


This item is held in Loughborough University's Institutional Repository (<https://dspace.lboro.ac.uk/>) and was harvested from the British Library's EThOS service (<http://www.ethos.bl.uk/>). It is made available under the following Creative Commons Licence conditions.



CC creative commons
COMMONS DEED

Attribution-NonCommercial-NoDerivs 2.5

You are free:

- to copy, distribute, display, and perform the work

Under the following conditions:

BY: **Attribution.** You must attribute the work in the manner specified by the author or licensor.


Noncommercial. You may not use this work for commercial purposes.

No Derivative Works. You may not alter, transform, or build upon this work.

- For any reuse or distribution, you must make clear to others the license terms of this work.
- Any of these conditions can be waived if you get permission from the copyright holder.

Your fair use and other rights are in no way affected by the above.

This is a human-readable summary of the [Legal Code \(the full license\)](#).

[Disclaimer](#) 

For the full text of this licence, please go to:
<http://creativecommons.org/licenses/by-nc-nd/2.5/>

**THE LLAB MODEL FOR QUANTIFYING COLOUR
APPEARANCE**

By

Mei-Chun Lo

A Doctoral Thesis

**Submitted in partial fulfilment of the requirement
for the award of
Doctor of Philosophy
of the Loughborough University of Technology**

August 1995

©Mei-Chun Lo 1995

ABSTRACT

A reliable colour appearance model is desired by industry to achieve high colour fidelity between images produced using a range of different imaging devices. The aim of this study was to derive a reliable colour appearance model capable of predicting the change of perceived attributes of colour appearance under a wide range of media/viewing conditions. The research was divided into three parts: characterising imaging devices, conducting a psychophysical experiment, and developing a colour appearance model.

Various imaging devices were characterised including a graphic art scanner, a Cromalin proofing system, an IRIS ink jet printer, and a Barco Calibrator. For the former three devices, each colour is described by four primaries: cyan (C), magenta (M), yellow (Y), and black (K). Three set of characterisation samples (120 and 31 black printer, and cube data sets) were produced and measured for deriving and testing the printing characterisation models. Four black printer algorithms (BPA), were derived. Each included both forward and reverse processes. A 2nd BPA printing model taking into account additivity failure, grey component replacement (GCR) algorithm gave the most accurate prediction to the characterisation data set than the other BPA models. The PLCC (Piecewise Linear interpolation assuming Constant Chromaticity coordinates) monitor model was also implemented to characterise the Barco monitor.

The psychophysical experiment was conducted to compare Cromalin hardcopy images viewed in a viewing cabinet and softcopy images presented on a monitor under a wide range of illuminants (white points) including: D93, D65, D50 and A. Two scaling methods: category judgement and paired comparison, were employed by viewing a pair of images. Three classes of colour models were evaluated: uniform colour spaces, colour appearance models and chromatic adaptation transforms. Six images were selected and processed via each colour model. The results indicated that the BFD chromatic transform gave the most accurate predictions of the visual results.

Finally, a colour appearance model, LLAB, was developed. It is a combination of the BFD chromatic transform and a modified version of CIELAB uniform colour space to fit the LUTCHI Colour Appearance Data previously accumulated. The form of the LLAB model is much simpler and its performance is more precise to fit experimental data than those of the other models.

ACKNOWLEDGEMENTS

The author is grateful to her supervisor Dr. H. E. Bez for his work on administrative support and encouragement.

The author wishes to express the most sincere thanks to her external supervisor Dr. M. R. Luo and his guidance in the writing of this thesis.

Particular thanks are due to The National Science Council, Taiwan, R.O.C., and The World College of Journalism and Communications, Taipei, Taiwan for the financial assistance.

This work was also supported by Crosfield Electronics Ltd. for preparing samples and supplying the tele-spectroradiometer for colour measurement. The author would also like to thank Mr. Tony Johnson and Professor R. W. G. Hunt for their technical advice.

The author is greatly indebted to every member of her family for their wonderful support and encouragement.

Many thanks are also due to the people who took part in many sessions of the psychophysical experiments.

CONTENTS

LIST OF TABLES

LIST OF FIGURES

LIST OF APPENDICES

Chapter 1	INTRODUCTION	1
1.1	WYSIWIG	1
1.2	Device Dependency	1
1.3	Variation of Colour Appearance Under Different Viewing Conditions	2
1.4	The Aim of the Study	2
Chapter 2	LITERATURE SURVEY	4
2.1	Colour Specification Systems	4
2.1.1	The CIE System	4
2.1.2	Colour Order System	6
2.1.2.1	The Munsell System	6
2.1.2.2	The Natural Color System (NCS)	7
2.2	Colour Difference Formulae	8
2.3	Colour Measurement Instruments	11
2.3.1	Tele-Spectroradiometer	12
2.3.2	Spectrophotometer	12
2.4	Colour Printing	13
2.4.1	Offset Colour Printing	13
2.4.2	Cromalin Proofing System and Continuous Ink-Jet Printing	13
2.4.3	Tone Reproduction	14
2.4.4	Black Printer and Grey Component Replacement (GCR)	15

2.4.4.1	Tone Reproduction for Black	15
2.4.4.2	Chromatic and Achromatic Colour Reproduction	16
2.4.4.3	GCR	17
2.4.5	Additivity Failure and Sub-Additivity Behaviour	18
2.5	Review of Mathematical Models for Characterising Printing and Monitor Devices	19
2.5.1	Printing Mathematical Models	19
2.5.1.1	Neugebauer-Type Equations	19
2.5.1.2	Masking-Type Equations	25
2.5.2	Monitor Models	27
2.5.2.1	PLCC (Piecewise Linear interpolation assuming constant Chromaticity Coordinates)	28
2.5.2.2	LIN-LIN2 (Linear-Linear 2nd-Order Model)	29
2.5.2.3	LOG-LOG (Log-Log Model)	29
2.5.2.4	LOG-LOG2 (Log-Log 2nd-Order Model)	29
2.5.2.5	Berns et al. (Modified Log-Log Model)	29
2.5.2.6	LOG-LIN2 (Log-Linear 2nd-Order Model)	30
2.5.2.7	PLVC (Piecewise Linear interpolation assuming Variable Chromaticity coordinates)	30
2.5.3	The Evaluation of Models' Performance	30
2.5.3.1	Printing Models' Performance	30
2.5.3.2	Monitor Models' Performance	32
2.6	The Psychological Laws	34
2.6.1	The Fecher's Logarithmic Law and the Stevens's Power Law	34
2.6.2	The Law of Comparative Judgement	36
2.6.3	The Law of Categorical Judgement	38

2.7 Chromatic Adaptation and Colour Appearance	39
2.7.1 Chromatic Adaptation Theory	39
2.7.1.1 Symmetric Matching	41
2.7.1.2 Asymmetric Matching	41
2.7.2 Some Colour Appearance Phenomena	42
2.7.2.1 Discounting of the Illuminant Colour (Object-Colour Constancy)	42
2.7.2.2 The Helson-Judd Effect	43
2.7.2.3 The Bezold-Brücke Effect	43
2.7.2.4 The Stevens Effect	43
2.7.2.5 The Hunt Effect	44
2.7.2.6 The Helmholtz-Kohlrausch Effect	44
2.7.3 Techniques For Studying Chromatic Adaptation and Assessing Colour Appearance	44
2.7.3.1 Haploscopic Matching	45
2.7.3.1.1 Simultaneous-Haploscopic Matching	45
2.7.3.1.2 Successive-Haploscopic Matching	46
2.7.3.2 Local Adaptation	47
2.7.3.3 Direct Scaling and Magnitude Estimation	47
2.7.3.4 Memory Matching	48
2.7.4 Chromatic Adaptation Transforms	49
2.7.4.1 The von Kries Chromatic Adaptation Transform	49
2.7.4.2 The BFD Chromatic Adaptation Transform	50
2.7.4.3 The Nayatani Chromatic Adaptation Transform (CIE Chromatic Adaptation Transform)	51
2.7.5 Colour Appearance Models	51

2.7.5.1	The Hunt Colour Appearance Model	51
2.7.5.2	The Nayatani Colour Appearance Model	53
2.7.5.3	The RLAB Colour Appearance Model	53
2.7.6	LUTCHI Colour Appearance Data	55
2.7.6.1	The Acquisition of LUTCHI Colour Appearance Data	55
2.7.6.1.1	Alvey Colour Appearance Data Set	55
2.7.6.1.2	CARISMA Colour Appearance Data Set	57
2.7.6.1.3	Kuo and Luo Colour Appearance Data Set	59
2.7.6.2	Testing Colour Models' Performance Using LUTCHI Colour Appearance Data	60
Chapter 3	CHARACTERISING PRINTING DEVICES	62
3.1	Objectives	62
3.2	Printing Devices Selected	63
3.3	Data Sets for Characterising Printers	63
3.3.1	Cube Data Set	63
3.3.2	Black Printer Data Set	64
3.4	Characterising Procedures	65
3.5	Printing Characterisation Models	67
3.5.1	Sub-Additivity Equations (SAE)	69
3.5.2	Modified Sub-Additivity Equations (MSAE)	71
3.5.3	Third-Order Polynomial Equations (3rd)	71
3.5.4	Second-Order Polynomial Equations (2nd)	71
3.6	Testing Models' Performance	72
3.6.1	The Performance of the Third-Order Masking Model	72
3.6.2	The Performance of the Forward BPA Models	74

3.6.3	The Performance of the Reverse BPA Models	76
3.6.4	The Reversibility Performance Between the Forward and Reverse BPA Models	78
3.7	Conclusions	81
Chapter 4	QUANTIFYING COLOUR APPEARANCE—COMPLEX IMAGES	83
4.1	Experimental Preparation	84
4.1.1	Device Characterisation	84
4.1.2	Image Preparation and Processing	88
4.2	Preliminary Experiment	89
4.2.1	Experimental Set-Up and Viewing Configuration	90
4.2.2	Data Analysis	92
4.2.3	Spatial Uniformity of Monitor Screen	96
4.2.4	Models' Performance	96
4.3	Main Experiment	98
4.3.1	Viewing Configuration	98
4.3.2	Viewing Conditions and Viewing Techniques	99
4.4	Data Analysis	101
4.5	Results and Discussion	102
4.5.1	Observer Precision and Repeatability	102
4.5.2	Models' Performance	103
4.5.3	Image Dependency	106
4.5.4	Difference Between Results From Paired Comparison and Category Judgement	107
4.5.5	Image Quality of Colour Fidelity	108
4.6	Conclusions	108

Chapter 5	THE LLAB COLOUR APPEARANCE MODEL	110
5.1	Drawbacks of the Hunt Model	111
5.2	Formulation of the LLAB Model	112
5.3	The Development of the LLAB Model	119
5.4	Testing the LLAB Model's Performance	121
5.5	Conclusions	125
Chapter 6	CONCLUSIONS	127
6.1	Summary of the Major Findings	127
6.2	Future Work	129
	REFERENCES	130
	COLOUR PLATE	
	TABLES	
	FIGURES	
	APPENDICES	

LIST OF TABLES

- Table 2.1 Summary of the experimental phases (the Alvey Colour Appearance Data Set).
- Table 2.2 Summary of the experimental phases (the CARISMA Colour Appearance Data–Surface Data Set).
- Table 2.3 Summary of the experimental phases (the CARISMA Colour Appearance Data–LT Data Set).
- Table 2.4 Summary of the experimental phases (the CARISMA Colour Appearance Data–35mm Data Set).
- Table 2.5 Summary of the experimental phases (the Kuo and Luo Colour Appearance Data Set).
- Table 3.1 The D_r , D_g , and D_b for each colour in the 120 data set (IRIS device).
- Table 3.2 The D_r , D_g , and D_b for each colour in the 120 data set (Cromalin device).
- Table 3.3 Summary of the 3rd-order masking equations' performance using the cube data set.
- Table 3.4 Summary of the forward BPA models' predictive performance.
- Table 3.5 Summary of the reverse BPA models' performance using IRIS device (K is known).
- Table 3.6 Summary of the reverse BPA models' performance using Cromalin device (K is known).
- Table 3.7 Summary of the reversibility performance between the forward and reverse BPA models (K ink is known).
- Table 3.8 Summary of the GCR's reversibility performance (IRIS device).
- Table 3.9 Summary of the GCR's reversibility performance (Cromalin device).
- Table 4.1 Mean colorimetric measures calculated between the XYZ values measured from TSR and MS and those calculated between the XYZ values measured from TSR and predicted (P) by the model under D65, D50, and A light sources.
- Table 4.2 Summary of the performance of the 2nd BPA model derived using newly characterisation data.
- Table 4.3 Parameters used for the Hunt and RLAB colour appearance models in the preliminary experiment.

- Table 4.4 The colorimetric and luminance values under D65 and D50 illuminants used in the preliminary experiment.
- Table 4.5 An example to illustrate method for calculating the category judgement results.
- Table 4.6 An example to illustrate method for calculating the paired comparison results.
- Table 4.7 The mean results in the preliminary experiment using the paired comparison and category judgement methods.
- Table 4.8 Summary of experimental phases for testing colour models in the main experiment.
- Table 4.9 The white point's colorimetric and luminance values in each phase in the main experiment.
- Table 4.10 Parameters used for the Hunt and RLAB colour appearance models in the main experiment.
- Table 4.11 The colorimetric, luminance, and monitor RGB DAC values of grey background used in the main experiment.
- Table 4.12 Summary of observer precision and repeatability performance (correlation coefficients (r) vs. frequencies).
- Table 4.13 Summary of models' performance from six images combined evaluated using the paired comparison method.
- Table 4.14 Summary of models' image dependency using the difference between the highest and the lowest z scores.
- Table 4.15 Summary of models' performance from six images combined evaluated using the category judgement method.
- Table 4.16 Mean rank of each model's performance from the paired comparison (pc) and category judgement (cj) methods (Case 2).
- Table 5.1 The F_S , F_L , and F_C parameters used in the LLAB model.
- Table 5.2 Values for converting hue angle to hue composition.
- Table 5.3 Example of input data and calculated results using the LLAB colour model.
- Table 5.4 Data used to formulate the S_C function in the LLAB colour model.
- Table 5.5 Summary the experimental conditions used in each LUTCHI data set.
- Table 5.6 Summary of observer precision (CVs) in each LUTCHI data set.
- Table 5.7 Parameters used in each space or model for testing colour appearance data.

- Table 5.8 CVs for set A of LUTCHI Colour Appearance Data (Alvey surface-colour high-luminance experimental results).
- Table 5.9 CVs for set B of LUTCHI Colour Appearance Data (Alvey surface-colour low-luminance experimental results).
- Table 5.10 CVs for set C of LUTCHI Colour Appearance Data (Alvey monitor-colour experimental results).
- Table 5.11 CVs for set D of LUTCHI Colour Appearance Data (CARISMA surface-colour experimental results).
- Table 5.12 CVs for set E of LUTCHI Colour Appearance Data (Kuo and Luo surface-colour experimental results).
- Table 5.13 CVs for set F of LUTCHI Colour Appearance Data (CARISMA large transparency (LT) experimental results).
- Table 5.14 CVs for set G of LUTCHI Colour Appearance Data (CARISMA 35mm projection experimental results).
- Table 5.15 Summary CVs for all models tested in predicting 7 sets of LUTCHI Colour Appearance Data.

LIST OF FIGURES

- Fig. 2.1 Hue, value, and chroma coordinates of the Munsell system.
- Fig. 2.2 The NCS hue arrangement.
- Fig. 2.3 Rectangular and cylindrical coordinates of CIELAB space.
- Fig. 2.4 Process for a printing colour reproduction.
- Fig. 2.5 Examples of three different types of black printer.
- Type 1: the amount of black is kept to an absolute minimum and is only used when the three-colour grey has reached its maximum.
- Type 2: the black is used to extend the maximum density for the three colours.
- Type 3: the full scale black printer.
- Fig. 2.6 (a) Conventional Chromatic, (b) Ideal 100% GCR, and (c) Practical GCR values.
- Fig. 2.7 Sub-additivity diagram representing the general sub-additivity behaviour of inks.
- Fig. 2.8 Schematic illustration of the eight Neugebauer primaries produced by overlapping of the Cyan, Magenta, and Yellow halftone dots.
- Fig. 2.9 “Cellular” corner-points of the eight cells determined using the combination of 0%, 50% and 100% for each of the CMY primaries.
- Fig. 2.10 One subset cell from the CMY space in Fig. 2.9.
- Fig. 2.11 The contents of the viewing pattern (Alvey Colour Appearance Data–Surface and Monitor Data Sets and CARISMA Colour Appearance Data–Surface Data Set).
- Fig. 2.12 Back-lit illuminator used in the LT (cut-sheet transparency) experiment.
- Fig. 2.13 Diagram of 35mm projected slide experimental situation.
- Fig. 3.1 Arrangement of colour patches in cube (or 729) data set (using cyan, magenta, and yellow primaries).
- Fig. 3.2 (a) Constant cyan plans with variation of magenta and yellow of the 729 cube data set plotted on CIE a^*b^* diagram for IRIS device.
- (b) Constant cyan plans with variation of magenta and yellow of the 729 cube data set plotted on CIE a^*b^* diagram for Cromalin device.
- Fig. 3.3 The computational procedures used in the forward BPA models.

- Fig. 3.4 The computational procedures used in the reverse BPA models (with known black ink (K)).
- Fig. 3.5 The computational procedures used in the full reverse BPA models (GCR).
- Fig. 3.6 (a) Sub-additivity diagram for red-colorimetric densities (D_r) of IRIS device.
(b) Sub-additivity diagram for red-colorimetric densities (D_r) of IRIS device. (Each line is plotted using a least-squares technique)
- Fig. 3.7 (a) Sub-additivity diagram for green-colorimetric densities (D_g) of IRIS device.
(b) Sub-additivity diagram for green-colorimetric densities (D_g) of IRIS device. (Each line is plotted using a least-squares technique)
- Fig. 3.8 (a) Sub-additivity diagram for blue-colorimetric densities (D_b) of IRIS device.
(b) Sub-additivity diagram for blue-colorimetric densities (D_b) of IRIS device. (Each line is plotted using a least-squares technique)
- Fig. 3.9 (a) Sub-additivity diagram for red-colorimetric densities (D_r) of Cromalin device.
(b) Sub-additivity diagram for red-colorimetric densities (D_r) of Cromalin device. (Each line is plotted using a least-squares technique)
- Fig. 3.10 (a) Sub-additivity diagram for green-colorimetric densities (D_g) of Cromalin device.
(b) Sub-additivity diagram for green-colorimetric densities (D_g) of Cromalin device. (Each line is plotted using a least-squares technique)
- Fig. 3.11 (a) Sub-additivity diagram for blue-colorimetric densities (D_b) of Cromalin device.
(b) Sub-additivity diagram for blue-colorimetric densities (D_b) of Cromalin device. (Each line is plotted using a least-squares technique)
- Fig. 3.12 (a) The $\Delta E(\text{CMC})$ distributions for the 5 forward BPA models tested using the 31 data set (IRIS device).
(b) The $\Delta E(\text{CMC})$ distributions for the 5 forward BPA models tested using the 31 data set (Cromalin device).
- Fig. 3.13 (a) The $\Delta E(\text{CMC})$ distributions for the 5 forward BPA models tested using the 110 data set (IRIS device).
(b) The $\Delta E(\text{CMC})$ distributions for the 5 forward BPA models tested using the 110 data set (Cromalin device).

- Fig. 3.14 (a) The $\Delta E(\text{CMC})$ distributions for the 2 forward 2nd BPA models tested using the cube data set (IRIS device).
(b) The $\Delta E(\text{CMC})$ distributions for the 2 forward 2nd BPA models tested using the cube data set (Cromalin device).
- Fig. 3.15 (a) The $|\Delta \text{FDA}_{3c}|$ distributions for the 5 reverse BPA models tested using the 31 data set (IRIS device).
(b) The $|\Delta \text{FDA}_{3c}|$ distributions for the 5 reverse BPA models tested using the 110 data set (IRIS device).
- Fig. 3.16 (a) The $|\Delta \text{FDA}_{3c}|$ distributions for the 5 reverse BPA models tested using the 31 data set (Cromalin device).
(b) The $|\Delta \text{FDA}_{3c}|$ distributions for the 5 reverse BPA models tested using the 110 data set (Cromalin device).
- Fig. 3.17 (a) The $\Delta E(\text{CMC})$ distributions for the 2 reverse 2nd BPA models tested using the 31 data set (K ink is known) (IRIS device).
(b) The $\Delta E(\text{CMC})$ distributions for the 2 reverse 2nd BPA models tested using the 110 data set (K ink is known) (IRIS device).
- Fig. 3.18 (a) The $\Delta E(\text{CMC})$ distributions for the 2 reverse 2nd BPA models tested using the 31 data set (K ink is known) (Cromalin device).
(b) The $\Delta E(\text{CMC})$ distributions for the 2 reverse 2nd BPA models tested using the 110 data set (K ink is known) (Cromalin device).
- Fig. 4.1 Flow chart showing the image processing procedures. The UCS, CAM and CAT processes represent uniform colour space, colour appearance model and chromatic adaptation transform respectively.
- Fig. 4.2 The experimental viewing configuration for a) a simultaneous (SS) display using a symmetric condition, b) a simultaneous (SS) display using a asymmetric condition (Background difference/With white border), c) a simultaneous (SS) display using a asymmetric condition (Background difference/ Without white border), d) a toggling (TG) display.
- Fig. 4.3 The plot of category results for the same image displayed on the right and left sides of the monitor screen.
- Fig. 4.4 Colour models' performance (combined from six images) evaluated using paired comparison results under a) D65, and b) D50 sources. The GW, BW, and BB represent the situations wherein the grey background with a white border, black background with a white border, and black background without a white border in the softcopy field for Experiments 1, 2, and 3 respectively.

- Fig. 4.5 Colour models' performance (combined from six images) evaluated using category judgement results under a) D65, and b) D50 sources. The GW, BW, and BB represent the situations wherein the grey background with a white border, black background with a white border, and black background without a white border in the softcopy field for Experiments 1, 2, and 3 respectively.
- Fig. 4.6 Colour models' performance (combined from six images) evaluated using paired comparison results from a) Phases 1 and 2, and b) Phases 3 to 7.
- Fig. 4.7 Performance difference between the models using the SS and TG display arrangements for Phases 5 and 6 respectively.
- Fig. 4.8 Colour models' performance (for individual image) evaluated using the paired-comparison method for a) Phase 1, b) Phase 2.
- Fig. 4.9 Colour models' performance (for individual image) evaluated using the paired-comparison method for a) Phase 3, b) Phase 4, c) Phase 5, d) Phase 6, e) Phase 7.
- Fig. 5.1 Graphical representation of corresponding a^* , b^* values showing direction and magnitude of the visual results under A (plotted using + symbol) and D65 (plotted using a \times symbol) light sources compared with those predicted by (a) the BFD model, (b) the Hunt model for LUTCHI–Alvey Data Set (plotted using o symbol).
- Fig. 5.2 Graphical representation of corresponding a^* , b^* values showing direction and magnitude of the visual results under A (plotted using + symbol) and D65 (plotted using a \times symbol) light sources compared with those predicted by (a) the BFD model, (b) the Hunt model for LUTCHI–Kuo and Luo Data Set (plotted using o symbol).
- Fig. 5.3 Flow chart for the calculation of LLAB model in predicting corresponding colours.
- Fig. 5.4 Scaling factor (S_c) vs. $\text{Log}(L)$ showing the Hunt effect (the increase in colourfulness due to increase of luminance level).
- Fig. 5.5 Flow chart for comparing colour models' prediction with visual results.

LIST OF APPENDICES

- Appendix A Equations used for black printer algorithms (BPAs).
- Appendix B The paired comparison results in terms of the z score together with 95% confidence limit for all phases in the main experiment.
- Appendix C The category judgement results for all phases in the main experiment.
- Appendix D Rank order of models' performance using the paired comparison method (using 95% confidence limits). (CL=1.39)
- Appendix E Rank order of models' performance using the category judgement method.
- Appendix F Colour-fidelity category of models' performance using the category judgement method.

Chapter 1 INTRODUCTION

1.1 WYSIWYG

“What You See Is What You Get” (WYSIWYG) has already been recognised as an area of considerable interest for the colour imaging industry, and as an aspect of computer imaging has recently been substantially researched. The essence of WYSIWYG is the accurate reproduction of colour images across a wide variety of media and applications.

CRT monitors are often used in the graphic arts industry as a softproofing device for previewing and editing the image before the hardcopy is printed. Both softcopy and hardcopy are widely used to simulate and communicate how the colours will appear in the final printed reproduction. However, the computer generated image a user sees on one monitor may not match that seen on another, and also cannot be truthfully reproduced onto the hardcopy. This often results in users spending hours interactively adjusting image colours on the monitor screen until a satisfactory match is obtained, after which the printed result still does not match that of the softcopy.

Thus WYSIWYG can not only tremendously improve operator confidence when making colour decisions, but can also enhance efficiency and hence there is potential for significant economic savings in industry by using WYSIWYG to prevent colour reproduction errors.

There are two main obstacles in achieving WYSIWYG: *device dependency* and *variation of colour appearance under different viewing conditions*.

1.2 DEVICE DEPENDENCY

It is common to use the device primaries to describe colours from a particular imaging device such as Red, Green and Blue (RGB) for a display monitor or film recorder, or Cyan, Magenta, Yellow and Black (CMYK) for an electronic printer. This is known as

device dependency. Since device primaries do not correspond to human colour perception and vary between different colour reproduction systems, a problem arises when colours are reproduced using the same set of device primaries for two different devices. Poor colour fidelity usually occurs. Control colours may be specified in a device-independent way to describe device primaries by means of an interchangeable and standardised colour specification system known as the CIE system. The process used to characterise each device in terms of the CIE system is called device characterization. Thus, a colorimetric match between colours presented on different media can be achieved.

1.3 VARIATION OF COLOUR APPEARANCE UNDER DIFFERENT VIEWING CONDITIONS

The CIE system was proposed in 1931 (CIE XYZ system) and was further refined in 1964 and 1976 to improve the overall visual uniformity of its colour space. It enabled any colour to be specified in terms of the light source, object and observer in a way that is truly independent of input and output devices. The purpose of this basic colorimetry is to determine how closely two colours match when seen under similar viewing conditions. It does not provide information about the appearance of colours in dissimilar viewing conditions such as different medium types, illuminants, luminance levels, backgrounds and surrounds. In practice, in colour reproduction systems such as photography, television, or printing, the viewing conditions for the original scene and its reproduction are often so different that simple colorimetric comparisons can be very misleading. Therefore, there is a considerable requirement for reliable colour models to predict the perceived appearance of colours presented on multiple media under various viewing conditions for industry use, to be developed.

1.4 THE AIM OF THE STUDY

The aim of this study was to derive a reliable colour appearance model capable of predicting the change of perceived attributes of colour appearance under a wide range of media/viewing conditions. The strategic approach was: to derive models to characterise

imaging devices, to test the performance of various existing colour spaces and colour appearance models using the experimental data involving complex images, and to derive a new model to adequately fit the existing data sets.

The above approaches correspond to the individual chapters in this thesis. A brief account of each chapter is given below.

- Chapter 2 to conduct literature survey covering all topics related to this study.
- Chapter 3 to characterise printing devices by developing mathematical transformations to convert between device dependent coordinates and colorimetric independent coordinates based on the CIE system.
- Chapter 4 to quantify colour appearance using complex images by conducting a psychophysical experiment to test various colour models. The comparison was made between hardcopy and softcopy images under a wide range of viewing conditions. The hardcopy images were viewed in a viewing cabinet, whereas the softcopy images, which had been processed using a number of colour models, were presented on a monitor.
- Chapter 5 to develop a colour appearance model by fitting a set of experimental data known as the LUTCHI (Loughborough University of Technology Computer Human Interface Research Centre) Colour Appearance Data based on the best performance colour model found in Chapter 4.
- Chapter 6 to summarise all results and findings from this study and to give implication of the application areas and future research works.

Chapter 2 LITERATURE SURVEY

This study encompassed a wide range of topics. A literature survey is given in this chapter to provide the background information related to this study.

2.1 COLOUR SPECIFICATION SYSTEMS

2.1.1 The CIE system

In CIE (1986a), it is stated that the Commission Internationale de l'Eclairage or International Commission Illumination (CIE) colour system, first standardised in 1931 and further refined in 1964 and 1976, allows the phenomenon of perceived colour to be described by the combination of the spectral power distribution of a light source, the spectral transmittances or reflectances of an object, and the spectral responses of the eyes from a panel of observers.

Tristimulus Values

In colorimetry (CIE 1986a), the tristimulus values X, Y, Z, are frequently used for colour specification and are calculated using Eqn. 2-1-1.

$$\begin{aligned} X &= k \sum P(\lambda) \rho(\lambda) \bar{x}(\lambda) \Delta\lambda \\ Y &= k \sum P(\lambda) \rho(\lambda) \bar{y}(\lambda) \Delta\lambda \\ Z &= k \sum P(\lambda) \rho(\lambda) \bar{z}(\lambda) \Delta\lambda \end{aligned} \quad (2-1-1)$$

where

- $k = \sum P(\lambda) \bar{y}(\lambda) \Delta\lambda / 100$
- $P(\lambda)$ is the spectral power distribution (SPD) of a light source at wavelength λ .
- $\rho(\lambda)$ is the spectral reflectance or transmittance of a colour stimulus at wavelength λ .
- $\bar{x}(\lambda)$, $\bar{y}(\lambda)$ and $\bar{z}(\lambda)$ are the colour matching functions of the CIE 1931 (2°) Standard Observer at wavelength λ .
- k is deliberately set so that $Y=100$ for a reference white.

The summation is carried out within the range of the visible spectrum from 360 to 830 nm, with a wavelength interval of ($\Delta\lambda$) say 5, 10 or 20 nm.

The CIE 1931 Standard Observer was defined by averaging the results from Wright (1928-29) and Guild (1931) on the colour matching of colours using a 2° bipartite matching field. Hence, the CIE 1931 Standard Observer (also referred to as the 2° Standard Observer) applies to colour matching fields of angular subtense less than 4°. In 1964 the CIE (1978) recommended a supplementary standard colorimetric observer ($\bar{x}_{10}(\lambda)$, $\bar{y}_{10}(\lambda)$ and $\bar{z}_{10}(\lambda)$) to be used with visual colour matching of fields of angular subtense of more than 4° at the eye of the observer.

Three standard illuminants A, B and C were initially recommended to represent tungsten filament lighting, direct sunlight and average daylight respectively. The standard illuminant D65 with a correlated colour temperature of approximately 6500K was recommended (together with a range of other D illuminants) due to the increasing demand for more accurate measurements on fluorescent materials. This overcame the problems caused by the inadequacy of standard illuminants B and C in the ultraviolet region. The CIE also recommended four illuminating and viewing conditions (45°/0°, 0°/45°, diffuse/0°, and 0°/diffuse) to be used for measuring the reflectances of opaque samples.

Chromaticity Coordinates

It is also usual to define a colour using chromaticity coordinates, which are types of relative tristimulus values.

$$x = X/(X + Y + Z)$$

$$y = Y/(X + Y + Z)$$

$$z = Z/(X + Y + Z)$$

$$\text{and } x + y + z = 1 \quad (2-1-2)$$

As shown in Eqn. 2-1-2, provided that x and y are known, z can be obtained by 1-x-y. It is therefore only necessary to quote two of the chromaticity coordinates which can then be

plotted on a y against x diagram (known as chromaticity diagram). The curve joining the x , y coordinates calculated from the $\bar{x}_{(\lambda)}$, $\bar{y}_{(\lambda)}$ and $\bar{z}_{(\lambda)}$ colour matching functions for the spectrum wavelengths is known as the spectrum locus. Any colour can be described by using x , y and Y .

2.1.2 Colour Order System

A colour order system is a rational method or a plan of ordering and specifying all object colours or colours within a limited domain, by means of a set of material standards selected and displayed so as to represent adequately the whole set of colours.

Of the many colour order systems (Wyszecki and Stiles 1982d), many have been widely used such as the Munsell system (Newhall et al. 1943), OSA system (MacAdam 1974), DIN system (Richter 1955), NCS system (Hård and Sivik 1981). The Munsell and NCS systems were used in the present work. A brief description of these systems is given in the following subsections.

2.1.2.1 The Munsell System

The Munsell system, developed by A. H. Munsell, is based on steps of equal visual-perception. The system arranges all colours on the basis of the equal colour difference between neighbouring steps and classifies colours according to three parameters: Munsell hue (H), Munsell value (V) and Munsell chroma (C), which closely correspond to hue, lightness, and saturation perceptions respectively. Each attribute was intended to be uniformly spaced in accordance with visual judgements.

The spacing of the chips was intensively studied by the Colorimetry Committee of the Optical Society of America in 1943. The CIE tristimulus values of ideally spaced chips were published as the Munsell Renotation System (Newhall et al. 1943). This revised spacing is defined under CIE illuminant C and the CIE 1931 Standard Observer. The current Munsell atlas, known as the Munsell Book of Color, is published in two types, glossy (1488 chips) and matt (1277 chips). Its spacing is illustrated in Fig. 2.1. The hue

circle is specified by ten hues: five principle hues, red (R), yellow (Y), green (G), blue (B) and purple (P), and five intermediate hues, YR, GY, BG, PB and RP. Each of the ten hues is subdivided into ten sub-hues numbered from 1 to 10. In total, there are 100 hue divisions. The Munsell value representing the lightness scale is divided into ten subjectively equal steps, with 0 being black and 10 being white. Similarly, by dividing into a series of steps, the Munsell chroma is an open-ended scale beginning with 0 for neutrals and up to about 12-16 for very saturated colours. The complete Munsell specification of a sample is expressed as:

H V/C

For example, 5R 6/12 is a very saturated red of moderate lightness.

2.1.2.2 The Natural Color System (NCS)

The NCS system was designed as a colour appearance system based on six psychologically unique colour perceptions: black (S), white (W), red (R) green (G), yellow (Y), and blue (B). The system is based upon Hering's opponent theory of colour (Hård and Sivik 1981). These six unique (primary) colours are arranged in opponent pairs on three orthogonal axes. The NCS hue plane includes the R-G versus Y-B opponent pairs. There are ten subdivisions between each neighbouring primaries, thus given 40 major hue angles at 9° intervals (Fig. 2.2). The four secondary colours lie at middle between two neighbouring primaries: Y50R, G50Y, B50G and R50B.

In the NCS colour system, colours can be specified by two methods. One uses the colour contents of six primaries. In other words, any colour can be described in terms of the relative amounts of unique colours appearing in the sample (but yellow and blue, and also red and green can not simultaneously exist). The six attributes are blackness (s), whiteness (w), redness (r) greenness (g), yellowness (y), and blueness (b) respectively. The r, g, y, and b are chromatic contents, whereas the s and w are achromatic contents. A typical specification of colour considered might be $w_{30}s_{20}g_{30}y_{20}$ which indicates the sample has 30% of whiteness, 20% of blackness, 30% of greenness, and 20% of yellowness. The scale is such that $w + s + g + y = 100$.

An alternative way to specify colours in the NCS system is to use three basic attributes—*hue* (Φ , the ratio of the two chromatic contents), blackness (s), and chromaticness (c , the sum of the two chromatic contents). The colours are marked as,

$$sc-\Phi,$$

where blackness (ranging from 0 to 100), and chromaticness (ranging from 0 to 100) correspond to magnitudes associated with lightness and saturation attributes respectively.

2.2 COLOUR DIFFERENCE FORMULAE

In any industry involved with the processing of coloured objects, maintaining the consistency of colours is a very important aspect of quality control. There is a considerable need for reliable colour difference formulae to be developed. These formulae provide a total colour difference (ΔE), which includes hue, lightness, and chroma components. Many colour difference formulae have been proposed over the years, but only a few, used in this work, are described below.

(1) 1976 CIE $L^*a^*b^*$ (CIELAB) formula (Robertson 1977, CIE 1978)

In 1976, the CIE recommended two uniform colour spaces: CIE $L^*a^*b^*$ and CIE $L^*u^*v^*$ for industries. The CIE $L^*a^*b^*$ was mainly concerned with the subtractive mixture (surface colorant) and the CIE $L^*u^*v^*$ for additive mixture of coloured light (lighting) (Hunt 1987). Both spaces have the same lightness scale, L^* , and opponent colour axes, red-green versus yellow-blue.

The CIE $L^*a^*b^*$ formula is a simplified version of the Adam-Nickerson or ANLAB formula (Adams 1942) which is a result of the nonlinear transformation of CIE space. A study carried out by Morley et al. (1975) showed that the CIE $L^*a^*b^*$ formula was one of the most reliable. In 1976 the Society of Dyers and Colourists recommended the use of CIE $L^*a^*b^*$ to replace the ANLAB formula to promote uniformity and simplicity for industrial application. The coordinates used to define the CIE $L^*a^*b^*$ are given in two forms as follows:

i) Rectangular Coordinates

$$L^* = 116 (Y / Y_n)^{1/3} - 16, \text{ or } L^* = 903.3 (Y / Y_n) \text{ if } Y/Y_n \leq 0.008856$$

$$a^* = 500 [f (X / X_n) - f (Y / Y_n)]$$

$$b^* = 200 [f (Y / Y_n) - f (Z / Z_n)]$$

If any one of the ratios X/X_n , Y/Y_n , or Z/Z_n is greater than 0.008856, the function of that particular ratio can be calculated using

$$f (X/X_n) = (X / X_n)^{1/3}$$

$$f (Y/Y_n) = (Y / Y_n)^{1/3}$$

$$f (Z/Z_n) = (Z / Z_n)^{1/3}$$

If any one of these ratios is less than or equal to 0.008856, the function of that particular ratio can be calculated using

$$f (X/X_n) = 7.787 (X / X_n) + 16/116$$

$$f (Y/Y_n) = 7.787 (Y / Y_n) + 16/116$$

$$f (Z/Z_n) = 7.787 (Z / Z_n) + 16/116$$

X , Y , and Z are the tristimulus values of the specimen, and X_n , Y_n , and Z_n are those of the appropriately chosen reference white.

The calculation of the total colour difference is given by:

$$\Delta E_{ab}^* = [(\Delta L^*)^2 - (\Delta a^*)^2 - (\Delta b^*)^2]^{1/2} \quad (2-2-1)$$

ii) Cylindrical Coordinates

$$C_{ab}^* = [(a^*)^2 + (b^*)^2]^{1/2}$$

$$h_{ab} = \arctan (b^* / a^*)$$

where C_{ab}^* is the metric chroma, and h is the metric hue angle and expressed using a $0^\circ - 360^\circ$ scale. In order to express the hue differences in the same unit as ΔE_{ab}^* , the quantity of hue difference (ΔH_{ab}^*) is defined by:

$$\Delta H_{ab}^* = [(\Delta E_{ab}^*)^2 - (\Delta L^*)^2 - (\Delta C_{ab}^*)^2]^{1/2} \quad (2-2-2)$$

where ΔE_{ab}^* is calculated from Eqn. 2-2-1.

A plot of the rectangular and cylindrical coordinates of CIE $L^*a^*b^*$ space is given in Fig. 2.3.

(2) 1976 CIE $L^*u^*v^*$ (CIELUV) formula (Robertson 1977, CIE 1978)

As mentioned above, along with CIELAB, CIE also recommended an alternative colour space, CIE $L^*u^*v^*$, which is a slightly modified version of the CIE (1964) $U^*V^*W^*$ formula. The new $u'v'$ UCS diagram is a projection transformation of the CIE 1931 x, y diagram. Straight lines in the x, y diagram remain straight in the u', v' diagram. This feature is considered important in cases where additive mixtures of lights are involved, such as in the colour television industry. It is produced by plotting in rectangular coordinates, the values of L^*, u^*, v^* defined as

$$L^* = 116 (Y / Y_n)^{1/3} - 16, \quad \text{or} \quad L^* = 903.3 (Y / Y_n) \quad \text{if } Y/Y_n \leq 0.008856$$

$$u^* = 13 L^* (u' - u_n')$$

$$v^* = 13 L^* (v' - v_n')$$

and,

$$u' = 4X / (X + 15Y + 3Z) = 4x / (-2x + 12y + 3)$$

$$v' = 9Y / (X + 15Y + 3Z) = 9y / (-2x + 12y + 3)$$

where

- Y_n is the Y value for the appropriately chosen reference white, taken to be 100;
- u', v' are the CIE 1976 uniform chromaticity scale;
- u_n', v_n' are the u' and v' coordinates for the particularly chosen reference white.

Colour difference can be calculated in the L^*, u^*, v^* space as follows:

$$\Delta E_{uv}^* = [(\Delta L^*)^2 + (\Delta u^*)^2 + (\Delta v^*)^2]^{1/2} \quad (2-2-3)$$

(3) CMC (*l*: *c*) Colour Difference Formula

McDonald (1980b) of J&P Coats developed the JPC79 formula which is a modification of the ANLAB colour space to fit a large collection of acceptability data (McDonald 1980a, 1980b). Further modifications were made by members of the Colour Measurement Committee of the Society of Dyers and Colourists (Clarke et al. 1984) to overcome problems arising from very dark colours, near neutral samples and hue angles for samples with low tristimulus values. The modified formula, CMC (*l*: *c*) is defined as follows:

$$\Delta E = [(\Delta L^* / l S_L) + (\Delta C^* / c S_C)^2 + (\Delta H^* / S_H)^2]^{1/2} \quad (2-2-4)$$

$$\text{where } S_L = 0.040975 L_1^* / (1 + 0.01765 L_1^*)$$

$$\text{unless } L_1^* < 16 \quad \text{when } S_L = 0.511$$

$$S_C = 0.063800 C_1^* / (1 + 0.01310 C_1^*) + 0.638$$

$$S_H = S_C (T f + 1 - f)$$

$$f = \{ (C_1^*)^4 / [(C_1^*)^4 + 1900] \}^{1/2}$$

$$T = 0.36 + | 0.4 \cos(h_1 + 35^\circ) |$$

$$\text{unless } h_1 \text{ is between } 164^\circ \text{ and } 345^\circ, \text{ when}$$

$$T = 0.56 + | 0.2 \cos(h_1 + 168^\circ) |$$

where

- L_1^* , C_1^* and h_1 refer to the standard of a pair of samples. These values and ΔL^* , ΔC^* , ΔH^* are calculated from the CIE $L^* a^* b^*$ formula.
- l and c values are the relative weightings of the CMC(*l*:*c*) formula required for a particular application.
- $l=c=1$ is used for judgement involving perceptibility of colour differences, while $l=2$ and $c=1$ are used for judgement involving acceptability of colour differences.

2.3 COLOUR MEASUREMENT INSTRUMENTS

There are three kinds of colour measurement instruments: the spectroradiometer, the spectrophotometer, and the tristimulus-filter colorimeter (Wyszecki and Stiles 1982a). Two instruments were used in this study: a tele-spectroradiometer (a kind of spectroradiometer) and a spectrophotometer.

2.3.1 Tele-Spectroradiometer (TSR)

A tele-spectroradiometer (TSR) is an apparatus designed to obtain spectral radiance which can be further multiplied by the colour matching functions ($\bar{x}(\lambda)$, $\bar{y}(\lambda)$ and $\bar{z}(\lambda)$ in Eqn. 2-1-1) to obtain tristimulus values that accurately represent a colour. It is set up at in the same position as that occupied by the observer's eyes with the same illuminant in the same surroundings. The instrument is made up of three basic components: a telescope to collect the light from the colour at the observing position, a monochromator which uses a grating or prism for analysing the data throughout the spectrum, and a detector to measure the spectral radiant power. The instrument has to be calibrated before measuring colour stimuli. There are two types of calibration. If measurements of absolute radiant power are required, then the instrument must be calibrated by using a standard light source with known absolute spectral power distribution. If only relative spectral power data are required, it is only necessary to know the relative spectral power distribution of the standard source. In practice, the TSR is frequently used to measure the spectral power distribution of a suitably chosen reference white under exactly the same conditions as the colours considered.

2.3.2 Spectrophotometer

A spectrophotometer is an apparatus designed to measure the spectral reflectance or transmittance factors of materials. It is the most widely used colour measurement equipment, applying a comparison of the radiant power leaving the material surface with that incident on it at each wavelength. Basically a modern spectrophotometer is made up of three components, a light source, such as a xenon flash lamp, a monochromator, and a photodetector. For modern instruments, the path of radiation is split into two parts within the instrument providing a sample beam and reference beam. When a sample is placed in the sample beam, the equality of the two beams is broken and the detector senses the difference and relates that to the transmittance or reflectance of the sample at that wavelength. For most purposes, it is usually considered sufficient to sample the spectrum at 20 nm intervals; but in some cases 10 nm is used.

2.4 COLOUR PRINTING

2.4.1 Offset Colour Printing

In a printing process, an image comprises three or four superimposed inks (cyan, magenta, yellow, or cyan, magenta, yellow, black). Theoretically only three process colours, cyan, magenta and yellow (CMY) are sufficient to give an accurate reproduction. However, in practice, a black printer is frequently added. Different colours are produced using a technique called halftoning (Stone et al. 1988), which reproduces the gradations in a picture using a pattern of dots of different sizes, i.e. fractional dot areas (FDAs). Originally, halftone patterns were produced by photographing an image through a fine screen, called a halftone screen. Modern systems produce halftone patterns digitally by scanning the original with a scanner. Fig. 2.4 is a simplified diagram of the various steps used in a four colour printing process. It starts with a continuous-tone original; produces four sets of screened separations on film containing information for each of the process colours (cyan, magenta, yellow and black); and culminates in printing plates ready for press printing on white paper with cyan, magenta, yellow, and black inks in registration. The initial procedure for producing four separations is similar in both conventional and scanning processes. The process consists of illuminating the original copy with white light. The reflected or transmitted light is then passed through a set of balanced red, green and blue filters to produce colour separations.

2.4.2 Cromalin Proofing System and Continuous Ink-Jet Printing

The Cromalin proofing system, a uniform thickness or concentration colorant system and one of the devices used in this study, is designed to match the full colour gamut of the printing inks. This system employs colourless photopolymer films, powdered coloured toners and conventional printing paper substrate. It allows respective printers to match spectral characteristics of their own inks by prescribed blending procedures with the basic coloured toners. The system can also compensate for certain individual press variations by making exposure or toner adjustments. Hence, Cromalin prepress proofs are often used instead of costly press proofs for customers' approval. Additionally, some printers

have used them to setup guides for multicolour printing because of their accuracy and consistency. Four-colour Cromalin proofs are produced by repeating the steps of laminating, exposing, and toning with each colour separation film (Sturge et al. 1989b).

Ink-jet printing is rapidly becoming one of the leading technologies in directly generating images on paper (non-impact printing). The ink-jet printer is a binary machine which can either put a dot at a particular location on a paper or leave it blank. In the process of continuous ink-jet printing, a stream of ink ejected through a nozzle is broken into droplets of equal size by ultrasonic vibration, typically of frequencies around 100 kHz. The droplets are charged and deflected to the desired position on the paper or other substrate to form an image. There are four nozzles, a black and three process inks, in a four-colour ink-jet printer. Halftone is obtained by a dither matrix (Sturge et al. 1989a).

The IRIS ink-jet printer, a continuous four-colour ink-jet printer and one of the devices used in this study, is typical of an increasing number of systems which combine frequency and amplitude modulation (Sturge et al. 1989b, Gur and O'Donnell 1987). A 5-bit resolution of a colorant "amount" is combined with a 4 x 4 dither matrix at 300 dpi to achieve modulation.

2.4.3 Tone Reproduction

The tone reproduction curve (TRC) is a measure frequently used for evaluating a reproduction system. This function defines a distribution of a set of reproduced tone values in relation to the original tone values. In traditional printing, these tone values are measured as density. An understanding of the densitometry is necessary for controlling the quality of halftone reproduction.

In principle, each original to be reproduced includes a range of brighter or darker shades, or tones. These are measured according to the degree of lightness and darkness. The measured values are known as density values. Density is actually a measurement of the light stopping ability of a tone area – less light will be stopped by a brighter tone, and conversely, more light will be absorbed by a darker tone. The density values are obtained by measuring the ratio between the amount of light reaching the original (i.e. incident

light), and the light reflected or transmitted from the original after it is partially absorbed. When the measurement is conducted from a reflected or transmitted tone area, it is called reflectance or transmission density respectively. It is expressed by a logarithmic function of reflectance factor (R) or transmittance factor (T) to produce numbers that relate to what observers see.

$$\text{Density} = \log_{10} (1/R)$$

$$\text{Density} = \log_{10} (1/T) \quad (2-4-1)$$

The tone reproduction curve characterises density values between the original and the reproduction images. An ideal reproduction maps the original values to identical values on the print (Molla 1988a).

2.4.4 Black Printer and Grey Component Replacement (GCR)

2.4.4.1 Tone Reproduction for Black

As mentioned earlier, a black printer is often used in the printing process. The black printer has two roles in the reproduction: extending the gamut of colours in the darkest regions of the image, and replacing appropriate amounts of the three coloured inks (Yule 1967d).

In a three-colour process, there is only one combination of the three inks for producing a given colour; but in a four-colour process, all except the cleanest colours can be reproduced either with minimum amounts of the three colours and a maximum black ink (or vice versa), or with many intermediate combinations between these two extremes. Three basic types of black printers (Kazuo 1986, Molla 1989b) are defined in terms of different TRCs as illustrated in Fig. 2.5. They are described below.

Type 1 the use of the black printer is simply to extend the maximum density of the three colours. This type is called a skeleton black printer.

Type 2 the maximum density for the three colours is extended by the use of the UCR (Under Colour Removal). The three colour primaries in the dark or near neutral shadow areas of the printed picture are removed and replaced

by black ink. In other words, black starts to print at a lower density and three-colour grey reduces accordingly.

Type 3 a full-scale black printer is produced along the entire tone reproduction curve.

With the advent of grey component replacement (GCR, see next section), the Types 2 and 3 black printers are more efficient than Type 1 and are commonly used in commercial situations. Therefore, some rules are required for using black ink as a replacement of the grey component produced using C, M, Y inks. These are introduced in the following sections.

2.4.4.2 Chromatic and Achromatic Colour Reproduction

Chromatic colour reproduction is the conventional reproduction of colours using cyan, magenta, and yellow inks, and reinforce their overprints with black ink where necessary. The black will give neutrality and depth. It will also extend the maximum density of the three colours and is mainly used to assist the coloured inks for Type 1 black printer. Achromatic colour reproduction is based on the theory that it is unnecessary to use cyan, magenta, and yellow inks to reproduce the grey (or achromatic) component in a colour when a single black can be used. Strictly speaking, achromatic colour reproduction consists of one or two chromatic primary colours and/or the achromatic black. So far even those reproductions which derive from the theory of achromatic colour reproduction have also been considered achromatic, although they do not entirely fulfill the requirement of not showing more than two chromatic or coloured inks and black ink in any part of the image. Since it is required to be able to select the intermediate stages between chromatic and achromatic colour reproduction in order to match customers' requirements, the choice of a new term is necessary. The term "Grey Component Replacement" (GCR) has been recognised as a new term instead of "Achromatic Colour Reproduction", and represents all the techniques which were originally developed from the theory of "Achromatic Colour Reproduction".

2.4.4.3 GCR

Whenever a colour is produced by overprinting cyan, magenta, and yellow primaries, the two primaries having more intensities determine the hue of that colour; and the least primary determines its purity, greyness, saturation or chroma. In fact, the latter primary is used to determine the amount of the colour for grey replacement. This amount of grey, called the grey component, can be removed from the colour and replaced with black ink. This process has been called “Grey Component Replacement” (GCR) as mentioned above.

With GCR, it is possible in the separation process to either completely or partly remove the grey component of all colours from highlight to shadow to different percentage values for certain printing characteristics, and replacing them with the black primary (Reiter 1984, Jung 1984, John 1985, Southworth 1990, Jackson 1990, Molla 1988c). The interpretation of a GCR percentage value has still not been standardised in the printing industry. Figs. 2.6 (a), (b), and (c) are examples for the chromatic, ideal 100% (or maximum) GCR, and practical 100% GCR colour reproductions respectively. The Fig. 2.6(a) illustrates the chromatic colour reproduction of a colour using 60% cyan (C), 70% magenta (M), and 90% yellow (Y) in an ideal printing condition. In this case, the achromatic value or grey component is formed by equal amount of 60% C, 60% M, and 60% Y ink coverage. Above this, it is the chromatic component, formed by 10% M and 30% Y. The C ink that has the least content in comparison with the other two, is called the tertiary colour or primary. When applying the 100% GCR to the ink percentages in Fig. 2.6(a) using ideal printing condition, the grey component is removed and replaced by black (K). The C, M, and Y inks would be reduced from 60% to 0%, 70% to 10%, and 90% to 30% respectively; and a 60% K would replace this three-colour grey component (Fig. 2.6(b)). Unfortunately, in reality, the GCR process is not that simple due to a number of external factors (Bruno 1985) such as the impurity of the pigments in the printing, deficiency of additivity failure (introduced below), and the printing conditions varying according to the different paper, press and inks used. Therefore, when applying

100% GCR, the grey component may only possibly be removed partially but not completely as illustrated in Fig. 2.6(c) (Jackson 1990).

2.4.5 Additivity Failure and Sub-Additivity Behaviour

When 3 or 4 inks are superimposed, it is assumed that the resultant density is equal to the sum of the densities from all of the inks. This is known as the additivity rule (Johnson 1988). In practice, the overall density is often much less than the sum of these inks. This deficiency is called additivity failure and is caused by several factors such as first-surface reflection, multiple internal reflection (Yule 1967a), opacity characteristics of the ink, ink trapping (Clapper and Yule 1953), back transfer effects, sideways scattering of light in the paper, halftone structure of the printed dots, spectral absorption characteristics of ink and paper, and spectral sensitivity characteristics of the measuring instruments. Empirically, this deficiency in multi-colour system can be characterised by deriving mathematical models, which are called Black Printer Algorithms (BPA). Yule (1967b) manifested that several of factors affecting additivity failure, when combined, tend to produce additivity curves in the form of approximately straight lines converging toward a point on the 45° line. Hamilton (1986) referred to it as sub-additivity behaviour. Both of Yule (1967b) and Kazuo (1986) devised the method of sub-additivity diagram to characterise the sub-additivity behaviour. Fig. 2.7 represents the general sub-additivity behaviour. For an ideal printing system without additivity failure, the function representing the relationship of densities of added black component and combination should be parallel to the 45° line. In practice, the increasing black ink superimposed on a fixed three-colour component in a four-colour system would approximately converge to a point on the 45° line as Yule found. Trigonometrically, it can be expressed as:

$$(D_{4c} - D_{3c}) / D_k = (k - D_{3c}) / k \quad (2-4-2)$$

where D_{4c} , D_{3c} , D_k are the densities of the resultant four-colour, three-colour and black components respectively. The k value represents the density at the converging point as shown in the sub-additivity diagram Fig. 2.7.

2.5 REVIEW OF MATHEMATICAL MODELS FOR CHARACTERISING PRINTING AND MONITOR DEVICES

One fundamental question for a colour reproduction system is:

“What is the mathematical relationship between how a colour looks and the amounts of printing colorants (CMY or CMYK) or monitor primaries (RGB) required to produce a visual match?”.

This is a question concerned with the form of mathematical transformations to correlate between the required output and generated input primary signals. As mentioned earlier, an accurate reproduction of colour images is needed to transform between the device dependent, and device independent coordinates, thereby the appearance of any colour can be colorimetrically specified.

Each mathematical model includes two forms: a forward and a reverse. The forward process predicts the CIE tristimulus values from a set of device primaries, for instance, CMY or CMYK for printing devices, RGB for monitors. The reverse process obtains the device primaries from a corresponding set of tristimulus values. This section introduces some of the mathematical models which have been proposed for characterising imaging devices.

2.5.1 Printing Mathematical Models

Printing models can be divided into two types of equations: Neugebauer-type and Masking-type.

2.5.1.1 Neugebauer-Type Equations

The basic Neugebauer (1937) model is a theoretical approach in relation to the ink amounts of the colour considered when a colour is produced by a halftone process. It predicts the colour which results from small halftone dots using data from large solid areas or 100% fractional dot areas (FDAs), known as Neugebauer Primaries. The model

is based on the assumption that the halftone dots are randomly distributed on the print. It is essentially an additive colour model based on the additive colour theory. The resultant colour appearance on a print seen by an observer is due to the fusion of the reproduction primaries (Cyan, Magenta, Yellow, Red, Green, Blue, White, Black for three-colour reproduction) in the eye. In other words, the tristimulus values of the reproduction colour pixel can simply be obtained by summing the tristimulus values of the combination of Neugebauer primaries, and weighting each by the relative fractional dot area.

Fig. 2.8 illustrates the generation of eight Neugebauer primaries from the overlap of Cyan (C), Magenta (M), and Yellow (Y) halftone dots in a three-colour reproduction system. If the XYZ tristimulus values of the eight Neugebauer primaries are represented as below:

<u>Colour</u>	<u>Tristimulus Values</u>
White	X_{PW}, Y_{PW}, Z_{PW}
Cyan	X_{CS}, Y_{CS}, Z_{CS}
Magenta	X_{MS}, Y_{MS}, Z_{MS}
Yellow	X_{YS}, Y_{YS}, Z_{YS}
Red	X_{RS}, Y_{RS}, Z_{RS}
Green	X_{GS}, Y_{GS}, Z_{GS}
Blue	X_{BS}, Y_{BS}, Z_{BS}
3-colour (Overprint)	$X_{3CS}, Y_{3CS}, Z_{3CS}$

the basic Neugebauer model can be expressed as Eqn. 2-5-1.

$$\begin{aligned}
 X &= f_p X_{PW} + f_c X_{CS} + f_m X_{MS} + f_y X_{YS} + f_r X_{RS} + f_g X_{GS} + f_b X_{BS} + f_{3c} X_{3CS} \\
 Y &= f_p Y_{PW} + f_c Y_{CS} + f_m Y_{MS} + f_y Y_{YS} + f_r Y_{RS} + f_g Y_{GS} + f_b Y_{BS} + f_{3c} Y_{3CS} \\
 Z &= f_p Z_{PW} + f_c Z_{CS} + f_m Z_{MS} + f_y Z_{YS} + f_r Z_{RS} + f_g Z_{GS} + f_b Z_{BS} + f_{3c} Z_{3CS}
 \end{aligned}
 \tag{2-5-1}$$

where

- X, Y, Z are the tristimulus values of the colour resultant or to be matched.
- f_i value is the fractional dot area (FDA) of the paper covered by the indicated primary (the value ranging between 0.0 and 1.0).
- subscripts p, c, m, y, r, g, b, 3c refer to the Paper White, Cyan, Magenta, Yellow, Red (i.e. Magenta + Yellow), Green (i.e. Cyan + Yellow), Blue (i.e. Cyan + Magenta) reproduction primaries (tints) respectively.

If the FDAs related to the halftone (tint) dot areas on paper of the single-coloured Cyan, Magenta, and Yellow are referred to as c , m , and y respectively, then, the FDAs of eight reproduction primaries (tints) can be represented as:

<u>Colour</u>	<u>Fractional Dot Area (FDA)</u>	
White	$f_p = (1-c)(1-m)(1-y)$	
Cyan	$f_c = c(1-m)(1-y)$	
Magenta	$f_m = m(1-c)(1-y)$	
Yellow	$f_y = y(1-m)(1-c)$	
Red	$f_r = m y (1-c)$	
Green	$f_g = c y (1-m)$	
Blue	$f_b = c m (1-y)$	
3-colour (Overprint)	$f_{3c} = c m y$	(2-5-2)

The c , m , y values can be computed using the Murray-Davies equations (Murray 1936) as follows:

$$\begin{aligned} c &= (1-10^{-D_c}) / (1-10^{-D_{cs}}) \\ m &= (1-10^{-D_m}) / (1-10^{-D_{ms}}) \\ y &= (1-10^{-D_y}) / (1-10^{-D_{ys}}) \end{aligned} \quad (2-5-3)$$

$$\begin{aligned} \text{where } D_c &= \log(X_{PW} / X_c) \\ D_m &= \log(Y_{PW} / Y_m) \\ D_y &= \log(Z_{PW} / Z_y) \end{aligned} \quad (2-5-4)$$

$$\begin{aligned} D_{cs} &= \log(X_{PW} / X_{CS}) \\ D_{ms} &= \log(Y_{PW} / Y_{MS}) \\ D_{ys} &= \log(Z_{PW} / Z_{YS}) \end{aligned} \quad (2-5-5)$$

where

- X_{PW} , Y_{PW} , Z_{PW} are the tristimulus values of white substrate.
- X_{CS} , Y_{MS} , and Z_{YS} are the X value of the solid Cyan primary, Y value of the solid Magenta primary, and Z value of the solid Yellow primary respectively.
- X_c , Y_m , Z_y are the X value of the required or generated Cyan amount (tint), the Y value of the required or generated Magenta amount, and Z value of the required or generated Yellow amount respectively.

The forward process of the Neugebauer-type models calculates the XYZ values directly from the dot area values (c , m , y). The c , m , y values have to be calculated by a numerical

method in the reverse process. With the addition of a Black primary (K), the number of possible overlaps is 16 rather than 8. The previous Neugebauer equations can be further extended to include the original eight primaries and the overprinting of the black primary.

There are a number of problems limiting the accuracy of the basic Neugebauer model. The major problem arises from the scattering of light within paper because the reflection does not occur at the ink-paper interface. This effect needs to be correctly predicted for an accurate colour reproduction. Although the Murray-Davies equation (Eqn. 2-5-3) does take this into account, it cannot predict this effect accurately.

Yule-Nielsen Modified Neugebauer Equations

Yule and Nielsen (1951), Clapper and Yule (1955), and Yule and Colt (1961) suggested that more accurate predictions could be made if the Neugebauer equation was modified to include an appropriate power factor (known as n value) to account for the internal reflections and scattering within the paper. With a power law, the basic Neugebauer model discussed in the above section was modified to include an exponent ($1/n$) for the tristimulus values in both sides of equation. This is known as the Yule-Nelson modified Neugebauer model. The new model is given in Eqn. 2-5-6.

$$\begin{aligned}
 X^{1/nc} &= f_p X_{PW}^{1/nc} + f_c X_{CS}^{1/nc} + f_m X_{MS}^{1/nc} + f_y X_{YS}^{1/nc} + f_r X_{RS}^{1/nc} + f_g X_{GS}^{1/nc} + \\
 &\quad f_b X_{BS}^{1/nc} + f_{3c} X_{3CS}^{1/nc} \\
 Y^{1/nm} &= f_p Y_{PW}^{1/nm} + f_c Y_{CS}^{1/nm} + f_m Y_{MS}^{1/nm} + f_y Y_{YS}^{1/nm} + f_r Y_{RS}^{1/nm} + f_g Y_{GS}^{1/nm} + \\
 &\quad f_b Y_{BS}^{1/nm} + f_{3c} Y_{3CS}^{1/nm} \\
 Z^{1/ny} &= f_p Z_{PW}^{1/ny} + f_c Z_{CS}^{1/ny} + f_m Z_{MS}^{1/ny} + f_y Z_{YS}^{1/ny} + f_r Z_{RS}^{1/ny} + f_g Z_{GS}^{1/ny} + \\
 &\quad f_b Z_{BS}^{1/ny} + f_{3c} Z_{3CS}^{1/ny} \qquad \qquad \qquad (2-5-6)
 \end{aligned}$$

and the Yule-Nielsen model for calculating the effective fractional dot areas is,

$$\begin{aligned}
 c &= (1-10^{-D_c/nc}) / (1-10^{-D_{cs}/nc}) \\
 m &= (1-10^{-D_m/nm}) / (1-10^{-D_{ms}/nm}) \\
 y &= (1-10^{-D_y/ny}) / (1-10^{-D_{ys}/ny}) \qquad \qquad \qquad (2-5-7)
 \end{aligned}$$

where nc , nm , ny are the Yule-Nielsen (1951) factors for each of tristimulus values used to compensate for the effect of the penetration of light into the paper, the other symbols are the same as those previously defined in Eqns. 2-5-4 and 2-5-5. The nc , nm , or ny values vary mainly according to the types of paper, screen frequencies of halftone ruling, the different printing devices' primaries, and the levels of dot area. A similar deviation can be applied for a four-colour reproduction case.

Spectral Yule-Nielsen Modified Neugebauer Equations

The Neugebauer models discussed above are based on broadband reflectance techniques using either colorimetry or densitometry. However, it has been argued that broadband techniques are inappropriate for the Neugebauer model due to large variations of each colour printer primary's reflectances across the visible spectrum. Vigginao (1985) devised the spectral Yule-Nielsen Equation which predicts the dot area on paper and XYZ of a single-coloured halftone tint throughout the visible spectrum. Furthermore, Vigginao (1990) extended the model to become the Spectral Yule-Nielsen Neugebauer to predict multi-colour halftone tints. If the symbol $R_{(\lambda)}$ denotes the reflectance of the multi-coloured halftone tint reproduced or the original colour matched at wavelength λ , and the reflectances of the primaries in an analogous manner, the Spectral Yule-Nielsen Neugebauer model is expressed in Eqn. 2-5-8.

$$R'_{(\lambda)} = f_p R'_{(\lambda)PW} + f_c R'_{(\lambda)CS} + f_m R'_{(\lambda)MS} + f_y R'_{(\lambda)YS} + f_r R'_{(\lambda)RS} + f_g R'_{(\lambda)GS} + f_b R'_{(\lambda)BS} + f_{3c} R'_{(\lambda)3CS} \quad (2-5-8)$$

where

- subscripts 1 to 8, indicate the particular primaries considered (corresponding to Paper White, Cyan, Magenta, Yellow, Red, Green, Blue, and 3-Colour overprints respectively).
- $R'_{(\lambda)} = R^{1/n}_{(\lambda)}$, $R'_{(\lambda)PW} = R^{1/n}_{(\lambda)PW}$, $R'_{(\lambda)CS} = R^{1/n}_{(\lambda)CS}$, etc.
where $R_{(\lambda)PW}$, $R_{(\lambda)CS}$, $R_{(\lambda)MS}$, ..., are the spectral reflectance at wavelength λ for Paper White, solid (100% FDA) Cyan primary, solid Magenta primary, etc., respectively.
- f_i term is defined in Eqn. 2-5-2.
- n value is the Yule-Nielsen factor as mentioned earlier.

Similarly, this model can be extended to a four-colour reproduction system.

Once the reflectance value of the colour considered at each wavelength (λ) is predicted, the CIE tristimulus values XYZ can be calculated by integrating those spectral reflectances using Eqn. 2-1-1.

“Cellular” Neugebauer-Type Equations

The previous Neugebauer-type models introduced were limited to use only a set of 8 samples or 16 samples for three- or four- colour cases respectively. Heuberger et al. (1992) found that the Neugebauer-type models, with the addition of partial dot area coverages, could produce more accurate results than the original model. A more accurate modified Neugebauer model can be derived using more than eight sample prints in a three-colour reproduction. The addition of these partial overprint samples is equivalent to partitioning the CMY space into rectangular cells and expanding the Neugebauer-type equations within each cell. Hence, a set of dot areas c , m , y can be represented as a point in a three-colour CMY space. This type of model is referred to as the “Cellular Neugebauer-Type Model”.

Provided that the combinations of 0%, 50%, and 100% of Cyan, Magenta, and Yellow colorant primaries are used, the CMY space will then be divided into 8 cells which are determined by the use of 3^3 (=27) corner points (Fig. 2.9). Similarly, using the combinations of 0%, 25%, 50%, 75% and 100%, will results in 64 cells determined by 5^3 (=125) corner points. By only using the combinations of 0% and 100% of Cyan, Magenta and Yellow primaries, the cellular Neugebauer-type equations have the geometric interpretation of linear interpolation in entire CMY space with 2^3 (=8) corner points. This then becomes the original Neugebauer model.

Heuberger et al. only extended the broadband Neugebauer model to the “cellular” case (i.e. cellular broadband Neugebauer equations). However, Rolleston (1993) stated that the cellular Yule-Nielsen modified equations or cellular spectral Neugebauer equations could be further derived to improve the accuracy of the prediction if the Yule-Nielsen equation

and spectral considerations were also incorporated into a cellular framework. These are described below.

Assuming a set of known dot areas c, m, y represented by a point in a three-colour CMY space, this point will fall into a rectangular cell bounded by the lower and upper extremes as in Fig. 2.10, i.e. one of the 8 subcells shown in Fig. 2.9. The cornerpoints' coordinates are denoted using $C_l, C_u, M_l, M_u, Y_l, Y_u$ along each of the three axes. Mathematically, the C_l and C_u, M_l and M_u, Y_l and Y_u may be specified as being the two points, along the cyan, magenta, and yellow axes respectively, that satisfy the constraints:

$$\begin{aligned} 0 \leq C_l \leq C_u \leq 1; & & C_l, C_u \in I_c \\ 0 \leq M_l \leq M_u \leq 1; & & M_l, M_u \in I_m \\ 0 \leq Y_l \leq Y_u \leq 1; & & M_l, M_u \in I_y \end{aligned} \quad (2-5-9)$$

where I_c, I_m, I_y are the set of points along the cyan, magenta, and yellow axes respectively that specify the cellular division in the entire CMY space. It is necessary to normalise the dot values c, m, y into the interval $[0,1]$ within the cell under consideration in order to perform the interpolation within a given cell. Using the same deviation technique as described earlier, the cellular broadband Neugebauer model, cellular broadband Yule-Nielsen modified Neugebauer model, cellular spectral Neugebauer and cellular spectral Yule-Nielsen modified Neugebauer models can be obtained and have similar forms as Eqns. 2-5-1, 2-5-6, 2-5-8 respectively.

2.5.1.2 Masking-Type Equations

Another model used to correlate the printing primaries and the CIE XYZ system is the masking model. The technique used for deriving forward and reverse processes in the Masking-type Models is the same. Therefore, only the forward models are introduced here.

The original first-order masking equations were devised by Yule (1938). They assume the occurrence of additivity and proportionality of ink densities as the halftone dot area, or colorant concentration or film thickness changes. Thus a simple linear transformation

would be sufficient to establish the amount of ink required in the reproduction in order to match the three colour intensities in the original copy. In practice, serious departures from additivity and proportionality arise because of the halftone screen and turgidity of the media. Hence, Clapper (1961) suggested an expansion of the original masking equations with the inclusion of 2nd-order terms to give a more accurate prediction than that of the first-order model. Yule (1967c) subsequently suggested that greater accuracy could be obtained by using higher order polynomials such as 2nd-order and 3rd-order. The forward 2nd-order and 3rd-order masking models are given in Eqns. 2-5-10 and 2-5-11 respectively.

$$\begin{aligned}
 D_r &= a_1 c + a_2 m + a_3 y + a_4 c^2 + a_5 m^2 + a_6 y^2 + a_7 cm + a_8 cy + a_9 my \\
 D_g &= b_1 c + b_2 m + b_3 y + b_4 c^2 + b_5 m^2 + b_6 y^2 + b_7 cm + b_8 cy + b_9 my \\
 D_b &= c_1 c + c_2 m + c_3 y + c_4 c^2 + c_5 m^2 + c_6 y^2 + c_7 cm + c_8 cy + c_9 my
 \end{aligned}
 \tag{2-5-10}$$

$$\begin{aligned}
 D_r &= a_1 c + a_2 m + a_3 y + a_4 c^2 + a_5 m^2 + a_6 y^2 + a_7 cm + a_8 cy + a_9 my + a_{10} c^3 + a_{11} m^3 + a_{12} y^3 + a_{13} c^2 m + a_{14} c^2 y + a_{15} m^2 c + a_{16} m^2 y + a_{17} y^2 c + a_{18} y^2 m + a_{19} c m y \\
 D_g &= b_1 c + b_2 m + b_3 y + b_4 c^2 + b_5 m^2 + b_6 y^2 + b_7 cm + b_8 cy + b_9 my + b_{10} c^3 + b_{11} m^3 + b_{12} y^3 + b_{13} c^2 m + b_{14} c^2 y + b_{15} m^2 c + b_{16} m^2 y + b_{17} y^2 c + b_{18} y^2 m + b_{19} c m y \\
 D_b &= c_1 c + c_2 m + c_3 y + c_4 c^2 + c_5 m^2 + c_6 y^2 + c_7 cm + c_8 cy + c_9 my + c_{10} c^3 + c_{11} m^3 + c_{12} y^3 + c_{13} c^2 m + c_{14} c^2 y + c_{15} m^2 c + c_{16} m^2 y + c_{17} y^2 c + c_{18} y^2 m + c_{19} c m y
 \end{aligned}
 \tag{2-5-11}$$

where

- a_i , b_i and c_i represent the coefficients for each equation.
- c , m and y values are the principal colorimetric densities on paper which can be obtained by establishing a one-dimensional look-up-table (LUT) between the dot areas on film (FDAs) and colorimetric densities on paper for each of three primaries.

The LUT is a technique whereby the relationship between two variables is specified as a table in which one group of variables is defined on one column of table, and the related group of variables listed in the other column. Therefore, the relationship between two

variables can be linearly interpolated. The a_i , b_i and c_i coefficients can be optimised using a least-squares technique (e.g. derived by Lawson and Hanson (1972)) to give the closest colorimetric predictions to those measured. The D_r , D_g , D_b and c , m , y are given by:

$$\begin{aligned} D_r &= \log (X_o / X) \\ D_g &= \log (Y_o / Y) \\ D_b &= \log (Z_o / Z) \end{aligned} \tag{2-5-12}$$

$$\begin{aligned} c &= \log (X_o / X_c) \\ m &= \log (Y_o / Y_m) \\ y &= \log (Z_o / Z_y) \end{aligned} \tag{2-5-13}$$

where

- (D_r , D_g , D_b) and (X , Y , Z) are the red-, green-, and blue- colorimetric densities and tristimulus values of a colour stimulus respectively.
- X_o , Y_o and Z_o are the tristimulus values of the paper substrate (white).
- X_c , Y_m , Z_y are the X value for the cyan, Y value for the magenta, and Z value for yellow tints (halftone) respectively.

In the following part of this thesis, the D_r , D_g , D_b are represented by D_{r-3c} , D_{g-3c} , D_{b-3c} respectively for a three-colour print or three-colour component in a four-colour print considered, and by D_{r-4c} , D_{g-4c} , D_{b-4c} respectively for a four-colour print. The c , m , y are represented by D_{r-c} , D_{g-m} , D_{b-y} (i.e. principal colorimetric densities) for each of three single-coloured tints respectively. The red-, green-, and blue- colorimetric densities of black ink are also calculated using Eqn. 2-5-12.

2.5.2 Monitor Models

The monitor model used in the graphics arts industry frequently assumes a linear gamma function and employs a matrix transformation for converting tristimulus values to drive voltage. It is considered to be insufficient for achieving the highest precision. Post and Calhoun (1989) and Luo et al. (1991c) investigated various models and concluded that the typical relationship between the monitor luminance in each of the R, G, and B channels and the CIE XYZ tristimulus values can be given by the matrix expression (Eqn. 2-5-14).

$$A = C T \quad (2-5-14)$$

where T is a 3x1 vector comprised of RGB gun luminances (T_R , T_G , and T_B), A is a 3x1 vector containing the resulting tristimulus values (X, Y, and Z), and

$$C = \begin{bmatrix} x_R/y_R & x_G/y_G & x_B/y_B \\ 1 & 1 & 1 \\ z_R/y_R & z_G/y_G & z_B/y_B \end{bmatrix} \quad (2-5-15)$$

$$T = \begin{bmatrix} T_R \\ T_G \\ T_B \end{bmatrix} \quad (2-5-16)$$

where C is a 3x3 coefficients' matrix in which x_R , y_R , z_R ; x_G , y_G , z_G and x_B , y_B , z_B are the chromaticity coordinates for each of the red (R), green (G) and blue (B) guns respectively. These can be determined by using a spectroradiometer or a tristimulus colorimeter with the monitor driven by the maximum DAC values for each of the three RGB guns.

Seven models were derived, the first six of which assume that the chromaticity coordinates for each channel are invariant and use the matrix above. Each of these six models simply transforms the normalised DAC value (D) to the normalised luminance for each of the three channels (T in Eqn. 2-5-16). Both normalised scales are ranged from zero to one assuming zero luminance at zero DAC value. A brief account of each model is given in the following subsections.

2.5.2.1 PLCC (Piecewise Linear interpolation assuming constant Chromaticity Coordinates)

The PLCC model is defined using a look up table including the XYZ values and its corresponding DAC values. The model then interpolates the intermediate values. It assumes that the luminance in each channel changes linearly between the points defined in the table.

2.5.2.2 LIN-LIN2 (Linear-Linear 2nd-Order Model)

The LIN-LIN2 model assumes that the relationship between D and T for each channel is given by Eqn. 2-5-17.

$$T = c_1 + c_2 D + c_3 D^2 \quad (2-5-17)$$

where c_i are the optimised coefficients for a particular channel obtained by a least-squares technique to fit the measured data.

2.5.2.3 LOG-LOG (Log-Log Model)

The LOG-LOG model given in Eqn. 2-5-18 has been widely used in the display industry and is more generally known as gamma correction.

$$\log T = c \log D \quad (2-5-18)$$

where c is the optimised coefficient for a particular channel obtained by a least-squares technique to fit measured data.

2.5.2.4 LOG-LOG2 (Log-Log 2nd-Order Model)

The LOG-LOG2 model was devised by Cowan (1983). The equation is written in Eqn. 2-5-19. It assumes that the relationship between D and T for each channel is an attempt to correct the departures from linearity, particularly at low luminance levels, assumed in the gamma correction model described above.

$$\log T = c_1 + c_2 \log D + c_3 (\log D)^2 \quad (2-5-19)$$

where c_i are the optimised coefficients for a particular channel obtained by a least-squares technique to fit measured data.

2.5.2.5 Berns et al. (Modified Log-Log Model)

Berns et al. (1993) modified the Log-Log Model described earlier by using only five neutral colours ranging from white point to the darkest neutral that can be measured with high precision. The model is given as follows:

$$\log T = c_1 \log [(1-c_2) D + c_3] \quad (2-5-20)$$

where c_i are the optimised coefficients for a particular channel obtained by a least-squares technique to fit the five measured neutral samples. In the later analysis, it was found that the c_2 and c_3 coefficients in the above equation are almost equal to each other. Thus, the equation was simplified as Eqn. 2-5-21.

$$\log T = c_1 \log [(1-c_2) D + c_2] \quad (2-5-21)$$

2.5.2.6 LOG-LIN2 (Log-Linear 2nd-Order Model)

The LOG-LIN2 model assumes that the relationship between D and T for each channel is given by Eqn. 2-5-22.

$$\log T = c_1 + c_2 D + c_3 D^2 \quad (2-5-22)$$

where c_i are the optimised coefficients for a particular channel obtained by a least-squares technique to fit the measured data.

2.5.2.7 PLVC (Piecewise Linear interpolation assuming Variable Chromaticity coordinates)

The PLVC model is similar to the “cellular” Neugebauer printing model (Section 2.5.1.1). It uses a large number of samples to create a 3D LUT. It also assumes that the chromaticity coordinates in each channel vary. This model is expected to give the most accurate correlation between the DAC values and colorimetric results because it takes into account the problems of gun interdependence and phosphor constancy. However, it requires much more complex algorithms and calibration procedures than the other models.

2.5.3 The Evaluation of Models' Performance

2.5.3.1 Printing Models' Performance

Pobboravsky (1966) proposed two methods for calculating the ink amounts required for grey balance in the printing process. One method used the Murray-Davies basic Neugebauer model and the other used the 2nd-order masking algorithm. He found that the 2nd-order masking model performed better than the basic Neugebauer model. He also

tried the modified Neugebauer model which had the same form as Eqn. 2-5-6, but the c , m , y values were computed using the Murray-Davies equations as given in Eqn. 2-5-3. The results showed that these modified equations did not improve its performance over the unmodified equations.

At a later stage, Pobboravsky and Pearson (1972) introduced the use of the Yule-Nielsen modified Neugebauer model for determining the halftone dot areas required to colorimetrically match a colour using the process inks. They claimed that the precision was improved but without giving much detail.

Heuberger et al. (1992) also tested six mathematical reverse models for predicting CMY dot areas. These six models were: three Neugebauer-type models (basic Neugebauer equations, Yule-Nielsen modified Neugebauer equations, and cellular broadband Neugebauer equations with 3^3 (=27) samples), and the other three masking models with first, second and fourth orders. Additionally, the results were also compared with those using a measured colour test chart as a look-up-table (LUT) consisting of 27 lookup points. The 27 lookup points are the corner points as shown in Fig. 2.9. In the LUT method, for each measured point the nearest four corner points were determined. A linear interpolation was then made using the four corner points. They concluded that the cellular broadband basic Neugebauer model had the best performance but it required the largest number of mathematical operations. The Neugebauer-type models required a large amount of computation time in the reverse process because of their interactive nature while matrix transformations only need analytical efforts. Matrix transformations could increase precision by using a higher order and were suitable for real time application. The deviations with the chosen look-up-table were slightly bigger than those with a fourth-order model. For good results using the LUT approach, the distance between neighbouring points should be 2% without interpolation and 6% when using linear interpolation. In other words, the LUT needs to have a large number of sampling points.

Bolleston et al. (1993) also investigated the use of the various Neugebauer-type models. The experimental results showed that introduction of the Yule-Nielsen correction (n

value) always improved a model's performance. A significant improvement was obtained by the use of a cellular model. The non-cellular spectral model, unlike the broadband case, with an appropriate choice of Yule-Nielsen values, yielded a performance equivalent to the cellular spectral model. They concluded that the choice of Yule-Nielsen value was crucial to the success of the non-cellular models in the spectral case; for the cellular models, as the number of cells increases, the performance of both broadband and spectral models improved by adding more cells, and the dependence on n became weak.

Johnson et al. (1995) and Luo et al. (1991c) summarised the results from research aiming to achieve high colour fidelity images across a wide range of colour imaging devices. They concluded that the 3rd-order masking equations gave more precise predictions than the 2nd-order masking and the Yule-Nielsen modified Neugebauer equations in three-colour reproduction system. The work in this thesis has further extended Johnson et al.'s work by including the black primary. It will be described in Chapter 3.

2.5.3.2 Monitor Models' Performance

For deriving and testing the performance of various monitor models, Johnson et al. (1995) produced both cube and uniform data sets including 729 and 267 colours respectively using a Barco Calibrator monitor. The cube data set was produced using nine unequal intervals for each of the RGB channels selected to give a reasonably uniform perceived colour difference between adjacent intervals in each channel. The uniform data set was comprised of 267 colours which were well distributed in the CIE $L^*a^*b^*$ space with ten equally spaced metric lightness and hue intervals, plus zero to maximum displayable metric chroma. The least-squares method derived by Lawson and Hanson (1972) was used to obtain the c_i coefficients in the monitor models described in Section 2.5.2.

The results indicated that all of the models gave very accurate predictions of the cube data set, but a bad fit to the uniform data set. The PLVC model, which would be expected to give the best prediction of any data set, performed the worst. Subsequent investigation showed that more than half of the colours in the uniform data set were either quite dark or

very saturated. The gun intensities for these were less than 0.3 (on a zero to one scale) for at least one of the three channels. This is the area of significant non-linearity in the gamma function but the visual “spacing” of the nine unequally spaced colours for each channel had not taken account of this. The lowest intensity was, in fact, only 0.3. It implies that the device space had not been properly linearised.

Therefore, new data was generated to improve the performance of these models. It included a set of 18 equally spaced colours for each gun, and a new cube data set produced using 9 equal intervals. The former set was used to derive all models except for the PLVC model. The cube data set was used as the LUT for the PLVC model. In addition, this LUT was determined using two types of colorimetric data: XYZ and CIE $L^*a^*b^*$. The XYZ form was used in the earlier test.

These new versions of the models were again tested using the two original data sets. The results showed that all models gave similarly accurate predictions of the cube data set, but very large improvements for the uniform data set. The general findings from the Johnson et al. (1995) study are summarised below:

- 1) The precision of all models was affected by the distribution of intensities chosen along each of the red, green, and blue channels. Reliable models could be derived by using either non-equal intervals, with more samples close to the low end or a greater number with equal intervals, such as the 18 used in Johnson et al.’s work.
- 2) The PLVC model did not perform as well as expected. Again, because it had not been properly linearised, its precision was greatly dependent upon the distribution of intensities chosen for the LUT. The model performance was slightly improved by using CIE $L^*a^*b^*$ rather than XYZ colour space to derive the LUT.
- 3) The PLCC, Berns et al. and LOG-LOG2 models gave the best overall performance, even better than that of the PLVC model. They assume invariance of each gun’s chromaticity coordinates. This result suggests that phosphor constancy does hold quite well for the Barco Calibrator monitor studied. These models are simple to implement and should be recommended for industrial application.

- 4) In Berns et al.'s study (1993), their model's coefficients were optimised using only five neutral colours which ranged from white point to the darkest neutral. Their results show that five samples are sufficient for defining an accurate CRT colorimetry. However, Johnson et al.'s (1995) results indicate that more samples are required to fit a reliable model capable of predicting dark and saturated colours.

The PLCC model was also used in this study for characterising the monitor used to display images for a psychophysical experiment. The PLCC model was employed as it was one of three models which gave the best overall performance found in Johnson et al.'s work and is simple to implement.

2.6 THE PSYCHOLOGICAL LAWS

Different experimental methods were used in this work for scaling colour appearance. Some of the fundamental psychological laws used are described in this section.

2.6.1 The Fechner's Logarithmic Law and the Stevens's Power Law

Modern experimental psychology had its beginnings in "the measurement of sensation", which started in the 1850's. At that time, two distinguished scientists, Fechner and Plateau, both considered the problem that the perceived relation between light and shade within the picture remains highly stable under two distinctive viewing conditions such as bright sunlight and a dimly lighted room. They reached quite opposite conclusions. Fechner concluded that the subjective *difference* between light and shade remains constant. Therefore the subjective brightness is a logarithmic function of stimulus intensity, i.e. equal stimulus ratios corresponding to equal sensation. This is known as Fechner's law. Plateau argued that the *ratio* remains constant is due to the subjective brightness as a power function of stimulus intensity, i.e. equal stimulus ratios corresponding to equal sensation ratios. Two different psychological laws were thus devised: Logarithmic Law and Power Law (Stevens 1958).

This controversy has generated considerable argument over the years. The Fechner function was more widely accepted than Plateau's before 1957. Stevens and Galanter

(1957) conducted a series of experiments using a direct psychophysical scaling technique. The results more or less agreed with the power relationship. Stevens (1957) published a paper entitled "To Honor Fechner and Repeal His Law" with the goal of replacing Fechner's Law with a power law. Moreover, growing evidence revealed that on prothetic or quantitative continua (Gordon 1989a), the form of the "psychophysical law" is a power function (Bartleson 1977, Pointer 1980, Padgham and Rowe 1973, de Mattiello 1987). The power law, originally proposed by Plateau, has therefore become the well-known Stevens's Law. These two laws are given in Eqn. 2-6-1 and Eqn. 2-6-2.

$$\text{Fechner's Law: } \psi = k_1 \log(\phi/\phi_0) \quad (2-6-1)$$

$$\text{Stevens's Law } \psi = k_2 \phi^n \quad (2-6-2)$$

where

- ψ is a psychophysical value (sensation response, or subjective magnitude).
- ϕ is a physical value (stimulus intensity of the scaled attribute).
- ϕ_0 is an absolute threshold.
- k_1 is a constant depending upon the particular sensory dimension and modality.
- k_2 is a arbitrary constant determining the scale unit.
- the exponent n is a constant whose value may vary with sensory modality and stimulation conditions.

The power law, when converted to a logarithmic form, produces a linear equation having a certain practical usefulness.

$$\log \psi = n \log \phi + \log k_2 \quad (2-6-3)$$

The function can then be represented by a straight line in log-log coordinates. The slope of this line corresponds to the exponent n .

As stated earlier, in most psychophysical experiments, $\psi = k_2 \phi^n$ has been found to be a very reliable relationship between sensory magnitude judgement and stimulus intensity. For weak stimuli near the absolute threshold, the equation becomes highly inaccurate. When log apparent magnitude is plotted against log stimulus intensity, the relationship is linear only at the higher stimulus values. For stimulus values near the absolute (effective)

threshold the relationship is concave downward. Fortunately, the derivation from the power law can be eliminated by a slight modification of the equation. The general form of the power function becomes

$$\psi = k_2 (\phi - \phi_0)^n \quad (2-6-4)$$

where ϕ_0 is the absolute (or effective) threshold. This formula has been successfully applied to a psychophysical scale such as Stevens and Stevens's (1963) brightness study. Stevens's attempt to replace the Fechner law was influential but not completely successful. Other investigators such as MacKay (1963) and Treisman (1964) were later to argue that Stevens's contention about the validity of magnitude estimation data was based largely on faith rather than fact. Treisman (1964) demonstrated that the power function did not provide a unique fit to direct scaling data in a careful mathematical analysis. He concluded that researchers should examine their application to the empirical data on scaling to see which description system handles the data with the greater facility or utility before choosing which law should be used. Gescheider (1985) stated that many papers examined these two laws, and suggested alternatives, but, there was no general agreement as to which law was correct.

2.6.2 The law of comparative judgement

A law of comparative judgement devised by Thurstone (1927) is a verification of Fechner's Law. It applies to both the comparison of physical stimulus intensities and also qualitative comparative judgements such as the acceptance of colour fidelity of reproduction in a matching scale. It states a set of equations relating the proportion of times any given stimulus (R_i) judged greater (better) on a given attribute than any other stimulus (R_j) in terms of the discriminial differences of the two stimuli on the psychological continuum. When two stimuli, R_i and R_j are presented for comparison in a particular scale such as in degree of colour fidelity, the difference in scale values S between the two stimuli R_i and R_j in question can be expressed using the law of comparative judgement as shown in Eqn. 2-6-5.

$$S_i - S_j = z_{ij} \sqrt{\sigma_i^2 + \sigma_j^2 - 2r_{ij}\sigma_i\sigma_j} \quad (2-6-5)$$

where

- S_i and S_j are the psychological scale values of the two compared stimuli.
- z_{ij} is the normal deviate corresponding to the observed proportion, $p_{i>j}$, of judgements “ R_i is judged greater or better than stimulus R_j ”.
- σ_i and σ_j denote the discriminial dispersions of stimuli R_i and R_j .
- r_{ij} is the correlation between the discriminial processes of R_i and R_j in the same judgement.

Eqn. 2-6-5 is the complete form of the law of comparative judgement. It fundamentally applies to the judgements of a single observer who compares a series of stimuli by the method of paired comparison when no “equal” judgements are allowed. It is assumed that a single observer compares each pair of stimuli a sufficient number of times so that a proportion, $p_{i>j}$, may be determined for each pair of stimuli. The law of comparative judgement is not solvable in its complete form. Since there are always more unknowns than observations in the equation, it is necessary to simplify the hypotheses in order to make the law workable. Six hypotheses were proposed. Five cases (Cases I to V) were proposed by Thurstone, and one case known as Case Va, was proposed by Mosteller (1951). In practice, the values of σ and r , although they can be estimated, are seldom known. Researchers normally assume one of the six cases instead. More often, Cases V and Va are used so that the scale values are simply in terms of z scores. The formulations are shown in Eqns. 2-6-6 and 2-6-7 for Cases V and Va respectively.

$$S_i - S_j = z_{ij}\sigma (2)^{1/2} \quad (2-6-6)$$

$$S_i - S_j = z_{ij}\sigma [2(1-r)]^{1/2} \quad (2-6-7)$$

In Eqns. 2-6-6 and 2-6-7, the only difference is the multiplying constant. In practice the unit of measurement can be arbitrarily specified so that the multiplying constant in each case is set to unity. The scale unit is simply equal to z_{ij} in both cases. The two equations therefore become indistinguishable. When applying these two cases, only the data in the form of “the proportion of times one stimulus is preferred over another in the attitude under study” is required, and then the standard normal deviates (z scores) corresponding

to that proportion can be subsequently calculated to determine the interval-scale value (also called *z* score) of a stimulus. The experimental method by which this is done, usually to obtain empirical estimates of scale values of stimuli under study, is known as *the method of paired comparison*. A paired comparison method applying the Thurstone's law of comparative judgement was used in this study (Chapter 4).

2.6.3 The Law of Categorical Judgement

Torgerson (1958) devised "The law of Categorical Judgement" which is also based on Thurstone's general judgement. It is an extension of Thurstone's law of comparative judgement. It is a set of equations relating parameters of stimuli and category boundaries to a set of cumulative proportions derived from the proportion of time, each stimulus (or model) is judged to be in each category of a set of subcategories which are ordered with respect to a given attribute such as colour fidelity.

The boundaries between adjacent categories behave like stimuli. The difference between the laws of comparative judgement and categorical judgement is simply that the law of categorical judgement relates to the relative positions of stimuli with respect to category boundaries rather than with respect to one another. This leads to the following form for the law of the categorical judgement:

$$T_i - S_j = z_{ij} \sqrt{\sigma_i^2 + \sigma_j^2 - 2r_{ij}\sigma_i\sigma_j} \quad (2-6-8)$$

$$(i = 1, 2, 3, \dots, n; j = 1, 2, 3, \dots, m)$$

where

- $n+1$ = the number of categories.
- m = the number of stimuli.
- T_i = the mean location of the i th category boundary
- S_j = the scale value of stimulus j .
- z_{ij} = the normal deviate corresponding to the observed proportion of judgements "stimulus j is placed below category boundary i ".
- σ_i = the discriminial dispersion of i th category boundary.
- σ_j = the discriminial dispersion of stimuli j .
- r_i = the correlation between the discriminial processes of stimulus j and category boundary i .

Essentially the same conditions making up the six cases of Eqn. 2-6-5 also apply to Eqn. 2-6-8. Similarly, the experimental method by which the empirical estimates of both of scale values of stimuli and category boundaries under study can be obtained is known as *the method of category judgement*. In addition to the paired comparison method described in Section 2.6.2, a category judgement method derived by Torgerson (1958) was also employed in this thesis (Chapter 4).

2.7 CHROMATIC ADAPTATION AND COLOUR APPEARANCE

The quantification of the appearance of a colour is of great importance in evaluating the colour fidelity across different media and illumination conditions in many colour reproduction applications. This however involves the human visual system's sophisticated mechanism to produce a stable perception of an object colour across changes in illumination. This important phenomenon is typically referred to as chromatic adaptation or colour constancy. Since colour images are often viewed under dissimilar conditions, such as spectral power distributions, luminances of background, and medium types, chromatic adaptation becomes essential for cross-media colour reproduction.

2.7.1 Chromatic Adaptation Theory

The word "*adaptatio*", originally coming from the Latin *adaptare*, means to adjust (Bartleson 1978). In the general sense, the word "adaptation" refers primarily to a process of adjustment by our visual-response mechanism to external conditions under which the eyes are exposed to radiant energy. It involves the action of transmitting any rapid changes in the environment, and temporally extending long-maintained conditions such as a tendency of constancy. There are different kinds of adaptation, the most important of which are dark (or scotopic) adaptation, light (or photopic) adaptation, and chromatic adaptation (Judd and Wyszecki 1975a). The dark and light adaptations refer to the adjustment of the visual-response mechanism to changes in the rate at which radiant energy enters the eye. Chromatic adaptation refers primarily to the adjustment of the visual-response mechanism to changes in radiant energy spectral distribution. The concept of "chromatic adaptation" represents transient and steady-physiological-state

activities, and sensitivities of the visual-response mechanism to chromatic (test) stimuli. Although the visual stimuli may appear quite different, after this transient and steady state of adaptation, a given physical stimulus retains its chromatic appearance nearly unchanged. The phenomenon of chromatic adaptation is of great importance in the prediction of object colour perceptions and in maintaining the colour constancy of objects seen under widely different qualities of light sources. Many studies on chromatic adaptation have been conducted over the years. Wright (1981) discussed why and how chromatic adaptation has been studied and made some suggestions for future directions. An entire section on experimental techniques and models were presented by Wyszecki and Stiles in the book, Color Science (1982). Terstiege (1972) and Bartleson (1978) also reviewed various studies of chromatic adaptation.

Fairchild (1992) classified chromatic adaptation mechanisms into two groups: sensory and cognitive mechanisms. The former responds automatically to the stimulus energy and is related to the function of individual components present in the organ of vision. Cognitive chromatic adaptation mechanisms are based upon the observers' knowledge of scene content which is related to memory colours.

Arend and Reeves (1986), however, divided chromatic adaptation mechanisms into two different classes: simultaneous and adaptation mechanisms. Simultaneous mechanisms are defined primarily in terms of spatial interactions among the response of chromatic channels to light at various locations in the retinal image. They only depend secondarily on temporal parameters. Adaptation mechanisms are defined primarily in terms of temporal interactions whereby the sensitivities of the chromatic channels of the visual system change over time in response to the change of illuminant. Adaptation mechanisms are spatially local, without spatial interactions. The adaptation is frequently affected by the conditions of colour matching which can be divided into two types, symmetric and asymmetric matching.

2.7.1.1 Symmetric Matching

Ordinary, “*symmetric*” colour matching occurs when two colours are presented under the same or closely similar viewing condition. In this case, two colours are imaged on the same or nearly the same portion of the retina(e) of one or both of an observer’s eyes at the same time (Bartleson 1977). The condition of the colour match, for two colours eliciting the same colour appearance under a symmetric viewing situation, is named as the symmetric match. In this condition, all the parameters such as spatial, temporal, physical, and physiological issues involved in the match are the same. The symmetric matching condition can be represented as shown in Eqn. 2-7-1.

$$\begin{aligned} f_1(X, Y, Z; A) &\equiv f_1(X, Y, Z; A) \\ f_2(X, Y, Z; A) &\equiv f_2(X, Y, Z; A) \\ f_3(X, Y, Z; A) &\equiv f_3(X, Y, Z; A) \end{aligned} \quad (2-7-1)$$

where X, Y, Z represent tristimulus specifications, A refers to the illuminant, and “ \equiv ” denotes “matches under symmetric conditions”.

2.7.1.2 Asymmetric Matching

In chromatic adaptation, a state of equal colour response under two different conditions of illumination is described as an “*asymmetric*” match by Wyszecki and Stiles (1982c). In this case, the two stimuli are physically different, and an identity set of viewing conditions does not exist. It may be assumed, for example, that by some means a colour match is obtained for two different stimuli that are imaged on the same area of the retina under two different illuminating conditions (A and A' respectively) to which the observer is adapted. Instead, an *equality* of terms rather than an *identity* of terms is used in the following functional forms for such an asymmetric matching condition.

$$\begin{aligned} f_1(X, Y, Z; A) &\Rightarrow f_1(X', Y', Z'; A') \\ f_2(X, Y, Z; A) &\Rightarrow f_2(X', Y', Z'; A') \\ f_3(X, Y, Z; A) &\Rightarrow f_3(X', Y', Z'; A') \end{aligned} \quad (2-7-2)$$

Eqn. 2-7-2 represents an equality condition rather than an identity. The “ \Rightarrow ” means “matches under asymmetric adaptation conditions”.

By assuming the linearity law holds for asymmetric colour matching, the two sets of tristimulus values (X, Y, Z and X', Y', Z') between adaptation conditions A and A' can be related by a constant linear transform with 3×3 matrix $T_{AA'}$ (Wyszecki and Stiles 1982c).

$$\begin{bmatrix} X' \\ Y' \\ Z' \end{bmatrix} = T_{AA'} \begin{bmatrix} X \\ Y \\ Z \end{bmatrix} \quad (2-7-3)$$

The best values of matrix elements of the $T_{AA'}$ can be determined using a least-squares method by optimising from a large group of matching pairs.

2.7.2 Some Colour Appearance Phenomena

2.7.2.1 Discounting of the Illuminant Colour (Object-Colour Constancy)

In the colour scaling experiment, observers are always unconsciously accustomed to make a judgement of an object colour by eliminating the differences in brightness and colour of illumination by which an object is illuminated. A colour could be perceived under a wide range of illuminants such as outdoor sunshine, blue light of the clear sky, weak white light of the overcast sky, red-yellow light of the setting sun, and red-yellow candle light. Consequently, observers realise a correct knowledge (idea) of the colours of objects by seeing the same colours under a wide range of illuminants. von Helmholtz suggested that the visual system relies on memory to maintain the colours of objects viewed under different viewing conditions; the memory of an object colour when viewed under “white light” is invoked if the object is seen under a “coloured” light. Observers judge how such an object would look in white light, and are not conscious at all of the separate sensations which contribute to make the visual judgement since they are only interested in the colour that an object permanently retains. This phenomenon of closely perceiving the colour of the object regardless of the colour of the light illuminating the object is known as object-colour constancy (Judd 1960).

2.7.2.2 The Helson-Judd Effect

Helson (Helson 1938, Helson and Jeffers 1940) carried out experiments to investigate the changes in hue, saturation, and lightness for neutral and chromatic samples illuminated using chromatic illuminant. The major finding is known as Helson-Judd effect:

Samples having a luminance factor, Y%, above that of the background are tinged with the illuminant hue. Samples having Y% below it, are tinged with the complementary hue of the illuminant. Samples having Y% near to that of the background are either achromatic or greatly reduced in saturation.

The effect is proportional to the difference between Y% of both the sample and background. For instance, on a white background dark samples are most saturated (in the complementary hue) while on a black background light samples are most saturated (in the hue of the illuminant).

2.7.2.3 The Bezold–Brücke Phenomenon

The Bezold–Brücke phenomenon was first discovered by von Bezold in 1873, and later by Brücke in 1878. It relates to the fact that the variation of luminance modifies the perception of hue when wavelength is held constant (Padgham and Saunders 1975b, Boynton and Gordon 1965). The effect shows that an increase in luminance not only increases the brightness of the aperture colour but also introduces a change in hue. For colours in the red, yellow-red, and yellow-green regions shift towards yellow and those in red-blue and blue-green regions move toward blue.

2.7.2.4 The Stevens Effect

Stevens and Stevens made an evaluation of brightness of various achromatic samples on a white background at various levels of adapting luminance under a white illuminant. The results show the perceived brightness of the grey sample changes due to the luminance level. It was found that brightness contrast increases when the adapting luminance increases because that lighter neutral samples and white background increase in apparent brightness, while darker neutral samples appear darker with a general increase in

luminance especially for very dark greys. (The medium-dark grey with 8.4 db, i.e. 14.5 of Y%, maintains approximately constant brightness).

2.7.2.5 The Hunt Effect

The effect on colourfulness of changes in luminance level was first investigated by Hunt (1950). It is referred to as the Hunt effect, in which by raising adapting luminance the apparent chroma and colourfulness of chromatic samples increase.

2.7.2.6 The Helmholtz-Kohlrausch Effect

von Helmholtz (1866) was the first to notice that the saturation of a colour affected its luminosity, some colours appear much brighter at higher saturations even though the constant luminance is maintained. This effect was also subsequently investigated by Kohlrausch (1935). It was found that if two patches of colour having the same luminance are placed side by side, one of high and the other of low saturation, the former will appear brighter. However, the differential luminosity effect disappears if they are flickered and thus seen alternately. This effect is referred to as the Helmholtz-Kohlrausch effect or heterochromatic brightness matching (Wyszecki and Stiles 1982b, Padgham and Saunders 1975a).

2.7.3 Techniques For Studying Chromatic Adaptation and Assessing Colour Appearance

Assessing colour appearance and chromatic adaptation has been extensively studied over years. The aim of these studies was to understand colour vision and establish useful engineering data for describing colour appearance. Bartleson (1977) and Wright (1981) reviewed why and how chromatic adaptation and colour appearance has been studied. They categorised the experimental methods into four techniques of gathering data:

- (a) haploscopic matching (differential ocular conditioning and comparison),
- (b) local adaptation (differential retinal conditioning and comparison),
- (c) direct scaling and magnitude estimation,
- (d) memory matching.

Methods (a) and (b) are carried out using specially designed visual colorimeters while methods (c) and (d) are carried out under normal viewing conditions.

2.7.3.1 Haploscopic Matching

2.7.3.1.1 Simultaneous-Haploscopic Matching

The simultaneous-haploscopic matching method has been prevalently used in the study of a wide variety of colour appearance and adaptation phenomena. It involves the presentation of independent images to an observer's two eyes simultaneously to form an interocular viewing condition for a direct comparison. It assumes that the mechanism of chromatic adaptation is essentially independent for the two eyes. The measurements of colour appearance are performed under asymmetric matching conditions (Section 2.7.1.2). Observers view the test stimulus in one eye under a set of viewing conditions and adjust a reference stimulus under another set of conditions viewed in the other eye to match the test stimulus (Burnham et al. 1952, 1957, Brewer 1954, Wassef 1958).

There are two advantages of the simultaneous-haploscopic matching technique:

- (a) the direct matching of colour appearance between two adapting conditions,
- (b) the well-defined state of adaptation of sensory chromatic adaptation mechanisms because of constant presentation of the adapting stimuli to each eye throughout a given experimental session.

The former is the main reason why the haploscopic technique is most frequently used in colour appearance research.

Contrarily, there are also two disadvantages of the haploscopic technique. First, it is questionable to assume that the two ocular channels are independent. Fairchild (1992, 1993) stated that there were cognitive mechanisms of chromatic adaptation that could not be independent for each eye. Thomas (1961), Valois and Walraven (1967), and Wright (1981) have pointed out that the validity of the assumption of two independent ocular channels is not fully true. The second disadvantage is the occurrence of binocular rivalry (Fairchild et al. 1994) from the perceptual experience tending to favour perception of one stimulus condition over the other. While the binocular rivalry might not affect colour

adaptation, it certainly makes haploscopic experiments more difficult and annoying for the observers.

2.7.3.1.2 Successive-Haploscopic Matching

The successive-haploscopic matching viewing method is similar to the previous simultaneous-haploscopic matching technique except that the observer is restricted to seeing both stimuli at the same time (Eastman and Brecher 1972, McCann et al. 1976). In the successive-haploscopic matching experiment one eye is exposed to a given adapting stimulus while the second eye is occluded. When the second eye is exposed to the second adapting stimulus, the first eye is occluded.

The successive-haploscopic technique allows for the direct matching of colour stimuli across different adapting conditions, and represents an improvement for eliminating binocular rivalry since only a single adapting condition is viewed at a time. The technique results in less confusion in the cognitive mechanisms of chromatic adaptation than the simultaneous haploscopic technique although the state of the sensory chromatic adaptation mechanisms are not as well defined.

Fairchild et al. (1994) devised a new haploscopic matching technique, referred to as the successive-*Ganzfeld* haploscopic matching technique. It relies on the use of a specific type of stimulus pattern, known as *Ganzfeld* (Hochberg et al. 1951, Gordon 1989b), which is spatially and temporally homogeneous. In the successive-*Ganzfeld* haploscopic matching technique, a neutral diffuse filter (*Ganzfeld*) covers one eye while the other eye inspects a stimulus. This technique assumes that the eye which is covered by the diffuse filter remains adapted to the appropriate white point. The main advantage is that the state of the sensory chromatic adaptation mechanisms is well defined and constant for each eye while binocular rivalry and confusion with cognitive mechanisms are eliminated. It is still an unnatural way to view and compare stimuli (images) because each stimulus is viewed in its respective adapted environment. Additionally, it has not been proven that each eye is fully adapted.

2.7.3.2 Local Adaptation

The local adaptation technique is similar to the haploscopic technique except that the comparison and matching is made between two retinal areas of the same eye. MacAdam (1956, 1961, 1963) has been the main investigator employing this technique. This technique eliminates the uncertainty of whether, in haploscopic matching, adaptation in one eye affects the sensitivity of the other. However, this technique still has drawbacks such as unnatural way of viewing and hybrid effects (Wyszecki and Stiles 1967).

2.7.3.3 Direct Scaling and Magnitude Estimation

The main idea of the magnitude estimation technique is to ask each observer to make a direct estimation of magnitude or ratio which corresponds to a visual attribute. The attributes might be hue, lightness, brightness, colourfulness, saturation, chroma, reproduction quality or colour fidelity (associated with complex stimuli). The observers are instructed to assign a number proportional to the magnitude of the chosen attribute in the stimulus being viewed, to assess the attribute using a more clearly defined scale (usually an equal-interval scale, or category-point scaling as in Steven and Galanter (1957)), or to compare two samples' attributes, such as judging the ratio of one saturation to the other (Pointer et al. 1977).

Stevens spent almost 40 years in developing a schema of direct scaling (Bartleson and Grum 1984c). This resulted in the wide acceptance of the magnitude estimation technique. The major appeal of employing this method is that the observations can be carried out under normal viewing conditions, using both eyes and without the interposition of any optical devices. Rowe (1973) and Padgham et al. (1973) carried out their work to scale hue and saturation using the magnitude estimation technique. They concluded that a surprising degree of precision could be achieved using this technique. Moreover, Bartleson (1977) found that the data obtained from three series of experiments using the magnitude estimation technique are remarkably similar to those obtained by other researchers utilising the memory and haploscopic methods. The magnitude estimation data obtained by Pointer et al. (1977), and Bartleson (1977), and Nayatani

(Sobagaki et al. 1974, 1975, Nayatani et al. (1972) are similar to those of Burnham et al.'s (1957) haploscopic data, and Helson et al.'s (1952) memory data respectively. Furthermore, Ishak et al. (1970) compared their magnitude estimation data to Helson et al.'s memory data and Wassef's (1955), Hunt's (1965), and Gibson's (1967) haploscopic data. The results confirmed to Bartleson's findings. Recently, Luo et al. (1991a and b), and Kuo et al. (1995) also employed this method for studying colour appearance and chromatic adaptation. They pointed out that the magnitude estimation method has several advantages:

- (a) It provides absolute perceptual values for colour attributes in the context of the interaction of various parameters, e.g. light sources, media, luminance levels, and induction colours;
- (b) The results are obtained in perceptual terms equivalent to those predicted by colour appearance models, and may be used directly for testing various existing colour models or consequently for deriving a more comprehensive model.
- (c) Colour appearance is expressed in a consciously reportable form.

Their data has therefore been used in this study to derive a new colour appearance model (see Section 2.7.6). There is a main concern in using this method. It requires a longer training period for observers than the haploscopic and local adaptation techniques to ensure that each observer clearly understands the perceptual attributes being scaled.

2.7.3.4 Memory Matching

In the memory matching method (Pearson et al. 1969), observers describe the colour appearance by means of a colour-order system such as the Munsell system. Each observer is asked to remember the hue, value, and chroma. Initially, they need to be familiarised with a colour order system's attributes such as hue, value and chroma. Subsequently, they describe the colour of any object using these terms with reasonable accuracy and precision. The memory matching method can also be carried out under normal viewing conditions, and has been widely used in the study of chromatic adaptation. The observer is asked to describe the colour appearance of objects seen under both the reference and test illuminants, in terms of the memorised colour scale (Helson et al. 1952).

This technique, like the magnitude estimation method, is suited to study colour appearance under steady-state adaptation. It is based on colorimetrically specified samples rather than arbitrary numerical scales used in the magnitude estimation method. The interpretation of results is therefore much easier. However, the memory matching method also poses some experimental problems. Substantial training periods are normally required and some observers tend to have a limited capability for retaining information, and the possibility of distortion may occur whenever memory is involved. Newhall et al. (1957) found that some systematic distortions occur in the relatively short-term memory for colours.

2.7.4 Chromatic Adaptation Transforms

A number of chromatic adaptation transforms have been proposed. Each is used to predict the corresponding colours in terms of chromaticity coordinates or tristimulus values. The corresponding colours are defined as two samples that evoke the same colour appearances when an observer is adapted to dissimilar illumination conditions. Three types of chromatic adaptation transforms, von Kries, BFD, and Nayatani, are described here.

2.7.4.1 The von Kries Chromatic Adaptation Transform

The most fundamental chromatic adaptation transform is known as the von Kries (1878, 1902, 1905) coefficient (proportionality) law, which is based on the Young-Helmholtz trichromatic theory of colour vision (Young 1802, von Helmholtz 1866). It postulates the existence of three independent cone types with different spectral sensitivity functions. The signals generated by these cones are transmitted directly to the brain where “colour sensations” are experienced.

A theoretical prediction transform based on von Kries coefficient law involving Judd’s (1945) fundamental primaries was developed by Helson et al. (1952) and is given below.

$$\begin{aligned} X_2 &= \beta X + 2.954 (\alpha - \beta) Y + 0.220 (\gamma - \beta) Z \\ Y_2 &= \alpha Y \\ Z_2 &= \gamma Z \end{aligned} \quad (2-7-4)$$

$$\begin{aligned}
 \text{where } \alpha &= (L_{n2} / L_{n1}) \\
 \beta &= (M_{n2} / M_{n1}) \\
 \gamma &= (S_{n2} / S_{n1})
 \end{aligned}
 \tag{2-7-5}$$

L_{n1}, M_{n1}, S_{n1} and L_{n2}, M_{n2}, S_{n2} are the cone responses, from the long-, middle-, and short-wavelength cone receptors, of the first and second adapting illuminants or light sources respectively. The calculation of the cone responses (L, M, S) is a linear transformation of CIE tristimulus values using Judd's cone responses (fundamental primaries) as below.

$$\begin{bmatrix} L \\ M \\ S \end{bmatrix} = A \begin{bmatrix} X \\ Y \\ Z \end{bmatrix}
 \tag{2-7-6}$$

$$A = \begin{bmatrix} 0.00 & 1.00 & 0.00 \\ -0.46 & 1.36 & 0.10 \\ 0.00 & 0.00 & 1.00 \end{bmatrix}
 \tag{2-7-7}$$

This transform was used in the later study and designated as the von Kries chromatic adaptation transform.

2.7.4.2 The BFD Chromatic Adaptation Transform

Lam and Rigg (Lam 1985) studied the degree of colour constancy for object colours with changing light sources, at Bradford University. The objective of their study was to provide basic data which may be used to derive a method of predicting the colour appearances of surface colour stimuli over a range of adaptation conditions of general interest in both commerce and industry. In their study, 58 textile samples having various degrees of colour constancy were accessed by a panel of five observers with normal colour vision in terms of Munsell value, chroma, and hue using a memory matching method under the simulated D65 and A light sources. A total of 3480 visual estimations were made. The BFD model (Lam 1985) keeps the achromaticity of neutral samples and allows for changes in different adapting illuminants. The results from their study also

showed a good prediction for the five other independent data sets (Burnham et al. data (1957), MacAdam data (1956) based on coloured lights, and Bartleson data (1977), Helson et al. data (1952), and Wassef data (1959) based on object colours).

2.7.4.3 The Nayatani Chromatic Adaptation Transform (CIE Chromatic Adaptation Transform)

Nayatani et al. (1981, 1982, 1990) also derived a nonlinear transform to predict corresponding colours. The cone responses are based on the fundamental primaries reported by Hunt and Pointer (1985). It also incorporates several effects related to adaptation such as the Hunt effect, Stevens effect, and Helson-Judd effect. In this model, the calculation of the cone responses (the Stiles-Estévez-Hunt-Pointer fundamentals (Hunt and Pointer 1985)) is a linear transformation of CIE tristimulus values.

In 1985, the transform was approved by the CIE Division 1 at a meeting in Paris, and was proposed for further field trials (CIE 1986b). Thus, it is also called the CIE chromatic adaptation transform in this study.

2.7.5 Colour Appearance Models

Colour appearance models taking into account the changes of the white point, luminance, surround, and other aspects of the viewing conditions, specify the colour appearance of a given stimulus in a defined set of viewing conditions.

In recent years, three colour appearance models, Hunt, Nayatani, and RLAB, have been developed and all of these were studied in this work. Some details of those models are given in the following sections.

2.7.5.1 The Hunt Colour Appearance Model

The Hunt colour appearance model is a comprehensive model of colour vision and fits well to not only psychophysical but also physiological experimental results. It has been refined over the years using the LUTCHI (Loughborough University of Technology Computer Human Interface Research Center) data sets (see Section 2.7.6). The Hunt

model begins with cone responses that represent the excitations of the three cone types. The cone excitations are then computed via a von Kries-type chromatic adaptation transform (Hunt et al. 1985) with additional terms that account for extent of luminance-level adaptation, degree of chromatic adaptation, discounting the colour of the illuminant and the Helson-Judd effect.

The cone signals in the Hunt model were normalised to be equal for the equi-energy stimulus, SE, with a colour temperature which appears neutral initially and throughout the adaptation no matter when desensitisation is complete or incomplete to the dark-adapted eye (Hurvich and Jameson 1951).

The calculation of an achromatic response and three chromatic responses is a linear combination of hyperbolic functions of the cone signals (Seim and Valberg 1986, Roynton and Whitten 1970). Appearance attributes are calculated from various combinations of these signals. Attributes of colour appearance predicted by the Hunt model include: hue, relative and absolute blueness-yellowness, relative and absolute redness-greenness, colourfulness, chroma, saturation, lightness, and brightness. Throughout these years, various modifications (Hunt89, Hunt91, Hunt94) (Hunt 1990, 1991, 1994) have been made to the original Hunt87 Model (Hunt 1987). The Hunt94 model is a modified version of Hunt91 model with an improved predictor of chroma (C_{94}) and colourfulness (M_{94}) (Hunt 1994).

The Hunt model is quite complicated involving various parameters (Hunt and Luo 1994) for computing colour appearance attributes. These parameter will be referred in the later stage. Hence, these are given below.

Brightness and chromatic surround induction factors	N_b	N_c	
		Hunt91	Hunt94
Small areas in uniform light background and surrounds	300	1.00	1.00
Normal scenes (reflecting samples viewed in booth)	75	1.00	1.00
Television and VDU displays in dim surrounds	25	0.95	1.00
Large transparencies on light boxes	25	0.95	0.70
Projected photographs in dark surrounds	10	0.90	0.70

2.7.5.2 The Nayatani Colour Appearance Model

The Nayatani colour appearance model (Nayatani et al. 1990, 1995a, 1995b) also transforms CIE tristimulus values to cone responses. The Nayatani86 model (Nayatani et al. 1986) used Pitt fundamental primaries whereas Nayatani87, Nayatani90, and Nayatani95 used Stiles-Estévez-Hunt-Pointer fundamental primaries (Nayatani et al. 1987a). The chromatic adaptation part is the same as the one previously discussed in Section 2.7.4.3 (Nayatani chromatic adaptation transform). Finally, corresponding to an interpretative stage (metric quantities), the signals are combined in multiplicative responses very similar in principle to the Hunt model (Hunt and Pointer 1985) introducing the idea in the transformation from trichromatic to opponent-colour responses. The main difference between the two models is that the nonlinear characteristics of cones in the Nayatani model are represented by power functions (Stevens power law) and in the Hunt model by hyperbolic function (Seim and Valberg 1986, Roynton and Whitten 1970). The Nayatani model has predictors for the same appearance attributes as the Hunt model but incorporates a new scale, a whiteness and blackness response of achromatic object colours (Nayatani et al. 1987b). The latest Nayatani95 (Nayatani et al. 1995a, 1995b) colour appearance model is different from Nayatani90 model (Nayatani et al. 1990) by adopting the new chromatic-strength function $E_s(\theta)$ instead of the eccentricity function $e_s(\theta)$.

2.7.5.3 The RLAB Colour Appearance Model

The original RLAB colour appearance model (denoted as the RLAB93 model) was developed by Fairchild and Berns (1993) for cross-media colour reproduction application where images are reproduced with different white points, luminance levels, and surrounds. It includes an extension of the CIELAB colour space, referred to as the RLAB colour space which incorporates a modified version of von Kries-type chromatic adaptation transform previously formulated by Fairchild (1991). The RLAB93 colour space has colour-appearance predictors similar to those of the CIELAB colour space, such as predictors of lightness, L^R , redness-greenness, a^R , yellowness-blueness, b^R ,

chroma, C^R , and hue angle, h^R . These appearance predictors are calculated using equations virtually identical to the CIELAB equations after the stimulus tristimulus values are transformed to the corresponding tristimulus values under a reference set of conditions (D65/2°, 318 cd/m², hard copy). In other words, the RLAB and CIELAB spaces are identical for a reference condition. However, for the other viewing conditions, the RLAB and CIELAB spaces differ. The model was further modified by Fairchild (1994) and is denoted as the RLAB94 model. The hue angle (h^R) in the RLAB94 model can be converted into hue composition (H^R) based on the notation of the NCS colour-order system (Derefeldt and Sahlin 1986).

The RLAB model also requires the input of various viewing parameters, which will be used later. The incomplete-chromatic-adaptation feature in RLAB93 can be turned on and off depending on whether or not cognitive “discounting-the-illuminant” mechanisms are active or not. This cognitive mechanisms are active when viewing hardcopy images in an illuminated environment and is inactive (i.e. the sensory mechanisms are on) when viewing soft-copy images. The other parameters are summarised below.

δ factors (surrounds)

	RLAB93	RLAB94
Average surrounds	1/3.00	1/2.30
Dim surrounds	1/3.75	1/2.90
Dark surrounds	1/4.50	1/3.50

D factors (mechanisms) (in RLAB94 model)

Hardcopy images	1.0
Softcopy displays	0.0
Projected transparencies	0.5

2.7.6 LUTCHI Colour Appearance Data

The LUTCHI Colour Appearance Data (Luo et al. 1991-995) was used in this thesis for deriving a reliable colour appearance model. The work was carried out at Loughborough University of Technology Computer Human Interface (LUTCHI) Research Centre. Hence this data is entitled “LUTCHI Colour Appearance Data”. The data was accumulated from two consecutive projects, named Alvey and CARISMA (Colour Appearance Research for Interactive Systems Management and Applications). Accordingly, the LUTCHI data can be divided into Alvey and CARISMA data sets. In the experiments, a magnitude estimation method was applied to quantify the colour appearance of a single colour stimulus under typical viewing conditions used for three media: reflective, monitor, and transmissive materials. The Hunt colour appearance model was also verified using this data set, its predictive performance proved to be quite satisfactory. Some details for obtaining the LUTCHI Colour Appearance Data and testing colour models’ performance using this data set conducted by Luo et al. are reviewed in the following sections.

2.7.6.1 The Acquisition of LUTCHI Colour Appearance Data

2.7.6.1.1 Alvey Colour Appearance Data Set

A research team was formed in 1986 under the auspices of the United Kingdom Government’s “Alvey” programme to carry out a research project entitled “Predictive Perceptual Colour Models”.

A large-scale experiment was carried out in which colour appearance was assessed under various viewing conditions including 23 phases. The parameters studied were:

- (a) four light sources having chromaticities close to those of D65, D50, a white fluorescent (WF), and tungsten (A),
- (b) two media: monitor colours and surface colours,
- (c) a high and a low luminance levels (about 40 and 240 cd/m^2) for surface colours, but only the low luminance level for monitor colours, and

- (d) five background conditions: white, grey, black, grey with white border, and grey with black border.

For the experiments conducted using surface colours, 105 colours covering a wide colour gamut and having Y values ranging from 6 to 60 (Munsell values 3-8), were chosen from the OSA Uniform Colour Scale. Colour measurements were carried out under the same experimental conditions using a Bentham tele-spectroradiometer (TSR) and the CIE 1931 colorimetric observer. Each surface colour was then transformed to a monitor colour in terms of CIE tristimulus values and luminance (with a CIE $L^*u^*v^*$ colour difference of less than 1 for the nonluminous colour), displayed on a Sigmex 6164 monitor. The experimental viewing pattern (Fig. 2.11) basically included a test colour being surrounded by 24 colours which were randomly selected from the Pantone Color Paper Selector, along with the “reference white” and “reference colourfulness”. For the experiments conducted using monitor colours, the observer viewed a similar pattern to that presented in the viewing cabinet, with a viewing geometry of $0^\circ/45^\circ$ (illuminating/viewing). For the luminous mode experiments, the observer was seated in a darkened room and was instructed to access each of the test colours in terms of the hue, lightness, and colourfulness attributes using the magnitude estimation method. The “reference white” and “reference colourfulness” samples were used as anchoring points for scaling colourfulness and lightness respectively in each phase. At the commencement of each new phase of experiment, the observers first visually readapted to the previous experimental conditions and had to fix in memory the appearance of standard reference colourfulness sample which was assigned a number. Afterwards, they adapted to the new experimental conditions under consideration and then scaled the new reference colourfulness sample with respect to the previous remembered standard colourfulness reference before they started scaling the required attributes of the test colours. The differences for each of 23 phases are listed in Table 2.1. In total, 43,332 estimations were made. This formed part of LUTCHI Colour Appearance Data, named the Alvey Colour Appearance Data Set including Surface and Monitor colours.

2.7.6.1.2 CARISMA Colour Appearance Data Set

(1) CARISMA Surface Data Set

The CARISMA project, as an extension of the previous Alvey project, included additional media and viewing conditions. One of the experiments in this project was designed to investigate changes in colour appearance under six luminance levels, covering a wider range of luminance conditions than those used in the Alvey project. In addition, a brightness attribute was added to the original lightness, colourfulness, and hue scales for colour assessment.

The experiment was divided into 12 phases (summarised in Table 2.2). At each luminance level, each colour was assessed twice using lightness, colourfulness, and hue attributes in one phase, and brightness, colourfulness and hue in another. The reference white was removed from the viewing pattern (similar to the one used in the Alvey project, Fig. 2.11) in phases 7 to 12 to avoid observers scaling lightness instead brightness.

A simulated D50 light source with a white diffuser distributing light evenly was used. Five large neutral half-tone transparencies with five levels of density were used to cover the diffuser to achieve the six luminance levels required for the experiment. In each phase, 40 glossy OSA reflection samples, selected from the 105 colours used in the Alvey experiments, were used.

Additionally, a “reference white” and a “reference colourfulness” samples were used as anchoring points for scaling colourfulness and lightness respectively in phases 7 to 12. The measuring conditions were the same as those used in the Alvey project. This part of the LUTCHI Data, is named the CARISMA Surface Data Set.

(2) CARISMA LT and 35mm Data Sets

In the graphic arts industry, the source image or “original” is often presented using a transmissive material and needed for reproduction onto paper. These “originals” can be either cut-sheet transparencies (Large Transparencies, designated as LT) or 35-mm projected transparencies (designated as 35mm). The research work in the CARISMA

project also covered these two types of transmissive media, both LT and 35mm. The viewing conditions used for these two types of media were:

- (a) using a back-lit illuminator including buttons for controlling light intensity (the device was designed to agree closely with ISO 3664 for observing large transparency),
- (b) using a 35mm slide projector to project an image onto a white screen.

CARISMA LT Data Set

The LT experiment was divided into ten phases according to the viewing parameters used. These are summarised in Table 2.3. The details of the experimental conditions were:

- 1) A transparency illuminator was used for viewing LT (shown as Fig. 2.12).
- 2) A simulated D50 light source (with x, y equal to 0.356, 0.377) was used to illuminate the transparency image with two additional D50 simulators from each side (designed as a flare diffuser) for introducing extra frontal flare falling on the LT image.
- 3) The whole illuminator was painted with a mid-grey colour except for the viewing area (30 x 40 cm²). The viewing pattern (17 x 23 cm², similar to Fig. 2.11), was placed in the viewing area centre. The black border and white border were simulated respectively with or without a mask covering the four sides of white light surround of the LT in the viewing area.
- 4) Two different types of viewing patterns were used, with luminance factors of 17% and 10% of grey backgrounds. Also, white and black borders were used for phases 1-4 and 10, and phases 5-9 respectively.
- 5) Each viewing pattern was designed with fixed decorating colours and the reference white, and with varied test and reference colourfulness colours (i.e. different reference colourfulness samples were used in different phases).
- 6) A panel of seven to eight experienced observers scaled each of 98 test colours, subtending a viewing angle of 1° from the viewing position (a distance of 60 cm in a darkened room) in terms of hue, lightness and colourfulness using the same scaling technique as described earlier.

In total, 21748 estimations were made. This LUTCHI subset, is named the CARISMA LT Data Set.

CARISMA 35mm Data Set

The 35mm projection experiment was divided into six phases according to different light sources, luminance levels and the spatial arrangement of colours in the viewing pattern (Fig. 2.11). These are summarised in Table 2.4, The details of the experimental conditions were:

- 1) A Kodak Carousel S-AV 2050 projector with a 250-W halogen lamp was used to project the image of a 35mm slide onto a white matte 120 x 120 cm² screen. The screen-to-projector was 400 cm (Fig. 2.13).
- 2) Two projector light sources were used. A halogen lamp (about 4000 K) with luminance levels of 113, 75, 45 cd/m² was used in phases 1 and 4, 5 and 6, and 3 respectively, and a simulated xenon light source (about 5600 K) with low luminance level of 47 cd/m² was used in phase 2.
- 3) 99, 95, and 36 test colours were assessed in phases 1-4, 5, and 6 respectively.
- 4) A TSR was used to measure the spectral radiance of test colours at a distance of 360 cm from screen.
- 5) Each test colour was assessed by a panel of five to six observers using the same magnitude estimation technique for scaling the attributes of the test colours.

In total, 9093 estimations were made. This data is named the CARISMA 35mm Data Set.

2.7.6.1.3 Kuo and Luo Colour Appearance Data Set

The Kuo and Luo Colour Appearance Data Set was accumulated after completion of the Alvey and CARISMA projects.

In the graphic arts industry, the colour samples under consideration mainly subtend an angle of around 2° at the observer's eye. In surface industries such as paint, textile, ink, plastics, large-field samples are usually used. The two different field sizes of subtended angular degree would affect the perceived colour appearance of a colour stimulus. Additionally, different media or substrates may also have an impact on colour appearance. A set of textile test colours was produced to investigate these issues.

The experiment was divided into three phases according to three light sources used (i.e. D65, tungsten (A) simulators, and TL84). The experimental conditions are summarised in Table 2.5. The details of experimental conditions are summarised below.

- 1) The test colours involved 240 samples of woven wool fabric, and were mounted on three inch squares of stiff cardboard that subtended 10° at the observer's eye.
- 2) The wool samples were distributed over CIE $L^*a^*b^*$ colour space with ten intervals of L^* scale from 10 to 100, and five unit intervals of a^* and b^* axes within the maximum to minimum achievable dye ranges.
- 3) Colour measurements were carried out using a Macbeth MS2020+ Spectrophotometer in terms of reflectance values of test colours under each of the three phases tested. The conditions were: 20 nm measured interval (400-700 nm), specular component included, without a UV cut-off filter, and using a large aperture.
- 4) A panel of five experienced observers scaled each of 240 samples illuminated by each of the three sources.

In total, 10770 estimations were made. This data is named the Kuo and Luo Data Set.

2.7.6.2 Testing Colour Models' Performance Using LUTCHI Colour Appearance Data

The acquisition of the LUTCHI Colour Appearance Data described above was used to test the accuracy of the predictions for various colour spaces and models. The studies were carried out using two test methods. In the first method, colour spaces (CIELAB, CIELUV, and CMC(1:1)) and colour appearance models (Hunt, Nayatani, and RLAB) were compared. In the second test, various chromatic adaptation transforms (von Kries, Bartleson, BFD, Nayatani, Hunt, RLAB, and CIELAB) were compared using the experimental grids selectively derived from the LUTCHI data. The results obtained using each set of the LUTCHI data are summarised below.

(1) Testing Results Using the Alvey Colour Appearance Data Set

Colour Spaces and Colour Appearance Models (not including RLAB)

The Hunt91 model gave a much better general performance for all three perceived attributes than the other models and spaces. Its performance was close to the typical variation between individual observer's and mean visual results.

Chromatic Adaptation Transforms

The BFD transform gave the best fit to the LUTCHI experimental grids, especially from adaptation to A to adaptation to D65. The Hunt91 model obtained from this study was not

the best in the area of chromatic adaptation, although it was almost consistently the second best. All transforms gave very similar performance when processing two adaptations having only a small difference in colour temperature, such as the adaptation from D50 to D65.

(2) Testing Results Using the CARISMA Surface Data Set

The results again showed that the Hunt91 colour appearance model outperformed the other spaces and models. Moreover, all spaces and models performed worse for the lower luminance phases, in which the somewhat larger experimental errors might occur.

(3) Testing Results Using the CARISMA LT and 35mm Data Sets

The predictive accuracy from the majority of the spaces and models was similar to those found above, except a poorer performance was found for the Hunt91 colour appearance model. The Hunt91 model was derived to fit the Alvey and CARISMA Surface data, and to give accurate predictions of these data within the typical-observer accuracy. The test results for the Hunt91 model indicated that there were large perceptual differences between the transmissive and non-transmissive viewing conditions. Additionally, it was also found that observers were effectively adapted in the dark surround conditions, despite the different colour temperature sources used. Hence, the Hunt91 model was modified, and a newer verified version, Hunt94 colour appearance model, was derived. Its predictive performance was proved to be quite satisfactory by evaluating using CV values.

(4) Testing Results Using the Kuo and Luo Data Set

Only chromatic adaptation transforms (including von Kries, Bartleson, BFD, Nayatani, Hunt, RLAB, and CIELAB) were compared using the experimental grids derived selectively from the new colour appearance data obtained from the Kuo and Luo's work. The results clearly indicated that the BFD transform gave the best fit to the experimental grids, especially for adaptation to A to adaptation to D65. It agreed with the findings of the testing model's performance using the Alvey Data Set.

Chapter 3 CHARACTERISING PRINTING DEVICES

As mentioned in Section 1.2, each imaging device must first be characterised to derive device independent colour reproduction. Device characterisation is a term which has crept into colour reproduction parlance in recent years and has slightly different meanings to different people. In this study, it is defined as the provision of data for developing a mathematical transformation which determines the conversion between device specific data and colorimetric data based on the CIE system.

Two approaches are commonly used in the field of device characterisation. One is a full characterisation method which is developed by measuring a large number of colours to define the transformation. The other is a modelling method which requires far less measurements. Although full characterisation methods would give accurate transformations for a range of device types, such procedures are time consuming. In addition, many devices cannot produce repeatable colours over time which results in a need to frequently re-characterise them. Therefore, it was decided to apply a modelling method in this study. Generally, the modelling method is often adequate for a general application in the graphic arts industry although it is recognised that this method is less accurate than the full characterisation method.

3.1 OBJECTIVES

In practice, commercial printers usually apply four-process colours (CMY plus black, K). This work formed part of a large research programme (as mentioned in Section 2.5.3.1). Previous research (Johnson et al. 1995, Luo et al. 1992) was focused on characterising printing models based upon three ink primaries (CMY). This research extended the three primaries by including black ink. Various models were derived and each consisted of both forward and reverse processes.

There were two objectives in these investigations.

- 1) To derive printing models. Each included both forward and reverse printing processes. The former predicts tristimulus values from a set of process primaries for a printing

device, i.e. from CMYK to XYZ. The reverse printing process was also derived for transforming tristimulus values into the four process primaries, i.e. XYZ to CMYK.

- 2) To evaluate printing models' predictive performance. These were tested using some data sets with known CMYK and XYZ values.

3.2 PRINTING DEVICES SELECTED

The two printing devices selected were a Cromalin colour proofing system, and an IRIS ink-jet printer (see Section 2.4.2).

3.3 DATA SETS FOR CHARACTERISING PRINTERS

For each printing device, both cube and black printer characterisation data sets were produced. The latter was composed of two subsets including 120 and 31 samples which are denoted as the 120, and 31 sample sets. The colours in the 120 sample set were all approximately neutral; the 31 sample set included colours, as colourful as possible, with a certain amount of black ink. A Macbeth MS2020+ spectrophotometer was used for colour measurements. The samples in these data sets were squares with approximately 1" × 1" inch square, and were large enough to be measured using a reasonably large aperture to avoid errors arising from internal scattering in the substrate and local print non-uniformity.

3.3.1 Cube Data Set

A 9×9×9 matrix colour chart, sampled from the CMY colour space, was produced for each device. The chart was designed to evenly sample the printing gamut considered. In the CMY colour space, each axis represented one of the three CMY primaries and was divided into nine divisions. These samples were selected to give approximately an equal perceived difference between neighbouring samples (see Fig. 3.1). This cube data set is also called 729 data set.

3.3.2 Black Printer Data Set

Two data sets (120 and 31 sample sets) were produced for each printing device for deriving black printer algorithms as described below.

(1) 31 Sample Set

For the 31 sample set, samples included a black ink together with at least one of the CMY inks. These samples were produced using the following c, m, y, and k fractional dot areas (FDAs).

No.	c	m	y	k	No.	c	m	y	k	No.	c	m	y	k
1	100	0	0	100	11	40	0	40	20	21	100	0	100	70
2	0	100	0	100	12	0	40	40	20	22	0	100	100	70
3	0	0	100	100	13	40	40	0	20	23	40	0	100	100
4	100	100	0	100	14	100	100	0	40	24	40	0	40	70
5	100	0	100	100	15	100	0	100	40	25	0	40	40	70
6	0	100	100	100	16	0	100	100	40	26	100	0	0	20
7	100	100	100	100	17	40	40	0	40	27	0	100	0	20
8	100	100	0	20	18	40	0	40	40	28	0	0	100	20
9	100	0	100	20	19	0	40	40	40	29	100	0	0	70
10	0	100	100	20	20	100	100	0	70	30	0	100	0	70
										31	0	0	100	70

It can be seen that all colours include a black ink content with FDAs ranging from 20 to 100.

(2) 120 Sample Set

The samples in the 120 sample set were arranged in a 12x10 array. In the first row, a grey scale was produced using only black ink with FDAs ranging from 10 to 100 with a 10 unit interval.

10	20	30	40	50	60	70	80	90	100
----	----	----	----	----	----	----	----	----	-----

In row 2, a near-neutral scale was made of three coloured inks (C, M, Y). For rows 3 to 12, samples in each column had the same C, M, Y FDAs as those in row 2 but varying in black contents. Their FDAs are listed below. For example, the sample in row 4 and column 3 had FDAs of 30, 21, 20 and 20 for C, M, Y and K.

Column		1	2	3	4	5	6	7	8	9	10
Row	C	10	20	30	40	50	60	70	80	90	100
	M	8	14	21	28	38	46	56	65	79	89
	Y	7	13	20	27	33	43	51	61	74	86
2	K	0	0	0	0	0	0	0	0	0	0
3		10	10	10	10	10	10	10	10	10	10
4		20	20	20	20	20	20	20	20	20	20
5		30	30	30	30	30	30	30	30	30	30
6		40	40	40	40	40	40	40	40	40	40
7		50	50	50	50	50	50	50	50	50	50
8		60	60	60	60	60	60	60	60	60	60
9		70	70	70	70	70	70	70	70	70	70
10		80	80	80	80	80	80	80	80	80	80
11		90	90	90	90	90	90	90	90	90	90
12		100	100	100	100	100	100	100	100	100	100

In a later stage, this data set, excluding the colours in the first row, was used to test various printing models' performance. This data set is renamed 110 sample set.

3.4 CHARACTERISING PROCEDURES

The procedures for obtaining colorimetric and densitometric data are as follows:

- 1) Measure each sample from the previously produced data sets in terms of the spectral reflectance values ($R_{(\lambda)}$) across the visible spectrum 400-700 nm with 20 nm interval using a Macbeth MS2020+ spectrophotometer. The measurement conditions were small aperture, UV included, and specular reflection excluded.

- 2) The TSR was used to measure the BaSO₄ tile against the real light sources considered (i.e. D65, D50, and A simulators). For each measurement, 81 spectral radiance values ($S_{(\lambda)}$) with 5 nm interval ranging from 380 to 780 nm were stored. These values were used to calculate the weights, $WX_{(\lambda)}$, $WY_{(\lambda)}$, and $WZ_{(\lambda)}$ (i.e. observer-illuminant products) using Eqn. 3-4-1.

$$\begin{aligned} WX_{(\lambda)} &= (1/k) S_{(\lambda)} \bar{x}_{(\lambda)} \\ WY_{(\lambda)} &= (1/k) S_{(\lambda)} \bar{y}_{(\lambda)} \\ WZ_{(\lambda)} &= (1/k) S_{(\lambda)} \bar{z}_{(\lambda)} \end{aligned} \quad (3-4-1)$$

Where $k = \sum S_{(\lambda)} \bar{y}_{(\lambda)} \Delta\lambda/100$ and the $\bar{x}_{(\lambda)}$, $\bar{y}_{(\lambda)}$ and $\bar{z}_{(\lambda)}$ are the 1931 CIE colour matching functions.

- 3) Each of the three weights was abridged from 81 to 16 points (ranging from 400–700 nm, with 20 nm interval) under the light source or illuminant considered. The method was derived from Stearns's (1975, 1985) abridged weights' method.
- 4) Calculate XYZ values for each sample using the abridged weights (designated as $WX'_{(\lambda)}$, $WY'_{(\lambda)}$, and $WZ'_{(\lambda)}$) obtained in step (3), i.e.

$$\begin{aligned} X &= \sum WX'_{(\lambda)} R_{(\lambda)} \Delta\lambda \\ Y &= \sum WY'_{(\lambda)} R_{(\lambda)} \Delta\lambda \\ Z &= \sum WZ'_{(\lambda)} R_{(\lambda)} \Delta\lambda \end{aligned} \quad (3-4-2)$$

where $\Delta\lambda = 20$ nm across the visible spectrum 400-700 nm.

- 5) Figs. 3.2(a) and 3.2(b) show the cube data plotted on CIE a^*b^* diagram for IRIS and Cromalin devices respectively with different L^* levels (only D65 simulator was used here). The diagram was used to check if the colour measurements were correct and the samples were reasonably spaced.
- 6) Generate two look-up-tables (LUTs) for the cube and black printer data sets. Each table was composed of colorimetric densities (Eqn. 2-5-12) and fractional dot areas (FDAs).

As mentioned in Section 2.5.1.2, the LUT is a technique whereby the relationship between two variables can be linearly interpolated.

3.5 PRINTING CHARACTERISATION MODELS

Five different black printer algorithms (BPAs) were derived. These were: sub-additivity model (SAM), modified sub-additivity model (MSAE), third-order polynomial model (3rd), and two second-order polynomial models (designated as 2nd(1) and 2nd(2)). Each model included both forward and reverse processes. Additionally, a third-order (3rd-order) masking model considering three-colour components (Section 2.5.1.2) was also included in each of the models derived.

Fig. 3.3 shows a schematic diagram for computing the forward process. The FDAs of CMYK inks are the input values. The FDAs of CMY are first converted to the principal colorimetric densities (i.e. D_{r-c} , D_{g-m} , and D_{b-y} respectively) via LUT, and the red-, green-, and blue- colorimetric densities of three-colour component (i.e. $(D_r, D_g, D_b)_{3c}$) are then computed using the forward masking model. The FDA of K ink is used to obtain the red-, green-, and blue- colorimetric densities of the black component $(D_r, D_g, D_b)_k$ via the LUT. Subsequently, a forward black printer algorithm (BPA) is applied to predict the $(D_r, D_g, D_b)_{4c}$ of a resultant colour by adding the black component $(D_r, D_g, D_b)_k$ to the three-colour component $(D_r, D_g, D_b)_k$ obtained in the earlier stage. Finally, the predicted tristimulus values (XYZ) are transformed from $(D_r, D_g, D_b)_{4c}$ using log density functions (Eqn. 2-5-12).

The reverse process includes a reverse black printer, and reverse masking models. The reverse BPA can be considered as a grey component replacement (GCR) algorithm as described in Section 2.4.4. The GCR algorithms were implemented to predict FDAs of CMYK inks using XYZ values. Fig. 3.4 shows the schematic diagram illustrating the reverse BPA model with known black ink. The observed FDA of the black ink and the measured XYZ values for the characterisation data sets (110, 31, or cube sample sets) are first entered. The XYZ values are transformed into $(D_r, D_g, D_b)_{4c}$ values using the log

density functions, and the FDA of the black ink is used to obtain $(D_r, D_g, D_b)_k$ values via the LUT. Subsequently, both the $(D_r, D_g, D_b)_{4c}$ and $(D_r, D_g, D_b)_k$ values are used to predict $(D_r, D_g, D_b)_{3c}$ values by applying a reverse BPA model. Finally, the predicted FDAs of CMY inks for three-colour component are obtained using the reverse 3rd-order masking model via the LUT. The full reverse BPA models applying grey component replacement (GCR) were also derived. A schematic diagram explaining the computational procedures is given in Fig. 3.5. Some parameters need to be defined as shown below.

D_{gcr}	critical density point below which no grey component replacement is performed. This is predetermined, say $D_{gcr} = 0.6$.
$(D_r, D_g, D_b)_{3c_max}$	the red-, green-, and blue- colorimetric densities obtained from the sample produced using FDAs of 100% C, 100% M, and 100% Y. (These are (1.20, 1.24, 1.20), and (1.31, 1.36, 1.28) for the IRIS and Cromalin devices respectively in this study)
$(D_r, D_g, D_b)_{k_max}$	the red-, green-, and blue- colorimetric densities obtained from the sample produced using only black ink with 100 % FDA.
gc	the grey component defined by the smallest density of $(D_r, D_g, D_b)_{4c}$.
r_o	the percentage of grey component removed from each channel of $(D_r, D_g, D_b)_{4c}$. This is also predetermined.
K_{lut}	the grey component removed from the set of the input $(D_r, D_g, D_b)_{4c}$ and replaced by black ink.

In Fig. 3.5, the XYZ values of a target colour are first entered and then converted into $(D_r, D_g, D_b)_{4c}$ using the log density functions given in Eqn. 2-5-12. The next step is to determine the amount of black ink (K) used. The full black content (i.e. solid black ink, $FDA_k = 100$) will be used if the red-, green-, and blue- colorimetric densities of the colour considered ($(D_r, D_g, D_b)_{4c}$) are larger than the respective channels of solid black ink (i.e. $(D_r, D_g, D_b)_{k_max}$ known previously). In this case (designated as Case 1), the $(D_r, D_g, D_b)_k$ used will be set to equal $(D_r, D_g, D_b)_{k_max}$. Otherwise, Case 2 or 3 black printers will be

used. Case 2 excludes black ink (i.e. $FDA_k = 0$). This is determined by the smallest density of the $(D_r, D_g, D_b)_{4c}$ (i.e. gc) less than D_{gcr} , and $(D_r, D_g, D_b)_{4c}$ less than $(D_r, D_g, D_b)_{3c-max}$. Hence the $(D_r, D_g, D_b)_{3c}$ are set equal to $(D_r, D_g, D_b)_{4c}$. In Case 3, the appropriate black content (i.e. K_{lut}) is calculated using the initially defined r_o , and followed by obtaining both the FDA_k and $(D_r, D_g, D_b)_k$ via the LUT. Subsequently, the $(D_r, D_g, D_b)_{3c}$ are obtained using a reverse BPA model for Cases 1 and 3. Then, the calculated $(D_r, D_g, D_b)_{3c}$ are used to obtain the principal colorimetric densities $(D_{r-c}, D_{g-m}, D_{b-y})$ via the reverse 3rd-masking model for Cases 1 to 3. Finally, the FDAs of CMY inks are obtained. As mentioned earlier, the r_o is initially fixed. However, this value can occasionally achieve $(D_{r-c}, D_{g-m}, D_{b-y}) > 1.0$ or < 0.0 . In these cases, the r_o can be optimised until a reasonable set of $(D_{r-c}, D_{g-m}, D_{b-y})$ values can be obtained.

3.5.1 Sub-Additivity Equations (SAE)

As described in Section 2.4.5, several factors causing the additivity failure of inks were mentioned. This deficiency can be characterised using a sub-additivity diagram (Yule 1967b, Reiter 1984, Kazuo 1986). The 120 black printer sample sets for IRIS and Cromalin devices were used to establish sub-additivity diagrams. For each sample, the colorimetric densities (D_r, D_g, D_b) were computed from the XYZ values using Eqn. 2-5-12. These are given in Tables 3.1 and 3.2 for IRIS and Cromalin devices respectively. They are also plotted in Figs. 3.6(a), 3.7(a), 3.8(a) and 3.9(a), 3.10(a), 3.11(a) for D_r, D_g, D_b of IRIS and Cromalin devices respectively. In each figure, the densities of the colours produced using three coloured inks (D_{3c}) and four primary inks (D_{4c}) are plotted against those (D_k) produced using black ink alone. Curves are drawn to go through the samples having the same content of three-colour component with variations in black ink. For each colour channel ten lines are plotted. In Figs. 3.6(b), 3.7(b), 3.8(b) (for IRIS) and Figs. 3.9(b), 3.10(b), 3.11(b) (for Cromalin), the best regression lines are plotted. If there is no additivity failure, all regression lines should be parallel to each other. However, for halftone printing, it is common to find that these lines approximately converge to a point on the 45° line. This is known as sub-additivity behaviour (Hamilton 1986) as described in Section 2.4.5. According to Eqn. 2-4-2 in Section 2.4.5 describing the sub-additivity

behaviour, the forward and reverse SAE models for four-colour reproduction can be expressed using Eqns. 3-5-1 and 3-5-2 respectively.

$$\begin{aligned} D_{r-4c} &= D_{r-3c} + D_{r-k} - (D_{r-3c} D_{r-k}) / k_r \\ D_{g-4c} &= D_{g-3c} + D_{g-k} - (D_{g-3c} D_{g-k}) / k_g \\ D_{b-4c} &= D_{b-3c} + D_{b-k} - (D_{b-3c} D_{b-k}) / k_b \end{aligned} \quad (3-5-1)$$

$$\begin{aligned} D_{r-3c} &= k_r (D_{r-4c} - D_{r-k}) / (k_r - D_{r-k}) \\ D_{g-3c} &= k_g (D_{g-4c} - D_{g-k}) / (k_g - D_{g-k}) \\ D_{b-3c} &= k_b (D_{b-4c} - D_{b-k}) / (k_b - D_{b-k}) \end{aligned} \quad (3-5-2)$$

where

- $(D_{r-4c}, D_{g-4c}, D_{b-4c}), (D_{r-3c}, D_{g-3c}, D_{b-3c}), (D_{r-k}, D_{g-k}, D_{b-k})$ terms are the red-, green-, and blue- colorimetric densities of four-colour, three-colour component, and black component respectively.
- $k_r, k_g,$ and k_b are the red-, green-, blue- colorimetric densities for the convergence points as described above.

From these diagrams, the converging densities D_r, D_g, D_b of 2.2, 2.1, 1.9 and 1.50, 1.50, 1.40 were obtained for IRIS and Cromalin devices respectively. These were obtained by averaging k values.

Some irregularities can be seen in the dark areas of the Cromalin samples in Figs. 3.9(a), 3.10(a) and 3.11(a) when compared with the IRIS's graphs (Figs. 3.6(a), 3.7(a) and 3.8(a)). This implies that noise existed in the shadow areas of the Cromalin samples. Further investigation found that dark Cromalin samples with a full black content (100%) appeared very similar. Their measurement results showed very little colorimetric differences between these dark samples (see Table 3.2, sample No. 101 to 110), but this did not occur in IRIS data (see Table 3.1). However, the human eye is less sensitive to the dark areas, and the loss of details in the shadow areas with large black content coverage (especially full 100% black) in colour reproduction is therefore insignificant (Molla 1988a). In other words, the noise existing in Cromalin samples is not important.

3.5.2 Modified Sub-Additivity Equations (MSAE)

It can be found that the converging point for each graph Figs. 3.6(b) to 3.11(b) is not an exact point, but a range of points. Especially, the range for the IRIS device is much larger than that for the Cromalin device. Therefore, modifications were made to improve the SAE model performance to derive a function k' , to replace k in Eqn. 3-5-1 for the forward model and k'' in Eqn. 3-5-2 for the reverse model. These factors were defined in Appendix A, Eqns. A.1.1 and A.1.2, for the forward and reverse models respectively.

3.5.3 Third-Order Polynomial Equations (3rd)

In addition to the two models described above, two alternative polynomial algorithms were also derived to correct the failure of additivity and proportionality for the four-colour case. These two models were extended from the approach proposed by Clapper (1961) using CMY primaries to CMYK. They are named third-order (3rd) and second-order polynomial equations (2nd) according to the order of polynomial used.

The third-order polynomial equations (3rd) were derived and are given in Eqns. A.2.1 and A.2.2 for the forward and reverse models with no cross products between D_r , D_g , D_b channels.

3.5.4 Second-Order Polynomial Equations (2nd)

The second-order polynomial (2nd) BPA model assumes that the three-colour component and black component (or black printer) are two separate parts in four-colour printing. Basically, this model is similar to the 2nd-order masking model in the three-colour reproduction described in Section 2.5.1.2 to apply all possible cross terms. In this case, 27 terms were used to include all possible combinations of $(D_r, D_g, D_b)_{4c}$ and $(D_r, D_g, D_b)_k$. The forward and reverse algorithms are given in Eqns. A.3.1 and A.3.2 respectively.

Five BPA models were successfully derived. Each model included both forward and reverse processes. These are SAE, MSAE, 3rd, 2nd(1) and 2nd(2) models. These models differ in calculating D_{4c} values using Eqns. 3-5-1, 3-5-1 and A.1.1, A.2.1, and A.3.1

respectively in the forward processes. In addition, D_{3c} values were calculated using Eqns. 3-5-2, 3-5-2 and A.1.2, A.2.2, and A.3.2 respectively in the reverse processes. For the first four BPA models (i.e. SAE, MSAE, 3rd, 2nd(1)), the coefficients in these equations were optimised using the D_{3c} and D_k values in forward processes (or the D_{4c} and D_{3c} in reverse processes) from the combined 110 and 31 sample set to predict D_{4c} (or D_{3c}) until the best least-squares fit to D_{4c} (or D_{3c}) measured. (The 110 data set used excluded the 10 grey-scale samples produced only using black ink from 120 sample data set.) For the 2nd(2) BPA model, all characterisation data sets (including cube data set and black printer data set) were used in the optimisation of the coefficients. Hence, the difference between the 2nd(1) and 2nd(2) BPA models is only due to different data sets involved for deriving models. As described earlier, the Lawson and Hanson least-squares technique was used to obtain the coefficients for each model.

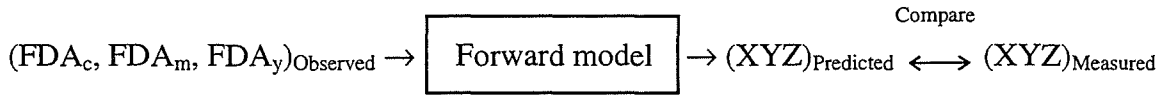
3.6 TESTING MODELS' PERFORMANCE

The models described in the earlier sections were tested using three characterisation data sets: the cube, 110 and 31 black printer, which were used to derive these models. For testing the forward models, the seven colorimetric measures were used, i.e. mean values of $|\Delta x|$, $|\Delta y|$, $\Delta u'v'$, $\Delta\%|Y|$, ΔE CIE $L^*a^*b^*$, ΔE CIE $L^*u^*v^*$, and ΔE CMC(1:1). For every colour in each data set, these seven measures were calculated between the measured and predicted XYZ values. The mean measures from all the samples in the data set considered were used to represent the models predicted performance. For the comparison of the reverse models, the mean values of $|\Delta FDA_{3c}|$ (i.e. $|\Delta FDA_c| + |\Delta FDA_m| + |\Delta FDA_y|$), $|\Delta FDA_c|$, $|\Delta FDA_m|$, and $|\Delta FDA_y|$ measures were used. The unit of FDA range from 1 to 100.

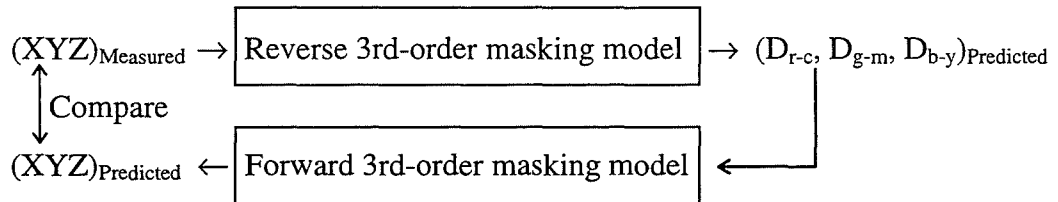
3.6.1 The Performance of the Third-Order Masking Model

All of the BPA models derived here employ the 3rd-order masking model (Eqn. 2-5-11). Thus the predictive and the reversibility performance between the forward and reverse masking models were also checked in this investigation. The forward model computes the XYZ from CMY and the reverse model calculates CMY from XYZ. The evaluation was

carried out using 729 samples in the cube data set. The procedures for testing the predictive performance are given below:



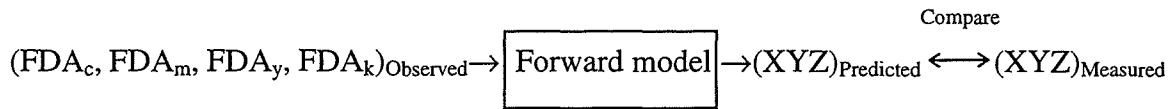
The observed FDAs of CMY inks of 729 colours were computed using the forward 3rd-order masking model to predict the XYZ values. The agreement between the predicted and measured XYZ values for the 729 cube colours in terms of seven colorimetric measures: mean values of $|\Delta x|$, $|\Delta y|$, $\Delta u'v'$, $\Delta\%|Y|$, $\Delta E \text{ CIE } L^*a^*b^*$, $\Delta E \text{ CIE } L^*u^*v^*$, and $\Delta E \text{ CMC}(1:1)$ (see Section 2.2), represents the 3rd-order masking model's reversibility performance. The results are given in Table 3.3. The procedures for testing reversibility are given as follows:



The measured XYZ tristimulus values $((XYZ)_{\text{Measured}})$ were first used to predict the CMY principal colorimetric densities $((D_{r-c}, D_{g-m}, D_{b-y})_{\text{Predicted}})$ using the reverse model. These were further used to predict XYZ tristimulus values $((XYZ)_{\text{Predicted}})$ using the forward model. The agreement between the $(XYZ)_{\text{Measured}}$ and $(XYZ)_{\text{Predicted}}$ for the 729 cube colours using each of the IRIS and Cromalin devices was assessed using the colorimetric measures mentioned above. The results are also given in Table 3.3. All measures for a perfect agreement, should equal zero for both the predictive and reversibility performance tests. The performance was considered to be very satisfactory. The mean CMC ΔE values of 0.61 and 0.63 were for the IRIS and Cromalin devices respectively for predictive performance, and mean CMC ΔE value of 0.62 and 0.67 were for the IRIS and Cromalin devices respectively for reversibility performance. Normally a CMC ΔE value of 1.0 is used as a typical tolerance limit for the colour quality control in the textile industry.

3.6.2 The Performance of the Forward BPA Models

This test was conducted to investigate the predictive performance of the forward models derived (see Fig. 3.3). The test procedures can be summarised as below:



The observed FDAs of CMYK inks of each colour in the 110, 31 or cube data sets were input values to predict the XYZ values via each of the five forward models. The predictive performance for each model was investigated by comparing the XYZ values between those predicted and measured, using the printing characterisation data sets.

Four BPA models (SAE, MSAE, 3rd, and 2nd(1)) were first derived using the 31 and 110 black printer sample sets. The 31 and 110 sample sets were used to test these four models. The results are summarised in Table 3.4. It can be seen that the 2nd(1) BPA model outperformed the other three models. However, when compared the 2nd(1) BPA model and 3rd-order masking equations in the test of cube data set, it was disappointing to find that the results (also given in Table 3.4) were not satisfactory. The mean CMC ΔE values are 1.78 and 3.11 for the IRIS and Cromalin devices respectively, much worse than the mean CMC ΔE values of 0.61 and 0.63 obtained using only the 3rd-order masking model for the IRIS and Cromalin devices respectively. This also implies that the 2nd(1) BPA model can not give reasonable predictions for the colours produced using small amounts of black ink. Therefore, it was decided that all three data sets were used to derive a new 2nd-order polynomial BPA model (named 2nd(2)). Subsequently, all data sets were used to test and compare these two 2nd BPA models (2nd(1) and 2nd(2)). The results are also given in Table 3.4. Although the 2nd(1) BPA model performed marginally better than the 2nd(2) BPA model in the test of the printer data sets for both IRIS and Cromalin devices (except in the test of 31 sample set for Cromalin device), the 2nd(2) BPA model gave much better performance than the 2nd(1) BPA model in the test of cube data set, close to those of the 3rd-order masking model.

The frequency histogram was also produced to show the distribution of prediction errors using the CMC ΔE values. It gives a snapshot of the overall pattern of variations. The smaller the number of high ΔE values, with narrower distribution indicates a better performance such as that of the 2nd(2) BPA model. For a perfect agreement, all ΔE values should be located at the zero point. The diagrams for both devices are displayed in Figs. 3.12, 3.13, and 3.14 for the 31 and 110 black printer, and cube data sets respectively.

The results obtained in this section are summarised below.

- Models' performance using the 31 sample set

For the IRIS device, the two 2nd BPA models 2nd(1) and 2nd(2) (see Fig. 3.12(a)) have narrower distributions and smaller ΔE values than those of the other models. The 2nd(1) BPA model with mean CMC ΔE values of 1.40 performed slightly better than the 2nd(2) BPA model with mean CMC ΔE values of 1.72, and the SAE BPA model the worst with a mean CMC ΔE value of 3.13. However, there was very little difference in performance amongst the five models for the Cromalin device with the 2nd(2) BPA model giving a slightly better performance (Fig. 3.12(b)). Generally, all models derived from the IRIS device performed better than those from the Cromalin device as expected due to some irregularities found in the dark areas of the Cromalin samples (explained in Section 3.5.1).

- Models' performance using the 110 sample set

The results clearly show that the two 2nd BPA models outperformed the other models for both devices (Fig. 3.13). As mentioned earlier, all characterisation data sets were used to derive the 2nd(2) BPA model while only the 31 and 110 black printer data sets were used to derive the 2nd(1) BPA model. In other words, there is more weight of the 110 sample set for deriving the 2nd(1) BPA model than the 2nd(2) BPA model. Hence, it is expected that the 2nd(1) BPA model performed better than the 2nd(2) BPA model using the 110 sample set.

- Models' performance using the cube sample set

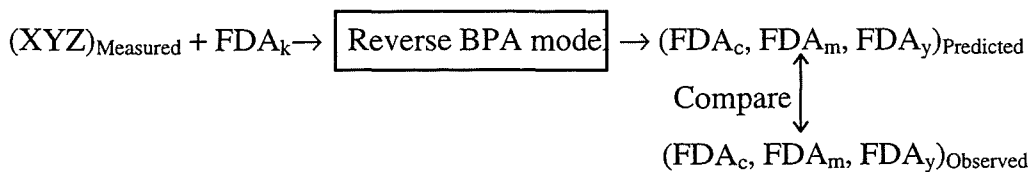
The 2nd(2) BPA model performed better than the 2nd(1) BPA model using the cube set. The distribution of the CMC ΔE values of the 2nd(2) BPA model is significantly narrower than that of the 2nd(1) BPA model (seen from Figs. 3.14(a) and (b)).

In conclusion, the 2nd(2) BPA model predicted the three data sets reasonably well, particularly the cube data set.

3.6.3 The Performance of the Reverse BPA Models

The five reverse models described earlier were also tested. These are briefly summarised as follows: the SAE BPA model using fixed k_r , k_g , k_b values in sub-additivity equations (Eqn. 3-5-2), the MSAE BPA model applying a modified sub-additivity equations (Eqn. A.1.2 with Eqn. 3-5-2), the 3rd BPA model employing a set of 3rd-order polynomial equations (Eqn. A.2.2), and the 2nd(1) and 2nd(2) BPA models using a set of 2nd-order polynomial equations (Eqn. A.3.2).

As mentioned in Section 3.5, these reverse models were initially implemented to predict FDAs of CMY inks using XYZ values with known FDA of K ink. This test was carried out to determine which model gave the best performance. The best performing model would be further applied to the BPA with the Grey Component Replacement Algorithm which is capable of predicting FDAs of all four primary inks from a set of XYZ values. (The BPA with known K ink has been given in Fig. 3.4.) The test procedures are summarised as follows:



The observed FDA of K ink and the measured XYZ for each colour in the black printer data sets (110 and 31 sample sets) were input values used to predict FDAs of CMY inks using five different models derived (following the procedures as described in Fig. 3.4).

The predictive performance for each model was investigated by comparing the FDAs of CMY values between the predicted and the observed values.

The results for the 31 and 110 sample sets are summarised in Tables 3.5 and 3.6 for the IRIS and Cromalin devices respectively. Again, frequency histograms were used to show the variations of the mean $|\Delta FDA_{3c}|$ values. Figs. 3.15(a) and (b) show the distribution of the mean $|\Delta FDA_{3c}|$ values for the 31 and 110 sample sets respectively for the IRIS device, and Figs. 3.16(a) and (b) for the Cromalin device.

- Models' performance using 31 sample set

For the IRIS device, the MSAE BPA model performed the best, but only slightly better than the two 2nd BPA models, 2nd(1) and 2nd(2), which had similar performance, and the SAE BPA model the worst. The 2nd BPA models predicted more accurate results than the other BPA models and the MSAE BPA model was the worst for the Cromalin device. All models gave better predictions to the IRIS data than to the Cromalin data. Again, this is due to the noise in the dark Cromalin samples as mentioned earlier.

- Models' performance using 110 sample set

For both devices, the 2nd(1) and 2nd(2) BPA models predictions were more accurate than the other BPA models, and the MSAE BPA the worst. Again, all models' predictions agreed more closely with the IRIS data than with the Cromalin data.

In conclusion, the 2nd BPA models gave the better overall performance than the other BPA models for both the IRIS and Cromalin devices. All five models derived from the Cromalin data performed much worse than those derived from the IRIS data. This can be clearly seen in Figs. 3.15 and 3.16; i.e. the variations of the mean $|\Delta FDA_{3c}|$ values for the all BPA models for the Cromalin device are much larger than those for the IRIS device. Both the 31 and 110 sample sets had four samples in which total FDA of four primary inks is more than 300 and the FDAs of both the black and at least one of the CMY inks are more than 90. It was found that these four samples in both 31 and 110 sample sets

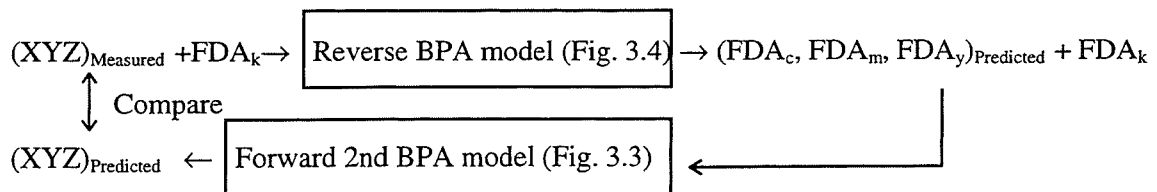
gave the worst predictions amongst the samples studied. However, with the knowledge of human visual insensitivity to the dark colour areas, these four samples were not considered to be significantly important to the results. Therefore, the mean measures from the full set including and excluding these four samples are also given in Tables 3.5 and 3.6 to show the difference. Additionally, as described, with the noise existing in the Cromalin samples with intense black content, the Cromalin samples performed badly as expected in the dark colour areas.

It was decided that the 2nd BPA models performed the best in this study, it was further extended to derive a BPA incorporated with GCR. The performance of GCR was investigated and described in the following section.

3.6.4 The Reversibility Performance Between the Forward and Reverse BPA Models

The Reversibility Performance Test Using Known K ink

Another test was carried out to examine the reversibility performance between the forward and reverse models using the 110 and 31 sample sets with known black content (K). Only two forward 2nd BPA models were used in the forward process due to the significantly better performance than the other BPA models found in the earlier test. All the reverse BPA models were tested in the reverse process. The forward 2nd(1) BPA model was used to calculate tristimulus values from the FDAs of CMYK inks predicted using the reverse SAE, MSAE, 3rd, and 2nd(1) BPA models respectively. The forward 2nd(2) BPA model was used for the reverse 2nd(2) BPA model only. All measures should equal zero for perfect reversibility between the forward and reverse models. This test was carried out using the following procedures:

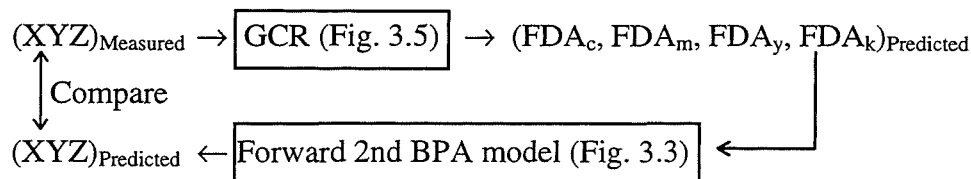


The results are summarised in Table 3.7 and the distribution of ΔE (CMC) results are also plotted in Figs. 3.17 and 3.18 for the IRIS and Cromalin devices respectively.

The results show that the two 2nd BPA models performed better than the other BPA models for all data sets for both the Cromalin and IRIS devices. Moreover, the results from the 31 sample set were inferior to those from the 110 sample set. This implies that the 31 sample set provides a more severe test for the models than that of the 110 sample set. Again, the two models performed much better with the IRIS data than with the Cromalin data. This is due to the reason given in Section 3.5.1.

The Reversibility Performance Using the GCR Algorithm

The GCR derived in Section 3.5 was tested by its reversibility performance between the forward and reverse processes based on 2nd BPA model using all three data sets. The 3rd-order masking and 2nd BPA models in the GCR were used in predicting all three data sets, even though the cube data set was produced using only three CMY colour primaries. The test procedures are given below.



First, the reverse 2nd BPA model (2nd(1) or 2nd(2)) was used to predict the FDAs of CMYK inks from the measured XYZ tristimulus values. Second, the corresponding forward 2nd BPA model was used to predict XYZ tristimulus values from these predicted FDAs of CMYK inks. Finally, the details of measures defining the reversibility performance were obtained by comparing between the predicted and the measured XYZ values. Five levels of r_0 values (the percentage of GCR) were tested, i.e. 0.00, 0.30, 0.70, 0.90, and 1.00 respectively for both the Cromalin and IRIS devices. Additionally, for each level of r_0 , except $r_0 = 0.00$, included three levels of D_{ger} (below this density without GCR) tested. These were 0.00, 0.60, and the smallest density of $(D_r, D_g, D_b)_{3c_max}$. An

initial value of $r_o = 0.00$ was set in order to compare two 2nd BPA model's capability in finding the optimised solutions for all colours considered. The smallest densities (gc) of $(D_r, D_g, D_b)_{3c_max}$ were 1.20, and 1.28 for the Cromalin and IRIS devices respectively in this study. The results varied with combination of r_o values (the percentage of GCR) and D_{gcr} (below this density without GCR) are shown in Tables 3.8 and 3.9 for the IRIS and Cromalin devices respectively.

- Models' performance for the IRIS device

Both 2nd BPA models gave quite satisfactory performance for each combination of r_o and D_{gcr} values (except when $r_o = 0.0$ and $D_{gcr} = 0.0$) in all characterisation data sets. The 2nd(2) BPA model performed much better than the 2nd(1) BPA model for the 110 black printer and cube data sets although both 2nd BPA models were very similar for the 31 sample set.

- Models' performance for the Cromalin device

The CMC ΔE values for r_o of 0.0 are much larger than those for the different levels of r_o with fixed D_{gcr} factors in the 2nd(1) BPA model (especially in the 31 black printer and cube sample sets) but not for 2nd(2) BPA model. It was also found that the 2nd(2) BPA model performed far better than the 2nd(1) BPA model for all the three data sets, especially for the cube set. However, the 2nd(1) BPA model gave reasonable predictions for all three data sets when the r_o factor is equal to or greater than 0.7, and D_{gcr} factor is equal to or greater than 0.6 but less than the maximum density of grey component produced by three CMY primary inks (i.e. D_{3c_max}). This confirms that 2nd(1) BPA model can not perform well when samples have low black contents. Both 2nd BPA models fit the 110 black printer and cube data sets much better than 31 black printer data set. This indicates that the 31 black printer data set provides a more severe test than those using the other two sets.

3.7 CONCLUSIONS

Various models were successfully derived to characterise the two printing devices studied. The following conclusions are reached:

For the forward models' performance, the two 2nd BPA models performed better than the other BPA models. There were no significant differences between these two 2nd BPA models for the 31 and 110 sample sets, but the 2nd(2) BPA model is significantly better than the 2nd(1) BPA for the cube data set. This implies that the 2nd(2) BPA model would give more accurate predictions than the 2nd(1) BPA model for those samples having small amounts of black ink.

For the reverse models' performance, the two 2nd BPA models again gave the better overall performance than the other BPA models.

For testing reversibility performance between the forward and reverse BPA models, the two 2nd BPA models performed much better than the other BPA models. There was hardly any difference between the results from two 2nd BPA models. The reversibility performance for the two 2nd BPA models were quite satisfactory.

For the reversibility performance of the GCR algorithm, the 2nd(2) BPA model performed better than the 2nd(1) BPA model, especially for the cube data set. The 2nd(2) BPA model always gave better performance than the 2nd(1) BPA when 0.00 of r_0 was used for both of the devices, especially for the Cromalin device. This implies that $r_0 = 0.00$, which was used to compare two 2nd BPA models' capability in finding the optimised solutions for all colours considered as mentioned earlier, provides a very critical tested point.

It was also found that, all BPA models performed better for the IRIS device than those for the Cromalin device in all tests due to the noise existing in the Cromalin samples which had intense black contents.

Overall, the 2nd(2) BPA model performed the best in comparison with the other BPA models. This indicates that the more samples used to derive a model, the better the overall performance of the model.

The 2nd(2) BPA model performed better than the 2nd(1) BPA model. However, a considerable amount of effort was required to produce and measure the large number of colour samples for deriving the 2nd(2) BPA model due to the inclusion of 729 samples in the cube data set. This is considered to be impractical in industry. A simplified procedure, by deriving mathematical models based on the measurement of fewer colour samples, should be recommended. This can be achieved by carefully selecting a few three-colour samples together with the 31 and 110 black printer set to derive a 2nd BPA model. Moreover, the 2nd(1) BPA model can also give a reasonable prediction for the GCR by carefully selecting r_o and D_{gcr} factors (e.g. $r_o = 0.7$ and $D_{gcr} = 0.6$ was found in this study).

Chapter 4 QUANTIFYING COLOUR APPEARANCE–COMPLEX IMAGES

As mentioned in Chapter 1, there is a considerable need by industry for high colour fidelity images to be reproduced using different imaging devices such as colour monitors and electronic printers. The core technology to achieve this requires a reliable colour appearance model to account for monitor and reflection print viewing conditions. Also described in Section 2.7.6, Luo et al. (Luo et al. 1991-1995, Kuo et al. 1995) carried out experiments to quantify the colour appearance of a single colour stimulus in a simple viewing field using a magnitude estimation method. The data set obtained is known as the LUTCHI Colour Appearance Data. The results have been used to refine the Hunt colour appearance model (Hunt 1994, Hunt and Luo 1994). In practice, complex images are frequently used in areas such as graphic arts and desktop publication. Hence, the work described in this chapter was carried out to extend the Luo et al's research by conducting psychophysical experiments using complex images.

In 1990, the CIE Technical Committee 1-27 on "Specification of Colour Appearance for Reflective Media and Self-Luminous Display Comparisons" was formed. The aim of this committee is to gather available data for the evaluation of various colour models to create visual matches for self-luminous display (softcopy) and reflection print (hardcopy) image comparison. The committee published guidelines (Alessi 1994) to encourage colour industrialists and researchers to perform experiments to contribute to this research programme.

This work was conducted closely following the CIE guidelines. An experiment was carried out to judge the matching performance of the softcopy image processed by a particular colour model against a standard (hardcopy) image viewed in a viewing cabinet by a panel of observers.

Eight colour models (described in Sections 2.2, 2.7.4 and 2.7.5) were evaluated. These were divided into four classes as follows:

- CIE 1931 XYZ system (CIE 1986),
- Uniform colour spaces: CIELAB and CIELUV (CIE 1986),
- Chromatic adaptation transforms: von Kries (Wyszecki and Stiles 1982c, Helson et al. 1952), Nayatani (Nayatani et al. 1990) (also named CIE), and BFD transforms (Lam 1985),
- Colour appearance models: Hunt (1991, 1994), and RLAB (Fairchild and Berns 1993, Fairchild 1994).

There was no need to use the Nayatani colour appearance model because the model has no capability in predicting colour appearance under different media/viewing conditions. Hence, only the chromatic adaptation transform (Nayatani et al. 1990) was used.

4.1 EXPERIMENTAL PREPARATION

4.1.1 Device Characterisation

Monitor Characterisation

A Barco Calibrator II monitor was used to display screen images in this work. The PLCC (Piecewise Linear interpolation assuming constant Chromaticity Coordinates) characterisation model (as described in Section 2.5.2.1) was used to calculate the monitor's RGB intensities from a given set of CIE 1931 XYZ values. The measurement equipment used was a Bentham tele-spectroradiometer (TSR). A set of characterisation data was produced for each of the three white points tested in this study: D53, D65 and D93. These colour temperatures were internally set by the Barco monitor, and were selected close to those used in the experiment. For each white point, 54 colours were produced, i.e. 18 colours for each of red, green and blue channels with 15 DAC interval ranging from 0 to 255 DAC values. The procedures for characterising the monitor were:

- 1) Calibrate the monitor and set the white point to either D53, D65 or D93 illuminants followed the Barco's calibration setup.
- 2) Display each of the characterisation colours in the centre of screen surrounded by a medium grey (L^* of 50).
- 3) Measure all colours in terms of 1931 CIE x , y , and luminance (cd/m^2) and store the measured data.
- 4) Calculate the matrix coefficients (described in Section 2.5.2.1) for the PLCC model for each of three white points under consideration.

The monitor was not switched off during the whole experimental period. This is to avoid the considerable warm-up period required to stabilise the display. In addition, a routine calibration procedure (same as procedure (1) above) was performed prior to each session to ensure the stability of screen images over time. It took approximately five minutes. Monitor calibration included two stages. The first stage simply invoked the Calibrator's own internal calibration routine which adjusted various internal parameters of the monitor based on the measurements with an external optical sensor. The second stage compensated for variations in the external video board used to drive the display. The second-stage calibration method was derived by Rhodes et al. (1992).

Printing Characterisation

A graphic arts scanner, applying photo-multiplier and external drum technology, manufactured by Crosfield Electronics Ltd., was used for producing conventional halftone colour separations. It outputs the CMYK (or CMY) DAC values or dot areas directly. A characterised Cromalin proofing system (Section 2.4.2) was used to produce the reflection prints required in the experiment. The Crosfield scanner was originally characterised to produce Cromalin hardcopies in terms of CMYK dot areas. Hence, the forward 2nd BPA printing model described in Section 3.5.4 was used to determine XYZ from CMYK dot areas of each pixel in an image.

Three light sources having chromaticities close to CIE D65, D50 and A illuminants were simulated in the viewing cabinet for viewing hardcopies in the psychophysical experiment (to be explained later). These light sources are named D65, D50 and A sources in the rest of the thesis. The Cromalin device was again used to produce a new set of characterisation samples and characterised. Each sample was measured using two colour measurement instruments, a Bentham tele-spectroradiometer (designated as TSR) using a 5 nm wavelength interval, and a Macbeth MS2020+ spectrophotometer (MS) using a 20 nm interval. As stated in Section 2.3.1, the TSR obtains measurements under the same viewing conditions as those used by observers. It provides a good correlation to what we see. However, it takes a much longer time to measure a colour using the TSR (about 3 minutes) than using the MS (4 seconds). The MS was mainly used for this research due to the large number of colour measurements required to characterise hardcopy devices. Hence, there was a need to transform the MS results to those of the TSR to avoid the problem of instrumental metamerism. (The monitor colours used in this study were measured using the TSR.) Luo and Xin (1991) derived an algorithm to convert the MS colour measurement results to those of the TSR. A 2nd-order polynomial given in Eqn. 4-1-1 was used to correlate the two sets of normalised spectral reflectance data (NR_{λ}) for each corresponding wavelength.

$$NR_{TSR,\lambda} = c1 + c2 (NR_{MS,\lambda}) + c3 (NR_{MS,\lambda})^2 \quad (4-1-1)$$

where $c1$, $c2$, and $c3$ are the coefficients which were optimised until the minimum measure of fit was achieved for the wavelength in question.

A set of 57 Cromalin samples was produced which was divided into two subsets: a single-coloured ink set and a 27-patch set. The former set consisted of 30 colours (10 colours ranging from 10 to 100 with a 10 unit interval for each of CMY inks). The latter set was composed of 27 samples which represent all combinations of CMY inks produced using three different levels: 0, 50, and 100 FDAs. The FDAs for each colour in the 27-patch set are shown as follows:

	Y0	Y50	Y100	Y0	Y50	Y100	Y0	Y50	Y100
C0									
C50									
C100									
	M100	M100	M100	M50	M50	M50	M0	M0	M0

These 57 samples covered a wide range of colour space and were measured using both the TSR and the MS. Again, the Lawson and Hanson least-squares technique (Lawson and Hanson 1974, Press et al. 1992) was used to optimise the coefficients in Eqn. 4-1-1.

The performance of this algorithm was tested using the 57 sample set. The XYZ values for the TSR, MS, and predicted values were computed by multiplying the reflectance values by the abridged weights as given in Eqn. 3-4-2. The seven colorimetric measures used in the previous chapter, i.e. mean values of $|\Delta x|$, $|\Delta y|$, Δu^*v^* , $\Delta\%|Y|$, ΔE CIE $L^*a^*b^*$, ΔE CIE $L^*u^*v^*$ and ΔE CMC(1:1), were again used. For each colour in the 57 sample set, these seven measures were calculated between the TSR and the MS XYZ values, and between the TSR and the predicted XYZ values under three different light sources (D65, D50, and A). The results are summarised in Table 4.1. It shows that the predicted results gave better agreement to the TSR results than those of the MS results. The method improves the correlation between the TSR and the MS results by about 70% for all three light sources investigated.

The Eqn. 4-1-1 was used to convert the MS measurement results to those of the TSR (see step (1), Section 3.4). Subsequently, the XYZ values for the black printer and cube data sets were recalculated. These were used to derive a new 2nd-order polynomial (2nd) BPA for converting CMYK to XYZ.

For each of the three sources, D65, D50, A used, four groups of data were obtained and used in the forward and reverse 2nd BPA models. These were:

- the 57 (i.e. 19×3) coefficients required in the 3rd-order masking equations (Eqn. 2-5-11) derived using the cube data set.
- a LUT containing FDA_{cmy} and $D_{\text{r-c}}, D_{\text{g-m}}, D_{\text{b-y}}$ data obtained using prints of single-coloured Cyan, Magenta, and Yellow primaries.
- the 81 (i.e. 27×3) coefficients required for 2nd BPA model derived using the cube, 31 and 110 black printer data sets.
- a LUT containing FDA_{k} and $D_{\text{r-k}}, D_{\text{g-k}}, D_{\text{b-k}}$ data obtained using a print of a single-coloured black primary.

Only the forward 2nd BPA model was used for the image preparation. The samples in the cube characterisation data set were again plotted on CIE a^*b^* diagram. It was found that the contours of the grid in the figure were still reasonably smooth and similar to Fig. 3.2(b). This indicates that the conversion algorithm from the MS to the TSR was working correctly and the colour measurement results were quite reasonable with no mistake being made in the sequence of measurements. The model was again tested as described in Chapter 2 in terms of its reversibility and predictive performance. The results are summarised in Table 4.2. It can be seen that the results obtained here were very similar to those in Section 3.6. and there is hardly any difference among all three sources (D65, D50, and A) studied. It indicates that the model performance did not vary with sources. Hence, the model's performance in general was considered to be quite satisfactory and was acceptable for use in the preparation of images in this study.

4.1.2 Image Preparation and Processing

Six transparency images were selected including three scene-content types: man-made objects, people, and natural scenes. Colour Plate I shows six images: "art", "golf", "girl2", "girl1", "musicians", and "flight" (from top right to bottom left). These images

were digitally scanned to obtain image data with a resolution of 300 dpi and also to produce the Cromalin hardcopies. The digital images were further adjusted to make the sizes of CRT images match those of hardcopies (about 5" x 7" in size).

Image processing software was developed to correlate the scanner's CMYK dot areas (FDAs) to the monitor's RGB intensities for a particular colour model on a pixel by pixel basis. The process is illustrated in Fig. 4.1. The 2nd BPA printing and the PLCC monitor models were used to transform CMYK dot areas to XYZ, and X'Y'Z' to RGB intensities respectively. The XYZ and X'Y'Z' represent the tristimulus values for hardcopy and softcopy viewing conditions respectively. For different categories of colour models, the computation procedures are different. For the XYZ system, XYZ values are directly transformed to monitor's RGB intensities. Three steps are needed for chromatic adaptation transforms which transform the XYZ to X'Y'Z' values.

For each uniform colour space or colour appearance model, the predicted lightness, chroma and hue were first calculated via its forward model, followed by calculating its corresponding X'Y'Z' using the model's reverse process. When applied to the Hunt and RLAB colour appearance models, the parameter defining the type of chromatic adaptation (Section 2.7.1) was set to "cognitive mechanism" or "discounting illuminant" in the forward model and "sensory mechanism" or "incomplete adaptation" in the reverse model. It was claimed by Fairchild (1992), that the cognitive and sensory chromatic adaptation mechanisms take place under the typical hardcopy and softcopy viewing conditions respectively.

4.2 PRELIMINARY EXPERIMENT

As described previously, the Hunt and RLAB colour appearance models include some arbitrary parameters whose values need to be determined according to different viewing conditions. Three sets of preliminary experiments (designated as Experiments 1, 2 and 3) were conducted to establish what values of these parameters should be used.

Additionally, the monitor screen used in the study could have a spatial uniformity problem which may have had a large impact on the results. Therefore, the location effect of the monitor was also included in the evaluation. Only the XYZ, Hunt, and RLAB models were used in the preliminary experiment. The Hunt91 and the RLAB93 models were used. The Hunt94 and RLAB94 (the latest versions of these two colour appearance models) were not available at that stage. The parameters used for the Hunt and RLAB colour appearance models are given in Table 4.3. For the hardcopy and softcopy viewing fields, the N_b and δ values used in the Hunt and RLAB models respectively were different. The dim and average surround conditions were used for the softcopy and hardcopy fields respectively (see Sections 2.7.5.1 and 2.7.5.3).

4.2.1 Experimental Set-Up and Viewing Configuration

The experimental set-up involved a hardcopy image illuminated in a VeriVide viewing cabinet, and two screen images with the same contents simultaneously displayed (SS) on a Barco Calibrator II monitor.

The experiments were carried out in a darkened room. The outside of the monitor was completely masked by a black cloth. Another black cloth was used to cover the surrounding walls of the viewing cabinet except for the viewing area. This allowed the observer's field of view to be filled with the image and background without interference from other areas. Two sources, D65 and D50, were investigated. The same set of chromaticities and luminance values (70 cd/m^2) for the softcopy's and hardcopy's white borders were used under the D65 and D50 sources. The colorimetric and luminance values for both the hardcopy and softcopy viewing fields under each of D65 and D50 sources are given in Table 4.4. The viewing cabinet was equipped with a luminance regulator. This allowed a close luminance match between the softcopy's and hardcopy's white borders (or reference white) determined by the TSR. Because identical chromaticities and luminance values were used for the softcopy's and hardcopy's white borders (or reference white), it was decided to apply the normal binocular simultaneous

matching (BSM) viewing technique. This technique is the most common method used in industry. The observer was instructed to use both eyes to look at one field at a time, but could switch between the two fields at any time. The softcopy images and the illuminated reflection hardcopy were located side by side and coplanar. The physical size of each screen image was the same as that of hardcopy image. The order of the softcopy image pair was randomised in each observing session to avoid possible trends in the comparisons.

Figs. 4.2(a) to (c) show the typical experimental viewing conditions used in Experiments 1 to 3 respectively. A grey background, with L^* of approximately 50, was used for both the hardcopy and softcopy fields in Experiment 1 (Fig. 4.2(a)). The symmetric viewing condition was used here, i.e. the same set of chromaticities and luminance values used for the softcopy's and hardcopy's white borders, and grey backgrounds. Experiments 2 and 3 used asymmetric conditions wherein different backgrounds were used for the softcopy and hardcopy fields. The black background was used for the softcopy field, and the grey background for the hardcopy field. The difference between Experiments 2 and 3 (Figs. 4.2(b) and (c) respectively) was that the softcopy and hardcopy images were displayed with and without a white border respectively. The white border was used as an anchor point for chromatic adaptation. Experiments 2 and 3 were intended to investigate the difference between the results obtained using with and without an anchor point for chromatic adaptation. Each image used included many objects. It was assumed that each observer unconsciously adapted to a colour, which was close to a "white" for chromatic adaptation in Experiment 3. In Experiment 1, each pair of softcopy images processed by two different models was judged by a panel of about 32 observers. Each pair was assessed twice by exchanging two images' left and right positions on the screen. In Experiments 2 and 3, each pair of softcopy images was repeatedly judged twice by each observer, but two images' left and right positions displayed on the monitor were randomised. This is due to the screen uniformity problem not found in Experiment 1 (to be explained later). Ten observers took part in Experiments 2 and 3.

4.2.2 Data Analysis

A forced-choice paired comparison method was employed in the experiment. Observers viewed a pair of displayed softcopy images, and judged which of the two gave a better match to the hardcopy. In addition, they also assessed the degree of match (i.e. colour fidelity) of the softcopy against the hardcopy using a 7-point category scale according to the appearance of the entire images, not part of the images. Each observer's results were entered via radio buttons numbered from 1 to 7 (see Fig. 4.2), which were located underneath each image. Another button marked "CONTINUE" was located in the lower middle area of the monitor for proceeding to the next pair of images. Data analysis was carried out using both the category judgement (Torgerson 1958) and paired comparison (Bartleson and Grum 1984) methods.

The category judgement method as described in Section 2.6.3, was used for obtaining empirical estimates of both the scale values of the colour models tested and the category boundaries of 7-point scale in this study. The 7-point category scale was defined from 1 (exact match), through 4 (acceptable match) to 7 (awful match) as below.

1. Exact match
2. good match
3. moderate match
4. acceptable match
5. poor match
6. bad match
7. awful match

This ranking method is recognised as a type of ordinal scale. The statistical treatment valid for it are: median, centile, and correlation coefficient. Theoretically, an ordinal scale involves ranking stimuli to be measured in the order of their magnitude according to the attribute considered. The rule for assigning numbers on an ordinal scale is that the ordinal position (rank order) of numbers on the scale must represent the rank order of the psychological attributes of the stimuli (McBurney 1990). The visual results from the

experiment were transformed to an interval scale using a method described by Torgerson (1958). It assumes that the distribution of visual scores for each stimulus is statistically normal. The data are not normally distributed as they are obtained on an ordinal scale, but, it is assumed that if they were transformed to an interval scale they would become so. The objective of the transformation in Torgerson's method is to force the data to fit the statistical normal distribution, accomplished by dealing with the cumulated distributions. A typical example (using the mean results), taken from Experiment 1, is given in Table 4.5. It includes each of the following 7 steps.

- Step 1: A frequency matrix is first established that contains the frequency of a model being judged in the seven categories.
- Step 2: As mentioned in Section 2.6.3, the law of categorical judgement deals with proportions of times that a given stimulus (model) is assigned to a position below a given category boundary. A cumulative frequency matrix is therefore constructed.
- Step 3: The cumulative frequency matrix is converted into a cumulative proportion matrix.
- Step 4: Transform the cumulative frequency matrix into a z score matrix.
- Step 5: A difference matrix between adjacent columns is established and the mean and sum for each column are also calculated.
- Step 6: The boundary estimates (T_1 to T_6 , i.e. scale values of boundaries) are determined by setting the origin at $T_1 = 0$ (which is between categories 7 and 6) and adding the adjacent mean values from difference matrix.
- Step 7: The scale value indicating image quality for each model is calculated by adding boundary estimates to the z score obtained in step 4. For each model, their mean and sum are also computed together with a rank which indicates the order of performance between the models investigated.

The category boundaries then can be decided as follows:

7.	$-\infty$ to 0.00	(awful match)
6.	0.00 to 0.960	(bad match)
5.	0.960 to 1.821	(poor match)
4.	1.821 to 2.605	(acceptable match)
3.	2.605 to 3.419	(moderate match)
2.	3.419 to 4.274	(good match)
1.	4.274 to ∞	(exact match)

The Category Boundary values for the “Aceptable Match” (designated as CBAM, i.e. T_3 and T_4) are the most critical points for defining the colour fidelity of the image (i.e. the performance of the model used to produce this image) in this study.

The paired comparison method is derived from Thurstone’s law of comparative judgement (see Sections 2.6.2). As described earlier, experimenters normally assume one of the six cases. More often Cases V and Va are used so that the scale values are described in terms of z scores (normal deviates) via a series of transformations. The score is linear with the visual response and is proportional to the quality of the image. For checking the calculation used in this study, the raw data from Kim et al’s paper (1993) was used and the calculation procedures are given in Table 4.6. It was found that the final z scores (in step 3) were the same as those calculated by Kim et al. This confirms that the computation method for obtaining z scores used in this study is correct. Table 4.6 illustrates three steps used for transforming the raw data to z scores.

Step 1: Raw data collected is constructed into a frequency matrix. Each number represents the frequency that the image represented by the column is judged better than the image represented by the row. For example, the value for column 6 and row 7 is 93, which indicates that the image produced using the Hunt model is judged 93 times out of 120 (the total number of judgements) and is better than that obtained using the Nayatani model.

Step 2: Each number in the frequency matrix is divided by the total number of judgements to produce a proportion matrix.

Step 3: The matrix values are then transformed to z scores. The summed z score for each column is on an interval scale where the higher the number, the better the model' performance. (From the results shown in step 3, it can be clearly seen that the CIELAB, RLAB, Hunt, and von Kries models perform better than the other models.)

However, there are difficulties with the Thurstone's method when there is a unanimous judgement, i.e. the images from one specific model are consistently judged better than those of another specific one. The z scores are infinity for 0.0 and 1.0, and these cannot be mathematically manipulated to form a response scale. Therefore, the method cannot be used for judgement where observer noise does not exist. A modified logistic transformation (LG) (Maxwell 1974), suggested by Bartleson (Bartleson and Grum 1984), can be used to overcome this problem and is defined as follows:

$$LG = \ln [(f+ c)/(N - f+ c)] \quad (4-1-2)$$

where N is the total number of pairs being judged, and f is the value in the frequency matrix. The c term is an arbitrary additive constant (0.5 is used here), and is used to prevent any zeros occurring in the frequency matrix.

The final step (step 4) in Table 4.6, shows how the LG values are calculated using Eqn. 4-1-2 from those in the frequency table in Step 1. Since, these values are linearly correlated to the z score values, a simple linear regression equation can be determined using a least-squares technique ($z = 0.587 LG - 5.16 \times 10^{-5}$ in this case). This equation has a correlation coefficient $r = 0.99983$, indicating an excellent agreement between the two scales. In other words, the LG function can be used to calculate z scores if there are missing figures in the z score table.

4.2.3 Spatial Uniformity of Monitor Screen

As mentioned earlier, the spatial uniformity of the monitor screen was also investigated in this evaluation. The paired comparison results from Experiment 1 were used to evaluate the monitor screen uniformity. The mean results from all observers in terms of the categories 1 to 7 for the same image presented on the left and right sides of the monitor are plotted in Fig. 4.3. For a perfect agreement (no spatial effect), all the points should lie on the 45° line. It can be seen that this is indeed the case. This implies that the spatial uniformity is insignificant for the particular Barco monitor used in this study. Similar results were also found by Berns et al. (Berns 1993). They concluded that the lack of uniformity for most monitors is below the visual system's contrast threshold to low spatial frequencies. Therefore, each pair of softcopy images was judged once or twice by randomly displaying the two images in each pair on either the right or the left side in the test of experiments. Fig. 4.3 also shows that the XYZ model performed better than the Hunt and RLAB models, i.e. the cross points (XYZ model) are located on the bottom part of the diagram representing a better performance.

4.2.4 Models' Performance

The paired comparison results in terms of the z scores with 95 % confidence limits (CL) and the category judgement mean results in terms of the scale values, for the combined six images (designated as "Total"), are summarised in Table 4.7. These z scores and scale values were calculated using all raw data from observations for six images for each model as illustrated in Tables 4.5 and 4.6 using the paired comparison and category judgement methods respectively. The CL represents two standard deviations (2σ) calculated from the z scores for each pair used. For instance, in Experiment 1, two images were compared at a time under D65 source. Thus the 95 % confidence limit is 1.39 units (i.e. $1.96/(2^{1/2})$, where 1.96 is the critical value of z under 5 % level of significant for two-tail test). The mean results with 95 % CL for using the paired comparison method are also plotted in Figs. 4.4(a) and (b) for D65 and D50 respectively, and the mean results using the category judgement method are plotted in Fig. 4.5(a) and (b) for D65 and D50 respectively. The

GW, BW, and BB represent the situations wherein the grey background with a white border, black background with a white border, and black background without a white border in the softcopy field for Experiments 1, 2 and 3 respectively. If the mean of one model overlaps another model's confidence limit (for using the paired comparison method), the two models are considered not to be significantly different. In comparison with Figs. 4.4 and 4.5, it can be seen that the ranks of three models' performance are the same. This indicates that two methods lead to same conclusion.

The results are summarised below.

- 1) The XYZ and Hunt model gave the similar performance and outperformed the RLAB model under the symmetric conditions (Experiment 1) where the grey background was used in both the hardcopy and softcopy fields.
- 2) The Hunt model gave the best predictions, XYZ second and RLAB the worst under the asymmetric conditions (Experiments 2 and 3) where the black background was used in the softcopy field while a grey background was used in the hardcopy field.
- 3) Under the asymmetric conditions, the ranking obtained using the white border was essentially the same as those obtained using without white border. i.e. the results obtained from Experiments 2 and 3 for each model were also similar.

Above results imply the following conclusions:

- there was no spatial uniformity problem with the monitor screen found from Experiment 1.
- the results from Experiment 1 show that a colorimetric match with a symmetric matching condition, where identical XYZ values are used for both the hardcopy and softcopy images, should provide a satisfactory visual match. This implies that, for the majority of the graphic arts, DTP and CAD applications using symmetric matching conditions, a simple colorimetric match is adequate.

- in comparison with the results obtained with and without a white border, the results indicate that there was very little difference between them.
- the results obtained from Experiments 2 and 3 indicate that there is a need to apply suitable surround parameters allowing for change of background colours. These parameters should be used according to different background used, not media used for viewing complex images. As found by Luo et al. (1991-1995) in their experiments using single stimuli, the models' surround parameters were greatly varied according to visual results obtained from different media. This was not found here using complex images.

From the above conclusions, it was decided that each pair of softcopy images was judged once by randomly displaying the two images' left and right positions in the main experiment. The surround parameters, N_b and δ , in the Hunt and RLAB models respectively, were set equal for both the hardcopy and softcopy fields.

4.3 MAIN EXPERIMENT

The experimental set-up was similar to that involved in the preliminary experiment. A detailed account is given below.

4.3.1 Viewing Configuration

Both simultaneous (SS) and toggled (TG) display arrangements were used in the main experiment. The experimental viewing configuration for the SS display arrangement was the same as that used in Experiment 1 of the preliminary experiment (Fig. 4.2(a)). Fig. 4.2(d) illustrates the TG visual configuration. The SS arrangement displays two images side by side (as mentioned above) whereas only one centralised image is shown for the TG arrangement. In the TG display arrangement, next to "CONTINUE" button, another button marked "TOGGLE" was also located in the lower area of the monitor for alternating between two images forming a pair. When the decision being made, the observer could click the "CONTINUE" button to proceed to the next pair in the sequence.

4.3.2 Viewing Conditions and Viewing Techniques

The experiment was divided into seven phases according to the light sources used for illuminating the hardcopies and the white points used to set up the softcopy displays. Table 4.8 summarises the differences for each phase. Nine normal colour vision observers took part in each phase. For some phases, observers assessed the same pair twice. These results were used to test observer repeatability performance. In total, 7,452 comparisons were made.

These seven phases can be further divided into two cases according to whether the same or different chromaticities of the white borders for softcopy and hardcopy images are used. As mentioned earlier, the border surrounding each image (see Figs. 4.2(a) and (d)) was used as a reference white which acted as an anchor point for chromatic adaptation purposes. The white border's and white point's colorimetric and luminance values used in the hardcopy and softcopy viewing fields for each phase are given in Table 4.9.

The Case 1 experiment was designed to investigate those softcopy and hardcopy images having the same set of chromaticities and luminance values. The grey backgrounds used in both fields had the same chromaticities as that of Experiment 1 of the preliminary experiment. Two sets of chromaticities close to those of D65 and D50 were used in Phases 1 and 2 respectively. As mentioned in Section 4.2, because the viewing conditions used in both fields were identical, the normal binocular simultaneous matching (BSM) viewing technique using the SS display (as shown in Fig. 4.1(a)) was applied. Only three colour models, XYZ, Hunt, and RLAB were evaluated in this case.

The Case 2 experiment used different sets of chromaticities for the monitor images' and hardcopies' white borders. Five phases (3 to 7) were included in this case. The TG display (Fig. 4.2(d)) was adopted for all Case 2 phases except for Phase 5 (for which the SS display was used (Fig. 4.2 (a))). Phases 5 and 6 had the same experimental conditions. The hardcopy was illuminated by a D50 source and the white border of the monitor image

was set to the chromaticity of D93. These were intended to investigate the differences between the results obtained using the SS and TG displays. For each of the Case 2 phases, all colour models except XYZ were compared. The latest versions of the Hunt and RLAB models (Hunt94 and RLAB94) were used. The surround parameters N_b and δ used in the Hunt and RLAB models respectively for the softcopy and hardcopy fields were identical, based upon the results obtained from the preliminary experiment, but the cognitive and sensory chromatic adaptation factors were differed for the hardcopy and softcopy fields. These are given in Table 4.10.

The binocular memory matching (BMM) viewing technique was adopted for all Case 2 phases. A comprehensive study was carried out by Braun and Fairchild (1994) to investigate methods for scaling the colour fidelity of complex images. They employed five different viewing techniques for comparing the standard hardcopy images with the softcopy images processed from five spaces and models. These were binocular memory, binocular successive, binocular simultaneous matching (as BSM used in Case 1 phases in this study), successive-*Ganzfeld* haploscopic matching, and simultaneous-haploscopic matching (Section 2.7.3.1). They concluded that the binocular memory matching technique gave more reliable results than the other techniques when the hardcopy's and softcopy's white borders had different colorimetric values. The decision to apply this technique was based upon their conclusions. In the current experiment, the viewing cabinet and monitor were arranged apart to ensure that observers could not view both fields at the same time. They initially looked at the hardcopy for at least 60 seconds and remembered the hardcopy image. They then turned toward the monitor showing a grey background for at least 60 seconds, and finally compared the pair of softcopy images and chose which gave a closer match to the hardcopy by toggling between two different softcopy images and ranking its quality on a 7-point category scale. The observers were allowed to look back at the hardcopy at any time. However, re-adaptation would take place for 60 seconds. (Fairchild and Reniff (1995) investigated the time required to complete adaptation when changing from one illuminant to another. They found that 90% adaptation can be achieved at a constant luminance for at least 60 seconds.)

The colorimetric and luminance values of the grey background used in the hardcopy field, together with the monitor RGB DAC values predicted by each space or model in each phase are given in Table 4.11. This table shows that, for Phases 1 and 2, the RGB DAC values predicted from the three models tested are nearly the same. The RLAB and Hunt models' RGB values slightly differed from those of XYZ model because the two models were set with cognitive and sensory chromatic adaptation mechanisms for the softcopy and hardcopy respectively. The results for Phases 3 to 7 are also nearly the same for all the models tested except the RLAB model, which is somewhat different from the others. Therefore, it was determined that the grey background on the monitor for Phases 3, 4, 6 and 7 used the XYZ values shown in Table 4.11. It was considered to be reasonable to vary the grey background for each model. The whole scene represents the overall model's performance, rather than using a fixed background for all models. For Phases 1, 2 and 5, the mean XYZ values, obtained by averaging those of grey backgrounds predicted using all colour models excluding the RLAB model, were used. This is because the SS display was used. To use a different background for viewing two screen images at the same time would produce incomplete adaptation.

The luminance levels of the borders of both the softcopy and hardcopy images for each phase were set to 64 cd/m^2 except for Phase 7 which was set to 54 cd/m^2 . This was necessary to reduce the number of out-of-gamut pixels in each image when transformed from sources A to D65. For all phases, the percentages of out-of-gamut pixels for the processed images ranged from 0% to 3%. A previous investigation had been conducted in which out of gamut pixels were identified by plotting them with a black colour on the screen. It was found that these colours did not occur in one particular image area and they had no significant effect on the appearance of the entire image.

4.4 DATA ANALYSIS

Again, both the forced-choice paired comparison and category judgement methods were employed in the main experiment. Observers viewed a pair of simultaneously (Phases 1, 2 and 5) or sequentially (Phases 3, 4, 6, and 7) displayed softcopy images and judged which

of the two gave a better match to the hardcopy using a 7-point category scale. The order of the image pair was randomised in each observing session to avoid possible trends in the comparisons as mentioned earlier.

The paired comparison results in terms of the z scores together with 95% confidence limits for each image and the six images combined for all phases are given in Appendix B. The category judgement results in terms of the scale values and boundary estimates (category boundaries) for each image and the six images combined ("Total") for all phases are given in Appendix C. As mentioned in Section 4.2.4, the z scores and scale values for "Total" using the paired comparison and category judgement methods respectively were calculated using all the raw data from observations for six images for each model in each phase. The z scores and scale values obtained using the paired comparison and category judgement methods respectively were also calculated using the raw data of each of the six individual images tested for each model in each phase.

4.5 RESULTS AND DISCUSSION

4.5.1 Observer Precision and Repeatability

The reliability of the experimental results was investigated in terms of observer precision and repeatability. The deviation between an individual's and the mean visual results (categories 1-7) representing observer precision was examined. The correlation coefficients (r) were calculated and these have been summarised in Table 4.12 for phases 1 to 7. It was found that observer precision is at its highest when larger colour temperature differences exist between the two fields (i.e. Phases 5 to 7), and at the lowest for the same colour temperature in two fields (i.e. r values of 0.28 and 0.30 for Phases 1 and 2 respectively).

The observer repeatability for Phases 1, 2 and 6 was also evaluated and is summarised in Table 4.12. In these three phases, each observer carried out the same experiment twice. The r measure was calculated between the individual's first and second results. It gave

similar results to the observer precision, i.e. a very poor repeatability performance for these phases having the same colour temperature in the two fields (r values of 0.57 and 0.46 for Phases 1 and 2 respectively), and better repeatability performance for the phase having a large colour temperature difference (0.68 for Phase 6). The performance of observer precision is better than that of observer repeatability for Phase 6 (i.e. 0.77 and 0.68 for repeatability and precision performance respectively).

4.5.2 Models' Performance

The paired comparison results will be primarily used to compare the models' performance to ease comparison. Two sets of results will also be compared at a later stage (Section 4.5.4).

The paired comparison results for "Total" (six images combined) are summarised in Table 4.13. These are also plotted in Figs. 4.6(a) and 4.6(b) for Phases 1 and 2, and 3 to 7 respectively. Additionally, for results in Phases 3 to 7, the rank order of each model's performance for each image was also determined. The average for each model's ranks over all images was then calculated and designated as "Mean Rank". These are given in Appendix D. Models that did not show a significant difference in z score were given identical ranks, i.e. a difference between models of less than 1.39 is statistically insignificant at a 95% confidence limit.

In Table 4.13 and Fig. 4.6 (a), the Phases 1 and 2 results show that all three models had similar performance, i.e. the mean of one model intersects each of the other two model's confidence limits. The two colour appearance models used here assume that an observer's cognitive and sensory mechanisms are automatically exchanged between viewing hardcopy and softcopy fields. The results do not support this theory, i.e. the two models actually performed marginally worse than the XYZ model.

The results indicate that a satisfactory visual match can be obtained by a colorimetric match (in which identical XYZ values are used for the hardcopy and softcopy images),

and it is adequate for the majority of graphic arts, DTP and CAD applications. However, for perceiving single stimuli, the results would vary largely according to different media/surround conditions as found by Luo et al. (1991-1995) and Kuo et al. (Kuo et al. 1995).

The models' performance for the experimental phases having different chromaticities for the softcopy's and hardcopy's white borders was evaluated using both "Total" (see Table 4.13 and Fig. 4.6 (b)) and "Mean Rank" (Appendix D) results. The "Total" results were used to give an overall feeling for these results obtained from all six images combined. It was considered that the "Mean Rank" results, obtained by averaging the rank order over all images tested, would give a more critical and reasonable comparison than those of "Total". These are summarised as follows:

- 1) In Phase 3, the "Total" results show the Nayatani, von Kries and Hunt models performed the best, and followed by the BFD model. The Nayatani model was slightly better than the von Kries and Hunt models. However, these differences were not statistically significant. The CIELAB and RLAB models were ranked the fifth, and the CIELUV the worst. In phase 4, the Nayatani performed the best, followed by the RLAB, von Kries, Hunt and BFD models (same rank), and the CIELAB and CIELUV the worst. The "Mean Rank" results obtained from Phases 3 and 4, indicates that the Nayatani model was superior to the other models. The BFD, Hunt and von Kries models gave the average level of predictions for Phases 3 and 4. The RLAB model gave mediocre performance in Phase 4 and it did not perform well in Phase 3.
- 3) By comparing the "Total" results, it was found that the BFD and RLAB gave better performance than the other models in Phase 5. The von Kries was ranked the second, followed by the Nayatani and Hunt, CIELAB, and CIELUV models. In Phase 6, the BFD, RLAB, and Hunt performed the best, Nayatani and von Kries third, and CIELAB and CIELUV the worst. The "Mean Rank" results clearly show

that the BFD model outperformed the other models in Phases 5 and 6. The Nayatani model gave a poorer performance for each of Phases 5 and 6 than that for each of Phases 3 and 4. However, in addition to the Hunt, von Kries and RLAB models, it gave an average level of prediction. Again, the CIELAB and CIELUV were the worst.

- 5) Both the “Total” and “Mean Rank” results from Phase 7, strongly indicate that the BFD gave the most precise predictions, followed by the von Kries model. The other models did not perform well in Phase 7. It can also be seen that the Nayatani performed much worse than the other models tested except for the CIELUV model.

The Nayatani models gave the best predictions when the colour temperatures between the hardcopy and softcopy viewing fields were close (Phases 3 and 4), but a poorer performance for each of Phases 5 to 7 with a large colour temperature difference between the two fields. This is mainly caused by the model’s overprediction of the Helson-Judd effect (Helson and Jeffers 1938, Helson 1940, Judd 1940) which results in a large hue shift and lightness change in the background. This has also been found in Luo et al’s study (1991-1995). The BFD model performed significantly better than the other models for Phase 7 which had a change in adaptation from A to D65. This agrees with those from Luo et al’s study using the Alvey Data (Section 2.7.6.1.1), and Kuo and Luo Data (Section 2.7.6.1.3) in testing chromatic adaptation transforms (see Section 2.7.6.2). All models in Phase 7, except BFD and von Kries, predicted results badly and produced a much lower colourfulness contrast for softcopy images in comparison with those of the hardcopy images. This indicates that there are problems existing in the area associated with chromatic-adaptation mechanisms in these models. It was particularly disappointing that the Hunt94 model, which has been refined using the LUTCHI Colour Appearance Data based upon single stimulus conditions, did not give the best performance. The present results, in agreement with Luo et al’s and Kuo et al’s corresponding colour data obtained using single stimuli, imply that the area associated with chromatic-adaptation mechanisms in the Hunt model needs to be further verified.

The z scores from six images combined (“Total”), evaluated using the paired comparison method for Phases 5 and 6 (given in Table 4.13), are also plotted in Fig. 4.7. It was used to give a snapshot to check whether the results vary between the SS and TG display arrangements. It shows a very slight change of models’ ranking orders and magnitudes between the same model using the SS and TG display arrangements. This inconsistency was due to each pair of the images differing only slightly in appearance. For instance in this case, the ranking orders of the Hunt and von Kries models were 3 and 5, and 5 and 3 for Phases 5 and 6 respectively while those of the other models were the same. The SS and TG viewing configurations basically made little difference to the visual results.

4.5.3 Image Dependency

It is possible that some of the models’ performance depends upon the particular image used. Kim et al. (1993) found that the models’ low to poor performance was highly image dependent. This was particularly notable for the Nayatani model. Therefore, the image dependency was also included into the investigation. The differences between the highest and the lowest z scores for each model were used to indicate the degree of image dependency. The larger the difference, the more image dependent of a model is. Table 4.14 summarises the differences for each model in each phase. These z score results for the six individual images processed using each model are also plotted in Figs. 4.8(a) and 4.8(b), and 4.9(a) to 4.9(e) for Phases 1 and 2, and 3 to 7 respectively. These figures were used to give a snapshot of the overall pattern of performance distribution and the z-score difference range for each model tested.

The results show that, in Case 1 especially for the Phase 2 using D50 (Fig. 4.8(b)), the XYZ model has the narrowest distribution range of z-score differences, while RLAB has the widest. The XYZ model not only performed the best but also had the least image dependency. In Case 2, the results shown in Figs. 4.9(a) to (d), indicate that the BFD model had the least image dependency in comparison with the other models (the narrowest range of the z-score distribution except for CIELUV). The CIELUV always

gave the worst performance leading to the least image dependency. The BFD model showed the least image dependency in comparison with the other models for almost all images, although its difference (Table 4.14) is the highest in Phase 7, and it has a wide range of z-score distribution as shown in Fig. 4.9(e).

4.5.4 Difference Between Results From Paired Comparison and Category Judgement

The last comparison was made to compare the results analysed using the paired comparison and category judgement methods. A direct comparison is not possible due to different scales for each set of results: z scores (with 95% CL) and scale values (with Category Boundary for Acceptable Match (CBAM)) for the paired comparison and category judgement respectively. It was decided to compare the best performing model in each phase, and the models' "Mean Ranks" between these two methods. The models' performance for six images combined ("Total") being evaluated using category judgement is summarised in Table 4.15. In comparison with the results using the paired comparison method (in Table 4.13), it was found that the best performing model using the category judgement method in each of seven phases is exactly the same as that using the paired comparison method.

As stated earlier, for calculating the models' individual "Mean Rank" values, the models' performance for each image in each phase (Case 2) was first ranked (given in Appendix D and E for the paired comparison and category judgement methods respectively); the individual "Mean Rank" value in each phase was then calculated across image content (for each of six images). For comparing models' performance, the individual "Mean Rank" values across the phase change for all the model were averaged to obtain the overall "Mean Rank" values, then the "Mean Rank" orders representing the models' performance were determined (shown at bottom of Table 4.16). These average "Mean Rank" values and orders for paired comparison and category judgement methods in the Case 2 experimental phases are summarised in Table 4.16. Although the individual "Mean Rank" values or orders for each model between two methods are different, the overall "Mean Rank" orders (shown at bottom of Table 4.16) are exactly the same. This

indicates that, in general, the models' performance would not be affected by the method used for analysing the results. However, inconsistency could occur for those models having very close performance. For instance, the Hunt, von Kries, and BFD models gave the similar performance for Phase 3. The ranking orders for 2 to 4 for these three models are slightly different between these two methods, i.e. von Kries, Hunt, and BFD in the paired comparison method, and von Kries, BFD, and Hunt in the category judgement respectively.

4.5.5 Image Quality of Colour Fidelity

As mentioned previously, in the experiment, the observers were instructed to judge the image quality of colour fidelity in terms of 1-7 category scale. Hence, the category results representing the image quality of colour fidelity were also evaluated. The results given in Table 4.15 and also Appendix F show that the category values, indicating the quality of colour fidelity as stated in Section 4.2.2, for those models performed the best, are at least above the lower limit of the "CBAM".

4.6 CONCLUSIONS

The results obtained here were included as part of the LUTCHI Colour Appearance Data by extending data to include that from complex images. This work closely followed CIE TC 1-27 guidelines for "coordinated research on the evaluation of reflection prints and self-luminous display image comparison". The experiment was divided into seven phases according to whether the same or different chromaticities for the hardcopy's and softcopy's reference white were used. The results, scaled using a 7-point image scale, were analysed using the paired comparison and category judgement methods. Analysis shows that the CIE XYZ system adequately predicted colour matches across media for the D65 and D50 using the same viewing conditions (as stated in Section 4.2) in both softcopy and hardcopy fields in this study. This indicates that for the majority of imaging applications, a simple colorimetric match is adequate as far as the same viewing

conditions are used in both fields. For dissimilar viewing conditions, a simple chromatic adaptation transform, BFD, gave more accurate predictions and had a greater image independency characteristic than the other models. Further work was carried out to extend the BFD transform to create a new colour appearance model. This will be described in the next chapter.

The results also reveal that the observer precision is mainly affected by the similarity of the image pairs compared. The larger the difference between images, the higher the precision occurs. This was clearly demonstrated in Phase 7, in which the colour temperatures between the hardcopy and softcopy fields were largely different. The issue of the spatial uniformity of the monitor was also examined. It was found that the effect is insignificant for tasks dealing with complex images. The results also show that no matter which display configuration is used (SS or TG), or which method is used to analyse the results (paired comparison or category judgement), the difference is very small and will not affect the conclusion. The results also reveal that, when comparing images using reference white points with closely similar colour temperatures, the observers' precision and repeatability will be reduced. Additionally, the models' performance will be very similar. This agrees with the results found by Luo et al. (1991b) using single stimuli.

Chapter 5 THE LLAB COLOUR APPEARANCE MODEL

As set out at the outset of this project, the aims of the research work were to characterise imaging devices, quantify colour appearance using complex images, and develop a reliable colour appearance model. The first two aims have been accomplished as described in Chapters 3 and 4 respectively. In this chapter, a colour appearance model named LLAB, is developed.

As mentioned in Section 2.7.6, Luo et al. (1991-1995) and Kuo et al. (1995) conducted a series of experiments to acquire the LUTCHI Colour Appearance Data. Their experiments were designed to investigate the change of colour appearance due to different viewing parameters such as illuminants, luminance levels, backgrounds, and surround conditions. These data can be considered as the most comprehensive data produced. Luo et al. (1991), and Kuo and Luo (1995) tested various chromatic adaptation transforms using the LUTCHI-Alvey, and Kuo and Luo Data Sets. Their results clearly indicate that the BFD transform gave the most precise predictions of the visual results amongst all the transforms tested. The results of BFD transform's predictive performance are shown in Figs. 5.1(a) and 5.2(a) for LUTCHI-Alvey, and Kuo and Luo data respectively. The predictions from the Hunt colour appearance model are also given in Figs. 5.1(b) and 5.2(b) for LUTCHI-Alvey and Kuo and Luo data respectively. For each figure, the experimental results are described using colour appearance representing the same colour appearance under sources simulating illuminants A and D65 plotted using the plus (+) and cross (×) symbols respectively. The predicted shift is drawn using an open circle (o). For a perfect agreement between the predicted and experimental results for each vector, the distance between the open circle and cross should be zero, or the two vectors should overlap. In comparing Figs. 5.1(a) and 5.2(a), it can be seen that the BFD transform predicts both sets of data with a similar degree of error. For example, the transform predicts well for colours in the Y, B, and RB regions for both data sets, the R, YR and GY regions for one of the data sets. Although it gives a worse prediction around the G

and BG regions, the prediction is the average of the two data sets. This indicates that much of the predictive error is due to a disagreement between the two data sets. In comparing Figs. 5.1(a), 5.2(a) and Figs. 5.1(b), 5.2(b), it can be seen that the BFD's predicted errors are much smaller than those from the Hunt model. The Hunt model gives reasonable predictions for colours between the BG to R regions. However, it also shows large systematic discrepancies in predicting colours around the YR to GY regions (much too low in chroma) no matter which data set used.

5.1 DRAWBACKS OF THE HUNT MODEL

As mentioned in Section 2.7.5.1, the Hunt colour appearance model is a comprehensive model of colour vision which adequately fits both psychophysical and physiological experimental results. It has been refined over the years using the LUTCHI data sets. However, the results in the last chapter show that the model did not perform well using complex images. The results from five phases, in which the chromaticities of the hardcopy's and softcopy's white borders were different, are summarised in Fig. 4.6(b) in terms of z scores. It shows that the Hunt model's performance was not good in comparison with the other models. The BFD chromatic adaptation transform performed the best, especially for the hardcopy under source A and softcopy's white point set to D65 conditions. This suggests that some predictive errors are occurring in the chromatic-adaptation mechanism of the Hunt colour appearance model. The BFD chromatic adaptation transform has been tested using many data sets (Lam 1985, Luo et al. 1991, Kuo et al. 1995, Lo et al. 1996) and all evidence indicates that it was superior to the other transforms.

Another drawback associated with the Hunt model is its complexity. For image processing tasks in cross-media reproduction, a reverse model is required to obtain the corresponding tristimulus values in order to reproduce colours with the same colour appearance from the source device/viewing conditions to those of destination conditions.

The reverse Hunt model is quite complicated and many parameters need to be predetermined. Additionally, the reverse model cannot be analytically expressed: a numerical approach is the only solution. For a typical complex image made up of hundreds of thousands of pixels, the processing power and calculation time required is considerable. This makes its practical application become questionable.

With this in mind, a much simpler model, LLAB, based upon the BFD chromatic adaptation transform was derived to fit the full set of LUTCHI colour appearance data. Many modelling techniques are followed those of the Hunt (1991, 1994) and RLAB (Fairchild and Berns 1993, Fairchild 1994) models.

5.2 FORMULATION OF THE LLAB MODEL

The LLAB model can be divided into two parts: the BFD chromatic adaptation transform and a modified version of CIELAB uniform colour space. The former is used to transform corresponding colours from a source illuminant to a fixed reference illuminant (D65/2°). The latter calculates perceived attributes (metrics of lightness, chroma, hue, and colour difference) similar to those of CIELAB. These attributes vary under different luminance levels, surrounds, and achromatic backgrounds. The uniform colour space is only valid under the D65/2° conditions. The two parts can be flexibly arranged according to different applications. Fig. 5.3 is a flow chart of the computational procedures of the LLAB model for predicting corresponding colours. For example, a colour needs to be reproduced from a source adapting field onto a destination adapting field. It consists of four stages:

- 1) Transform the tristimulus values ($X_s Y_s Z_s$) from the source illuminant to those ($X_r Y_r Z_r$) in the reference illuminant (D65/2°).
- 2) Compute the colour appearance attributes (L_L, A_L, B_L, C_L, h_L and H_L) under D65 illuminant and other viewing parameters under the source viewing conditions.
- 3) Calculate the corresponding tristimulus values ($X_r' Y_r' Z_r'$) under D65 illuminant and other viewing parameters under the destination viewing conditions.

- 4) Obtain the corresponding tristimulus values ($X_d Y_d Z_d$) under the destination illuminant.

The details of each stage are given below.

Data preparation

X_s, Y_s and Z_s	Tristimulus values of a test sample under the source adapting field.
X_{os}, Y_{os} and Z_{os}	Tristimulus values of the illuminant under the source adapting field.
X_{od}, Y_{od} and Z_{od}	Tristimulus values of the illuminant under the destination adapting field.
X_{or}, Y_{or} and Z_{or}	Tristimulus values of the reference illuminant in the reference adapting field, which are set equal to those for the CIE D65 illuminant/1931 Standard Colorimetric Observer (i.e. 95.05, 100.0, 108.88 for X_{or}, Y_{or} and Z_{or} , respectively).
L_{ls}, L_{ld}	Luminance of the reference whites under the source and destination adaptation fields respectively (in cd/m^2).
Y_{bs}, Y_{bd}	Luminance factor, $Y\%$, of the achromatic backgrounds under the source and destination adapting fields respectively.

Three extra parameters are required according to different viewing conditions considered. These are the Surround induction factors (i.e. F_{Ss} and F_{Sd}), the Lightness induction factors (F_{Ls} and F_{Ld}), and the Chroma induction factors (F_{Cs} and F_{Cd}) for the source and destination fields. The values which correspond to each set of viewing conditions are summarised in Table 5.1.

Stage 1. Compute the tristimulus values (X_r, Y_r, Z_r) of a test colour stimulus under the reference illuminant via the BFD chromatic adaptation transform.

$$\begin{bmatrix} L \\ M \\ S \end{bmatrix} = T \begin{bmatrix} X/Y \\ Y/Y \\ Z/Y \end{bmatrix} \quad (5-2-1)$$

$$\text{where } T = \begin{bmatrix} 0.8951 & 0.2664 & -0.1614 \\ -0.7502 & 1.7135 & 0.0367 \\ 0.0389 & -0.0685 & 1.0296 \end{bmatrix}$$

The *LMS* cone responses for the reference and source illuminants, and the test colour under the source illuminant are calculated using Eqn. 5-2-1 and are designated as (L_{or} , M_{or} , S_{or}), and (L_{os} , M_{os} , S_{os}) and (L_s , M_s , S_s) respectively.

$$\begin{aligned} L_r &= L_{or} L_s / L_{os} \\ M_r &= M_{or} M_s / M_{os} \\ S_r &= S_{or} (S_s / S_{os})^{P_s}, \text{ where } P_s = (S_{os} / S_{or})^{0.0834} \end{aligned} \quad (5-2-2)$$

$$\begin{bmatrix} X_r \\ Y_r \\ Z_r \end{bmatrix} = T^{-1} \begin{bmatrix} L_r & Y_s \\ M_r & Y_s \\ S_r & Y_s \end{bmatrix} \quad (5-2-3)$$

Stage 2. Calculate the appearance attributes: lightness (L_L), redness-greenness (A_L), yellowness-blueness (B_L), chroma (C_L), hue angle (h_L) and hue composition (H_L) under the $D65/2^\circ$ illuminant and other viewing parameters under the source adapting field.

$$L_L = 116 f(Y)^Z - 16 \quad (5-2-4)$$

$$A = 500 [f(X) - f(Y)] \quad (5-2-5)$$

$$B = 200 [f(Y) - f(Z)] \quad (5-2-6)$$

$$\text{where } z = 1 + F_{Ls} (Y_{bs} / 100)^{1/2} \quad (5-2-7)$$

If $X/95.05$, $Y/100$ or $Z/108.88 > 0.008856$

$$f(X) = (X_r / 95.05)^{1/F_{Ss}}$$

$$f(Y) = (Y_r / 100.00)^{1/F_{Ss}} \quad (5-2-8)$$

$$f(Z) = (Z_r / 108.88)^{1/F_{Ss}}$$

If $X/95.05$, $Y/100$ or $Z/108.88 \leq 0.008856$

$$f(X) = [(0.008856^{1/F_{Ss}} - 16/116)/0.008856] X_r / 95.05 + 16/116$$

$$f(Y) = [(0.008856^{1/F_{Ss}} - 16/116)/0.008856] Y_r / 100.00 + 16/116 \quad (5-2-9)$$

$$f(Z) = [(0.008856^{1/F_{Ss}} - 16/116)/0.008856] Z_r / 108.88 + 16/116$$

$$C = (A^2 + B^2)^{1/2} \quad (5-2-10)$$

$$C_L = [4.907 + 0.162 C + 10.92 \ln(0.638 + 0.07216 C)] \cdot F_{Cs} \cdot S_C \quad (5-2-11)$$

$$\text{where } S_C = 1.0 + 0.47 \log(L_{ts}) - 0.057 [\log(L_{ts})]^2 \quad (5-2-12)$$

$$h_L = \tan^{-1}(B / A) \quad (5-2-13)$$

$$A_L = C_L \cos(h_L) \quad (5-2-14)$$

$$B_L = C_L \sin(h_L) \quad (5-2-15)$$

$$H_L = H_{L1} + (H_{L2} - H_{L1})(h_L - h_{L1})/(h_{L2} - h_{L1}) \quad (5-2-16)$$

where H_{L1} is either 0, 50, 100, 150, 200, 250, 300, or 350 according to whether R, YR, Y, GY, G, BG, B or RB, respectively, is the hue composition having the nearest lower value of h_L . The values of h_L , H_L and the NCS expression are given in Table 5.2.

Stage 3. Compute the tristimulus values (X_r, Y_r, Z_r) under $D65/2^\circ$ illuminant and other viewing parameters under the destination adapting field.

If $L_L > 116 (0.008856)^{1/F_{sd}} - 16$,

$$Y_r' = 100 [(L_L + 16) / 116]^{F_{sd}/Z} \quad (5-2-17)$$

If $L_L \leq 116 (0.008856)^{1/F_{sd}} - 16$,

$$Y_r' = 100 \{ [(L_L + 16) / 116]^{1/Z} - 16/116 \} / \{ [0.008856^{1/F_{sd}} - 16/116] / 0.008856 \} \quad (5-2-18)$$

where $z = 1 + F_{Ld} (Y_{bd} / 100)^{1/2}$ (5-2-19)

$$h_L = h_{L1} + (h_{L2} - h_{L1})(H_L - H_{L1}) / (H_{L2} - H_{L1}) \quad (5-2-20)$$

where above figures can be found in Table 5.2.

$$C_L = [4.907 + 0.162 C + 10.92 \ln (0.638 + 0.07216 C)] \cdot F_{Cd} \cdot S_C \quad (5-2-11)$$

where $S_C = 1.0 + 0.47 \log (L_{ld}) - 0.057 [\log(L_{ld})]^2$ (5-2-21)

C can be obtained using a numerical method such as the Newton-Raphson (Dalton 1991). The algorithm is given as follows.

To obtain a solution of the equation $f(C) = 0$, i.e.

$$f(C) = [4.907 + 0.162 C + 10.92 \ln (0.638 + 0.07216 C)] \cdot F_{Cd} \cdot S_C - C_L = 0$$

input: C_0 (a starting value, using C value obtained under the $D65/2^\circ$ and source viewing conditions).

for $n = 0, 1, \dots$, until satisfied

$b := f(C_n)$

$c := f'(C_n)$

$C_{n+1} := C_n - (b/c)$

endloop

output: C_0, C_1, C_2, \dots : a sequence of approximations to be required solution.

(where $f'(C) = [0.162 + 0.788 / (0.638 + 0.07216 C)] \cdot F_{Cd} \cdot S_C$)

$$A = C \cos(h_L) \quad (5-2-22)$$

$$B = C \sin(h_L) \quad (5-2-23)$$

If $Y_r'/100 > 0.008856$

$$f(Y_r') = (Y_r' / 100)^{1/F_{sd}} \quad (5-2-24)$$

If $Y_r'/100 \leq 0.008856$

$$f(Y_r') = [(0.008856^{1/F_{sd}} - 16/116)/0.008856] Y_r' / 100 + 16/116 \quad (5-2-25)$$

$$f(X_r') = (A/500) + f(Y_r') \quad (5-2-26)$$

$$f(Z_r') = f(Y_r') - (B/200) \quad (5-2-27)$$

If $f(X_r') > (0.008856)^{1/F_{sd}}$

$$X_r' = 95.05 f(X_r')^{F_{sd}} \quad (5-2-28)$$

If $f(X_r') \leq (0.008856)^{1/F_{sd}}$

$$X_r' = 95.05 (f(X_r') - 16/116) / [(0.008856^{1/F_{sd}} - 16/116)/0.008856] \quad (5-2-29)$$

If $f(Z_r') > (0.008856)^{1/F_{sd}}$

$$Z_r' = 108.88 f(Z_r')^{F_{sd}} \quad (5-2-30)$$

If $f(Z_r') \leq (0.008856)^{1/F_{sd}}$

$$Z_r' = 108.88 (f(Z_r') - 16/116) / [(0.008856^{1/F_{sd}} - 16/116)/0.008856] \quad (5-2-31)$$

Stage 4. Compute the tristimulus values ($X_d Y_d Z_d$) under the destination illuminant via the BFD chromatic adaptation transform.

The same procedures as stage 1 are used. However, the input values should be changed from $X_s Y_s Z_s$, $X_{os} Y_{os} Z_{os}$, and $X_{or} Y_{or} Z_{or}$ to $X_r' Y_r' Z_r'$, $X_{or} Y_{or} Z_{or}$, and $X_{od} Y_{od} Z_{od}$, respectively. The output values $X_d Y_d Z_d$ are the tristimulus values under the destination adapting illuminant.

Calculate colour difference

$$\begin{aligned}\Delta E_L &= (\Delta L_L^2 + \Delta C_L^2 + \Delta H_L^2)^{1/2} \\ &= (\Delta L_L^2 + \Delta A_L^2 + \Delta B_L^2)^{1/2}\end{aligned}\quad (5-2-32)$$

where $\Delta L_L = L_{L,bat} - L_{L,std}$

$$\Delta A_L = A_{L,bat} - A_{L,std}$$

$$\Delta B_L = B_{L,bat} - B_{L,std}$$

$$\Delta C_L = C_{L,bat} - C_{L,std}$$

$$\Delta H_L = 2 (C_{L,bat} C_{L,std})^{1/2} \sin(\Delta h_L/2)$$

$$\Delta h_L = h_{L,bat} - h_{L,std}$$

where the LLAB coordinates with subscripts of “std” and “bat” represents those for standard and batch samples.

An example is provided by calculating a test colour’s colour appearance attributes under average, dim, and dark surrounds respectively. The input data and calculated results are summarised in Table 5.3.

5.3 THE DEVELOPMENT OF THE LLAB MODEL

The BFD chromatic adaptation transform has been proven to be the most reliable transform in predicting corresponding data sets such as the author's results in Chapter 4, Helson et al. (1952), Lam and Rigg (Lam 1985), Luo et al. (1991), and Kuo and Luo (Kuo et al. 1995). The transform considers only full chromatic adaptation (cognitive) excluding "incomplete adaptation" (sensory). This results in a "white point" remaining "white" under all illuminants. Not enough evidence was found in the tests described in Chapter 4 and in the LUTCHI data to establish a relationship for controlling the degree of adaptation. Efforts were therefore made to keep the BFD chromatic adaptation transform and to extend its function for predicting various colour appearance effects found in the LUTCHI colour appearance data. The model should reliably predict both single stimulus data and complex images.

The model includes a modified version of CIELAB to predict six appearance attributes: lightness (L_L), redness-greenness (A_L), yellowness-blueness (B_L), chroma (C_L), hue angle (h_L) and hue composition (H_L). The method for modifying CIELAB space is similar to that of the RLAB model.

The lightness, colourfulness and hue composition attributes have been consistently used in Luo et al's, and Kuo and Luo's magnitude estimation experiments. Additionally, they have been proven to be the most efficient, precise and easily understood attributes in scaling colour appearance. These attributes are all included in the LLAB model. The chroma predictor is actually a colourfulness scale capable of predicting the Hunt effect (see later).

From Luo et al's earlier results (Luo et al. 1991b) in testing the performance of various spaces and models, the CMC chroma scale in general gave quite reasonable predictions of the visual colourfulness results, and was better than those in the other models except for the Hunt model. Furthermore, the CMC scale corrects the problem of uniformity

occurring in the CIELAB space (Alman 1993, Clarke 1984, Luo and Rigg 1987b, Berns et al. 1991), which predicts much smaller differences around the neutral area than those in other areas. Hence, this scale was used to replace the C^* scale in the CIELAB space. As described in Luo et al's paper (1991a), the colourfulness scale in the LUTCHI colour appearance data was an unconstrained open-ended scale with no maximum. Therefore, the geometric mean was used to compute the mean results. These consistently showed the Hunt effect: the increase in colourfulness due to an increase in the level of luminance (Section 2.7.2.5). For comparing the visual results and C_L in Eqn. 5-2-11 (without multiplying F_{Cs} and S_C), the scaling factors were calculated. These phases were selected from the Alvey and CARISMA surface subsets of the LUTCHI data (see Section 2.7.6.1), which covered a wide range of luminance levels. The factors are summarised in Table 5.4 and are plotted in Fig. 5.4 together with the S_C function. Fig. 5.4 shows that the S_C function gives quite a reasonable fit to the visual data. In other words, this function represents the typical relationship between luminance and colourfulness found from the LUTCHI data. When testing the new scale with the visual results from the LUTCHI experiments using the monitor and transparency media, it was found that extra scaling factors were required, i.e. 1.15 and 0.95 respectively. These are named chroma induction factors (F_C) as shown in Table 5.1. Consequently, by multiplying the S_C and F_C factors (Eqn. 5-2-21) with the CMC chroma scale in the LLAB model, the scale should predict accurate colour appearance under different luminance levels and provide uniform steps in evaluating the colour difference.

The lightness scale is a modification of the L^* scale. A z function (Eqn. 5-2-19) was used. This function was derived by Hunt (1994) to formulate the change in lightness due to different Y values of the background (the lightness contrast effect). It gave quite an accurate prediction of all previous experimental results using small size stimuli (less than 4° subtended at the observer's eyes). However, this equation gave a poor performance with the Kuo and Luo data (Luo et al. 1996) using 10° samples, but the L^* scale gave an excellent prediction of the visual results. Hence, a F_L (lightness induction) factor was used to switch on and off (1 or 0 respectively) the lightness contrast effect. Further work

is required to obtain the experimental data for large size stimuli against different achromatic backgrounds.

It is well known that the luminance of the surround condition is a dominant factor affecting colour appearance. The image contrast is smaller with the dim and dark surrounds in comparison to that with an average surround. The surround induction factor, F_s (Eqns. 5-2-8 and 5-2-9), was optimised for predicting this effect. It was obtained by optimising these values to fit the LUTCHI monitor and transparency results. The F_s factors are 1/3.0, 1/3.5 and 1/4.2 and close to those suggested by Hunt (1987), i.e. 1/3.0, 1/3.75 and 1/4.5 for the average, dim and dark surrounds respectively.

The model's hue angle is identical to that of CIELAB and its hue composition is based upon the work of Derefeldt and Sahlin (1986). They established a look-up-table between the relationship of the NCS's hue compositions and CIELAB's hue angles. Only those of four unitary hues and their 50% mixtures are used in the model as shown in Table 5.2. A simple linear interpolation technique (Eqn. 5-2-16) is used to determine these two attributes.

5.4 TESTING THE LLAB MODEL'S PERFORMANCE

The LUTCHI Colour Appearance Data (Section 2.7.6) previously accumulated by Luo et al. was again used to evaluate seven uniform colour spaces and colour appearance models. In this study, the data was regrouped into seven sets (A–G) according to different viewing conditions, i.e. medium/surround, size of stimuli, light source and luminance level. The experimental conditions used in each set are summarised in Table 5.5 (see Section 2.7.6 for more details). Each set is interesting to people from different industries and research fields. For example, the CIE TC 1-27 on “Comparison between Softcopy and Hardcopy Images” is interested the results from B and C sets. The CIE TC 1-34 on “Colour Appearance Model Comparison” is interested on A, B, D and E sets (all surface colours).

In total, the seven models (described in Sections 2.2, and 2.7.5) were tested, i.e. three uniform colour spaces (CIELAB, CIELUV and CMC) and four colour appearance models (Nayatani95, Hunt94, RLAB94 and LLAB).

The LLAB model is calculated using stages 1 and 2 described in the earlier section. The tristimulus values measured under the original experimental source were first transformed using the BFD chromatic transform to those under the reference adapting field ($D65/2^\circ$). Subsequently, the L_L , C_L and H_L were calculated using the LLAB uniform colour space (stage 2).

As shown in Table 5.5, each data set is divided into a number of phases, in which each includes many test colours. For each colour, the results are presented in terms of mean visual results (lightness (L_v), colourfulness (C_v), and hue (H_v)). For obtaining mean visual results in the LUTCHI data, the geometric mean was used in the computation of colourfulness, instead of the arithmetic mean value, due to the unconstrained visual scale used to scale colourfulness. The arithmetic mean value was used for the calculation of hue and lightness. The geometric mean automatically established a basis for normalising the results of an individual's colourfulness data using a scaling factor and an exponent factor according to the Stevens's power law (see Section 2.6.1) as adopted by Bartleson (1979) and Pointer (1980). The deviation between the individual's and the mean visual results, representing corporate panel results, was investigated in terms of CV measures. The coefficient of variation, CV, was used as a statistical measure to investigate the agreement between any two sets of data, say x (individual's results) and y (mean visual results). The CV is a measure of the distance along the y axis of the points from the 45° line in the x (each observer's results), y (mean visual results) plot. It expresses the root-mean-square deviation of the distances of the points from the line as a percentage of the mean value of the set y , giving results independent of the size of the set y . In other words, it represents observer precision or the relative percentage error of individual's results compared to mean visual results. Therefore, a CV value of 20 means a 20% error of

individual from the mean. For a perfect agreement, the CV should equal zero (i.e. 0% error). The calculation of CV is defined as below.

$$CV = 100 [\sum(x_i - y_i)^2 / n]^{1/2} / \bar{y} \quad (5-5-1)$$

where n is the number of samples in x (individual's results) and y (mean visual results) sets and \bar{y} is the mean value of the y set. These mean CV results representing observers' precision are given in Table 5.6 for each of the three attributes in each data set. It can be seen that the CV values of colourfulness > lightness > hue is consistent throughout all of the data sets. It indicates that the hue is the easiest of the three attributes to scale while the colourfulness is the most difficult (about 2 to 3 times as difficult to scale as hue). The results, say in D data set, imply that for a satisfactory colour appearance model or space, it is unlikely to achieve better than a 90%, 84%, and 94% agreement for lightness, colourfulness, and hue respectively.

The method for testing each space's or model's performance is the same as those described by Luo et al. (Luo et al. 1991-1995). The computational procedures for comparing colour models' performance are given in Fig. 5.5. For different spaces and models, each colour's measurement results (x , y and L) were used to compute the lightness (L_p), chroma (C_p), and hue composition (H_p , ranging from 0 to 400) predictions. Similarly, the coefficient of variation (CV) was also used as a statistical measure to indicate the agreement between the visual results and the model's predictions for each of the three attributes.

The hue scale for each uniform colour space is intended to predict hue colour difference, not colour appearance. Thus the three colour spaces' hue scales were not evaluated. Each space or model's lightness scale runs from 0 (black) to 100 (white) having the same scale as the visual results. Hence, their predictions and visual results can be directly compared. However, their chroma scales are in different scales. These were adjusted by multiplying a mean scaling factor (SF) to bring each predicted chroma result onto the same scale as

the visual results. This method was applied to the RLAB, Hunt94, and LLAB models, but not for three uniform colour spaces which are incapable of predicting changes in colourfulness under different luminance levels. It was found that the Nayatani model's chroma scale varied greatly between different data sets so that different SFs had to be used for each set. Kuo and Luo data set was used a different reference colourfulness sample to that used in the other LUTCHI experiments. Hence, it is necessary to apply a different SF value for each space or model.

The input parameters used for each space and model for each data set could be different. These are summarised in Table 5.7. For all spaces and models, the chroma scaling factor (SF) is listed for each combination of model/set. The Hunt colour appearance model is somewhat more complicated and needs six parameters. Its lightness was calculated using either the J_p or the J scale for the 35 mm projected transparency and the other colours respectively. These scales also require a power factor, which is calculated using the function of z or z' , or fixed values for different sets (similar to the z function in the LLAB model Eqn. 5-2-4). The lightness formulae in the Hunt model are given below.

$$J = 100 (Q/Q_w)^z,$$

$$\text{where } z = 1 + (Y_b/Y_w)^{1/2},$$

except for transparencies viewed on a light box when z is replaced by z' :

$$z' = 0.36 + 1.55 (Y_b/Y_w)^{1/2},$$

and except for projected transparencies when J is replaced by J_p :

$$J_p = J'' \{1.14[1-(J''/100)^3] + (J''/100)^5\} \text{ and } J'' = 100 (Q/Q_w)^{1/2}.$$

where Q and Q_w are the brightness values for the colour considered and reference white respectively. The Y_b and Y_w are the luminance factors of the background and reference white respectively. For the Kuo and Luo's data set (E), it was found that a z value of 1.10 is needed to give the best fit to the visual results. The Helson-Judd effect in the model was removed in the calculation for the Kuo and Luo (E), and 35 mm projected slide (G) experimental sets, although it was included for the other data sets. For the RLAB model,

the D parameters allowing for the extent of adaptation, were suggested by Fairchild (1994) as 1.0, 0.0 and 0.5 for reflection, self-luminous and transparency viewing conditions.

The seven spaces and models were tested using seven data sets and the results in terms of CV value are given in Tables 5.8 to 5.14 for A to G respectively. The mean CV value for each model/set was also calculated. These are also summarised in Table 5.15 together with observer precision, which represents a single observer agreeing with the average of a group of observers as previously mentioned.

5.5 CONCLUSIONS

In Table 5.15, the results show that the Hunt94 model gave an overall better performance amongst all spaces/models tested. However, the LLAB model performed the best for hue, and second best for lightness and chroma. This implies that the LUTCHI experimental data agrees well with the NCS hue results, which is incorporated with the LLAB model. Both the Hunt and BFD models outperformed the other models by a large margin and their errors of prediction were similar to the CV values of observer precision. It is particularly encouraging that the LLAB model gave a better prediction of hue visual results than that of the Hunt model for almost all phases except for phases C10, C11 and Set G (35 mm projected transparency results). This is particularly marked for non daylight surface-colour phases (phases A-5, A-6, B-5, B-6 and E-3). As described by Luo et al. (1991a), the visual results in C10 and C11 phases had lower observer precision than the other phases due to problems in adaptation under low luminance monitor viewing conditions. Thus their results are less reliable than the other phases.

A comparison of the two models' lightness scales shows that the LLAB model performed the best in five out of seven data sets except for Sets D (CARISMA surface-colour) and G (CARISMA 35 mm projected transparency) data. It was also found by Luo et al. (1993) that the higher part of the lightness scale for the 35 mm projected transparency results,

from 85 to 100, had a sharp transition towards the reference white. This resulted in a separate Hunt94 lightness scale (J_p) which was developed specifically for predicting this set of results. However, the LLAB lightness scale still performed the second best amongst all the spaces/models tested. For predicting colourfulness results, the LLAB model performed worse than the Hunt94 model by about 3 CV units except for large surface colours (Set E) with 9 CV unit's difference.

In summary, a reliable colour appearance model has already been successfully developed. It is recommended that the LLAB colour appearance model can be applied to a wide range of applications, such as the cross-media colour reproduction, where colour appearance is to be taken into account, the prediction of metamerism and colour constancy, and the evaluation of colour rendering properties. For future work, the LLAB model should be extended to predict colour difference and other uncertain areas such as the verification of the F_L factors, by conducting experiments using large size stimuli against different achromatic backgrounds, and the investigation of the cognitive and sensory chromatic adaptation mechanisms.

Chapter 6 CONCLUSIONS

As mentioned in Chapter 1, there is a need to develop WYSIWYG colour technology for achieving accurate colour reproduction between images presented on different imaging devices. Three major aims were set in this study: to characterise monitor and printing devices, to compare colour models' performance using complex images and to develop a colour appearance model. All these aims were successfully accomplished. The major findings are summarised below.

6.1 SUMMARY OF THE MAJOR FINDINGS

In Chapter 3, a complete printing characterisation model was developed. It includes two processes: forward and reverse for XYZ to CMYK, and CMYK to XYZ respectively. The model was based on a set of 2nd-order polynomial equations (named as 2nd BPA model in the thesis). It performs better than the other models (SAE, MSAE, and 3rd-order) also developed in this study. Furthermore, the 2nd BPA model incorporating with the Grey Component Removal (GCR) technique was also derived. This automatically calculates the percentage of black ink together with the C, M and Y chromatic inks. The GCR provides both technical and economic benefits. Technical advantages include less hue shifts as a result of dot gain and density fluctuations, and neutral colours mainly produced using the black ink to avoid using conventional chromatic C, M and Y inks. The economic advantages are high image quality and less more expensive chromatic inks used in the reproduction. The model can be applied to any printing processes using C, M, Y and K process primaries. The most potential application area is the desktop publication.

In Chapter 4, a comprehensive psychophysical experiment was conducted. The aim was to compare colour models' performance between the hardcopy (illuminated using light

sources) and softcopy (displayed using a colour monitor) complex images. The experiment was divided into seven phases according to different adapting light sources and display configurations. Software was developed to carry out image processing to transform scanner images onto those displayed on a monitor via eight colour models. The results showed that for symmetric viewing conditions such as the same background, chromaticity and luminance of the reference white between the hardcopy and softcopy fields, the XYZ model gave a satisfactory results. For asymmetric conditions, the BFD chromatic adaptation transform gave the most precise prediction than the other models (CIELAB, CIELUV, von Kries, Nayatani, Hunt and RLAB). This is particularly marked when the colour temperatures used in both fields were largely differed. The experimental data is also valuable to increase the LUTCHI colour appearance data from only single stimulus to complex images.

Chapter 5 describes the development of a colour appearance model, named LLAB. As found in Chapter 4, the BFD chromatic adaptation transform gave the most precise prediction for complex images presented in hardcopy and softcopy viewing fields under asymmetric conditions. The LLAB colour appearance model is based on the BFD chromatic adaptation transform by extending its function to predict the colour appearance attributes under a wide range of viewing conditions. The model was derived to fit the most comprehensive data set to date (LUTCHI) using single stimuli. The model gave the similar degree of predictive performance to that of the state of the art colour appearance model, Hunt model. However, the Hunt model suffers its complexity making practical use in imaging industry questionable. The LLAB model is much simpler than the Hunt model, and should be applied for computer image processing to achieve high precision for cross-media colour reproduction in industry.

By combining all research results from this study, it should be able to establish a colour management framework in a computer system, which processes the input and output

images according to different media/viewing conditions, and demonstrates the advantages in using the WYSIWYG colour technology.

6.2 FUTURE WORK

For future work, more work should be carried out to make the 2nd BPA model giving more precise prediction. One method is to linearise the characterisation database using some mathematical smoothing techniques. A linearised database can correct the typical problems of poor repeatability occurring for a particular printing device and of colour measurement errors. Another approach is to include more characterisation samples having large chromatic but little black contents. This would make printing models more effective in predicting colours in these colour areas. The model should also be further tested using other printing technologies such as dye sublimation.

The LLAB colour appearance model should also be further extended to predict other colour appearance attributes, e.g. saturation, colourfulness and brightness, and to evaluate the extent of colour difference between a pair of samples. This would make the LLAB model a more comprehensive model. There is a need to clarify F_L parameter in the model, i.e. the luminance factors of neutral backgrounds affecting lightness appearance for large size samples. Further experiments are required to verify this effect.

REFERENCES

REFERENCES

- Adams, E. Q., X-Z plans in the 1931 ICI system of colorimetry, *J. Opt. Soc. Am.*, **32**, 168-173 (1942).
- Alessi, P. J., CIE guidelines for coordinated research on valuation of colour appearance models for reflection prints and self-luminous display image comparisons, Central Bureau of the CIE, *Color Res. Appl.*, **19**, 48-58 (1994).
- Alman, D. H., CIE TC 1-29 Industrial color-difference evaluation progress report, *Color Res. Appl.*, **18**, 137-139 (1993).
- Arend, L. E. and Reeves, A., Simultaneous color constancy, *J. Opt. Soc. Am.*, **3**, 1743-1751 (1986).
- Bartleson, C. J. and Grum, F., Optical Radiation Measurements Volume 5: Visual Measurement, Academic Press, Inc., 455-467 (1984a).
- Bartleson, C. J. and Grum, F., Optical Radiation Measurements Volume 5: Visual Measurement, Academic Press, Inc., 472-475 (1984b).
- Bartleson, C. J. and Grum, F., Optical Radiation Measurements Volume 5: Visual Measurement, Academic Press, Inc., 493 (1984c).
- Bartleson, C. J., A review of chromatic adaptation, *AIC Proceedings*, in *Colour 77*, Troy, NY (Billmeyer, F. W., Jr and Wyszecki, G., Eds.), 63-96, Adam Hilger, Bristol (1978).
- Bartleson, C. J., Changes in color appearance with variations in chromatic adaptation, *Color Res. Appl.*, **4**, 119-138 (1979).
- Bartleson, C. J., Comparison of chromatic-adaptation transforms, *Color Res. Appl.*, **3**, 129-136 (1978a).
- Bartleson, C. J., Factors Affecting Colour Appearance and Measurement by Psychophysical Methods, Ph.D. Thesis, The City University, London (1977).
- Bartleson, C. J., Predicting corresponding colours with changes in adaptation, *Color Res. Appl.*, **4**, 143-155 (1979).
- Berns, R. S., Alman, D., Reniff, H., L., Gnyder, G. D. and Bolonon-Rosen, M. R., Visual determination of suprathreshold color-difference tolerances using probit analysis, *Color Res. Appl.*, **16**, 297-316 (1991).

- Berns, R. S., Motta, R. J. and Gorynski, M. E., CRT colorimetry. Part I: Theory and practice, *Color Res. Appl.*, **18**, 299-314 (1993).
- Birkenshaw, J. W., Johnson, A. J. and Sunderland, B. H. W., Colour Reproduction, *Pira Report*, Appendix 2 (1985).
- Birkenshaw, J. W., Scott-Taggart, M. and Tritton, K. T., The black printer, *TAGA Proc.*, 403-429 (1986).
- Bolleston, R. and Balasubramanian, R., Accuracy of various types of Neugebauer model, *Final Program and Proceeding of the IS&T/SID Color Imaging Conference: Transforms & Transportability of Color*, 32-37 (1993).
- Boynton R. M. and Gordon J., Bezold-Brücke hue shift measured by color-naming technique, *J. Opt. Soc. Am.*, **55**, 78-86 (1965).
- Boynton, R. M. and Whitten, D. N., Visual Adaptation in monkey cones: recordings of late receptor potential, *Science*, **170**, 1423-1426 (1970).
- Braun, K. and Fairchild, M. D., Viewing environments for cross-media image comparison, *IS&T's 47th Annual Conference/ICPS*, 391-396 (1994).
- Brewer, W. L., Fundamental response functions and binocular colour matching, *J. Opt. Soc. Am.*, **44**, 207-212 (1954).
- Bruno, M. H., Four-color printing that isn't, *AMERICAN PRINTER*, 40-44 (1985).
- Burnham, R. W., Evans, R. M. and Newhall, S. M., Influence on color perception of adaptation to illumination, *J. Opt. Soc. Am.*, **42**, 597-605 (1952).
- Burnham, R. W., Evans, R. M. and Newhall, S. M., Prediction of color appearance with different adaptation illuminations, *J. Opt. Soc. Am.*, **47**, 35-42 (1957).
- CIE Proceeding 1963 (Vienna Session)*, Vol. B., 209-220 (Committee Report E-1.4.1), Bureau de la CIE, Paris (1964).
- CIE, Colorimetry, 2nd edition, CIE Publication No. 15.2, Central Bureau of the CIE (1986a).
- CIE Research Note, Method for predicting corresponding colours with a change in chromatic adaptation to illumination proposed for testing, *CIE-Jor.* **5**, No. 1, 16-18 (1986b).
- CIE, Method of measuring and specifying colour-rendering properties of light sources, Bureau Central de la CIE, Paris (1974).

- CIE, Supplement No. 2 to CIE Publication No. 15 (E-1.3.1) 1971/(TC-1.3), Bureau Central de la CIE, Paris, France (1978).
- Clapper, F. R. and Yule, J. A. C., Reproduction of color with halftone images, *TAGA Proc.*, 1-14 (1955).
- Clapper, F. R. and Yule, J. A. C., The effect of multiple internal reflection on the densities on halftone-tone printing paper, *J. Opt. Soc. Am.*, **43**, 600-603 (1953).
- Clapper, F. R., An empirical determination of half-tone colour-reproduction requirement, *TAGA Proc.*, 31-41 (1961).
- Clarke, F. J. J., McDonald, R. and Rigg, B., Modification to the JPC79 Colour-Difference Formula, *J. Soc. Dyers Col.*, **100**, 117-148 (1984).
- Cowan, W. B., An inexpensive scheme for calibration of colour monitors in terms of CIE standard coordinates, *Computer Graphics*, **17**, 2315-321 (1983).
- Dalton, B., Numerical Analysis, Longman Group UK Limited, 204-210 (1991).
- de Mattiello, M. L. F., On the exponents of saturation, *Color Res. Appl.*, **12**, 327-333 (1987).
- Derefeldt, G. and Sahlin, C., Transformation of NCS data into CIELAB colour space, *Color Res. Appl.*, **11**, 146-152 (1986).
- Eastman, A. A. and G. A. Brecher, The subjective measurement of color shift with and without chromatic adaptation, *J. Illum. Eng. Soc.*, **1**, 239-246 (1972).
- Fairchild, M. D. and Reniff, L., Time-course of chromatic adaptation for colour-appearance judgements, *J. Opt. Soc. Am.*, **A12**, 824-833 (1995).
- Fairchild, M. D., and Berns, R. S., image color-appearance specification through extension of CIELAB, *Color Res. Appl.*, **18**, 178-190 (1993).
- Fairchild, M. D., Chromatic adaptation in hard-copy/soft-copy comparison, *SPIE Proceeding*, **1912**, 47-61 (1993).
- Fairchild, M. D., Chromatic adaptation to image displays, *TAGA Proc.*, **2**, 803-824 (1992).
- Fairchild, M. D., Formulation and testing of an incomplete-chromatic-adaptation model, *Color Res. Appl.*, **16**, 243-250 (1991).
- Fairchild, M. D., Pirrotta, E. and Kim, T., Successive-*Ganzfeld* haploscopic viewing technique for color-appearance research, *Color Res. Appl.*, **19**, 214-221 (1994).

- Fairchild, M. D., Visual evaluation and evolution of the RLAB color space, *The Second IS&T/SID Color Imaging Conference: Color Science, Systems and Applications*, 9-13 (1994).
- Gentile, R. S., Walowit, E. and Allebach, J. P., A comparison of techniques for color gamut mismatch compression, *Journal of Imaging Technology*, **16**, 176-181 (1990).
- Gescheider, G. A., Psychophysics: Method, Theory, and Application, Hillsdale, NJ: Erlbaum. 2nd ed., 215-262 (1985).
- Gibson, N., The measurement of subject colour, *Optica Acta*, **14**, 219-243 (1967).
- Gill, P. E. and Murray, W., Quasi-Newton methods for unconstrained optimisation, *J. Int. Mat. Appl.*, **9**, 91-108 (1982).
- Gordon, I. E., Theories of Visual Perception, John Wiley & Sons, 30-33 (1989a).
- Gordon, I. E., Theories of Visual Perception, John Wiley & Sons, 97 (1989b).
- Grassman, H. G., Theory of component colors (1853), Sources of Color Sciences (selected and edited by David L. MacAdam), The MIT Press, 53-60 (1970).
- Guild, J., The colorimetric properties of the spectrum, *Phi. Trans. Roy. Soc.*, London, **A230**, 149-187 (1931).
- Gur, Y. and O'Donnell, F. X. D., Image quality assessment of ink-jet printer, *TAGA Proc.*, 630-641 (1987).
- Hård, A. and Sivik, L., NCS-Natural Color System: a Swedish standard for color notation, *Color Res. Appl.*, **6**, 129-138 (1981).
- Hamilton, J. F., Jr., A new ink-trap formula for newsprint, *TAGA Proc.*, 158-165 (1986).
- Helson, H. and Jeffer, V. B., Fundamental problems in color vision. II. Hue, lightness, and saturation of selective samples in chromatic illumination, *J. Exp. Psychol.*, **26**, 1-27 (1940).
- Helson, H., Fundamental problems in color vision. I. The principles governing changes in hue, saturation, and lightness of nonselective samples in chromatic illumination, *J. Exp. Psychol.*, **23**, 439-476 (1938).
- Helson, H., Judd, D. B., and Warren, M. H., Object-Color Changes from Daylight to Incandescent Filament Illumination, *Illum. Eng.*, **47**, 221-233 (1952).
- Heuberger, K. J., Jing, Z. M. and Persiev, S., Color transformations and lookup tables, *TAGA/ISCC Proc.*, **2**, 863-881 (1992).

- Hochberg, J. E., Triebel, W. and Seaman, G., Color adaptation under conditions of homogeneous visual stimulus (*Ganzfeld*), *J. Exp. Psychol.*, **41**, 153-59 (1951).
- Hunt, R. W. G. and Pointer, M. R., A colour-appearance transform for the CIE 1931 standard colorimetric observer, *Color Res. Appl.*, **10**, 165-179 (1985).
- Hunt, R. W. G., A model of colour vision for predicting colour appearance, *Color Res. Appl.*, **7**, 95-112 (1982).
- Hunt, R. W. G. and Luo, M. R., Evaluation of a model of colour vision by magnitude scalings: discussion of collected results, *Color Res. Appl.*, **19**, 27-33 (1994).
- Hunt, R. W. G., An improved predictor of colourfulness in a model of colour vision, *Color Res. Appl.*, **19**, 23-26 (1994).
- Hunt, R. W. G., Measurement of colour appearance, *J. Opt. Soc. Am.*, **55**, 1540-1551 (1965).
- Hunt, R. W. G., Procedures for using a revised colour appearance model, *J. Photo. Sci.*, **38**, 109-113 (1990).
- Hunt, R. W. G., Revised colour-appearance model for related and unrelated colours, *Color Res. Appl.*, **16**, 146-165 (1991).
- Hunt, R. W. G., The effects of daylight and tungsten light-adaptation on colour perception, *J. Opt. Soc. Am.*, **40**, 362-371 (1950).
- Hunt, R. W. G., A model of colour vision for predicting colour appearance in various viewing conditions, *Color Res. Appl.*, **12**, 297-314 (1987).
- Hunt, R. W. G., The Reproduction of Colour in Photography, Printing, and Television, 4th ed., Fountain, England (1987).
- Hunt, W. G., Specifying colour appearance, *Lighting Research & Technology*, Vol. **11** No. 4, 175-183 (1979).
- Hurvich, L. M. and Jameson, D., A psychophysical study of white. III. Adaptation as variant, *J. Opt. Soc. Am.*, **41**, 787-801 (1951).
- Ishak, I. G. H., Bouma, H. and Van Bussel, H. J. J., Subjective estimates of colour attributes for surface colours, *Vision Res.*, **10**, 489-500 (1970).
- Jackson, L. L., Undercolor removal and component replacement, *GATFWORLD*, 19-26 (1990).

- Johnson, A. J., Luo M. R., Lo, M. C., Xin J. H. and Rhodes, P. A., Aspects of colour management. Part I. Characterisation of three-colour imaging devices, *Color Res. Appl.*, **20**, 000-000 (1995a).
- Johnson, A. J., Luo M. R., Lo, M. C., Xin J. H. and Rhodes, P. A., Aspects of colour management. Part II. Characterisation of four-colour imaging devices and colour gamut compression, *Color Res. Appl.*, **20**, 000-000 (1995b).
- Johnson, A. J., Techniques for reproducing images in different media: advantages and disadvantages of current methods, *TAGA Proc.*, **2**, 739-756 (1992).
- Johnson, A. J., The application of printing specification to grey component, *TAGA Proc.*, 502-510 (1988).
- Johnson, A., J., Polychromatic colour removal evolution or revolution?, *TAGA Proc.*, 1-15 (1985).
- Judd, D. B. and Wyszecki, G., Color in Business, Science and Industry, 3rd ed., New York & Sons, 352 (1975a).
- Judd, D. B. and Wyszecki, G., Color in Business, Science and Industry, 3rd ed., New York & Sons, 352-362 (1975b).
- Judd, D. B., Appraisal of Land's work on two-primary color projections, *J. Opt. Soc. Am.*, **50**, 254-268 (1960).
- Judd, D. B., Color appearance, *Die Farbe*, **14**, 2-26 (1965).
- Judd, D. B., Hue, saturation, and lightness of surface colors with chromatic illumination, *J. Opt. Soc. Am.*, **30**, 2-32 (1940).
- Judd, D. B., Standard response functions for protanopic and deuteranopic vision, *J. Opt. Soc. Am.*, **35**, 199-221 (1945).
- Judd, D. B., Wyszecki, G., Color in Business, Science and Industry, John Wiley & Sons, 3rd ed. (1975).
- Jung, D. E., Programmed and complementary color reduction, *TAGA Proc.*, 135-150 (1984).
- Kazuo, S., Black printer UCR and UCA, *TAGA Proc.*, 402-429 (1986).
- Kim, T. G., Berns, R. S. and Fairchild, M. D., Comparing appearance models using pictorial images, *IS&T/SID Color Imaging Conference: Transforms&Transportability of Color*, 78-82 (1993).

- Kohlrusch, V. A., Zur Photometrie farbiger Lichter, *Das Licht*, **5**, 259-275 (1935).
- Kuo, W. G., Luo, M. R. and Bez, H. E., Various chromatic-adaptation transformations tested using new colour appearance data in textile, *Color Res. Appl.*, **20**, 000-000 (1995).
- Lam, K. M., Ph.D. Thesis, Metamerism and Colour Constancy, University of Bradford, (Postgraduate School of Studies in Colour Chemistry and Colour Technology) (1985).
- Lawson, C. L. and Hanson, R., Solving Least Squares Problems, Englewood Cliffs, NJ: Prentice-Hall (1974).
- Leibowitz, H., Myers, N. A. and Chinetti, P., The role of simultaneous contrast in brightness constancy, *J. Exp. Psychol.*, **50**, 15-18 (1955).
- Lo, M. C. and Luo, M. R., Models for characterizing four-primary printing devices, *J. Photo. Sci.*, **42**, 94-96 (1994).
- Lo, M. C., Luo, M. R. and Rhodes, P. A., Quantifying colour appearance. Part VI. Complex Images, *Color Res. Appl.*, **21**, 000-000 (1996).
- Luo, M. R., Johnson, Xin, A., J. H., Rhodes, P.A. and Scrivener, S. A. R., Mathematical models for characterising printing devices, *SID'92 Digest*, Boston, May, 753-756 (1992).
- Luo, M. R. and Xin, J., Methods for correlating between TSR and MS measurement results, IED CARISMA PROJECT - COLOUR APPEARANCE RESEARCH FOR INTERACTIVE SYSTEM MANAGEMENT AND APPLICATION, REPORT WP2-8 (1991).
- Luo, M. R. and Rigg, B., BFD(*l:c*) colour-difference formula Part 1 – Development of the formula, *J. Soc. Dyers. Col.*, **103**, 86-94 (1987a).
- Luo, M. R. and Rigg, B., BFD(*l:c*) colour-difference formula, Part II – Performance of the formula, *J. Soc. Dyers. Col.*, **103**, 126-132 (1987b).
- Luo, M. R. and Rigg, B., Chromaticity-discrimination ellipses for source colours, *Color Res. Appl.*, **11**, 25-42 (1986).
- Luo, M. R., Clarke, A. A., Rhodes, P. A., Schappo, A., Scrivener, S. A. R. and Tait, C., Quantifying colour appearance. Part I. LUTCHI colour appearance data, *Color Res. Appl.*, **16**, 166-180 (1991a).
- Luo, M. R., Clarke, A. A., Rhodes, P. A., Schappo, A., Scrivener, S. A. R. and Tait, C., Quantifying colour appearance. Part II. Testing colour models performance using LUTCHI colour appearance data, *Color Res. Appl.*, **16**, 181-197 (1991b).

- Luo, M. R., Gao, X. W. and Scrivener, S. A. R., Quantifying colour appearance. Part V. Simultaneous contrast, *Color Res. Appl.*, **20**, 18-28 (1995).
- Luo, M. R., Lo, M. C. and Kuo, W. G., The LLAB colorimetric model, *Color Res. Appl.*, **21**, 000-000 (1996).
- Luo, M. R., Gao, X. W., Rhodes, P. A., Xin, J. H., Clarke, A. A. and Scrivener, S. A. R., Quantifying colour appearance. Part III. Supplementary LUTCHI colour appearance data, *Color Res. Appl.*, **18**, 98-113 (1993a).
- Luo, M. R., Gao, X. W., Rhodes, P. A., Xin, J. H., Clarke, A. A. and Scrivener, S. A. R., Quantifying colour appearance. Part IV. Transmissive media, *Color Res. Appl.*, **18**, 191-209 (1993b).
- Luo, M. R., Johnson, A. J., Xin, J. H., Rhodes, P. A. and Scrivener, S. A. R., Mathematical models for characterizing printing devices, *SID'92 Digest*, Boston, May, 753-756 (1992).
- Luo, M. R., Xin, J. H., Rhodes, P. A., Scrivener, S. A. R. and MacDonald, L. W., Studying the performance of high resolution colour displays, *CIE 22nd SESSION—Division I*, Melbourne, 97-100 (1991c).
- MacAdam, D. L., Chromatic Adaptation, *J. Opt. Soc. Am.*, **46**, 500-513 (1956).
- MacAdam, D. L., A nonlinear hypothesis for chromatic adaptation, *Vision Res.*, **1**, 9-40 (1961).
- MacAdam, D. L., Chromatic adaptation. II. Nonlinear hypothesis, *J. Opt. Soc. Am.*, **53**, 1441-1445 (1963).
- MacAdam, D. L., Uniform color scales, , *J. Opt. Soc. Am.*, **64**, 1691-1702 (1974).
- MacDonald, L. W., Johnson, A. J. and Luo, M. R., Four stage transform, British Patent No: 9005030.3, Crosfield Electronics Limited, March (1990).
- Mackay, D. M., Psychophysics of perceived intensity: a theoretical basis for Fechner's and Stevens' laws, *Science*, **139**, 1213-1216 (1963).
- Maier, T. O. and Rinehart, C. E., Design Criteria for an Input Colour Scanner Evaluation Test Object, *J. Photo. Sci.*, **38**, 169-172 (1990).
- Maxwell, A. E., The logistic transformation in the analysis of paired-comparison data, *Br. J. Mach. Statist. Psychol*, **27**, 62-71 (1974).

- McBurney, D. H., Experimental Psychology, Wadsworth Publishing Company, 2nd edition, 94-95 (1990).
- McCann, J. J., Mckee, S. P., and Taylor, T. H., Quantitative studies in retinex theory: a comparison between theoretical predictions and observer responses to the "colour mondrian" experiments, *Vision Res.*, **16**, 445-458 (1976).
- McDonald, R, Industrial pass/fail colour matching Part I—Preparation of visual colour-matching data, *J. Soc. Dyers Col.*, **96**, 372-376 (1980a).
- McDonald, R, Industrial pass/fail colour matching Part III—Development of a pass/fail for use with instrumental measurement of colour difference, *J. Soc. Dyers Col.*, **96**, 486-496 (1980b).
- Molla, R. K., Electronic Color Separation, R. K. Printing & Publishing Company, 140-142 (1988a).
- Molla, R. K., Electronic Color Separation, R. K. Printing & Publishing Company, 146-149 (1988b).
- Molla, R. K., Electronic Color Separation, R. K. Printing & Publishing Company, 216-223 (1988c).
- Mori, L., Sobagaki, H., Komatsubara, H. and Ikeda, K., Field trials on CIE chromatic adaptation formula, *CIE Proceeding 22nd Session*, Melbourne, Vol. 1, Part 1, Division 1, 55-58 (1991).
- Morley, D. I., Munn, R. and Billmeyer, F. W., Jr., Small and moderate colour differences : II The Morley data, *J. Soc. Dyers Col.*, **91**, 229-242 (1975).
- Mosteller, F., Remarks on the method of paired comparisons: I. The least square solution, assuming equal standard deviations and equal correlations, *Psychometrika*, **16**, 3-6 (1951).
- Murray, A., Monochrome reproduction in photoengraving, *J. Franklin Inst.*, **221**, 721-744 (1936).
- Nayatani, Y., Hashimoto, K., Takahama, K. and Sobagaki, H., A nonlinear colour-appearance model using Estéves-Hunt-Pointer primaries, *Color Res. Appl.*, **12**, 231-242 (1987a).
- Nayatani, Y., Hashimoto, K., Takahama, K. and Sobagaki, H., Whiteness-blackness and brightness response in a nonlinear colour-appearance model, *Color Res. Appl.*, **12**, 121-127 (1987b).

- Nayatani, Y., Revision of chroma and hue scales of a nonlinear color-appearance model, *Color Res. Appl.*, **20**, 143-155 (1995a).
- Nayatani, Y., Sobagaki, H. and Hashimoto, K., Lightness dependency of chroma scales of a nonlinear color-appearance model, *Color Res. Appl.*, **20**, 156-167 (1995b).
- Nayatani, Y., Takahama, K. and Sobagaki, H. and Hirono, H., On exponents of a non-linear model of chromatic adaptation, *Color Res. Appl.*, **7**, 34-45 (1982).
- Nayatani, Y., Takahama, K. and Sobagaki, H., Formulation of non-linear model of chromatic adaptation, *Color Res. Appl.*, **6**, 161-171 (1981).
- Nayatani, Y., Takahama, K. and Sobagaki, H., Prediction of colour appearance under various adapting conditions, *Color Res. Appl.*, **11**, 62-71 (1986).
- Nayatani, Y., Takahama, K., Sobagaki, H. and Hashimoto, K., Colour-appearance model and chromatic-adaptation transform, *Color Res. Appl.*, **15**, 210-221 (1990).
- Nayatani, Y., Yamanaka, T., Sobagaki, H., Subjective estimation of colour attributes for surface colour, Part I: Reproducibility of estimations, *Acta Chromatica*, **2**, 129-138 (1972).
- Nemcsics, A., Colour Dynamics-Environmental Colour Design, Akadémiai Kiadó, Budapest, 44-45 (1993).
- Neugebauer, H. E. J., Die Theoretischen Grundlagen des Mehrfarbendruckes, *Zeitschrift wissenschaften photograph*, **36**, 73-89 (1937).
- Newhall, S. M., Burnham, R. W., and Clark, J. R., Comparison of successive with simultaneous color matching, *J. Opt. Soc. Am.*, **47**, 43-56 (1957).
- Newhall, S. M., Nickerson, D. and Judd, D. B., Final report of the O.S.A. Subcommittee on the spacing of the Munsell colors, *J. Opt. Soc. Am.*, **33**, 385-418 (1943).
- Padgham, C. A. and Rowe, S. C. H., A mass colour scaling experiment, in *Colour 73*, Adam Hilger, London, 393-398 (1973).
- Padgham, C. A. and Saunders, J. E., The Perception of Light and Colour, London, G. Bell & Sons Ltd., London, 135-137 (1975a).
- Padgham, C. A. and Saunders, J. E., The Perception of Light and Colour, London, G. Bell & Sons Ltd., London, 137-140 (1975b).

- Pearson, D. E., Rubinstein, C. B. and Spivack, G. J., Comparison of perceived color in two-primary computer-generated artificial images with predictions based on the Helson-Judd Formulation, *J. Opt. Soc. Am.*, **59**, 644-658 (1969).
- Pearson, M. L., The use of the color gamut of an ink set in the selection of process inks, *TAGA Proc.*, 59-74 (1964).
- Pobboravsky, I. and Pearson, M. L., Computation of dot areas required to match a colorimetrically specified color using the modified Neugebauer equations, *TAGA Proc.*, 65-77 (1972).
- Pobboravsky, I., Methods of computing ink amounts to produce a scale of neutrals for photomechanical reproduction, *TAGA Proc.*, 10-34 (1966).
- Pointer, M. R., Ensell, J. S. and Bullock, L. M., Grid for assessing colour appearance, *Color Res. Appl.*, **2**, 131-136 (1977).
- Pointer, M. R., The concept of colourfulness and its use for deriving grids for assessing colour appearance, *Color Res. Appl.*, **5**, 99-107 (1980).
- Post, D. L. and Calhoun, C. S., An Evaluation of methods for producing desired colours on CRT monitors, *Color Res. Appl.*, **14**, 172-186 (1989).
- Press, W. H., Teukolsky, S. A., Vetterling, W. T. and Flannery, B. P., Numerical Recipes in FORTRAN- The Art of Scientific Computing, 2nd Edition, Cambridge University Press, 51-63 (1992).
- Reiter, C., Computer calculated optimum black printer, *TAGA Proc.*, 123-134 (1984).
- Rhodes, P. A., Scrivener, S. A. R. and Luo, M. R., ColourTalk—a system for colour communication, *Display*, **13**, 89-96 (1992).
- Richter, M., The official German standard color chart, *J. Opt. Soc. Am.*, **45**, 223-227 (1955).
- Robertson, A. R., The CIE 1976 color-difference formulas: clarification concerning usage, *J. Opt. Soc. Am.*, **2**, 7-11 (1977).
- Rolleston, R. and Balasubramanian, R., Accuracy of various types of Neugebauer model, *IS&T and SID's Colour Imaging Conference: Transforms & Transportability of color*, 32-37 (1993).
- Rowe, S. C. H., The subjective scaling of hue and saturation, in *Colour 73*, Adam Hilger, London, 391-393 (1973).

- Roynton, R. M. and Whitten, D. N., Visual adaptation in monkey cones: recording of late receptor potentials, *Science*, **170**, 1423-1426 (1970).
- Seim, T. and Valberg, A., Toward a uniform colour space: a better formula to describe the Munsell and OSA colour scales, *Color Res. Appl.*, **11**, 11-24 (1986).
- Sobagaki, H., Takahama, K., Yamanaka, T., Nishimoto, A. and Nayatani, Y., A study on chromatic adaptation by the subjective-estimation method, Proceeding, London, *18th session of CIE* (1975), Publication CIE No. 36, Bureau Central de la CIE, Paris (1976).
- Sobagaki, H., Yamanaka, T., Takahama, K. and Nayatani, Y., Chromatic-adaptation study by subjective-estimation method, *J. Opt. Soc. Am.*, **64**, 743-749 (1974).
- Southworth, M. F., The black printer, *The Quality Control Scanner*, **V10**, N2 (1990).
- Stearns, E. I., Calculation of tristimulus values and weights with the revised CIE recommendations, *Textile Color Col. Chemist and Colorist*, **53**, 162-168 (1985).
- Stearns, E. I., Weights for calculation of tristimulus values, *Clemson University Review of Industrial Management and Textile Science*, **14**, 79-112 (1975).
- Stevens, J. C. and Stevens, S. S., Brightness function: effects of adaptation, *J. Opt. Soc. Am.*, **53**, 375-385 (1963).
- Stevens, J. C. and Stevens, S. S., Brightness function: parametric effects of adaptation and contrast, *J. Opt. Soc. Am.*, **50**, 1139 (1960).
- Stevens, S. S. and Galanter, E. H., Ratio scales and category scales for a dozen perceptual continua, *J. Exp. Psychol.*, **54**, 377-411 (1957).
- Stevens, S. S., Measurement and man, *Science*, **127**, 383-389 (1958).
- Stevens, S. S., On the psychological law, *The Psychological Review*, **64**, 153-181 (1957).
- Stevens, S. S., To honor Fechner and repeal his law, *Science*, **133**, 80-86 (1961).
- Stokes, M. D. Fairchild and R. S. Berns, Precision requirements for digital color reproduction, *ACM Transaction on Graphics*, **11**, 406-422 (1992).
- Stone, M. C., Cowan, W. B. and Beatty, J. C., Color gamut mapping and the printing of digital color images, *ACM Transaction Graphics*, **7**, 249-292 (1988).
- Sturge, J. M., Walworth, V. and Shepp, A., Imaging Processes and Materials, Van Norstrand Reinhold, 250-251 (1989a).

- Sturge, J. M., Walworth, V. and Shepp, A., Imaging Processes and Materials, Van Norstrand Reinhold, 379-384 (1989b).
- Terstiege, Chromatic adaptation: A state-of-the-art report, *J. Col. & Appear.*, **1**, 19-23 (1972).
- Thomas, F. H., Dimmick, F. L. and Luria, S. M., A study of binocular colour mixture, *Vision Res.*, **1**, 108-120 (1961).
- Thurstone, L. L., A law of comparative judgement, *Psychological Review*, **34**, 273-286 (1927).
- Torgerson, W. S., Theory and Methods of Scaling, John Wiley & Sons, 159-246 (1958).
- Treisman, M., What do sensory scales measure?, *Quarterly J. of Experimental Psychology*, **16**, 387-391 (1964).
- Valois, R. L. D. and Walraven, J., Monocular and binocular aftereffects of chromatic adaptation, *Science*, **155**, 463-465 (1967).
- Viggiano, J. A. S., Color matching functions for observers of arbitrarily sized targets, *TAGA Proc.*, 56-64 (1984).
- Viggiano, J. A. S., Modeling the color of multi-colored halftone, *TAGA Proc.*, 44-62 (1990).
- Viggiano, J. A. S., The color of halftone tint, *TAGA Proc.*, 647-661 (1985).
- von Helmholtz, H., Physiological optics (1866), Sources of Color Sciences (selected and edited by David L. MacAdam), The MIT Press, 84-100 (1970).
- von Helmholtz, H., Theory of component colors (1866), Sources of Color Sciences (selected and edited by David L. MacAdam), The MIT Press, 84-100 (1970).
- von Kries, J., Chromatic adaptation (1902), Sources of Color Sciences (selected and edited by David L. MacAdam), The MIT Press, 109-119 (1970).
- von Kries, J., Contribution to the physiology of visual sensations (1878), Sources of Color Sciences (selected and edited by David L. MacAdam), The MIT Press, 101-108 (1970).
- von Kries, J., Influence of adaptation on the effects produced by luminous stimuli (1905), Sources of Color Sciences (selected and edited by David L. MacAdam), The MIT Press, 109-119 (1970).

- Wassef, E. G. T., Application of the binocular matching method to the study of the subjective appearance of surface colours, *Optica Acta*, **2**, 144-150 (1955).
- Wassef, E. G. T., Investigations into the theory of prediction of the appearance of colours and its bearing on the theory of colour vision, *Optica Acta.*, **5**, 101-110 (1958).
- Wassef, E. G. T., Linearity of the relationship between the tristimulus values of corresponding colours seen under different conditions of chromatic adaptation, *Optica Acta*, **6**, 378-386 (1959).
- Wright, W. D., A re-determination of the trichromatic coefficients of the spectral colours, *Trans. Opt. Soc.*, **30**, 141-164 (1928-1929).
- Wright, W. D., Why and how chromatic adaptation has been studied, *Color Res. Appl.*, **6**, 147-152 (1981).
- Wyszecki, G. and Stiles, W. S., Color Science: Concept and Methods, Quantitative Data and Formulae, 1st ed., John Wiley & Sons, 429 (1967).
- Wyszecki, G. and Stiles, W. S., Color Science: Concept and Methods, Quantitative Data and Formulae, 2nd ed., John Wiley & Sons, 228-235 (1982a).
- Wyszecki, G. and Stiles, W. S., Color Science: Concept and Methods, Quantitative Data and Formulae, 2nd ed., John Wiley & Sons, 410 (1982b).
- Wyszecki, G. and Stiles, W. S., Color Science: Concept and Methods, Quantitative Data and Formulae, 2nd ed., John Wiley & Sons, 429-432 (1982c).
- Wyszecki, G. and Stiles, W. S., Color Science: Concept and Methods, Quantitative Data and Formulae, 2nd ed., John Wiley & Sons, 506-513 (1982d).
- Wyszecki, G. and Stiles, W. S., Color Science: Concept and Methods, Quantitative Data and Formulae, 2nd ed., John Wiley & Sons, 582-583 (1982e).
- Young, T., On the theory of light and colors, *Philosophical Transaction of the Royal Society of London*, **92**, 12-49 (1802).
- Yousif, W. S. and Luo, M. R., An image process for achieving WYSIWYG Colour, *IMACS '91, 13th World Congress on Computation and Applied Mathematics*, **4**, 1841-1843 (1991).
- Yule, J. A. C. and Colt, R. S., Colorimetric investigations in multi-colour printing, *TAGA Proc.*, 77-82 (1951).

- Yule, J. A. C. and Nielsen, W. J., The penetration of light into paper and its effect on halftone reproduction, *TAGA Proc.*, 65-76 (1951).
- Yule, J. A. C., Principle of Colour Reproduction, John Wiley & Sons, 205-232 (1967a).
- Yule, J. A. C., Principle of Colour Reproduction, John Wiley & Sons, 230-231 (1967b).
- Yule, J. A. C., Principle of Colour Reproduction, John Wiley & Sons, 275-277 (1967c).
- Yule, J. A. C., Principle of Colour Reproduction, John Wiley & Sons, 282 (1967d).
- Yule, J. A. C., The theory of subtractive colour photography; I. The conditions for perfect colour rendering, *J. Opt. Soc. Am.*, **28**, 419-430 (1938).

COLOUR PLATE

COLOUR PLATE

Colour Plate I six images: 'art', 'golf', 'girl2', 'girl1', 'musicians', and 'flight' (from top right to bottom left) selected for testing colour models' performance.



TABLES

Table 2.1 Summary of the experimental phases (the Alvey Colour Appearance Data Set).

Phase	Light Source	Luminance (cd/m ²)	Background	Mode	No. of Colours	No. of Observer	No. of Estimations
1	D50	264.0 (High)	White	NL	105	6	1890
2	D50	252.0 (High)	Grey	NL	105	6	1890
3	D50	252.0 (High)	Black	NL	105	6	1890
4	D50	44.0 (Low)	White	NL	105	6	1890
5	D50	42.0 (Low)	Grey	NL	105	6	1890
6	D50	42.0 (Low)	Black	NL	105	6	1890
7	D50	40.0 (Low)	White	L	94	6	1692
8	D50	44.5 (Low)	Grey	L	100	6	1800
9	D50	44.5 (Low)	Black	L	100	6	1800
10	D50	44.5 (Low)	Grey/WB	L	100	6	1800
11	D50	44.5 (Low)	Grey/BB	L	100	6	1800
12	D65	243.0 (High)	Grey	NL	105	7	2205
13	D65	40.5 (Low)	Grey	NL	105	7	2205
14	D65	40.5 (Low)	Grey	L	103	7	2163
15	D65	40.5 (Low)	Grey/WB	L	103	7	2163
16	WF	252.0 (High)	Grey	NL	105	6	1890
17	WF	42.0 (Low)	Grey	NL	105	6	1890
18	WF	28.4 (Low)	Grey	L	86	7	1806
19	WF	28.4 (Low)	Grey/WB	L	86	7	1806
20	A	232.0 (High)	Grey	NL	105	7	2205
21	A	42.0 (Low)	Grey	NL	105	7	2205
22	A	20.3 (Low)	Grey	L	61	7	1281
23	A	20.3 (Low)	Grey/WB	L	61	7	1281
Total Number					2254		43,332
No. of Observers Used in the Experiment						10	

Note:

WB: White Border BB: Black Border
L: Monitor (Luminous) NL: Surface (Non-Luminous)

Table 2.2 Summary of the experimental phases (the CARISMA Colour Appearance Data–Surface Data Set).

Phase	Light Source	Luminance (cd/m ²)	Y% Background	Scale Attributes	No. of Colours	No. of Observer	No. of Estimations
1	D50	843.1	21.8	L, C, H*	40	4	480
2	D50	200.3	22.5	L, C, H	40	4	480
3	D50	61.9	23.4	L, C, H	40	4	480
4	D50	16.6	22.3	L, C, H	40	4	480
5	D50	6.2	23.2	L, C, H	40	4	480
6	D50	0.4	19.2	L, C, H	40	4	480
7	D50	843.1	21.8	B, C, H*	40	4	480
8	D50	200.3	22.5	B, C, H	40	4	480
9	D50	61.9	23.4	B, C, H	40	4	480
10	D50	16.6	22.3	B, C, H	40	4	480
11	D50	6.2	23.2	B, C, H	40	4	480
12	D50	0.4	19.2	B, C, H	40	4	480
Total Number					480		5,760
No. of Observers Used in the Experiment						4	

Note:

L, C, H: Stand for Lightness, Colourfulness, and Hue

B, C, H: Stand for Brightness, Colourfulness, and Hue

Table 2.3 Summary of the experimental phases (the CARISMA Colour Appearance Data–LT Data Set).

Phase	Light Source	Luminance (cd/m ²)	Y% Background	Border	No. of Colours	No. of Observer	No. of Estimations
1	D50	2259 (High)	15.9	White	98	7	2058
2	D50	689 (Medium)	17.1	White	98	8	2352
3	D50	325 (Low)	16.7	White	98	7	2058
4	D50	670 (Medium+F)	17.4	White	98	7	2058
5	D50	1954 (High)	9.6	Black	98	8	2352
6	D50	619 (Medium)	9.5	Black	98	7	2058
7	D50	319 (Low)	9.8	Black	98	8	2352
8	D50	642 (Medium+F)	9.4	Paper	98	8	2352
9	D50	658 (Medium)	9.6	White	98	7	2058
10	D50	680 (Medium)	17.5	Black	98	7	2058
Total							21,748

Note:

F: Flare

Table 2.4 Summary of the experimental phases (the CARISMA Colour Appearance Data-35mm Data Set).

Phase	Light Source	Luminance (cd/m ²)	Y% Background	Viewing Pattern	No. of Colours	No. of Observer	No. of Estimations
1	Halogen (4000 K)	113 (High)	18.88	1*	99	6	1782
2	Xenon (5600 K)	47 (Low)	19.18	1	99	6	1782
3	Halogen (4000 K)	45 (Low)	18.91	1	99	6	1782
4	Halogen (4000 K)	113 (High)	18.88	1	99	6	1782
5	Halogen (4000 K)	75(Medium)	16.00	2*	95	5	1425
6	Halogen (4000K)	75(Medium)	16.00	2	36	5	540
Total							9093

Note:

Viewing Pattern 1: the reference white, the reference colourfulness, and test colours are placed at the same angular distance from the center of the projected image (i.e. placed closely in the centre triangle).

Viewing Pattern 2: the spatial arrangement of the reference white is further away from the test colours.

Table 2.5 Summary of the experimental phases (the Kuo and Luo Colour Appearance Data Set).

Phase	Light Source	Luminance (cd/m ²)	Y% Background	No. of Colours	No. of Observer	No. of Estimations
1	D65 (6461 K)	250	16	240	5	3600
2	TL84 (4019 K)	540	16	239	5	3585
3	A (2544 K)	250	16	239	5	3585
Total						10,770

Table 3.1 The D_r , D_g , and D_b for each colour in the 120 data set (IRIS device).

FDA _k = 0	No	D _{r3c}	D _{rk}	D _{g3c}	D _{gk}	D _{b3c}	D _{bk}
	1	.07843	.00000	.07978	.00000	.05661	.00000
	2	.13585	.00000	.14723	.00000	.10756	.00000
	3	.18921	.00000	.19589	.00000	.15807	.00000
	4	.26379	.00000	.26821	.00000	.20529	.00000
	5	.35829	.00000	.37349	.00000	.29215	.00000
	6	.41825	.00000	.43368	.00000	.35587	.00000
	7	.51782	.00000	.54624	.00000	.44432	.00000
	8	.60444	.00000	.62814	.00000	.53918	.00000
	9	.75361	.00000	.76623	.00000	.68975	.00000
	10	.99397	.00000	.99473	.00000	.85176	.00000
FDA _k = 10	No	D _{r4c}	D _{rk}	D _{g3c}	D _{gk}	D _{b3c}	D _{bk}
	11	.12986	.05353	.12667	.05338	.10507	.05076
	12	.18255	.05353	.19131	.05338	.15765	.05076
	13	.24165	.05353	.24774	.05338	.21329	.05076
	14	.31416	.05353	.31529	.05338	.25769	.05076
	15	.40448	.05353	.41245	.05338	.33629	.05076
	16	.46068	.05353	.47183	.05338	.39708	.05076
	17	.56158	.05353	.58502	.05338	.49104	.05076
	18	.64775	.05353	.66744	.05338	.58275	.05076
	19	.79424	.05353	.80387	.05338	.72711	.05076
	20	1.02253	.05353	1.02138	.05338	.88212	.05076
FDA _k = 20	No	D _{r4c}	D _{rk}	D _{g3c}	D _{gk}	D _{b3c}	D _{bk}
	21	.20787	.13070	.20369	.12909	.18252	.12820
	22	.25210	.13070	.25120	.12909	.22487	.12820
	23	.30606	.13070	.30417	.12909	.28556	.12820
	24	.39361	.13070	.39189	.12909	.33275	.12820
	25	.47096	.13070	.47404	.12909	.39608	.12820
	26	.51870	.13070	.52584	.12909	.45978	.12820
	27	.62363	.13070	.64198	.12909	.55513	.12820
	28	.70684	.13070	.72164	.12909	.64341	.12820
	29	.84961	.13070	.85532	.12909	.78293	.12820
	30	1.07362	.13070	1.07015	.12909	.93069	.12820
FDA _k = 30	No	D _{r4c}	D _{rk}	D _{g3c}	D _{gk}	D _{b3c}	D _{bk}
	31	.28710	.20860	.28007	.20519	.26091	.20536
	32	.31450	.20860	.31311	.20519	.28658	.20536
	33	.37418	.20860	.36823	.20519	.35378	.20536
	34	.45459	.20860	.44607	.20519	.40233	.20536
	35	.53719	.20860	.53133	.20519	.46766	.20536
	36	.57899	.20860	.57820	.20519	.53073	.20536
	37	.68817	.20860	.70063	.20519	.62692	.20536
	38	.76639	.20860	.77728	.20519	.70485	.20536
	39	.90398	.20860	.90604	.20519	.80361	.20536
	40	1.11892	.20860	1.11212	.20519	.97700	.20536
FDA _k = 40	No	D _{r4c}	D _{rk}	D _{g3c}	D _{gk}	D _{b3c}	D _{bk}
	41	.39394	.32389	.37952	.31715	.36704	.32211
	42	.43099	.32389	.42311	.31715	.41353	.32211
	43	.49059	.32389	.47563	.31715	.46815	.32211
	44	.56631	.32389	.54982	.31715	.50758	.32211
	45	.63766	.32389	.62268	.31715	.56224	.32211
	46	.67899	.32389	.66705	.31715	.62799	.32211
	47	.77896	.32389	.78244	.31715	.71858	.32211
	48	.85204	.32389	.85318	.31715	.79226	.32211
	49	.98299	.32389	.97726	.31715	.91058	.32211
	50	1.17491	.32389	1.16389	.31715	1.03519	.32211
FDA _k = 50	No	D _{r4c}	D _{rk}	D _{g3c}	D _{gk}	D _{b3c}	D _{bk}
	51	.51330	.44403	.49384	.43282	.48732	.44157
	52	.55649	.44403	.54161	.43282	.53489	.44157
	53	.60283	.44403	.58545	.43282	.58753	.44157
	54	.67917	.44403	.66162	.43282	.62995	.44157
	55	.74447	.44403	.72858	.43282	.67577	.44157
	56	.77733	.44403	.76711	.43282	.72452	.44157
	57	.87005	.44403	.86956	.43282	.80983	.44157
	58	.94073	.44403	.94083	.43282	.88130	.44157
	59	1.05798	.44403	1.04866	.43282	.98666	.44157
	60	1.23074	.44403	1.21732	.43282	1.09173	.44157

Table 3.1 The D_r , D_g , and D_b for each colour in the 120 data set (IRIS device).
(continued)

$FDA_k = 60$	No.	D_{r4c}	D_{rk}	D_{g4c}	D_{gk}	D_{b4c}	D_{bk}
	61	.60670	.54740	.58572	.53209	.58484	.54443
	62	.66012	.54740	.64093	.53209	.63406	.54443
	63	.70215	.54740	.68089	.53209	.68353	.54443
	64	.76742	.54740	.74928	.53209	.72788	.54443
	65	.83012	.54740	.81149	.53209	.76946	.54443
	66	.85876	.54740	.84436	.53209	.80847	.54443
	67	.94222	.54740	.93818	.53209	.88307	.54443
	68	1.00937	.54740	1.00447	.53209	.94914	.54443
	69	1.12533	.54740	1.11242	.53209	1.05066	.54443
	70	1.27986	.54740	1.26453	.53209	1.14235	.54443
$FDA_k = 70$	No.						
	71	.76765	.70048	.74087	.67976	.74704	.69566
	72	.80874	.70048	.78533	.67976	.78145	.69566
	73	.84892	.70048	.82332	.67976	.82423	.69566
	74	.89730	.70048	.87162	.67976	.85742	.69566
	75	.96170	.70048	.94243	.67976	.90983	.69566
	76	1.00077	.70048	.98039	.67976	.94704	.69566
	77	1.07027	.70048	1.06022	.67976	1.00551	.69566
	78	1.12778	.70048	1.11625	.67976	1.06092	.69566
	79	1.21663	.70048	1.20015	.67976	1.13820	.69566
	80	1.33177	.70048	1.31534	.67976	1.20011	.69566
$FDA_k = 80$	No.						
	81	.88843	.83413	.85962	.80937	.86644	.82626
	82	.92324	.83413	.89806	.80937	.89284	.82626
	83	.97254	.83413	.94412	.80937	.93988	.82626
	84	1.02032	.83413	.99022	.80937	.97638	.82626
	85	1.07608	.83413	1.05297	.80937	1.02266	.82626
	86	1.09912	.83413	1.07565	.80937	1.04299	.82626
	87	1.15437	.83413	1.14215	.80937	1.08717	.82626
	88	1.20415	.83413	1.19148	.80937	1.13594	.82626
	89	1.28595	.83413	1.26902	.80937	1.20457	.82626
	90	1.39658	.83413	1.38039	.80937	1.26226	.82626
$FDA_k = 90$	No.						
	91	1.05306	.98594	1.02082	.95804	1.02583	.97278
	92	1.08302	.98594	1.05393	.95804	1.04581	.97278
	93	1.12290	.98594	1.09148	.95804	1.08257	.97278
	94	1.15571	.98594	1.12293	.95804	1.10492	.97278
	95	1.21839	.98594	1.19379	.95804	1.15946	.97278
	96	1.23535	.98594	1.21011	.95804	1.17102	.97278
	97	1.27899	.98594	1.26340	.95804	1.20317	.97278
	98	1.31615	.98594	1.30053	.95804	1.23825	.97278
	99	1.37254	.98594	1.32034	.95804	1.27302	.97278
	100	1.44671	.98594	1.43143	.95804	1.31387	.97278
$FDA_k = 100$	No.						
	101	1.23903	1.16962	1.20517	1.13984	1.20010	1.14650
	102	1.27095	1.16962	1.24081	1.13984	1.22113	1.14650
	103	1.28709	1.16962	1.25565	1.13984	1.23544	1.14650
	104	1.31881	1.16962	1.28616	1.13984	1.25637	1.14650
	105	1.35289	1.16962	1.32852	1.13984	1.28423	1.14650
	106	1.36089	1.16962	1.33663	1.13984	1.28653	1.14650
	107	1.39390	1.16962	1.37780	1.13984	1.30887	1.14650
	108	1.41999	1.16962	1.40417	1.13984	1.33332	1.14650
	109	1.44783	1.16962	1.43047	1.13984	1.35409	1.14650
	110	1.48082	1.16962	1.46727	1.13984	1.35320	1.14650

Table 3.2 The D_r , D_g , and D_b for each colour in the 120 data set (Cromalin device).

FDA _k = 0	No.	D _{r3c}	D _{rk}	D _{g3c}	D _{gk}	D _{b3c}	D _{bk}
	1	.13507	.00000	.13025	.00000	.09809	.00000
	2	.24771	.00000	.24222	.00000	.19842	.00000
	3	.35467	.00000	.34839	.00000	.29557	.00000
	4	.46241	.00000	.45321	.00000	.38786	.00000
	5	.58935	.00000	.58181	.00000	.48753	.00000
	6	.69941	.00000	.68707	.00000	.60279	.00000
	7	.82593	.00000	.81938	.00000	.72627	.00000
	8	.96569	.00000	.95185	.00000	.85405	.00000
	9	1.13538	.00000	1.12958	.00000	1.03512	.00000
	10	1.27926	.00000	1.27872	.00000	1.20080	.00000
FDA _k = 10	No.	D _{r4c}	D _{rk}	D _{g3c}	D _{gk}	D _{b3c}	D _{bk}
	11	.22850	.11847	.22639	.12062	.19050	.10799
	12	.33033	.11847	.32690	.12062	.27964	.10799
	13	.43199	.11847	.42711	.12062	.37040	.10799
	14	.53431	.11847	.52631	.12062	.45670	.10799
	15	.65700	.11847	.65138	.12062	.55566	.10799
	16	.76477	.11847	.75444	.12062	.66730	.10799
	17	.88438	.11847	.87898	.12062	.78261	.10799
	18	1.01586	.11847	1.00257	.12062	.90427	.10799
	19	1.17907	.11847	1.17318	.12062	1.07633	.10799
	20	1.31789	.11847	1.31602	.12062	1.23392	.10799
FDA _k = 20	No.						
	21	.31829	.22026	.31751	.22384	.27391	.20259
	22	.41409	.22026	.41122	.22384	.35811	.20259
	23	.50777	.22026	.50405	.22384	.44486	.20259
	24	.60426	.22026	.59821	.22384	.52709	.20259
	25	.72440	.22026	.71898	.22384	.62022	.20259
	26	.82962	.22026	.81967	.22384	.72857	.20259
	27	.94258	.22026	.93707	.22384	.83619	.20259
	28	1.06541	.22026	1.05200	.22384	.94982	.20259
	29	1.21809	.22026	1.21174	.22384	1.11403	.20259
	30	1.35462	.22026	1.35342	.22384	1.27171	.20259
FDA _k = 30	No.						
	31	.41059	.32469	.41051	.32945	.36308	.30104
	32	.49675	.32469	.49423	.32945	.43751	.30104
	33	.59067	.32469	.58558	.32945	.52119	.30104
	34	.67923	.32469	.67092	.32945	.59642	.30104
	35	.79528	.32469	.79037	.32945	.68990	.30104
	36	.89246	.32469	.88247	.32945	.79079	.30104
	37	1.00141	.32469	.99593	.32945	.89600	.30104
	38	1.12058	.32469	1.10788	.32945	1.00596	.30104
	39	1.26530	.32469	1.26039	.32945	1.16535	.30104
	40	1.39457	.32469	1.39032	.32945	1.30582	.30104
FDA _k = 40	No.						
	41	.51214	.42807	.51278	.43323	.46061	.39945
	42	.59200	.42807	.59021	.43323	.53009	.39945
	43	.67446	.42807	.67101	.43323	.60546	.39945
	44	.75824	.42807	.75178	.43323	.67736	.39945
	45	.86357	.42807	.85776	.43323	.76105	.39945
	46	.95801	.42807	.94883	.43323	.85773	.39945
	47	1.06053	.42807	1.05506	.43323	.95643	.39945
	48	1.17569	.42807	1.16342	.43323	1.06195	.39945
	49	1.31459	.42807	1.30768	.43323	1.21253	.39945
	50	1.43776	.42807	1.43173	.43323	1.34470	.39945
FDA _k = 50	No.						
	51	.62829	.54848	.62971	.55410	.57404	.51653
	52	.69410	.54848	.69256	.55410	.63185	.51653
	53	.76878	.54848	.76518	.55410	.69892	.51653
	54	.84774	.54848	.84093	.55410	.76729	.51653
	55	.94456	.54848	.93904	.55410	.84355	.51653
	56	1.03049	.54848	1.02077	.55410	.93146	.51653
	57	1.13242	.54848	1.12547	.55410	1.02469	.51653
	58	1.23525	.54848	1.22125	.55410	1.12265	.51653
	59	1.36889	.54848	1.35999	.55410	1.26393	.51653
	60	1.47493	.54848	1.46633	.55410	1.37893	.51653

Table 3.2 The D_r , D_g , and D_b for each colour in the 120 data set (Cromalin device).
(continued)

$FDA_k = 60$	No.	D_{r4c}	D_{rk}	D_{g3c}	D_{gk}	D_{b3c}	D_{bk}
	61	.75124	.67134	.75272	.67653	.69504	.63505
	62	.80842	.67134	.80709	.67653	.74354	.63505
	63	.87270	.67134	.86914	.67653	.80302	.63505
	64	.94563	.67134	.93872	.67653	.86447	.63505
	65	1.03449	.67134	1.02824	.67653	.93358	.63505
	66	1.11160	.67134	1.10159	.67653	1.01165	.63505
	67	1.20425	.67134	1.19660	.67653	1.09759	.63505
	68	1.30794	.67134	1.29386	.67653	1.19214	.63505
	69	1.42336	.67134	1.41293	.67653	1.31624	.63505
	70	1.52443	.67134	1.51249	.67653	1.41769	.63505
$FDA_k = 70$	No.						
	71	.87786	.79123	.87890	.79610	.81851	.75230
	72	.92721	.79123	.92522	.79610	.86004	.75230
	73	.99311	.79123	.98849	.79610	.91862	.75230
	74	1.05474	.79123	1.04663	.79610	.97109	.75230
	75	1.13511	.79123	1.12773	.79610	1.03417	.75230
	76	1.20263	.79123	1.19166	.79610	1.10135	.75230
	77	1.28183	.79123	1.27289	.79610	1.17446	.75230
	78	1.36486	.79123	1.34999	.79610	1.24880	.75230
	79	1.45778	.79123	1.44475	.79610	1.34431	.75230
	80	1.54643	.79123	1.53082	.79610	1.43245	.75230
$FDA_k = 80$	No.						
	81	.97261	.95081	.97330	.95481	.92390	.90688
	82	1.01758	.95081	1.01521	.95481	.96185	.90688
	83	1.08839	.95081	1.08233	.95481	1.02357	.90688
	84	1.15570	.95081	1.14661	.95481	1.08011	.90688
	85	1.24335	.95081	1.23336	.95481	1.14354	.90688
	86	1.32023	.95081	1.30484	.95481	1.21200	.90688
	87	1.40147	.95081	1.38786	.95481	1.29012	.90688
	88	1.47785	.95081	1.45691	.95481	1.35943	.90688
	89	1.57695	.95081	1.55375	.95481	1.44929	.90688
	90	1.66581	.95081	1.63928	.95481	1.53010	.90688
$FDA_k = 90$	No.						
	91	1.16171	1.15609	1.16125	1.15761	1.10535	1.10437
	92	1.20380	1.15609	1.19949	1.15761	1.14081	1.10437
	93	1.26540	1.15609	1.25710	1.15761	1.19184	1.10437
	94	1.32067	1.15609	1.30936	1.15761	1.23883	1.10437
	95	1.40293	1.15609	1.38929	1.15761	1.29860	1.10437
	96	1.45535	1.15609	1.43736	1.15761	1.34599	1.10437
	97	1.52412	1.15609	1.50523	1.15761	1.40629	1.10437
	98	1.58403	1.15609	1.55899	1.15761	1.45886	1.10437
	99	1.67699	1.15609	1.64749	1.15761	1.53893	1.10437
	100	1.75148	1.15609	1.71772	1.15761	1.60743	1.10437
$FDA_k = 100$	No.						
	101	1.37089	1.37485	1.36742	1.37248	1.30525	1.31318
	102	1.41759	1.37485	1.40942	1.37248	1.33954	1.31318
	103	1.47579	1.37485	1.46386	1.37248	1.38602	1.31318
	104	1.50624	1.37485	1.49096	1.37248	1.40652	1.31318
	105	1.58326	1.37485	1.56351	1.37248	1.46494	1.31318
	106	1.60987	1.37485	1.58438	1.37248	1.48570	1.31318
	107	1.65208	1.37485	1.62617	1.37248	1.52560	1.31318
	108	1.70315	1.37485	1.67183	1.37248	1.56347	1.31318
	109	1.76651	1.37485	1.73062	1.37248	1.61365	1.31318
	110	1.79201	1.37485	1.75349	1.37248	1.62834	1.31318

Table 3.3 Summary of the 3rd-order masking equations' performance using the cube data set.

<u>Predictive Performance</u>							
Device	$ \Delta x $	$ \Delta y $	$\Delta u'v'$	$\% \Delta Y $	$\Delta E L^*u^*v^*$	$\Delta E L^*a^*b^*$	$\Delta E CMC(1:1)$
IRIS	0.0013	0.0012	0.0013	0.92	0.90	1.38	0.61
Cromalin	0.0014	0.0016	0.0015	1.35	0.91	1.14	0.63

<u>Reversibility Performance</u>							
Device	$ \Delta x $	$ \Delta y $	$\Delta u'v'$	$\% \Delta Y $	$\Delta E L^*u^*v^*$	$\Delta E L^*a^*b^*$	$\Delta E CMC(1:1)$
IRIS	0.0016	0.0012	0.0015	0.95	0.92	1.36	0.62
Cromalin	0.0015	0.0017	0.0017	1.56	1.22	0.98	0.67

Table 3.4 Summary of the forward BPA models' predictive performance.

<u>Black Printer-31 Sample Set</u>								
Device	Model	$ \Delta x $	$ \Delta y $	$\Delta u'v'$	$\% \Delta Y $	$\Delta E L^*u^*v^*$	$\Delta E L^*a^*b^*$	$\Delta E CMC(1:1)$
IRIS	SAE	0.0062	0.0101	0.0090	7.58	4.49	3.96	3.13
	MSAE	0.0078	0.0094	0.0091	6.06	4.30	3.64	2.55
	3rd	0.0060	0.0082	0.0083	5.76	3.96	3.51	2.47
	2nd(1)	0.0029	0.0040	0.0042	3.09	2.38	1.97	1.40
	2nd(2)	0.0036	0.0060	0.0059	4.42	2.79	2.43	1.72
Cromalin	SAE	0.0077	0.0094	0.0096	12.85	3.71	3.57	3.51
	MSAE	0.0087	0.0076	0.0099	9.87	3.36	3.42	3.07
	3rd	0.0090	0.0088	0.0098	12.24	3.61	3.43	3.26
	2nd(1)	0.0065	0.0093	0.0099	12.95	3.74	3.50	3.34
	2nd(2)	0.0058	0.0086	0.0081	8.18	3.46	3.24	2.73

<u>Black Printer-110 Sample Set</u>								
Device	Model	$ \Delta x $	$ \Delta y $	$\Delta u'v'$	$\% \Delta Y $	$\Delta E L^*u^*v^*$	$\Delta E L^*a^*b^*$	$\Delta E CMC(1:1)$
IRIS	SAE	0.0029	0.0046	0.0041	4.18	2.61	2.12	2.48
	MSAE	0.0032	0.0024	0.0032	3.11	2.13	1.70	1.98
	3rd	0.0034	0.0028	0.0032	3.29	2.01	1.52	1.70
	2nd(1)	0.0028	0.0024	0.0028	2.88	1.85	1.45	1.62
	2nd(2)	0.0028	0.0027	0.0030	3.20	1.95	1.53	1.72
Cromalin	SAE	0.0025	0.0024	0.0023	4.83	1.34	1.18	1.31
	MSAE	0.0036	0.0033	0.0036	5.79	1.93	1.69	2.02
	3rd	0.0033	0.0029	0.0034	5.30	1.82	1.62	1.89
	2nd(1)	0.0026	0.0027	0.0024	2.63	1.27	1.00	1.06
	2nd(2)	0.0022	0.0024	0.0022	4.18	1.28	1.09	1.23

<u>Cube Data Set</u>								
Device	Model	$ \Delta x $	$ \Delta y $	$\Delta u'v'$	$\% \Delta Y $	$\Delta E L^*u^*v^*$	$\Delta E L^*a^*b^*$	$\Delta E CMC(1:1)$
IRIS	2nd(1)	0.0032	0.0034	0.0040	4.19	3.58	2.73	1.78
	2nd(2)	0.0016	0.0013	0.0015	0.97	1.40	0.94	0.65
Cromalin	2nd(1)	0.0060	0.0081	0.0096	9.87	5.17	4.52	3.11
	2nd(2)	0.0016	0.0018	0.0017	1.72	1.30	1.03	0.71

Table 3.5 Summary of the reverse BPA models' performance using IRIS device (K is known).

Model	SAE			MSAE			3rd			2nd(1)			2nd(2)		
	$ \Delta c $	$ \Delta m $	$ \Delta y $	$ \Delta c $	$ \Delta m $	$ \Delta y $	$ \Delta c $	$ \Delta m $	$ \Delta y $	$ \Delta c $	$ \Delta m $	$ \Delta y $	$ \Delta c $	$ \Delta m $	$ \Delta y $
110 sample set															
110	3	3	3	2	3	3	3	3	4	3	2	3	3	2	4
106	3	2	4	2	2	2	3	2	3	3	2	3	3	2	3
4	11	13	19	3	23	13	3	14	9	5	7	9	6	7	9
31 sample set															
31	3	2	5	1	2	2	2	2	3	2	2	2	1	2	2
27	2	1	3	1	1	2	2	1	2	1	2	1	1	1	2
4	10	7	20	0	6	2	1	5	9	4	8	7	4	9	9

Table 3.6 Summary of the reverse BPA models' performance using Cromalin device (K is known).

Model	SAE			MSAE			3rd			2nd(1)			2nd(2)		
	Δc	Δm	Δy	Δc	Δm	Δy	Δc	Δm	Δy	Δc	Δm	Δy	Δc	Δm	Δy
110 sample set															
110	5	5	4	8	6	6	6	6	5	5	5	5	5	5	5
106	4	4	4	7	5	5	5	5	4	4	4	4	4	4	4
4	32	33	21	43	37	33	36	38	32	31	35	30	31	35	31
31 sample set															
31	3	10	6	8	9	9	7	8	9	5	8	7	5	8	8
27	3	7	3	4	5	7	5	6	8	5	6	5	4	6	6
4	1	30	25	33	38	21	19	24	20	9	20	20	15	23	24

Table 3.7 Summary of the reversibility performance between the forward and reverse BPA models (K ink is known).

<u>Black Printer-31 Sample Set</u>								
Device	Model	$ \Delta x $	$ \Delta y $	$\Delta u'v'$	$\% \Delta Y $	$\Delta EL*u*v*$	$\Delta EL*a*b*$	ΔE CMC(1:1)
IRIS	SAE	0.0059	0.0077	0.0073	4.58	3.84	3.22	2.37
	MSAE	0.0043	0.0060	0.0057	4.21	3.20	2.68	2.09
	3rd	0.0037	0.0057	0.0050	3.93	3.10	2.45	1.84
	2nd(1)	0.0023	0.0043	0.0039	3.26	2.05	1.81	1.24
	2nd(2)	0.0027	0.0047	0.0044	3.45	2.12	1.88	1.26
Cromalin	SAE	0.0075	0.0118	0.0116	14.75	4.37	4.17	4.24
	MSAE	0.0082	0.0117	0.0117	15.53	4.86	4.48	4.17
	3rd	0.0079	0.0101	0.0096	14.11	4.21	3.85	3.76
	2nd(1)	0.0060	0.0061	0.0063	10.33	3.55	2.85	2.69
	2nd(2)	0.0076	0.0070	0.0073	8.22	3.16	2.72	2.49

<u>Black Printer-110 Sample Set</u>								
Device	Model	$ \Delta x $	$ \Delta y $	$\Delta u'v'$	$\% \Delta Y $	$\Delta EL*u*v*$	$\Delta EL*a*b*$	ΔE CMC(1:1)
IRIS	SAE	0.0014	0.0038	0.0030	1.99	2.04	1.72	2.03
	MSAE	0.0017	0.0020	0.0020	1.68	1.11	0.93	1.06
	3rd	0.0022	0.0024	0.0026	2.17	1.61	1.33	1.50
	2nd(1)	0.0010	0.0011	0.0012	1.64	0.89	0.69	0.78
	2nd(2)	0.0013	0.0011	0.0012	1.64	0.89	0.69	0.78
Cromalin	SAE	0.0034	0.0023	0.0030	3.28	1.36	1.17	1.34
	MSAE	0.0052	0.0037	0.0046	5.10	2.17	1.82	2.15
	3rd	0.0033	0.0036	0.0036	4.88	1.90	1.66	1.88
	2nd(1)	0.0021	0.0024	0.0022	3.25	1.24	1.05	1.16
	2nd(2)	0.0028	0.0025	0.0024	3.95	1.38	1.13	1.27

Table 3.8 Summary of the GCR's reversibility performance (IRIS device).

<u>Black Printer-31 Sample Set</u>									
r_o	D_{gcr}	Model	$ \Delta x $	$ \Delta y $	$\Delta u'v'$	$\% \Delta Y $	$\Delta E L^*u^*v^*$	$\Delta E L^*a^*b^*$	$\Delta E CMC(1:1)$
0.00	0.00	2nd(1)	0.0106	0.0131	0.0117	9.69	6.45	5.29	3.56
		2nd(2)	0.0031	0.0046	0.0045	4.86	2.48	2.14	1.49
0.30	0.00	2nd(1)	0.0028	0.0052	0.0046	3.95	2.74	2.35	1.53
		2nd(2)	0.0033	0.0052	0.0050	5.03	2.89	2.49	1.63
	0.60	2nd(1)	0.0027	0.0043	0.0042	4.11	2.37	2.10	1.47
		2nd(2)	0.0033	0.0049	0.0048	4.58	2.49	2.21	1.47
	1.20	2nd(1)	0.0047	0.0061	0.0063	6.22	2.89	2.68	1.83
		2nd(2)	0.0051	0.0058	0.0062	6.50	2.68	2.46	1.76
0.70	0.00	2nd(1)	0.0026	0.0042	0.0042	3.71	2.65	2.18	1.39
		2nd(2)	0.0030	0.0048	0.0046	4.68	2.55	2.24	1.47
	0.60	2nd(1)	0.0028	0.0038	0.0042	4.01	2.61	2.20	1.43
		2nd(2)	0.0032	0.0047	0.0046	4.40	2.40	2.13	1.40
	1.20	2nd(1)	0.0049	0.0059	0.0064	6.43	3.22	2.86	1.90
		2nd(2)	0.0050	0.0057	0.0061	6.50	2.65	2.42	1.73
0.90	0.00	2nd(1)	0.0028	0.0044	0.0043	3.89	2.69	2.21	1.40
		2nd(2)	0.0033	0.0050	0.0049	4.86	2.74	2.39	1.57
	0.60	2nd(1)	0.0028	0.0038	0.0041	4.20	2.53	2.14	1.42
		2nd(2)	0.0033	0.0047	0.0047	4.46	2.43	2.16	1.43
	1.20	2nd(1)	0.0049	0.0060	0.0064	6.66	3.22	2.86	1.93
		2nd(2)	0.0051	0.0058	0.0062	6.50	2.68	2.46	1.76
1.00	0.00	2nd(1)	0.0028	0.0044	0.0043	3.90	2.70	2.22	1.41
		2nd(2)	0.0033	0.0051	0.0049	4.81	2.76	2.40	1.57
	0.60	2nd(1)	0.0028	0.0038	0.0041	4.21	2.55	2.15	1.42
		2nd(2)	0.0033	0.0048	0.0047	4.41	2.45	2.18	1.43
	1.20	2nd(1)	0.0049	0.0060	0.0064	6.66	3.22	2.86	1.93
		2nd(2)	0.0051	0.0058	0.0062	6.50	2.68	2.46	1.76

Table 3.8 Summary of the GCR's reversibility performance (IRIS device). (continued)

<u>Black Printer-110 Sample Set</u>									
r_o	D_{gcr}	Model	$ \Delta x $	$ \Delta y $	$\Delta u'v'$	$\% \Delta Y $	$\Delta E L^*u^*v^*$	$\Delta E L^*a^*b^*$	$\Delta E CMC(1:1)$
0.00	0.00	2nd(1)	0.0046	0.0080	0.0058	8.09	3.81	2.85	3.17
		2nd(2)	0.0009	0.0013	0.0012	1.49	0.75	0.62	0.71
0.30	0.00	2nd(1)	0.0014	0.0026	0.0020	3.16	1.48	1.20	1.26
		2nd(2)	0.0015	0.0023	0.0018	2.86	1.41	1.07	1.14
	0.60	2nd(1)	0.0012	0.0026	0.0019	2.92	1.39	1.14	1.24
		2nd(2)	0.0012	0.0019	0.0015	2.04	0.99	0.77	0.87
	1.20	2nd(1)	0.0022	0.0020	0.0025	2.75	1.51	1.27	1.42
		2nd(2)	0.0023	0.0015	0.0021	1.81	1.13	0.89	1.04
0.70	0.00	2nd(1)	0.0010	0.0016	0.0012	2.28	1.06	0.86	0.86
		2nd(2)	0.0008	0.0013	0.0010	2.06	0.89	0.71	0.72
	0.60	2nd(1)	0.0007	0.0015	0.0012	1.99	0.93	0.78	0.83
		2nd(2)	0.0007	0.0010	0.0008	1.19	0.59	0.46	0.52
	1.20	2nd(1)	0.0022	0.0019	0.0024	2.66	1.47	1.23	1.38
		2nd(2)	0.0022	0.0014	0.0019	1.69	1.09	0.84	0.98
0.90	0.00	2nd(1)	0.0009	0.0016	0.0013	2.24	1.06	0.87	0.89
		2nd(2)	0.0009	0.0015	0.0011	2.16	1.01	0.80	0.80
	0.60	2nd(1)	0.0007	0.0016	0.0012	2.17	0.97	0.84	0.90
		2nd(2)	0.0007	0.0011	0.0009	1.25	0.60	0.47	0.54
	1.20	2nd(1)	0.0022	0.0019	0.0024	2.63	1.48	1.25	1.40
		2nd(2)	0.0022	0.0014	0.0020	1.66	0.84	1.08	0.98
1.00	0.00	2nd(1)	0.0011	0.0016	0.0013	1.67	1.05	0.82	0.84
		2nd(2)	0.0011	0.0014	0.0012	2.10	1.02	0.78	0.80
	0.60	2nd(1)	0.0008	0.0014	0.0012	1.65	0.90	0.75	0.80
		2nd(2)	0.0009	0.0010	0.0009	1.27	0.61	0.47	0.53
	1.20	2nd(1)	0.0022	0.0019	0.0024	2.62	1.47	1.24	1.39
		2nd(2)	0.0022	0.0014	0.0020	1.69	1.10	0.85	0.99

Table 3.8 Summary of the GCR's reversibility performance (IRIS device). (continued)

<u>Cube Data Set</u>									
r_o	D_{gcr}	Model	$ \Delta x $	$ \Delta y $	$\Delta u'v'$	$\% \Delta Y $	$\Delta E L^*u^*v^*$	$\Delta E L^*a^*b^*$	ΔE CMC(1:1)
0.00	0.00	2nd(1)	0.0107	0.0091	0.0100	5.14	8.27	5.63	3.09
		2nd(2)	0.0008	0.0010	0.0010	0.78	0.93	0.68	0.45
0.30	0.00	2nd(1)	0.0045	0.0042	0.0048	4.17	4.65	3.24	1.94
		2nd(2)	0.0034	0.0040	0.0038	3.41	4.07	2.84	1.75
	0.60	2nd(1)	0.0028	0.0035	0.0039	4.03	3.47	2.69	1.74
		2nd(2)	0.0009	0.0011	0.0011	0.78	1.00	0.73	0.47
	1.20	2nd(1)	0.0027	0.0033	0.0038	4.01	3.43	2.67	1.72
		2nd(2)	0.0009	0.0010	0.0011	0.72	0.96	0.69	0.45
0.70	0.00	2nd(1)	0.0045	0.0041	0.0047	3.96	4.66	3.20	1.93
		2nd(2)	0.0032	0.0036	0.0036	3.12	3.83	2.67	1.68
	0.60	2nd(1)	0.0027	0.0033	0.0038	3.96	3.42	2.65	1.71
		2nd(2)	0.0009	0.0010	0.0010	0.72	0.98	0.71	0.45
	1.20	2nd(1)	0.0027	0.0033	0.0038	4.01	3.43	2.67	1.72
		2nd(2)	0.0009	0.0010	0.0011	0.72	0.96	0.69	0.45
0.90	0.00	2nd(1)	0.0046	0.0041	0.0048	3.91	4.67	3.20	1.93
		2nd(2)	0.0032	0.0037	0.0036	3.17	3.85	2.69	1.69
	0.60	2nd(1)	0.0027	0.0033	0.0038	3.97	3.42	2.65	1.71
		2nd(2)	0.0009	0.0010	0.0011	0.72	0.98	0.71	0.45
	1.20	2nd(1)	0.0027	0.0033	0.0038	4.01	3.43	2.67	1.72
		2nd(2)	0.0009	0.0010	0.0011	0.72	0.96	0.69	0.45
1.00	0.00	2nd(1)	0.0046	0.0041	0.0048	3.91	4.66	3.19	1.92
		2nd(2)	0.0032	0.0037	0.0036	3.19	3.86	2.69	1.69
	0.60	2nd(1)	0.0027	0.0033	0.0038	3.97	3.42	2.65	1.71
		2nd(2)	0.0093	0.0010	0.0011	0.72	0.98	0.71	0.45
	1.20	2nd(1)	0.0027	0.0033	0.0038	4.01	3.43	2.67	1.72
		2nd(2)	0.0009	0.0010	0.0011	0.72	0.96	0.69	0.45

Table 3.9 Summary of the GCR's reversibility performance (Cromalin device).

<u>Black Printer-31 Sample Set</u>									
r_o	D_{gcr}	Model	$ \Delta x $	$ \Delta y $	$\Delta u'v'$	$\% \Delta Y $	$\Delta EL*u*v*$	$\Delta EL*a*b*$	ΔE CMC(1:1)
0.00	0.00	2nd(1)	0.0410	0.0490	0.0445	41.04	25.37	20.37	14.68
		2nd(2)	0.0081	0.0066	0.0076	7.66	2.81	2.47	2.22
0.30	0.00	2nd(1)	0.0131	0.0114	0.0120	18.07	6.96	5.76	4.60
		2nd(2)	0.0116	0.0084	0.0106	9.46	5.22	4.04	3.07
	0.60	2nd(1)	0.0093	0.0088	0.0098	15.13	4.86	4.18	3.75
		2nd(2)	0.0093	0.0070	0.0088	8.56	3.70	3.05	2.50
	1.28	2nd(1)	0.0069	0.0086	0.0093	11.12	4.04	3.68	3.32
		2nd(2)	0.0095	0.0061	0.0089	8.52	3.17	2.89	2.52
0.70	0.00	2nd(1)	0.0069	0.0084	0.0077	13.57	4.24	3.69	3.28
		2nd(2)	0.0097	0.0084	0.0093	8.16	4.55	3.70	2.77
	0.60	2nd(1)	0.0062	0.0083	0.0077	12.38	3.87	3.46	3.17
		2nd(2)	0.0093	0.0078	0.0089	8.45	3.86	3.23	2.55
	1.28	2nd(1)	0.0066	0.0085	0.0090	10.94	4.00	3.64	3.28
		2nd(2)	0.0096	0.0065	0.0089	8.49	3.19	2.92	2.54
0.90	0.00	2nd(1)	0.0082	0.0084	0.0082	13.93	4.39	3.78	3.37
		2nd(2)	0.0113	0.0093	0.0107	9.16	5.15	4.11	3.07
	0.60	2nd(1)	0.0055	0.0075	0.0072	11.76	3.55	3.17	2.97
		2nd(2)	0.0100	0.0081	0.0093	8.57	4.05	3.35	2.64
	1.28	2nd(1)	0.0066	0.0085	0.0090	10.94	4.00	3.64	3.28
		2nd(2)	0.0102	0.0068	0.0094	8.61	3.38	3.05	2.63
1.00	0.00	2nd(1)	0.0082	0.0084	0.0082	13.98	4.40	3.78	3.37
		2nd(2)	0.0107	0.0090	0.0102	9.04	4.96	3.98	2.97
	0.60	2nd(1)	0.0062	0.0083	0.0077	12.38	3.87	3.46	3.17
		2nd(2)	0.0081	0.0074	0.0081	7.69	3.55	2.97	2.38
	1.28	2nd(1)	0.0066	0.0085	0.0090	10.94	4.00	3.64	3.28
		2nd(2)	0.0096	0.0066	0.0089	8.49	3.19	2.92	2.54

Table 3.9 Summary of the GCR's reversibility performance (Cromalin device).
(continued)

<u>Black Printer-110 Sample Set</u>									
r_o	D_{gcr}	Model	$ \Delta x $	$ \Delta y $	$\Delta u'v'$	$\% \Delta Y $	$\Delta E L^*u^*v^*$	$\Delta E L^*a^*b^*$	$\Delta E CMC(1:1)$
0.00	0.00	2nd(1)	0.0086	0.0092	0.0080	7.41	3.63	2.85	2.89
		2nd(2)	0.0013	0.0022	0.0021	2.50	0.99	0.93	1.11
0.30	0.00	2nd(1)	0.0033	0.0040	0.0036	4.54	2.10	1.70	1.77
		2nd(2)	0.0024	0.0036	0.0029	3.54	1.83	1.44	1.50
	0.60	2nd(1)	0.0018	0.0026	0.0024	2.99	1.07	0.99	1.11
		2nd(2)	0.0010	0.0021	0.0017	2.62	0.89	0.83	0.94
	1.28	2nd(1)	0.0028	0.0026	0.0033	2.72	1.41	1.32	1.57
		2nd(2)	0.0022	0.0013	0.0021	2.36	1.00	0.90	1.14
0.70	0.00	2nd(1)	0.0032	0.0025	0.0026	3.91	1.57	1.23	1.32
		2nd(2)	0.0018	0.0021	0.0017	3.50	1.19	0.96	1.03
	0.60	2nd(1)	0.0023	0.0016	0.0019	2.93	0.89	0.74	0.88
		2nd(2)	0.0011	0.0014	0.0011	2.94	0.70	0.64	0.73
	1.28	2nd(1)	0.0028	0.0026	0.0033	2.72	1.41	1.32	1.57
		2nd(2)	0.0022	0.0014	0.0020	2.43	0.97	0.86	1.09
0.90	0.00	2nd(1)	0.0028	0.0025	0.0024	3.64	1.51	1.18	1.23
		2nd(2)	0.0023	0.0025	0.0021	4.11	1.46	1.17	1.23
	0.60	2nd(1)	0.0023	0.0020	0.0020	2.96	1.07	0.86	0.94
		2nd(2)	0.0018	0.0019	0.0016	3.38	1.05	0.87	0.96
	1.28	2nd(1)	0.0026	0.0026	0.0032	2.63	1.37	1.29	1.52
		2nd(2)	0.0021	0.0011	0.0019	2.33	0.95	0.84	1.07
1.00	0.00	2nd(1)	0.0026	0.0025	0.0024	7.26	1.72	1.55	1.80
		2nd(2)	0.0015	0.0020	0.0016	7.14	1.55	1.41	1.64
	0.60	2nd(1)	0.0021	0.0020	0.0019	6.77	1.34	1.27	1.55
		2nd(2)	0.0011	0.0015	0.0012	6.23	1.17	1.10	1.37
	1.28	2nd(1)	0.0026	0.0026	0.0032	3.07	1.43	1.35	1.61
		2nd(2)	0.0022	0.0012	0.0020	3.05	1.05	0.94	1.21

Table 3.9 Summary of the GCR's reversibility performance (Cromalin device).
(continued)

<u>Cube Data Set</u>									
r_o	D_{gcr}	Model	$ \Delta x $	$ \Delta y $	$\Delta u'v'$	$\% \Delta Y $	$\Delta EL*u*v*$	$\Delta EL*a*b*$	$\Delta E CMC(1:1)$
0.00	0.00	2nd(1)	0.0787	0.0637	0.0677	48.55	50.96	36.28	22.51
		2nd(2)	0.0011	0.0014	0.0014	1.11	1.09	0.87	0.58
0.30	0.00	2nd(1)	0.0254	0.0231	0.0213	21.43	18.23	13.63	8.30
		2nd(2)	0.0080	0.0073	0.0076	5.63	6.16	4.45	2.67
	0.60	2nd(1)	0.0080	0.0075	0.0091	11.19	5.97	4.96	3.31
		2nd(2)	0.0024	0.0020	0.0024	1.93	1.87	1.37	0.87
	1.28	2nd(1)	0.0059	0.0076	0.0091	9.51	5.12	4.44	3.01
		2nd(2)	0.0013	0.0013	0.0014	1.31	1.16	0.90	0.61
0.70	0.00	2nd(1)	0.0168	0.0151	0.0152	15.64	12.43	9.41	5.96
		2nd(2)	0.0071	0.0072	0.0072	5.75	5.86	4.31	2.65
	0.60	2nd(1)	0.0070	0.0070	0.0085	10.14	5.49	4.62	3.04
		2nd(2)	0.0023	0.0023	0.0024	1.80	1.82	1.38	0.86
	1.28	2nd(1)	0.0059	0.0076	0.0091	9.51	5.12	4.44	3.01
		2nd(2)	0.0013	0.0013	0.0014	1.31	1.16	0.90	0.61
0.90	0.00	2nd(1)	0.0173	0.0157	0.0155	15.94	12.71	9.65	6.09
		2nd(2)	0.0072	0.0073	0.0072	5.81	5.83	4.29	2.66
	0.60	2nd(1)	0.0070	0.0071	0.0085	10.16	5.50	4.63	3.05
		2nd(2)	0.0023	0.0024	0.0025	1.83	1.84	1.39	0.87
	1.28	2nd(1)	0.0059	0.0076	0.0091	9.51	5.12	4.44	3.01
		2nd(2)	0.0013	0.0013	0.0014	1.31	1.16	0.90	0.61
1.00	0.00	2nd(1)	0.0174	0.0159	0.0156	16.09	12.86	9.77	6.16
		2nd(2)	0.0071	0.0071	0.0071	5.77	5.81	4.28	2.64
	0.60	2nd(1)	0.0070	0.0070	0.0085	10.15	5.49	4.62	3.04
		2nd(2)	0.0023	0.0024	0.0025	1.80	1.81	1.39	0.87
	1.28	2nd(1)	0.0059	0.0076	0.0091	9.51	5.12	4.44	3.01
		2nd(2)	0.0013	0.0013	0.0014	1.31	1.16	0.90	0.61

Table 4.1 Mean colorimetric measures calculated between the XYZ values measured from TSR and MS and those calculated between the XYZ values measured from TSR and predicted (P) by the model under D65, D50, and A light sources.

Illuminant	$ \Delta x $	$ \Delta y $	$\Delta u'v'$	$\Delta %Y $	$\Delta E L^*a^*b^*$	$\Delta E L^*u^*v^*$	$\Delta E CMC(1:1)$
D65							
TSR and MS	0.0126	0.0113	0.0139	16.96	6.67	7.56	4.12
TSR and P	0.0026	0.0026	0.0031	3.39	1.99	2.51	1.35
D50							
TSR and MS	0.0129	0.0106	0.0135	16.64	6.53	7.43	4.06
TSR and P	0.0027	0.0024	0.0030	3.41	1.96	2.48	1.34
A							
TSR and MS	0.0116	0.0068	0.0112	16.52	5.97	6.63	3.88
TSR and P	0.0025	0.0016	0.0024	3.44	1.81	2.21	1.26

Table 4.2 Summary of the performance of the 2nd BPA model derived using newly characterisation data.

<u>Reversibility Performance Using Third-Order Masking Equations</u>							
Source	$ \Delta x $	$ \Delta y $	$\Delta u'v'$	$\% \Delta Y $	$\Delta E L^*u^*v^*$	$\Delta E L^*a^*b^*$	$\Delta E CMC(1:1)$
D65	0.0014	0.0015	0.0016	1.43	1.20	0.94	0.68
D50	0.0015	0.0013	0.0015	1.44	1.15	0.92	0.66
A	0.0013	0.0009	0.0013	1.50	1.08	0.87	0.63

<u>Reverse Model' Performance</u>									
Light Source	D65			D50			A		
Mean delta FDA	$ \Delta c $	$ \Delta m $	$ \Delta y $	$ \Delta c $	$ \Delta m $	$ \Delta y $	$ \Delta c $	$ \Delta m $	$ \Delta c $
110 Sample Set									
110	2	3	2	2	3	2	2	4	2
106	2	3	2	2	3	1	2	4	2
4	3	4	6	2	4	3	2	5	5
31 Sample Set									
31	2	4	3	2	5	3	1	6	5
27	2	3	1	2	3	1	1	5	2
3	6	13	15	5	14	16	3	17	26

<u>Predictive performance for the Forward Model</u>								
Source	Samples	$ \Delta x $	$ \Delta y $	$\Delta u'v'$	$\% \Delta Y $	$\Delta E L^*u^*v^*$	$\Delta E L^*a^*b^*$	$\Delta E CMC(1:1)$
D65	31	0.0052	0.0059	0.0061	5.52	2.65	2.36	2.09
	110	0.0054	0.0019	0.0042	3.02	1.81	2.32	2.27
D50	31	0.0054	0.0057	0.0060	5.47	2.65	2.33	2.07
	110	0.0058	0.0017	0.0044	2.90	2.43	1.86	2.30
A	31	0.0051	0.0051	0.0060	5.08	2.82	2.25	2.01
	110	0.0064	0.0030	0.0057	2.27	3.02	2.04	2.62

Table 4.2 Summary of the performance of the 2nd BPA model derived using newly characterisation data. (continued)

Reversibility Performance Between the Forward and Reverse Models

Source	Samples	$ \Delta x $	$ \Delta y $	$\Delta u'v'$	$\% \Delta Y $	$\Delta E L^*u^*v^*$	$\Delta E L^*a^*b^*$	$\Delta E CMC(1:1)$
D65	31	0.0040	0.0040	0.0045	3.10	1.65	1.53	1.17
	110	0.0018	0.0014	0.0016	1.17	0.83	0.69	0.82
D50	31	0.0041	0.0045	0.0047	3.12	1.94	1.75	1.24
	110	0.0014	0.0007	0.0011	0.96	0.56	0.48	0.57
A	31	0.0044	0.0041	0.0047	3.04	1.84	1.68	1.30
	110	0.0012	0.0007	0.0011	0.91	0.56	0.48	0.57

Reversibility Performance of the GCR Algorithm
($r_o = 0.70, D_{gcr} = 0.60$).

Source	Samples	$ \Delta x $	$ \Delta y $	$\Delta u'v'$	$\% \Delta Y $	$\Delta E L^*u^*v^*$	$\Delta E L^*a^*b^*$	$\Delta E CMC(1:1)$
D65	31	0.0079	0.0068	0.0082	3.83	3.12	2.71	1.71
	110	0.0014	0.0018	0.0018	1.43	0.85	0.77	0.98
	729	0.0014	0.0014	0.0015	1.00	1.12	0.88	0.58
D50	31	0.0057	0.0041	0.0058	3.25	2.28	1.88	1.25
	110	0.0013	0.0014	0.0014	1.08	0.69	0.60	0.74
	729	0.0011	0.0011	0.0012	0.94	0.94	0.76	0.51
A	31	0.0055	0.0039	0.0036	3.65	2.43	2.27	1.61
	110	0.0010	0.0010	0.0011	1.00	0.61	0.55	0.65
	729	0.0012	0.0010	0.0013	1.06	1.08	0.85	0.57

Table 4.3 Parameters used for the Hunt and RLAB colour appearance models in the preliminary experiment.

Hunt							
Field	N_c	N_b	$(LMS)_D = 0.0$	$F_L = F_M = F_S = 1$	Lightness	z scale	
Hardcopy	0.95	75	no	yes	J	z	
Softcopy	0.95	25	no	no	J	z	
RLAB							
Field	δ factor (Surround)			Mechanism			
Hardcopy	1/3.00 (Average)			Cognitive			
Softcopy	1/3.75 (Dim)			Sensory			

Table 4.4 The colorimetric and luminance values under D65 and D50 illuminants used in the preliminary experiment.

<u>White (substrate)</u>									
Source	x	y	L	u'	v'	X	Y	Z	C. T.
D50	0.3491	0.3613	70.00	0.2104	0.4899	96.62	100.00	80.15	4830 K
D65	0.3235	0.3411	70.00	0.2007	0.4762	94.84	100.00	98.33	6415 K
<u>Grey Background</u>									
Source	x	y	L	u'	v'	X	Y	Z	Y%
D50	0.3330	0.3415	14.70	0.2071	0.4778	20.57	21.10	20.11	21.00
D65	0.3110	0.3231	14.70	0.1989	0.4649	20.68	21.48	24.33	21.00

Note: 1) C. T. : Colour Temperature

2) $Y\% = L_{\text{grey}}/L_{\text{white}}$

Table 4.5 A example to illustrate method for calculating the category judgement results

Step 1: Frequency Matrix

Model	7	6	5	4	3	2	1
XYZ	2	44	221	537	708	607	185
Hunt	13	110	417	690	602	398	74
RLAB	510	745	654	288	96	9	2

Step 2: Cumulative Frequencies Matrix

Model	7	6	5	4	3	2	1
XYZ	2	46	267	804	1512	2119	2304
Hunt	13	123	540	1230	1832	2230	2304
RLAB	510	1255	1909	2197	2293	2302	2304

Step 3: Cumulative Proportion Matrix

Model	7	6	5	4	3	2
XYZ	0.001	0.020	0.116	0.349	0.656	0.920
Hunt	0.006	0.053	0.234	0.534	0.795	0.968
RLAB	0.221	0.545	0.829	0.954	0.995	0.999

Step 4: Z Score Matrix

Model	7	6	5	4	3	2
XYZ	-3.133	-2.055	-1.196	-0.388	0.402	1.403
Hunt	-2.535	-1.613	-0.725	0.085	0.825	1.851
RLAB	-0.768	0.112	0.949	1.681	2.595	3.133

Step 5: Difference Matrix

Model	7	6	5	4	3
XYZ	1.078	0.859	0.808	0.791	1.001
Hunt	0.922	0.889	0.810	0.740	1.026
RLAB	0.880	0.836	0.733	0.913	0.538
Sum	2.880	2.584	2.350	2.444	2.566
Mean	0.960	0.861	0.783	0.815	0.855

Step 6: Category Boundary Estimate

	T1	T2	T3	T4	T5	T6
	0.000	0.960	1.821	2.605	3.419	4.274

Step 7: Scale Value

	1	2	3	4	5	6	sum	Mean	Rank
XYZ	3.133	3.015	3.017	2.993	3.017	2.871	18.046	3.008	1
Hunt	2.535	2.573	2.546	2.519	2.594	2.423	15.191	2.532	2
RLAB	0.768	0.847	0.872	0.923	0.824	1.141	5.377	0.896	3

Table 4.6 An example to illustrate method for calculating the paired comparison results.

Step 1: Frequency Matrix

	VK	CLAB	CLUV	LABH	RT	Hunt	Nay	RLAB
VK	.	67	9	9	25	69	28	61
CLAB	53	.	4	20	12	47	29	58
CLUV	111	116	.	112	113	113	101	114
LABH	111	100	8	.	62	105	66	107
RT	95	108	7	58	.	103	65	97
Hunt	51	73	7	15	17	.	27	59
Nay	92	91	19	54	55	93	.	89
RLAB	59	62	6	13	23	61	31	.

Step 2: Proportion Matrix

	VK	CLAB	CLUV	LABH	RT	Hunt	Nay	RLAB	sum
VK	.	0.558	0.075	0.075	0.208	0.575	0.233	0.508	
CLAB	0.442	.	0.033	0.167	0.100	0.392	0.242	0.483	
CLUV	0.925	0.967	.	0.933	0.942	0.942	0.842	0.950	
LABH	0.925	0.833	0.067	.	0.517	0.875	0.550	0.892	
RT	0.792	0.900	0.058	0.483	.	0.858	0.542	0.808	
Hunt	0.425	0.608	0.058	0.125	0.142	.	0.225	0.492	
Nay	0.767	0.758	0.158	0.450	0.458	0.775	.	0.742	
RLAB	0.492	0.517	0.050	0.108	0.192	0.508	0.258	.	
sum	4.767	5.142	0.500	2.342	2.558	4.925	2.892	4.875	28.000

Step 2: Z Score Matrix (Normal Deviates)

	VK	CLAB	CLUV	LABH	RT	Hunt	Nay	RLAB	sum
VK	.	0.147	-1.440	-1.440	-0.813	0.189	-0.728	0.021	
CLAB	-0.147	.	-1.835	-0.968	-1.282	-0.275	-0.701	-0.042	
CLUV	1.440	1.835	.	1.501	1.570	1.570	1.002	1.645	
LABH	1.440	0.968	-1.501	.	0.042	1.150	0.126	1.236	
RT	0.813	1.282	-1.570	-0.042	.	1.073	0.105	0.872	
Hunt	-0.189	0.275	-1.570	-1.150	-1.073	.	-0.755	-0.021	
Nay	0.728	0.701	-1.002	-0.126	-0.105	0.755	.	0.648	
RLAB	-0.021	0.042	-1.645	-1.236	-0.872	0.021	-0.648	.	
sum	4.063	5.249	-10.561	-3.460	-2.533	4.484	-1.601	4.360	-0.000
average	0.508	0.656	-1.320	-0.433	-0.317	0.560	-0.200	0.545	-0.000

Step 4: Logistic Matrix (LG-scale)

	VK	CLAB	CLUV	LABH	RT	Hunt	Nay	RLAB	sum
VK	0.000	0.232	-2.463	-2.463	-1.320	0.300	-1.177	0.033	
CLAB	-0.232	0.000	-3.254	-1.590	-2.161	-0.437	-1.132	-0.066	
CLUV	2.463	3.254	0.000	2.583	2.717	2.717	1.650	2.869	
LABH	2.463	1.590	-2.583	0.000	0.066	1.918	0.199	2.075	
RT	1.320	2.161	-2.717	-0.066	0.000	1.777	0.166	1.423	
Hunt	-0.300	0.437	-2.717	-1.918	-1.777	0.000	-1.224	-0.033	
Nay	1.177	1.132	-1.650	-0.199	-0.166	1.224	0.000	1.044	
RLAB	-0.033	0.066	-2.869	-2.075	-1.423	0.033	-1.044	0.000	
sum	6.858	8.872	-18.252	-5.727	-4.064	7.532	-2.563	7.345	-0.000

Table 4.7 The mean results in the preliminary experiment using the paired comparison and category judgement methods.

Mean results Using Paired Comparison Method

Experiment	Source	XYZ	Hunt	RLAB	No. of Obs.	Hardcopy Field		Softcopy Field		95% CL.
						BG	Border	BG	Border	
1	D65	2.422	1.565	-3.986	64	Grey	White	Grey	White	1.39
	D50	4.693	4.638	-4.440	36	Grey	White	Grey	White	1.39
2	D65	0.877	3.640	-4.521	20	Grey	White	Black	White	1.39
	D50	0.805	2.560	-3.365	20	Grey	White	Black	White	1.39
3	D65	0.536	2.335	-2.872	20	Grey	Grey	Black	Black	1.39
	D50	0.883	2.630	-3.513	20	Grey	Grey	Black	Black	1.39

Mean Results Using Category Judgement Method

Experiment	Source	XYZ	Hunt	RLAB	No. of Obs.	Hardcopy Field		Softcopy Field	
						BG	Border	BG	Border
1	D65	3.008	2.532	0.896	64	Grey	White	Grey	White
	D50	2.707	2.224	0.230	36	Grey	White	Grey	White
2	D65	3.938	4.104	2.041	20	Grey	White	Black	White
	D50	3.894	4.212	2.211	20	Grey	White	Black	White
3	D65	3.091	3.678	1.626	20	Grey	Grey	Black	Black
	D50	2.957	3.397	1.725	20	Grey	Grey	Black	Black

Note:

- 1) The 95% CL represents 95% confidence limit (equal to 2σ)
- 2) Obs.: Observations
- 3) BG: Background

Table 4.8 Summary of experimental phases for testing colour models in the main experiment.

Phase	Hardcopy	Softcopy	Viewing Technique	Monitor Display	No. of Observers	Repetition	Pairs	No. of Comparisons
CASE 1								
1	D65	D65	BSM	SS	9	2	36	324
2	D50	D50	BSM	SS	9	2	36	324
CASE 2								
3	D50	D65	BMM	TG	9	1	126	1,134
4	D65	D93	BMM	TG	9	1	126	1,134
5	D50	D93	BMM	SS	9	1	126	1,134
6	D50	D93	BMM	TG	9	2	252	2,268
7	A	D65	BMM	TG	9	1	126	1,134
Total					9		828	7,452

Note:

- 1) BSM: Binocular Simultaneous Matching, BMM: Binocular Memory Matching
- 2) SS: Simultaneous Display, TG: Toggling Display.

Table 4.9 The white point's colorimetric and luminance values in each phase in the main experiment.

Phase	1	2	3	4	5,6	7
Hardcopy field						
White border	D65	D50	D50	D65	D50	A
Colour Temperature	6539 K	5104 K	5104 K	6539 K	5104 K	2309 K
L (cd/m ²)	64	64	64	64	64	54
u'	0.2001	0.2089	0.2089	0.2001	0.2089	0.2742
v'	0.4700	0.4856	0.4856	0.4700	0.4856	0.5328
Softcopy field						
White border	D65	D50	D65	D93	D93	D65
Colour Temperature	6539 K	5104 K	6539 K	9703 K	9703 K	6539 K
L (cd/m ²)	64	64	64	64	64	54
u'	0.2001	0.2089	0.2001	0.1895	0.1895	0.2001
v'	0.4700	0.4856	0.4700	0.4464	0.4464	0.4700
White Point	D65	D53	D65	D93	D93	D65
Colour Temperature	6646K	5257 K	6646 K	9703 K	9703 K	6646 K
L (cd/m ²)	78	80	78	78	78	78
u'	0.1982	0.2070	0.1982	0.1895	0.1895	0.1982
v'	0.4693	0.4843	0.4693	0.4464	0.4464	0.4693

Table 4.10 Parameters used for the Hunt and RLAB colour appearance models in the main experiment.

Phase	1	2	3	4	5,6	7
Hunt						
Hardcopy Field						
Flas	1.097	0.957	0.957	1.097	0.957	1.097
Nc	1.00	1.00	1.00	1.00	1.00	1.00
Nb	75	75	75	75	75	75
$(LMS)_D=0.0$	no	no	no	no	no	no
$F_L=F_M=F_S=1$	yes	yes	yes	yes	yes	yes
Lightness	J	J	J	J	J	J
z	z	z	z	z	z	z
Soft Field						
Flas	1.097	0.957	1.097	1.265	1.265	0.562
Nc	1.00	1.00	1.00	1.00	1.00	1.00
Nb	75	75	75	75	75	75
$(LMS)_D=0.0$	no	no	no	no	no	no
$F_L=F_M=F_S=1$	no	no	no	no	no	no
Lightness	J	J	J	J	J	J
z	z	z	z	z	z	z
RLAB						
Hardcopy Field						
D factor	1.00	1.00	1.00	1.00	1.00	1.00
δ	1/2.30	1/2.30	1/2.30	1/2.30	1/2.30	1/2.30
Softcopy Field						
D factor	0.00	0.00	0.00	0.00	0.00	0.00
δ	1/2.30	1/2.30	1/2.30	1/2.30	1/2.30	1/2.30

Note:

- 1) For Hunt Model, the $F_L = F_M = F_S$ equal 1 or the F_L, F_M, F_S vary corresponds to cognitive or sensory chromatic mechanisms respectively.
- 2) For RLAB Model, the D factor equals 1 or 2 corresponds to cognitive or sensory chromatic mechanisms respectively.

Table 4.11 The colorimetric, luminance, and monitor RGB DAC values of grey background used in the main experiment.

Hardcopy Field						
Source	x	y	L	X	Y	Z
D50	0.3334	0.3425	12.25	18.63	19.14	18.11
D65	0.3099	0.3212	12.54	18.91	19.60	22.51
A	0.4750	0.4123	10.48	22.36	19.41	5.31

Softcopy Field								
Model	x	y	X	Y	Z	DAC Values		
						R	G	B
Phase 1								
Hunt	0.3104	0.3204	15.45	15.95	18.38	121	119	124
RLAB	0.3152	0.3222	15.81	16.16	18.18	123	119	123
XYZ	0.3099	0.3212	15.50	16.06	18.45	121	120	124
Phase 2								
Hunt	0.3332	0.3420	14.91	15.31	14.54	117	117	123
RLAB	0.3303	0.3354	14.84	15.08	15.03	117	116	125
XYZ	0.3334	0.3425	14.92	15.33	14.50	117	117	123
Phase 3								
Hunt	0.3079	0.3185	15.10	15.63	18.33	119	118	124
Nayatani	0.3083	0.3189	15.16	15.68	18.34	119	119	124
RLAB	0.3133	0.3192	15.49	15.78	18.17	122	118	124
von Kries	0.3081	0.3181	15.19	15.69	18.43	119	118	124
BFD	0.3079	0.3186	15.18	15.70	18.41	119	119	124
CIELAB	0.3070	0.3186	15.11	15.69	18.43	119	119	124
CIELUV	0.3086	0.3202	15.12	15.69	18.19	119	119	124
Phase 4								
Hunt	0.2781	0.2881	15.54	16.10	24.24	122	121	124
Nayatani	0.2782	0.2881	15.62	16.18	24.35	122	121	124
RLAB	0.2933	0.3003	16.44	16.84	22.78	129	122	121
von Kries	0.2780	0.2871	15.66	16.18	24.51	122	121	125
BFD	0.2777	0.2877	15.64	16.20	24.48	122	121	124
CIELAB	0.2766	0.2877	15.56	16.18	24.51	121	121	125
CIELUV	0.2781	0.2891	15.57	16.18	24.22	121	121	124
Phases 5 and 6								
Hunt	0.2762	0.2847	15.21	15.68	24.18	120	119	124
Nayatani	0.2856	0.2766	15.30	15.80	24.22	121	120	124
RLAB	0.2915	0.2972	16.13	16.44	22.76	127	121	121
von Kries	0.2764	0.2838	15.39	15.80	24.49	121	119	125
BFD	0.2758	0.2851	15.33	15.85	24.42	120	120	124
CIELAB	0.2736	0.2849	15.18	15.80	24.49	119	120	125
CIELUV	0.2882	0.2769	15.18	15.80	23.84	120	120	123
Phase 7								
Hunt	0.3077	0.3165	12.86	13.23	15.70	111	110	117
Nayatani	0.3102	0.3225	12.91	13.42	15.28	112	111	115
RLAB	0.3176	0.3132	13.32	13.51	15.71	115	111	117
von Kries	0.3079	0.3163	13.06	13.42	15.94	112	111	118
BFD	0.3072	0.3190	13.00	13.50	15.82	112	112	117
CIELAB	0.3035	0.3184	12.79	13.42	15.94	110	112	117
CIELUV	0.3116	0.3278	12.76	13.42	14.76	111	112	113

Table 4.12 Summary of observer precision and repeatability performance (correlation coefficients (r) vs. frequencies).

Phase	Hard-copy	Soft-copy	Monitor Display	r						Mean
				< 0.50	0.50-0.60	0.60-0.70	0.70-0.80	0.80-0.90	0.90-1.00	
Observer precision										
1	D65	D65	SS	13	4	1	0	0	0	0.28
2	D50	D50	SS	13	2	3	0	0	0	0.30
3	D50	D65	TG	0	2	2	4	1	0	0.69
4	D65	D93	TG	0	2	3	4	0	0	0.69
5	D50	D93	SS	0	0	3	2	4	0	0.77
6	D50	D93	TG	0	0	1	8	7	2	0.77
7	A	D65	TG	0	0	0	3	6	0	0.78
Observer repeatability										
1	D65	D65	SS	6	2	0	1	0	0	0.57
2	D50	D50	SS	8	0	0	1	0	0	0.46
6	D50	D93	TG	1	1	3	3	1	0	0.68

Note:

SS: Simultaneous Display, TG: Toggling Display.

Table 4.13 Summary of models' performance from six images combined evaluated using the paired comparison method.

Phase	Hardcopy	Softcopy	XYZ		Hunt	RLAB		95% CL		
1	D65	D65(ss)	<u>0.544</u> (1)		-0.023 (1)		-0.520 (1)		1.39	
2	D50	D50(ss)	<u>0.210</u> (1)		0.070 (1)		-0.280 (1)		1.39	
			CIELAB	CIELUV	Hunt	Nayatani	von Kries	BFD	RLAB	95% CL
3	D50	D65(ss)	0.757 (5)	-11.879 (7)	2.709 (1)	<u>3.660</u> (1)	2.365 (1)	1.853 (3)	0.535 (5)	1.39
4	D65	D93(ss)	-1.753 (6)	-12.888 (7)	2.317 (2)	<u>4.409</u> (1)	2.634 (2)	2.242 (2)	2.891 (2)	1.39
5	D50	D93(tg)	-4.022 (6)	-14.450 (7)	2.744 (3)	2.871 (3)	3.260 (2)	<u>4.948</u> (1)	4.299 (1)	1.39
6	D50	D93(ss)	-3.303 (6)	-16.281 (7)	3.833 (1)	2.937 (3)	2.676 (3)	<u>4.956</u> (1)	3.854 (1)	1.39
7	A	D65(ss)	1.178 (3)	-16.092 (7)	0.879 (5)	-0.050 (5)	4.776 (2)	<u>7.423</u> (1)	1.602 (3)	1.39

Note:

1) The figure underlined indicates the best model in a particular phase and CL represents confidence limit.

2) The figure in the bracket indicates the rank order in each phase (using 95% CL).

Table 4.14 Summary of models' image dependency using the difference between the highest and the lowest z scores.

Phase	Hardcopy	Softcopy	XYZ	Hunt	RLAB
1	D65	D65 (SS)	2.095	2.358	2.227
2	D50	D50 (SS)	1.555	2.365	3.347

Phase	Hardcopy	Softcopy	CIELAB	CIELUV	Hunt	Nayatani	von Kries	BFD	RLAB
3	D50	D65 (TG)	1.538	2.059	3.747	3.185	2.993	1.776	3.764
4	D65	D93 (TG)	4.111	2.986	6.480	3.786	3.704	2.882	5.688
5	D50	D93 (SS)	7.534	1.694	3.649	4.055	5.602	2.764	9.224
6	D50	D93 (TG)	8.325	1.864	3.447	2.316	4.849	1.018	6.353
7	A	D65 (TG)	7.674	0.847	5.367	7.753	5.884	7.834	5.205

Note:

SS: Simultaneous Display, TG: Toggling Display.

Table 4.15 Summary of models' performance from six images combined evaluated using the category judgement method.

Phase	Hardcopy	Softcopy	XYZ	Hunt	RLAB	CBAM
1	D65	D65	<u>2.427</u> (1)	2.237 (3)	2.249 (2)	1.241–2.340
2	D50	D50	<u>2.839</u> (1)	2.754 (3)	2.818 (2)	1.549–2.676

Phase	Hardcopy	Softcopy	CIELAB	CIELUV	Hunt	Nayatani	von Kries	BFD	RLAB	CBAM
3	D50	D65	3.656 (6)	1.679 (7)	4.055 (2)	<u>4.188</u> (1)	3.981 (3)	3.928 (4)	3.719 (5)	2.509–3.748
4	D65	D93	2.276 (6)	0.826 (7)	2.642 (5)	<u>3.125</u> (1)	2.931 (2)	2.797 (3)	2.710 (4)	1.604–2.709
5	D50	D93	1.941 (6)	0.192 (7)	3.081 (2)	2.918 (5)	2.992 (4)	<u>3.286</u> (1)	3.038 (3)	2.233–3.227
6	D50	D93	2.472 (6)	0.277 (7)	3.487 (2)	3.358 (4)	3.421 (3)	<u>3.656</u> (1)	3.290 (5)	2.314–3.299
7	A	D65	1.912 (5)	-1.651 (7)	2.080 (3)	1.637 (6)	2.589 (2)	<u>2.941</u> (1)	1.973 (4)	2.083–2.996

Note:

- 1) The figure underlined indicates the best model in a particular phase and CBAM represents category boundaries for acceptable match.
- 2) The figure in the bracket indicates the rank order in each phase.

Table 4.16 Mean rank of each model's performance from the paired comparison (pc) and category judgement (cj) methods (Case 2).

Phase	Hard-copy	Soft-copy	CIELAB		CIELUV		Hunt		Nayatani		von Kries		BFD		RLAB	
			pc	cj	pc	cj	pc	cj	pc	cj	pc	cj	pc	cj	pc	cj
3	D50	D65	3.5 (5)	5.2 (5)	7.0 (7)	7.0 (7)	2.0 (3)	3.3 (4)	1.0 (1)	1.7 (1)	1.8 (2)	2.5 (2)	2.5 (4)	3.0 (3)	3.5 (5)	5.3 (6)
4	D65	D93	5.5 (6)	5.8 (6)	7.0 (7)	7.0 (7)	3.0 (5)	4.2 (5)	1.0 (1)	1.0 (1)	2.8 (4)	2.7 (2)	1.8 (2)	3.5 (3)	2.7 (3)	3.8 (4)
5	D50	D93	5.7 (6)	6.0 (6)	7.0 (7)	7.0 (7)	2.7 (4)	3.3 (3)	3.0 (5)	4.0 (5)	2.3 (2)	3.3 (3)	1.3 (1)	1.3 (1)	2.3 (2)	3.0 (2)
6	D50	D93	5.8 (6)	5.8 (6)	7.0 (7)	7.0 (7)	2.0 (2)	2.3 (2)	2.7 (4)	4.2 (5)	3.2 (5)	3.5 (3)	1.2 (1)	1.7 (1)	2.3 (3)	3.5 (3)
7	A	D65	3.7 (5)	4.3 (5)	7.0 (7)	7.0 (7)	3.3 (3)	4.0 (3)	4.7 (6)	5.3 (6)	1.8 (2)	2.0 (2)	1.0 (1)	1.2 (1)	3.5 (4)	4.2 (4)
Average			4.8	5.4	7.0	7.0	2.6	3.4	2.5	3.2	2.4	2.8	1.6	2.1	2.9	4.0
Rank			6	6	7	7	4	4	3	3	2	2	1	1	5	5

Note:

The figure in the bracket indicates the rank order in each phase.

Table 5.1 The F_S , F_L and F_C parameters used in the LLAB model.

	F_S	F_L	F_C
Reflection samples and images in average surround			
Subtending 10°	3.0	0.0	1.00
Subtending 2°	3.0	1.0	1.00
Television and VDU displays in dim surround	3.5	1.0	1.15
Transparency in dark surround	4.2	1.0	0.95

Table 5.2 Values for converting hue angle to hue composition.

h_L	H_L	R	Y	G	B	NCS expression
25	0	100	0	0	0	R
62	50	50	50	0	0	R50Y
93	100	0	100	0	0	Y
118	150	0	50	50	0	Y50G
165	200	0	0	100	0	G
202	250	0	0	50	50	G50B
254	300	0	0	100	0	B
322	350	50	0	0	50	B50R

Table 5.3 Example of input data and calculated results using the LLAB colour model.

Input Data									
Surround	X_s	Y_s	Z_s	X_o	Y_o	Z_o	F_S	F_L	F_C
Average	9.12	8.94	23.50	94.82	100.00	107.30	3.0	1.0	1.00
Dim	9.12	8.94	23.50	94.82	100.00	107.30	3.5	1.0	1.15
Dark	9.12	8.84	23.50	94.82	100.00	107.30	4.2	1.0	0.95
Perceived Attribute									
Surround	X_d	Y_d	Z_d	L_L	A_L	B_L	C_L	h_L	H_L
Average	9.17	8.95	23.81	20.21	7.11	-38.81	39.45	280.38	B19R
Dim	9.17	8.95	23.81	26.76	8.02	-42.92	43.66	280.59	B20R
Dark	9.17	8.95	23.81	34.50	6.39	-33.48	34.09	280.80	B20R

Table 5.4 Data used to formulate the S_C function in the LLAB colour model.

Data Set	Luminance	Log (Luminance)	Sc
Alvey(Surface_BB)	42	1.62	1.6
	252	2.4	1.73
Alvey(Surface_WB)	44	1.64	1.69
	264	2.42	1.89
Alvey(Surface_GB)	42	1.62	1.68
	42	1.62	1.59
	40.5	1.61	1.65
	42	1.62	1.63
	232	2.37	1.82
	252	2.4	1.83
	243	2.39	1.86
	252	2.4	1.81
CARISMA(Surface)	843	2.93	1.73
	200	2.3	1.79
	62	1.79	1.58
	17	1.23	1.49
	6	0.78	1.33
	0.4	-0.4	0.88
	843	2.93	1.9
	200	2.3	1.84
	62	1.79	1.59
	17	1.23	1.44
	6	0.78	1.38
0.4	-0.4	0.8	

Note:

BB: Black Background, WB: White Background, GB: Grey Background

Table 5.5 Summary the experimental conditions used in each LUTCHI data set

Data Set	A	B	C	D	E	F	G
Research Project	Alvey	Alvey	Alvery	CARISMA	Kuo & Luo	CARISMA	CARISMA
Medium	Surface	Surface	Self-luminous	Surface	Surface	Transparency	
Material	Paint	Paint	Monitor	Paint	Textile	LT	35mm
No. of Phases	6	6	11	6	3	10	6
Light source	(D50, D65, W, A)			D50	(D65, TL84, A)	D50	A, Xenon
Luminance (cd/m ²)	250	40	40	850-0.3	250-540	2000-300	110-45
Background+	W,G,B	W,G,B	W,G,B	G	G	G	G
Sample size	2°	2°	2°	2°	10°	2°	2°
Colours/ phase	105	105	103-61	40	270	98-94	99-36
No. of Observers	6-7	6-7	6-7	4	8	7-8	5-6

Note +: W, G and B represents white, grey and black backgrounds used in the experiment.

Table 5.6 Summary of observer precision (CVs) in each LUTCHI data set.

Data Set	A	B	C	D	E	F	G
Lightness	13	13	13	10	11	15	16
Colourfulness	18	18	18	16	17	17	16
Hue	9	9	9	6	7	6	7

Table 5.7 Parameters used in each space or model for testing colour appearance data

Data Set		A	B	C	D	E	F	G
Uniform Colour Space								
CMC	SF	1.80	1.64	1.64	1.64	1.47	1.59	1.47
CIELAB	SF	1.02	0.94	0.94	0.94	0.80	0.88	0.80
CIELUV	SF	0.80	0.69	0.69	0.69	0.69	0.87	0.69
Colour Appearance Model								
Nayatani	SF	1.20	2.00	2.00	1.80	0.76	0.70	1.30
RLAB	D	1.00	1.00	0.00	1.00	1.00	0.50	0.50
	s	2.30	2.30	2.90	2.30	2.30	2.90	3.50
	SF	1.00	1.00	1.00	1.00	0.83	1.00	1.00
Hunt94	Nb	75	75	25	75	75	25	10
	Nc	1.00	1.00	1.00	1.00	1.00	0.70	0.70
Lightness scale	J	J	J	J	J	J	J	Jp
	z	z	z	z	z	1.10	z'	1.20
Helson-Judd effect	inc.	inc.	inc.	inc.	inc.	exc.	inc.	exc.
	SF	0.89	0.89	0.89	0.89	0.71	0.89	0.89
LLAB	F _L	1.00	1.00	1.00	0.00	1.00	1.00	1.00
	F _S	3.00	3.00	3.50	3.00	3.00	4.20	4.20
	F _C	1.00	1.00	1.15	1.00	1.00	0.95	0.95
	SF	1.00	1.00	1.00	1.00	0.80	1.00	1.00

Note:

For calculating Hunt's lightness values, two scales plus different z values are required (Luo et al. 1993b, Hunt and Luo 1994).

Table 5.8 CVs for Set A of LUTCHI Colour Appearance Data (Alvey surface-colour high-luminance experimental results).

Phase	A-1	A-2	A-3	A-4	A-5	A-6	
Source	D50	D50	D50	D65	WF	A	
Luminance (cd/m ²)	264	252	252	243	252	232	
Background (Y%)	100	6	21	21	21	21	Mean
LIGHTNESS							
CIE	40	13	24	20	18	18	22
CMC	63	31	44	40	37	37	42
Nayatani	44	16	27	23	21	21	25
RLAB	36	11	21	17	15	16	19
Hunt94	16	9	14	13	12	11	13
LLAB	14	8	11	13	12	12	12
CHROMA							
CIELAB	30	28	28	22	32	23	27
CIELUV	31	33	26	25	34	35	31
CMC	23	27	24	13	20	19	26
Nayatani	21	47	29	24	30	26	30
RLAB	31	30	30	23	32	22	28
Hunt94	19	20	15	15	19	18	18
LLAB	23	27	24	13	20	16	21
HUE							
Nayatani	8	20	9	7	14	14	13
RLAB	8	7	7	6	12	8	8
Hunt94	8	7	7	6	9	8	8
LLAB	8	7	6	5	9	5	7

Table 5.9 CVs for Set B of LUTCHI Colour Appearance Data (Alvey surface-colour low-luminance experimental results).

Phase	B-1	B-2	B-3	B-4	B-5	B-6	
Source	D50	D50	D50	D65	WF	A	
Luminance (cd/m ²)	44	42	42	41	42	42	
Background (Y%)	100	6	21	21	21	21	Mean
LIGHTNESS							
CIE	48	19	24	21	21	22	26
CMC	72	38	44	41	42	42	47
Nayatani	52	22	27	24	24	24	29
RLAB	44	16	21	18	18	18	23
Hunt94	15	11	11	10	11	11	12
LLAB	11	10	9	10	9	10	10
CHROMA							
CIELAB	30	28	28	27	34	23	28
CIELUV	30	26	26	28	36	35	30
CMC	23	24	23	20	24	20	24
Nayatani	24	33	24	23	30	23	26
RLAB	30	32	30	28	37	26	31
Hunt94	20	18	17	15	19	17	18
LLAB	24	24	23	20	23	17	22
HUE							
Nayatani	7	27	16	10	15	20	16
RLAB	8	6	7	8	11	10	8
Hunt94	7	7	6	6	10	14	8
LLAB	7	5	6	7	8	6	7

Table 5.10 CVs for Set C of LUTCHI Colour Appearance Data (Alvey monitor-colour experimental results).

Phase	C-1	C-2	C-3	C-4	C-5	C-6	C-7	C-8	C-9	C-10	C-11	
Source	D50	D50	D50	D50	D50	D65	D65	WF	WF	A	A	
Luminance (cd/m ²)	40	45	45	45	45	41	41	28	28	20	20	
Background (Y%)	100	6	21	21	21	21	21	21	21	21	21	Mean
LIGHTNESS												
CIE	36	12	20	11	21	21	18	19	16	21	18	18
CMC	62	21	32	42	31	41	37	41	37	44	40	39
Nayatani	39	9	15	23	14	25	21	21	18	23	19	21
RLAB	46	11	20	28	19	27	24	30	26	34	30	27
Hunt94	13	9	9	9	8	12	9	10	9	9	9	10
LLAB	14	7	8	9	6	13	10	10	8	10	8	9
CHROMA												
CIELAB	26	21	18	18	21	25	24	33	31	45	39	27
CIELUV	30	25	22	23	23	25	25	43	43	37	32	30
CMC	21	17	17	15	19	19	18	25	21	37	32	22
Nayatani	32	30	17	19	19	24	20	46	45	50	47	32
RLAB	29	25	21	22	26	27	24	35	34	35	40	29
Hunt94	16	15	15	16	13	16	12	27	25	30	28	19
LLAB	28	21	22	22	20	19	20	20	17	29	25	22
HUE												
Nayatani	9	30	15	16	15	9	9	14	14	18	16	15
RLAB	10	8	7	7	8	7	7	13	13	17	24	11
Hunt94	8	7	7	6	6	6	6	8	9	12	9	8
LLAB	8	6	6	6	5	6	7	8	9	18	13	8

Table 5.11 CVs for Set D of LUTCHI Colour Appearance Data (CARISMA surface-colour experimental results).

Phase	D-1	D-2	D-3	D-4	D-5	D-6		
Source	D50	D50	D50	D50	D50	D50		
Luminance (cd/m ²)	843	200	62	17	6	0.4	6 Phases	5 Phases
Background (Y%)	21	21	21	21	21	21	Mean	Mean+
LIGHTNESS								
CIE	11	14	15	16	16	23	16	14
CMC	27	33	33	35	37	44	35	33
Nayatani	12	16	18	18	18	25	18	16
RLAB	10	12	13	14	14	21	14	13
Hunt94	14	13	14	12	13	18	14	13
LLAB	20	16	16	13	14	17	16	16
CHROMA								
CIELAB	23	24	21	28	41	129	44	27
CIELUV	27	27	21	25	27	93	37	25
CMC	19	21	18	24	36	128	41	24
Nayatani	177	70	26	36	57	71	73	73
RLAB	26	29	28	35	48	137	50	33
Hunt94	22	16	19	18	21	41	23	19
LLAB	19	20	19	21	28	38	24	21
HUE								
Nayatani	8	9	15	19	18	25	15	14
RLAB	6	7	7	8	6	9	7	7
Hunt94	6	7	7	9	7	11	7	7
LLAB	5	6	6	7	4	9	6	6

Note+: Mean calculated from 5 phases excluding phase 6 (Very low luminance).

Table 5.12 CVs for Set E of LUTCHI Colour Appearance Data (Kuo and Luo surface-colour experimental results).

Phase	E-1	E-2	E-3	
Source	D65	TL84	A	
Luminance (cd/m ²)	250	540	250	
Background (Y%)	16	16	16	Mean
LIGHTNESS				
CIE	7	7	7	7
CMC	28	29	26	28
Nayatani	9	8	8	8
RLAB	7	7	8	7
Hunt94	8	7	8	8
LLAB	7	7	7	7
CHROMA				
CIELAB	33	38	35	35
CIELUV	35	36	41	37
CMC	27	30	27	28
Nayatani	31	47	38	39
RLAB	36	41	36	37
Hunt94	16	20	21	19
LLAB	27	29	27	28
HUE				
Nayatani	19	13	19	17
RLAB	9	7	12	10
Hunt94	9	7	11	9
LLAB	8	7	9	8

Table 5.13 CVs for Set F of LUTCHI Colour Appearance Data (CARISMA large transparency (LT) experimental results).

Phase	F-1	F-2	F-3	F-4	F-5	F-6	F-7	F-8	F-9	F-10	
Source	D50	D50	D50	D50	D50	D50	D50	D50	D50	D50	
Luminance (cd/m ²)	2100	660	320	660	2100	660	320	660	660	660	
Background (Y%)	17	17	17	17	10	10	10	10	10	17	Mean
LIGHTNESS											
CIE	21	16	16	18	28	23	24	18	19	21	20
CMC	13	23	19	20	9	14	11	19	17	15	16
Nayatani	22	16	16	18	27	23	24	17	18	21	20
RLAB	10	11	10	14	16	10	11	10	9	9	11
Hunt94	10	10	10	12	10	9	8	12	10	12	10
LLAB	10	9	9	12	13	9	9	10	9	11	10
CHROMA											
CIELAB	24	22	24	18	22	21	21	22	20	25	22
CIELUV	27	26	26	25	29	27	27	24	25	29	26
CMC	21	19	23	17	21	18	20	18	15	22	21
Nayatani	54	26	27	21	57	33	35	27	28	33	34
RLAB	27	26	27	23	27	26	26	27	24	29	26
Hunt94	20	17	20	19	22	14	16	16	13	20	18
LLAB	21	20	23	19	20	19	21	20	17	24	20
HUE											
Nayatani	18	15	18	18	18	18	12	18	18	16	17
RLAB	7	8	7	6	7	6	7	6	6	7	7
Hunt94	7	5	8	7	7	8	8	8	7	6	7
LLAB	7	7	7	6	7	6	7	7	5	7	7

Table 5.14 CVs for Set G of LUTCHI Colour Appearance Data (CARISMA 35mm projection experimental results).

Phase	G-1	G-2	G-3	G-4	G-5	G-6	
Source	A	Xenon	A	A	A	A	
Luminance (cd/m ²)	113	47	45	113	75	75	Mean
LIGHTNESS							
CIE	20	20	19	17	20	13	18
CMC	37	41	40	32	36	24	35
Nayatani	21	22	21	19	21	13	19
RLAB	34	37	36	30	33	22	32
Hunt94	13	13	13	11	13	10	12
LLAB	19	19	18	16	19	13	17
CHROMA							
CIELAB	19	19	17	17	19	20	18
CIELUV	27	23	26	25	24	21	24
CMC	18	19	16	17	18	20	18
Nayatani	20	18	30	27	28	32	26
RLAB	25	24	24	24	25	22	24
Hunt94	18	19	17	17	20	19	18
LLAB	20	19	18	20	23	22	20
HUE							
Nayatani	17	17	17	18	18	16	17
RLAB	10	10	9	10	10	13	10
Hunt94	8	8	7	8	7	10	8
LLAB	7	9	8	8	9	12	9

Table 5.15 Summary CVs for all models tested in predicting 7 sets of LUTCHI colour appearance data.

Data Sets	A	B	C	D	E	F	G	
Phase	6	6	11	6	3	10	6	Mean
Lightness								
CIE	22	26	18	14	7	20	18	18
CMC	42	47	39	33	28	16	35	34
Nayatani	25	29	21	16	8	20	19	20
RLAB	19	23	27	13	7	11	32	19
Hunt94	13	12	10	13	8	10	12	11
LLAB	12	10	9	16	7	10	17	12
Obs. precision	13	13	13	10	11	15	16	13
Chroma								
CIELAB	27	28	27	27	35	22	18	26
CIELUV	31	30	30	25	37	26	24	29
CMC	26	24	22	24	28	21	18	23
Nayatani	30	26	32	73	39	34	26	37
RLAB	28	31	29	33	37	26	24	30
Hunt94	18	18	19	19	19	18	18	18
LLAB	21	22	22	21	28	20	20	22
Obs. precision	18	18	18	16	17	17	16	17
Hue								
Nayatani	13	16	15	14	17	17	17	16
RLAB	8	8	11	7	10	7	10	9
Hunt94	8	8	8	7	9	7	8	8
LLAB	7	7	8	6	8	7	9	7
Obs. precision	9	9	9	6	7	6	7	8

FIGURES

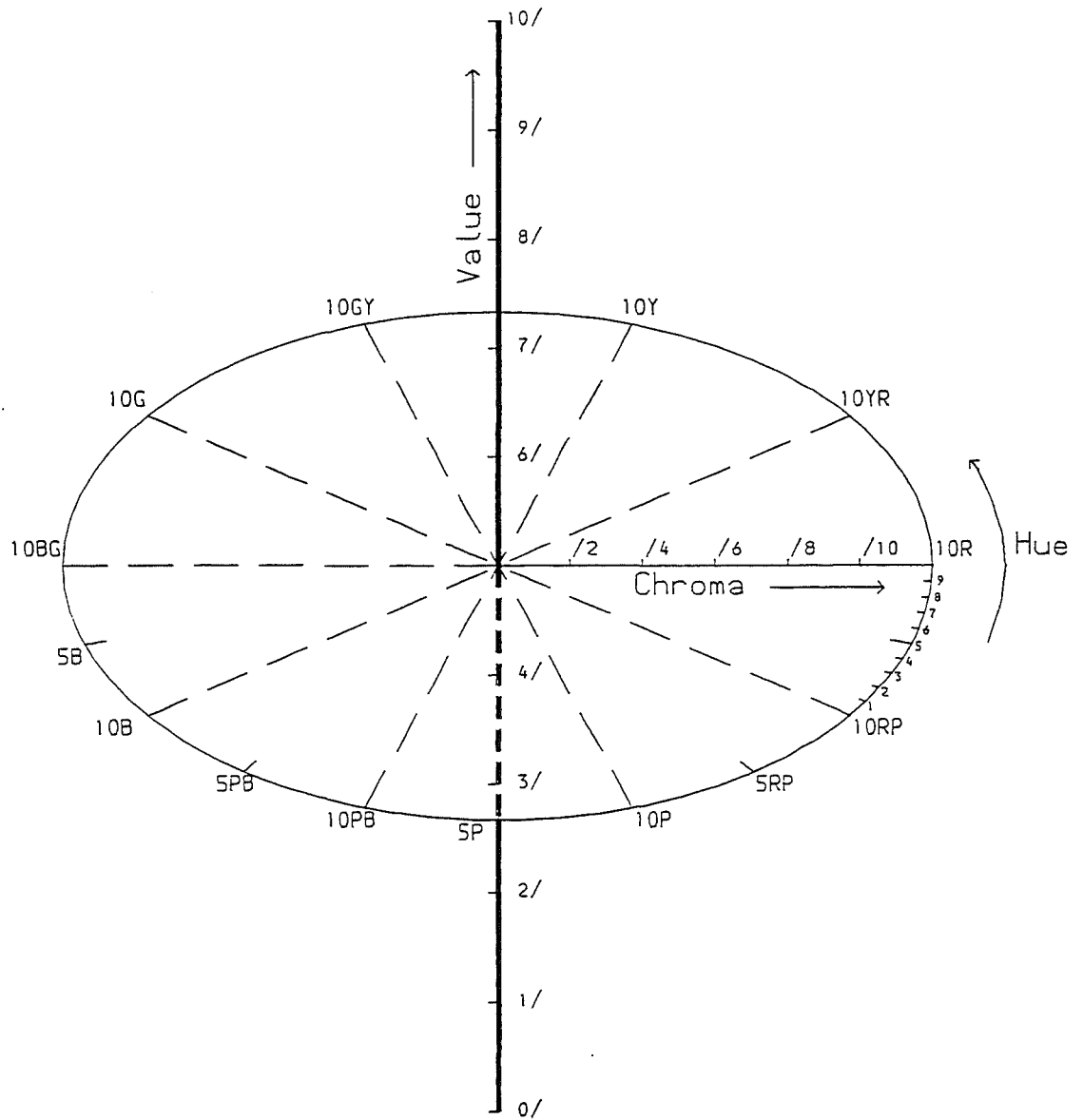


Fig. 2.1 Hue, value, and chroma coordinates of the Munsell system.

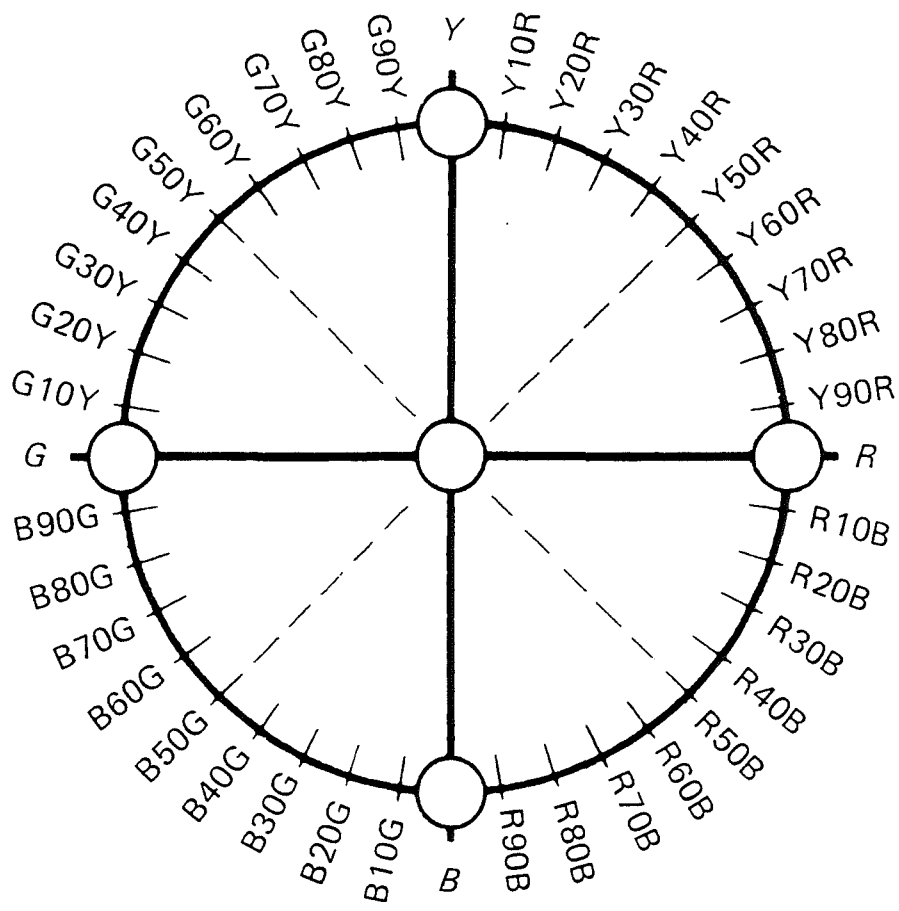


Fig. 2.2 The NCS hue arrangement.

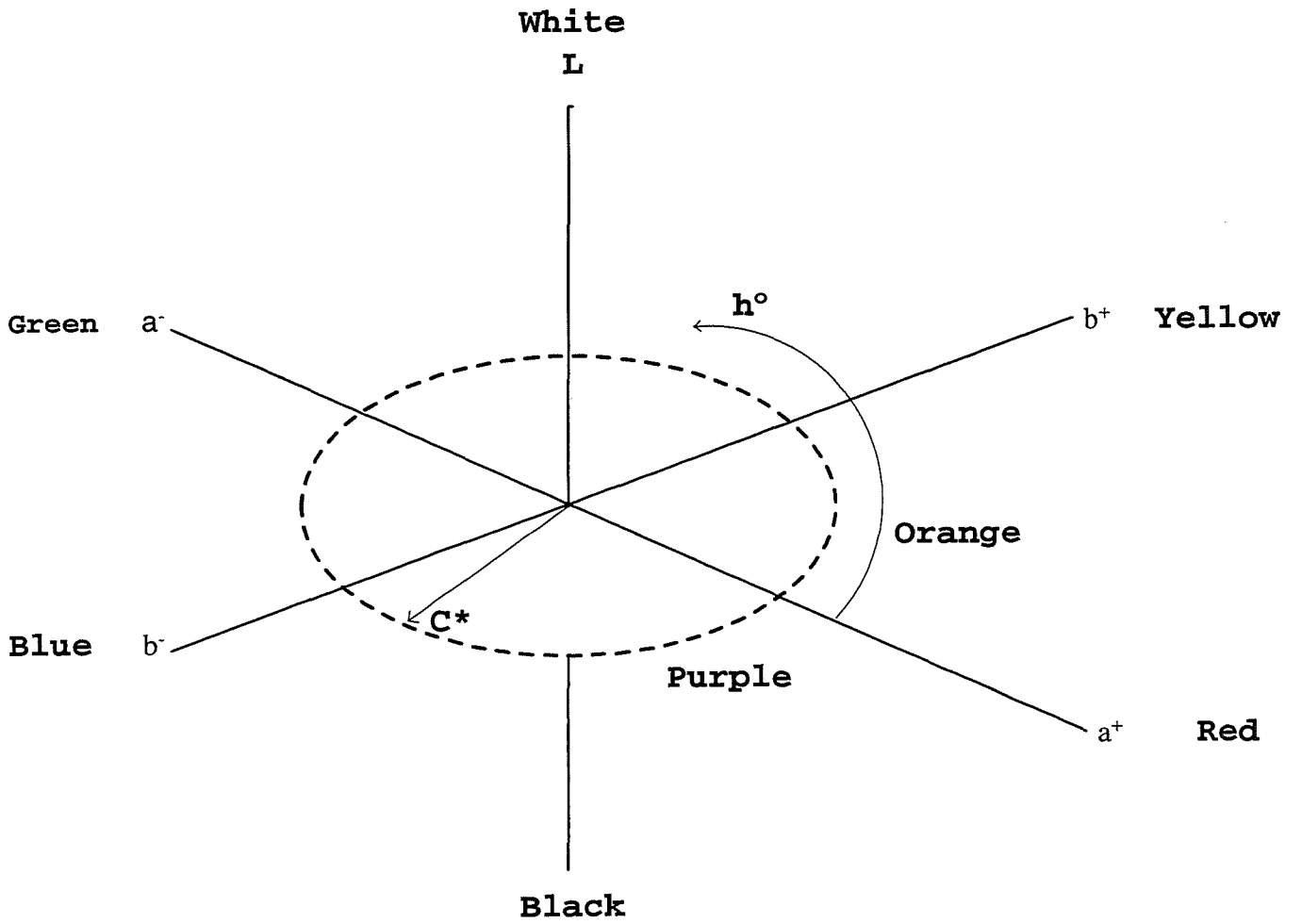


Fig. 2.3 Rectangular and cylindrical coordinates of CIELAB space.

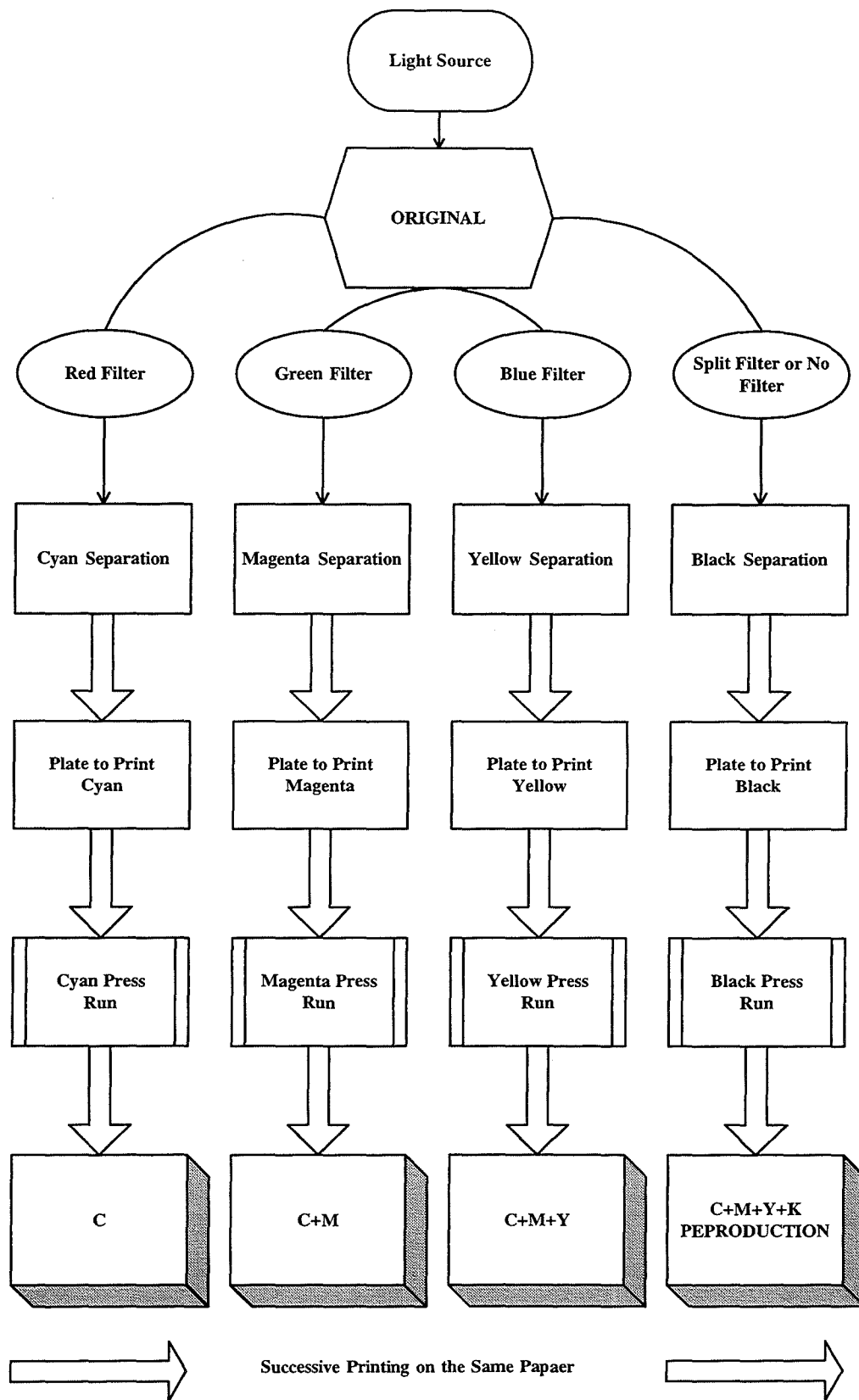


Fig. 2.4 Process for a printing colour reproduction .

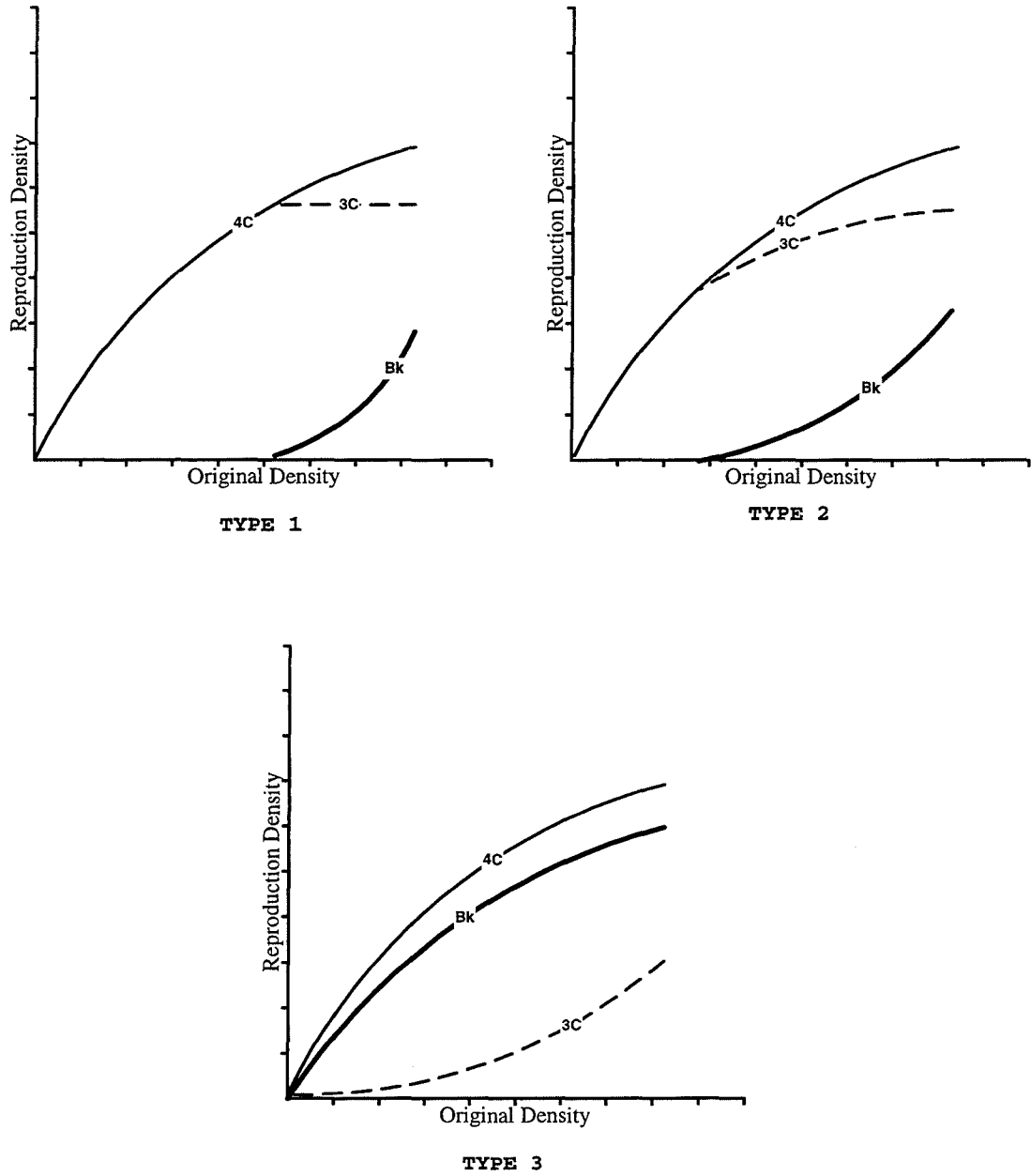


Fig. 2.5 Examples of three different types of black printer.

Type 1: The amount of black is kept to an absolute minimum and is only used when the three-colour grey has reached its maximum.

Type 2: The black is used to extend the maximum density for the three colours.

Type 3: The full scale black printer.

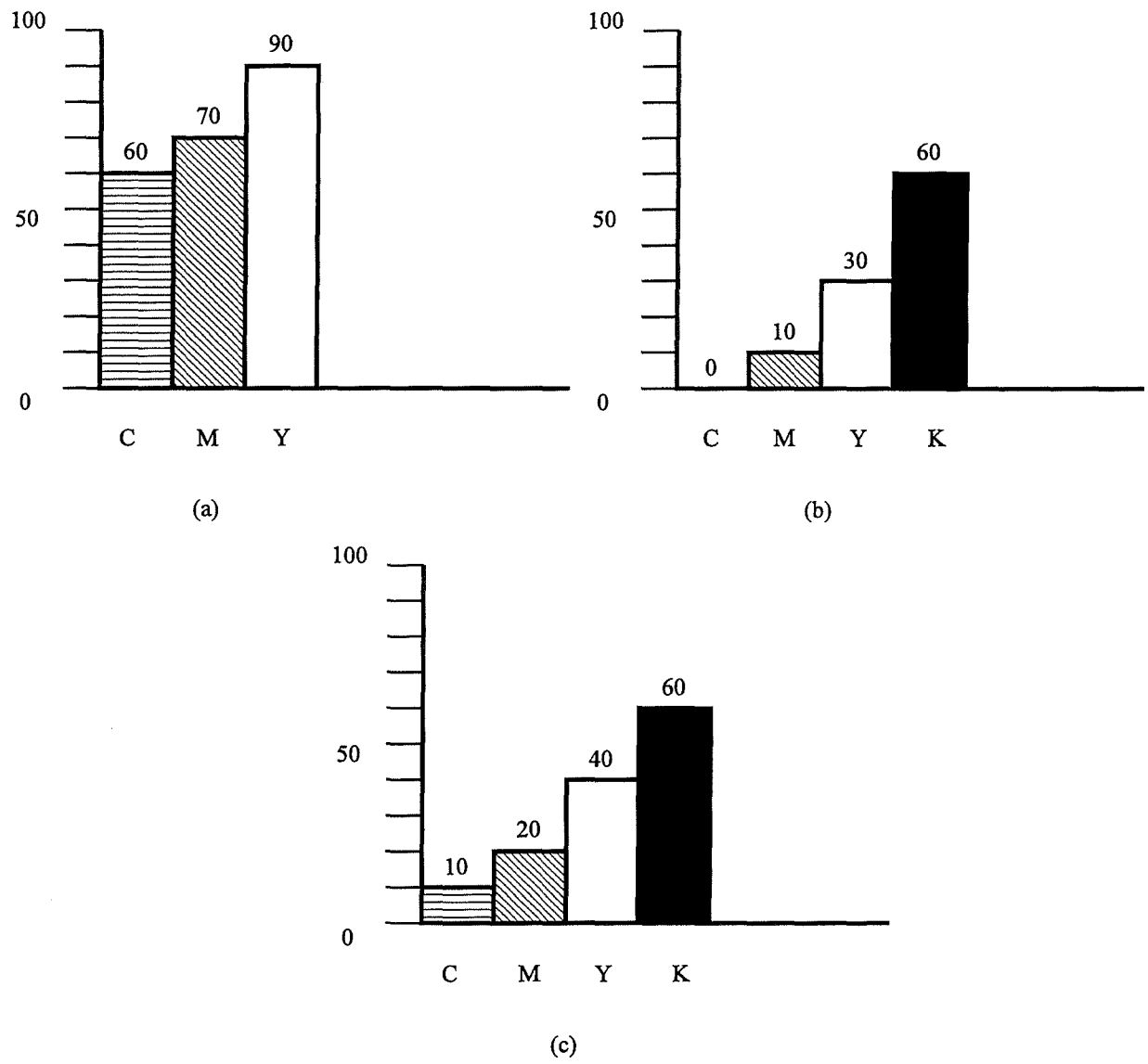


Fig. 2.6 (a) Conventional Chromatic, (b) Ideal 100% GCR, and (c) Practical 100% GCR values.

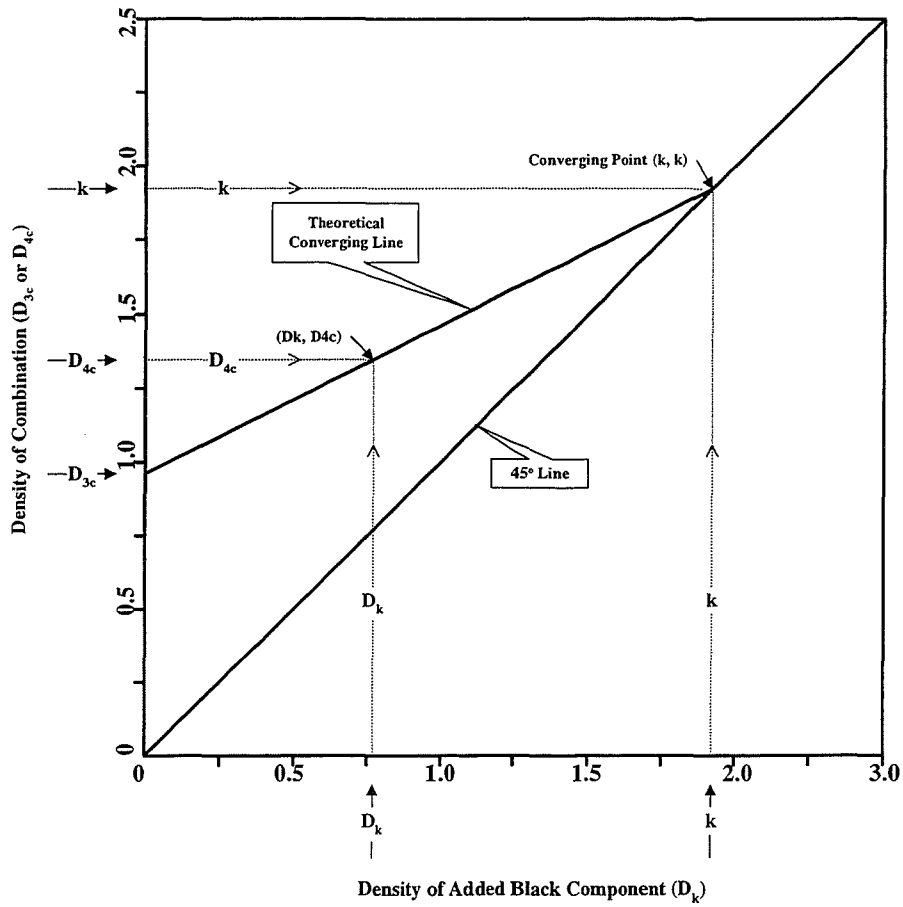


Fig. 2.7 Sub-additivity diagram representing the general sub-additivity behaviour of inks.

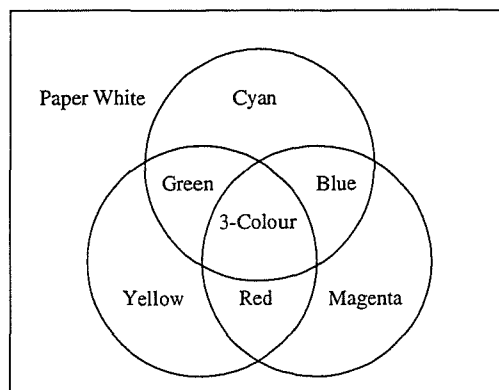


Fig. 2.8 Schematic illustration of the eight Neugebauer primaries produced by overlapping of the Cyan, Magenta, and Yellow halftone dots.

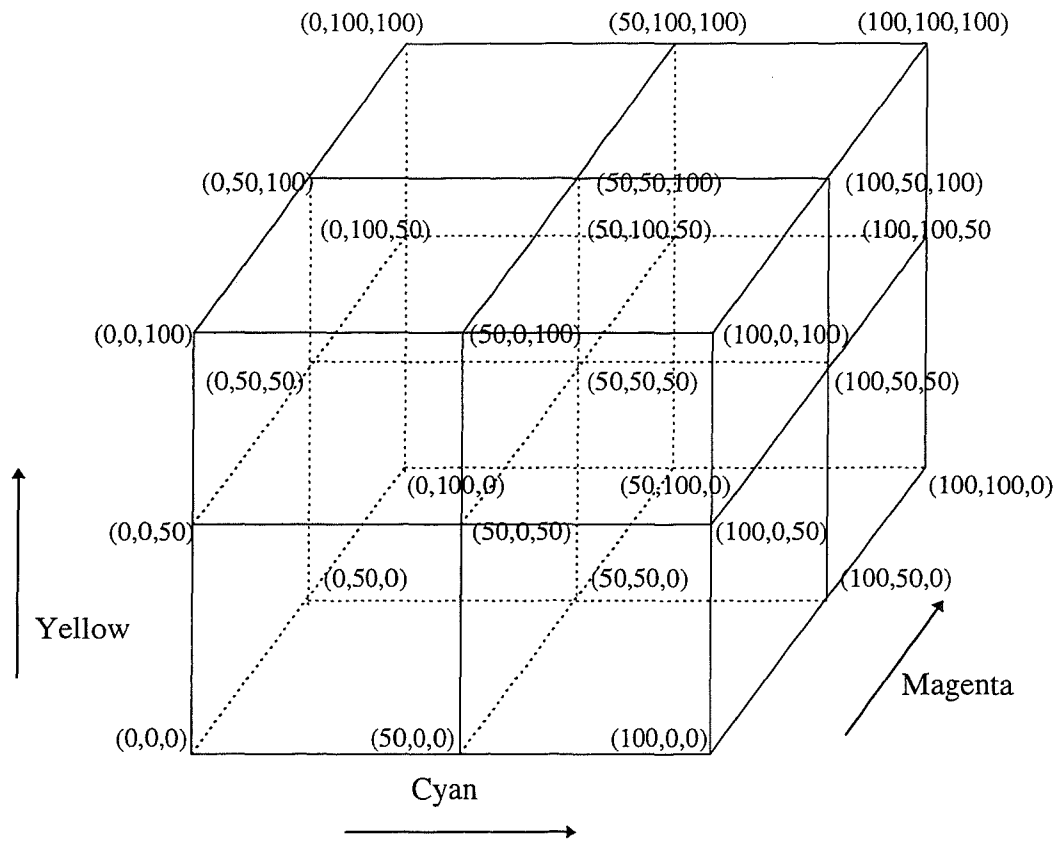


Fig. 2.9 "Cellular" corner-points of the eight cells determined using the combination of 0%, 50% and 100% for each of the CMY primaries.

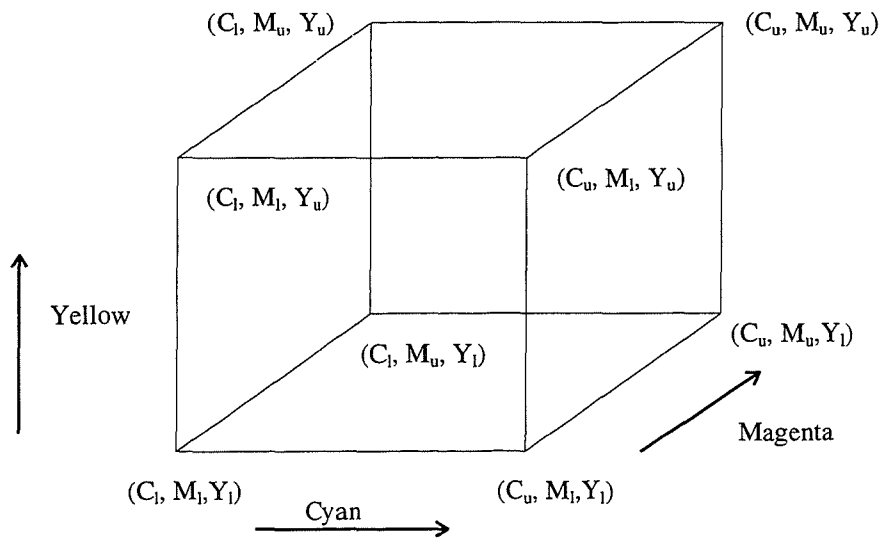


Fig. 2.10 One subset cell from the CMY space in Fig. 2.9.

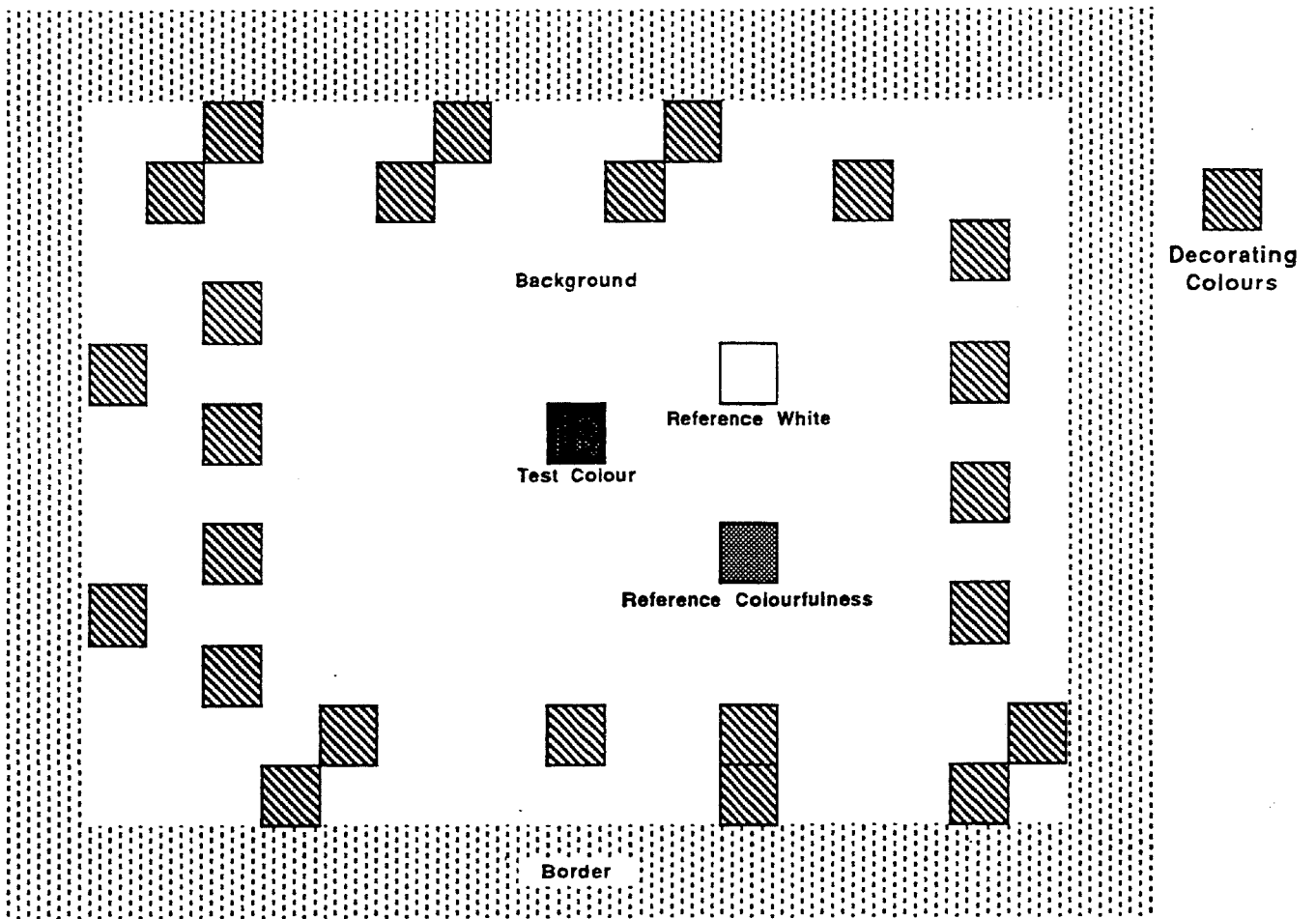


Fig. 2.11 The contents of the viewing pattern (Alvey Colour Appearance Data-Surface and Monitor Data Sets and CARISMA Colour Appearance Data-Surface Data Set).

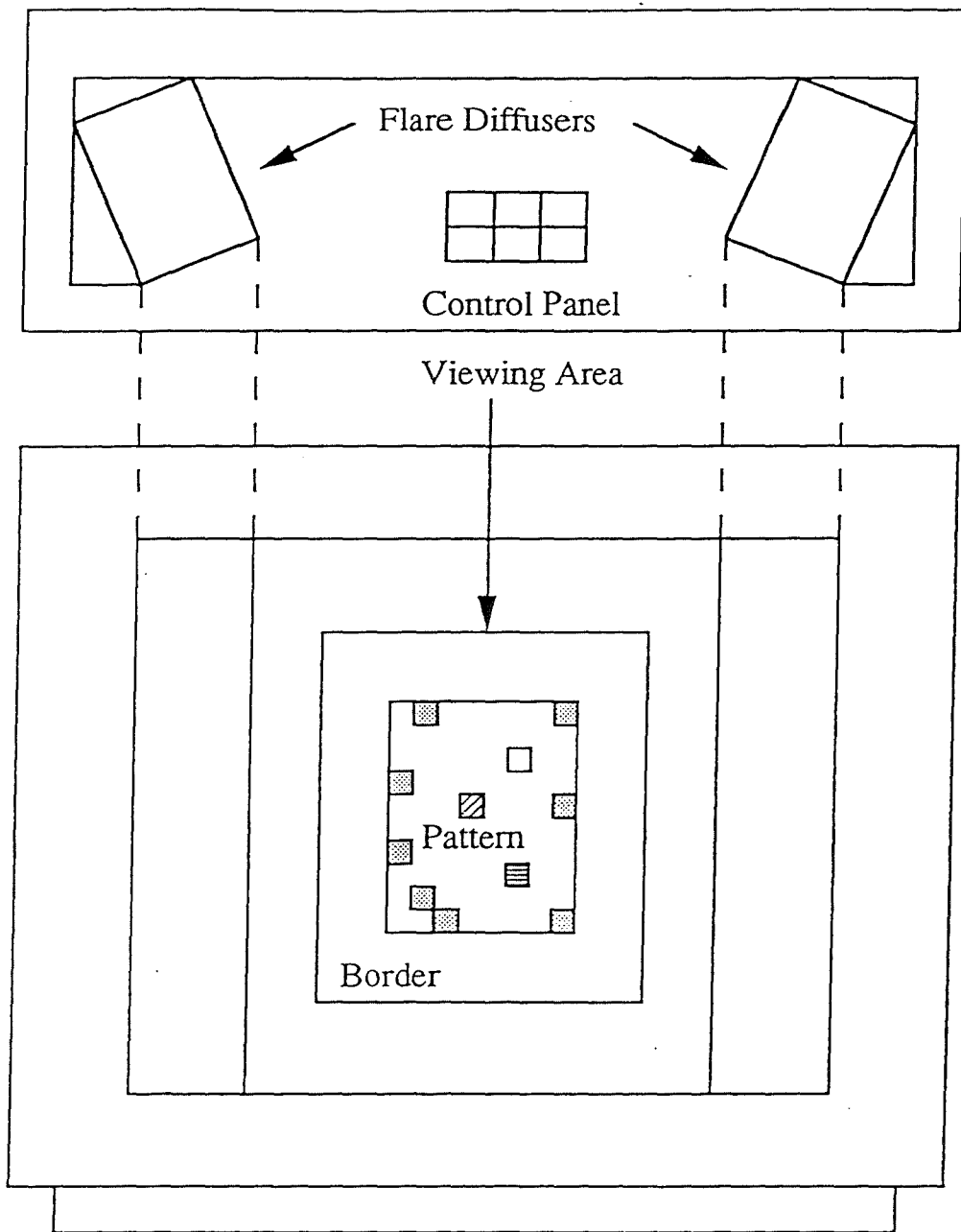


Fig. 2.12 Back-lit illuminator used in the LT (cut-sheet transparency) experiment.

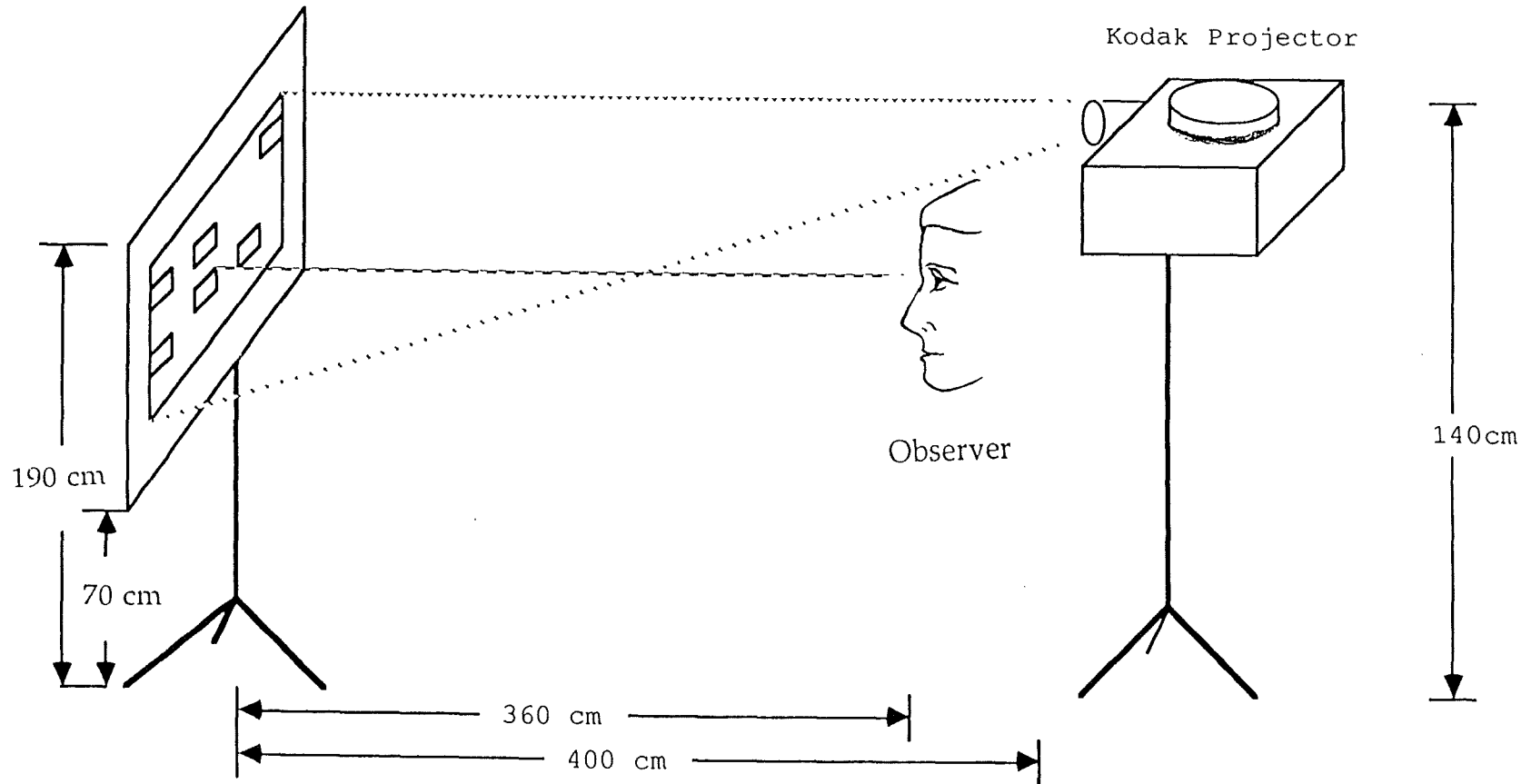


Fig. 2.13 Diagram of 35mm projected slide experimental situation.

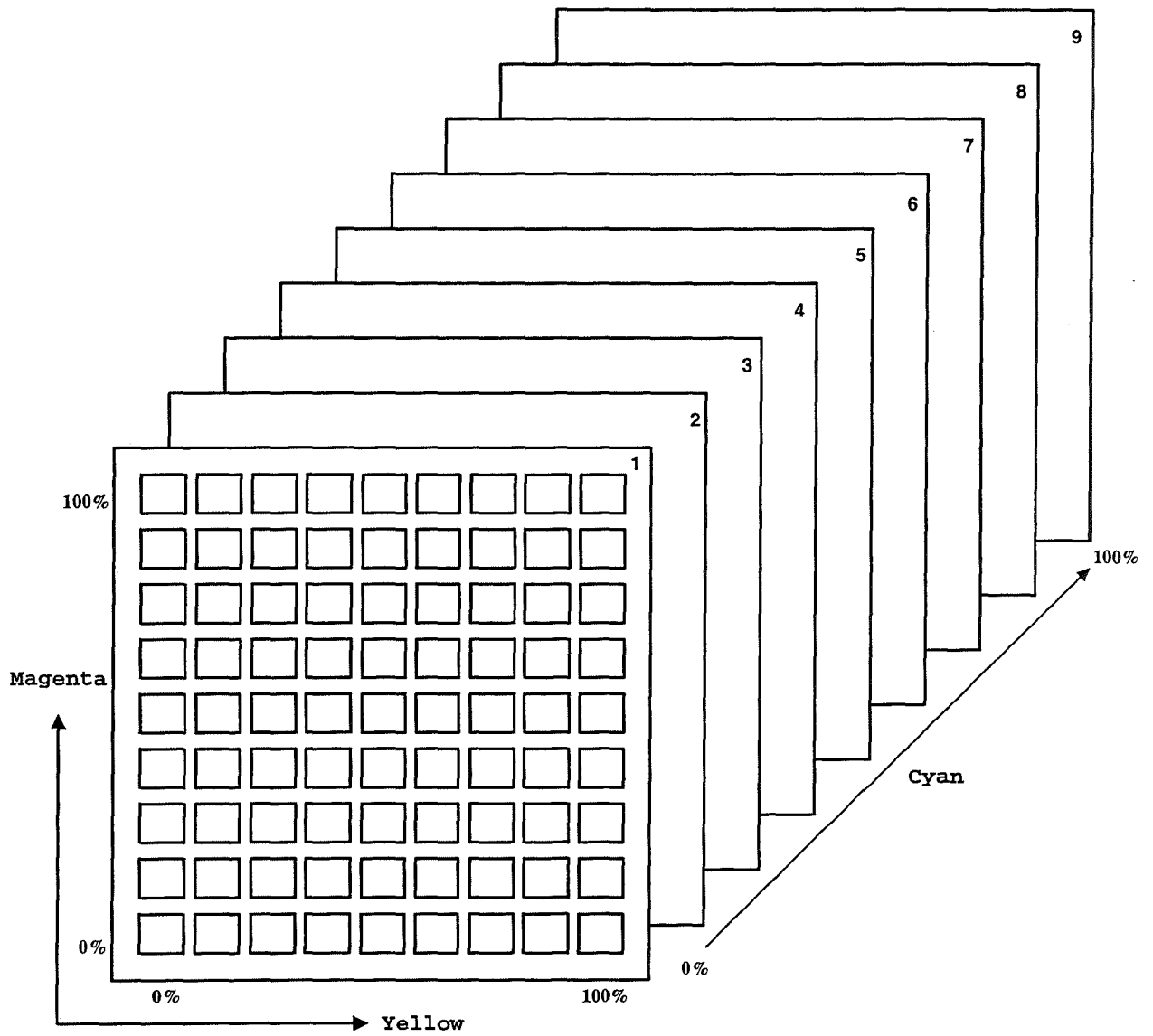


Fig. 3.1 Arrangement of colour patches in cube (or 729) data set (using cyan, magenta, and yellow primaries).

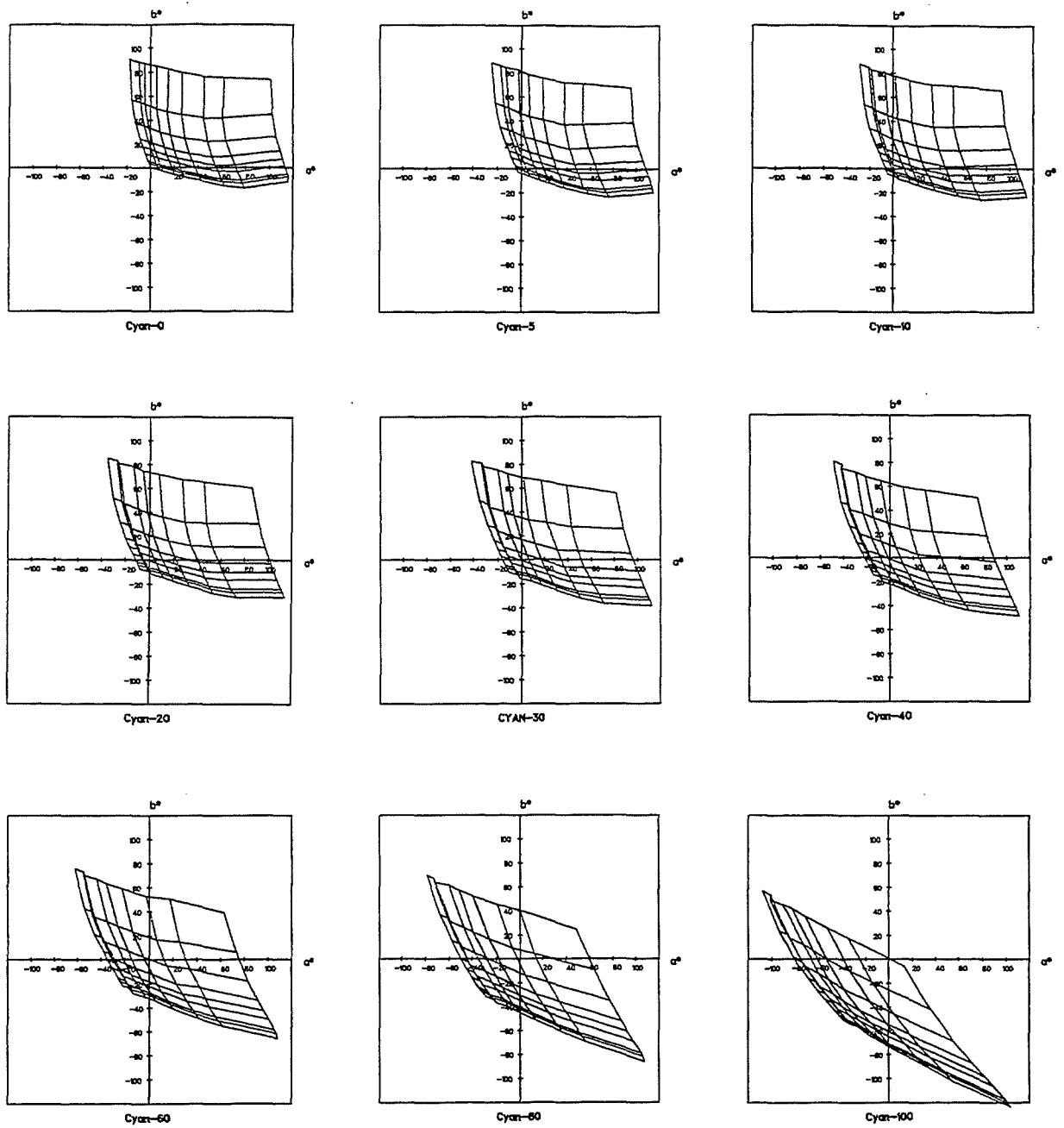


Fig. 3.2 (a) Constant cyan plans with variation of magenta and yellow of the 729 cube data set plotted on CIE a^*b^* diagram for IRIS device.

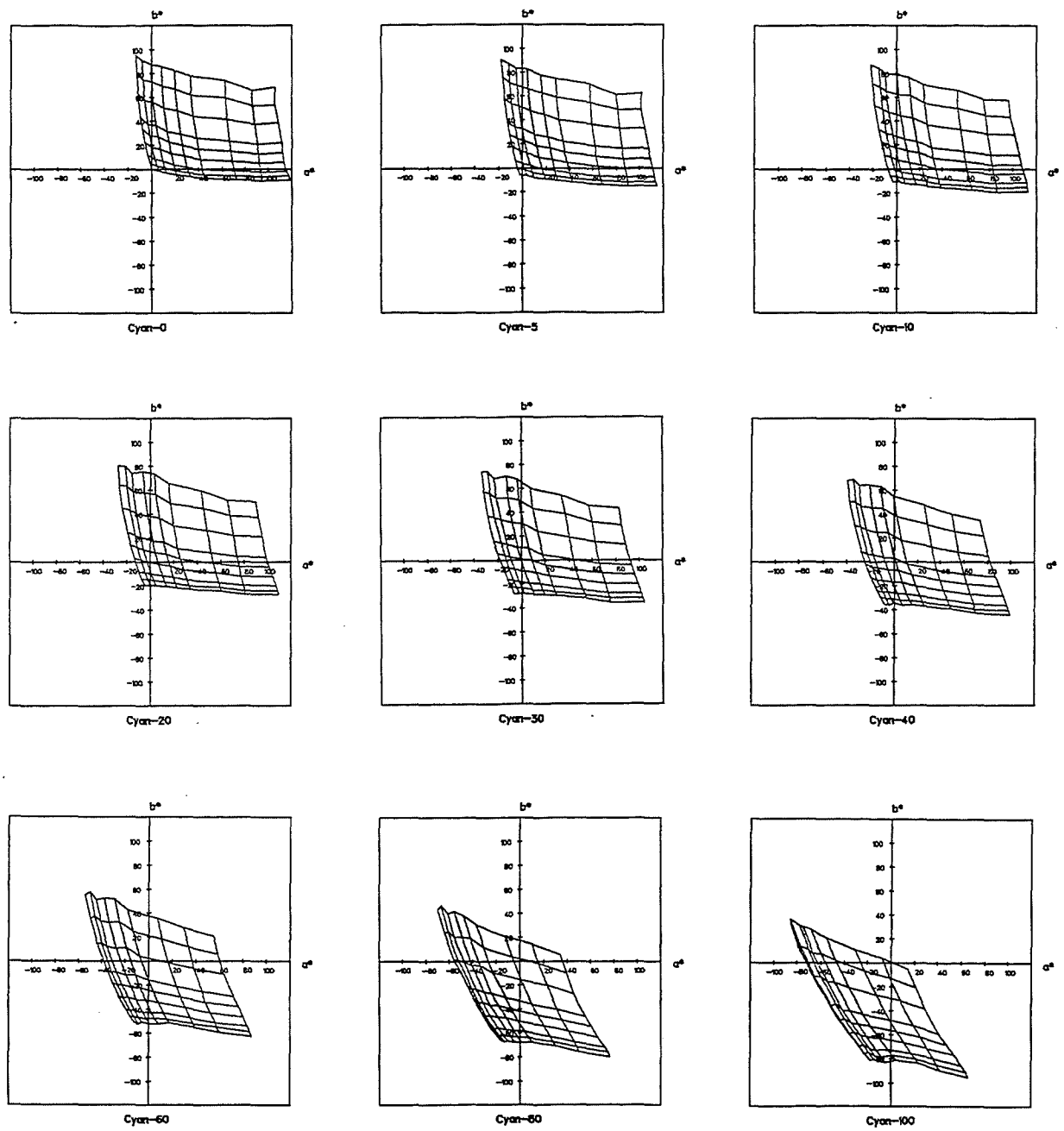


Fig. 3.2 (b) Constant cyan plans with variation of magenta and yellow of the 729 cube data set plotted on CIE a^*b^* diagram for Cromalin device.

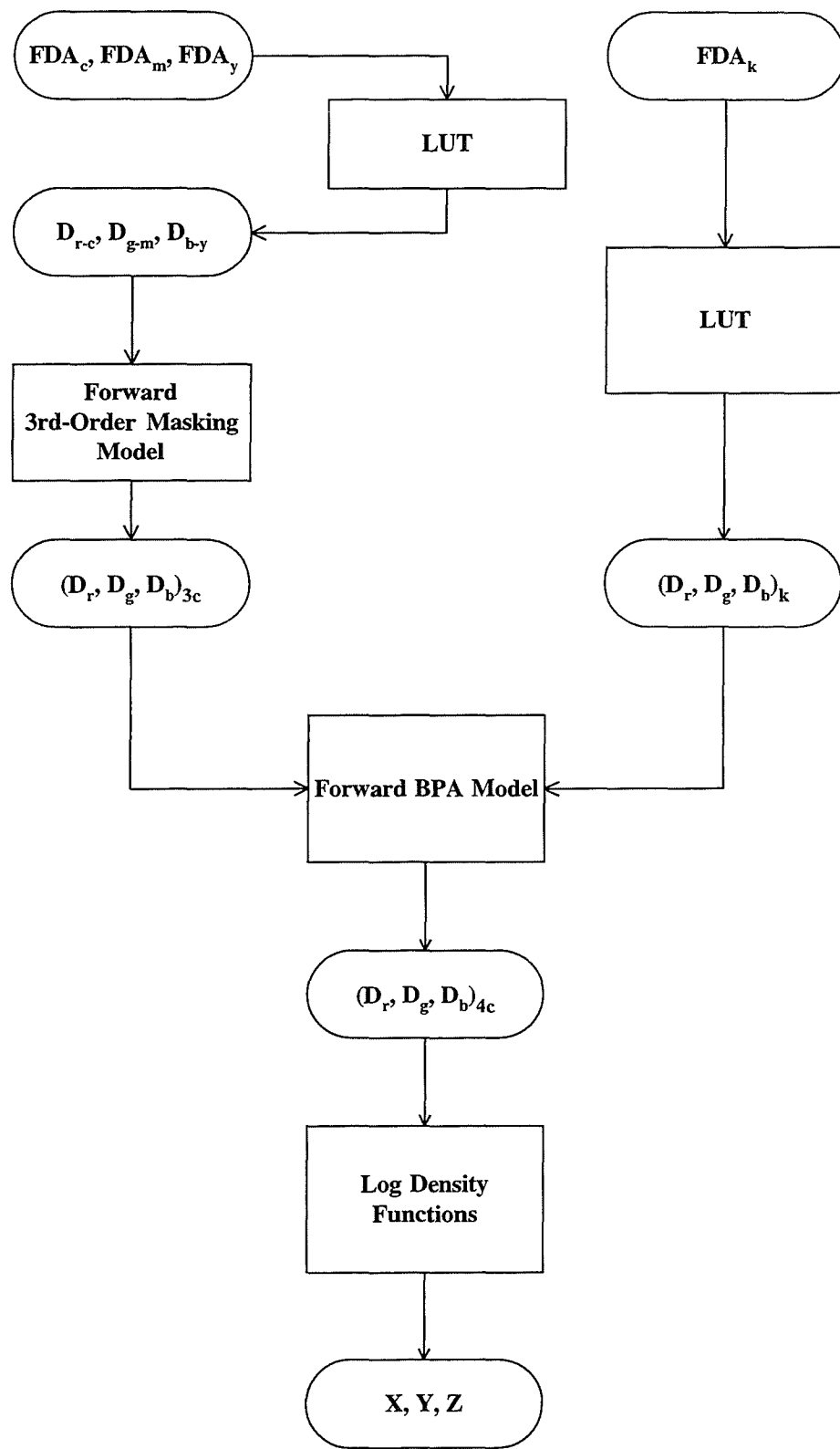


Fig. 3.3 The computational procedures used in the forward BPA models.

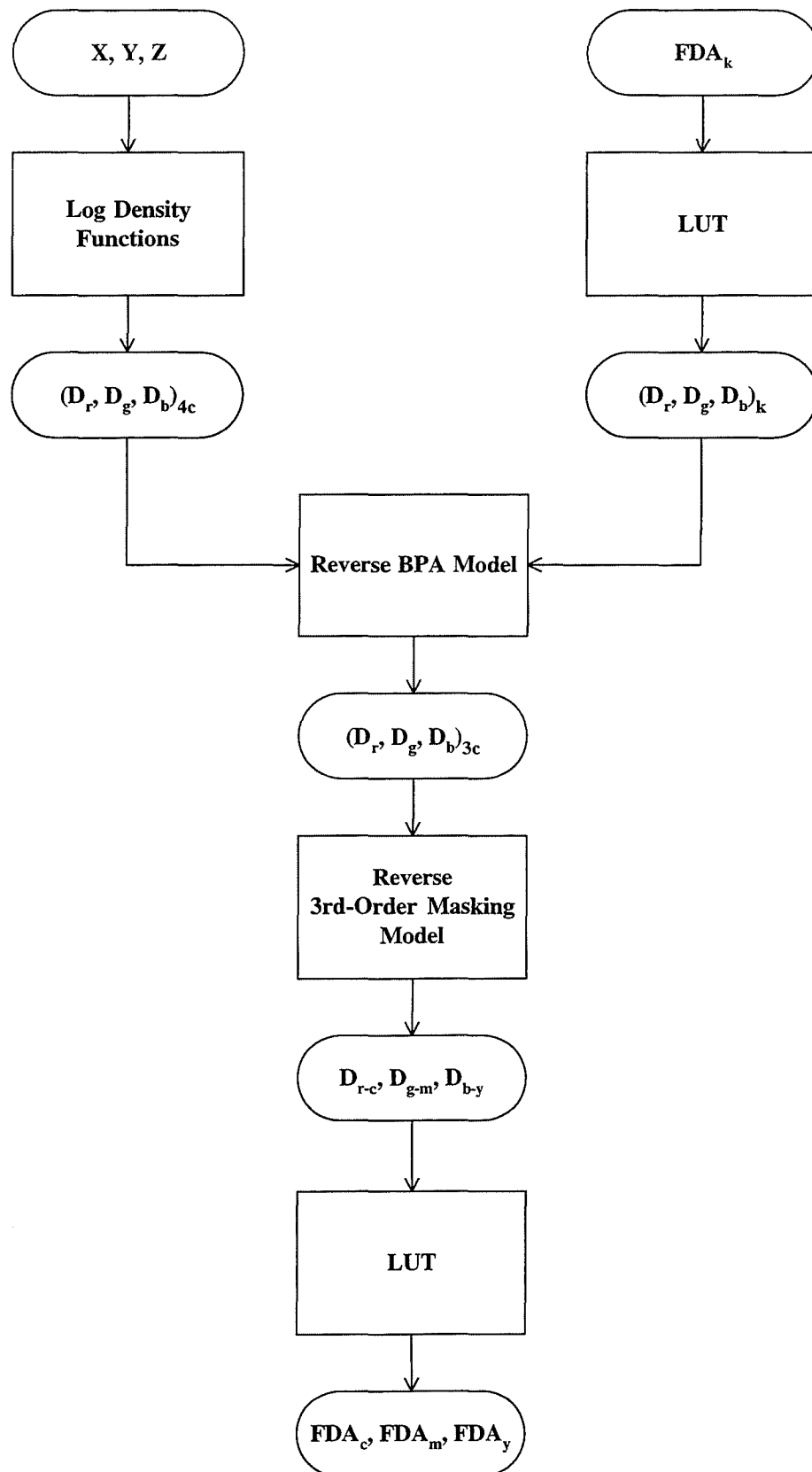


Fig. 3.4 The computational procedures used in the reverse BPA models (with known black ink (K)).

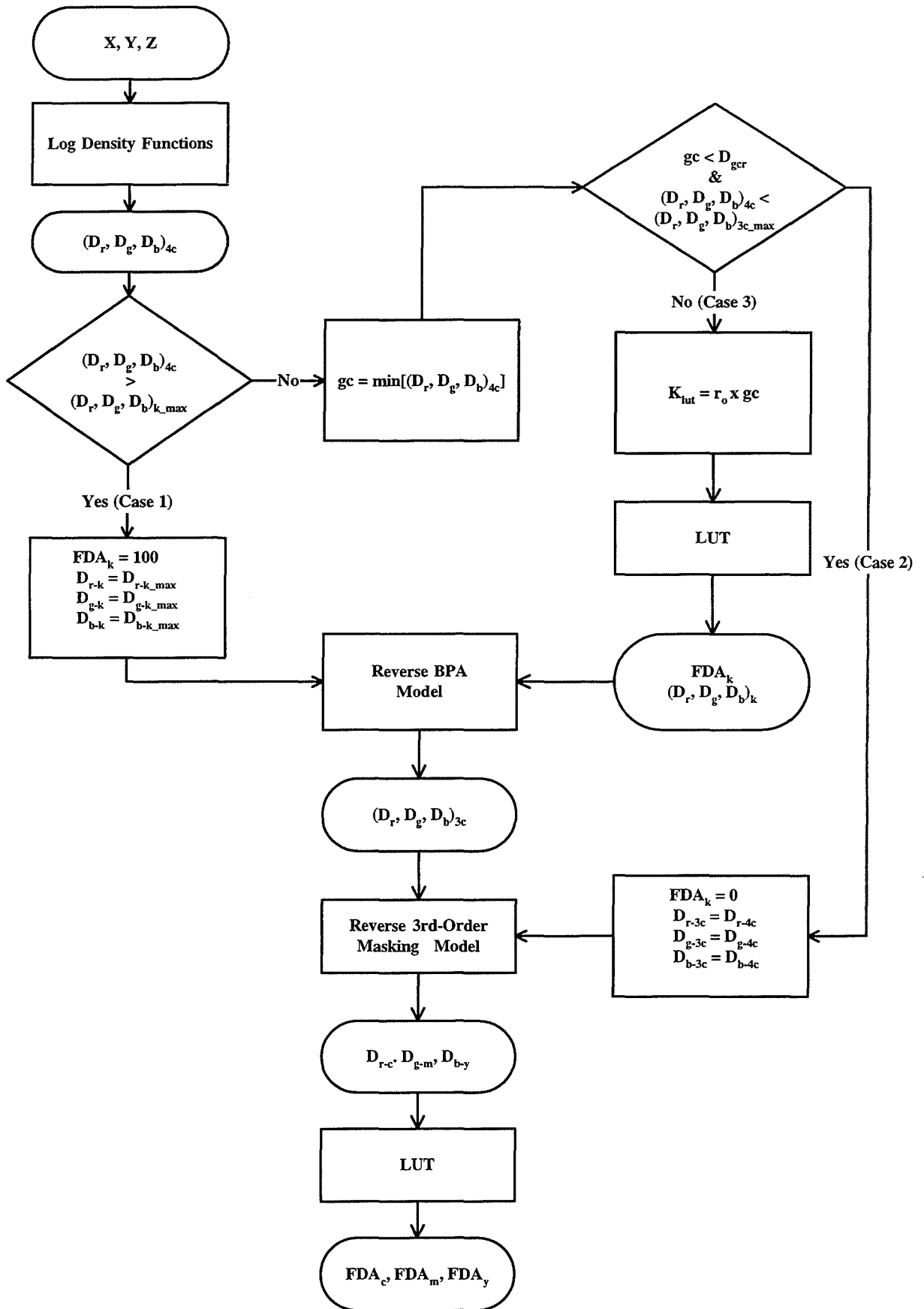


Fig. 3.5 The computational procedures used in the full reverse BPA models (GCR).

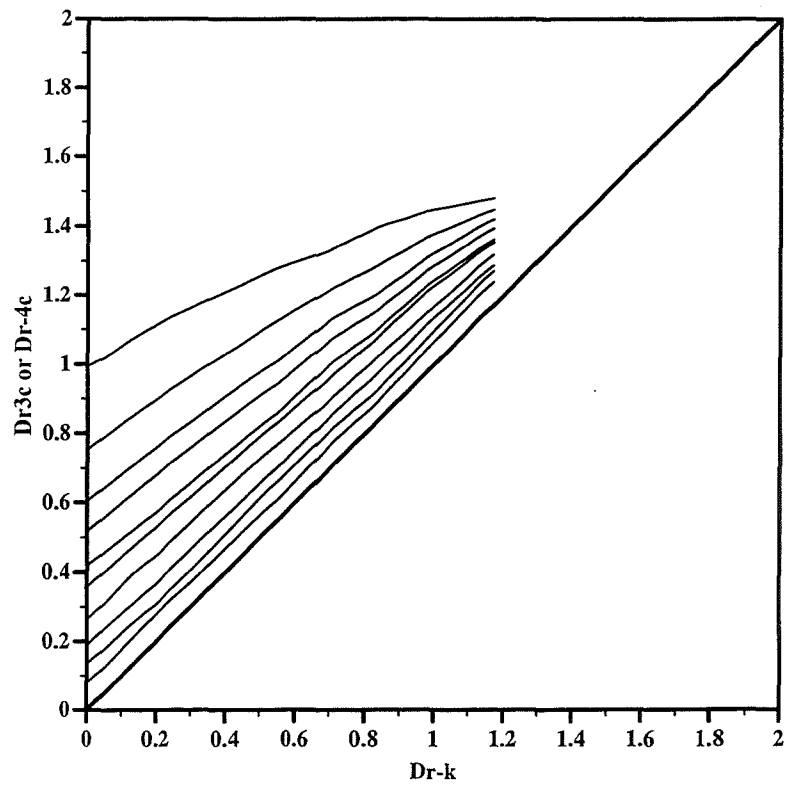


Fig. 3.6 (a) Sub-additivity diagram for red-colorimetric densities (D_r) of IRIS device.

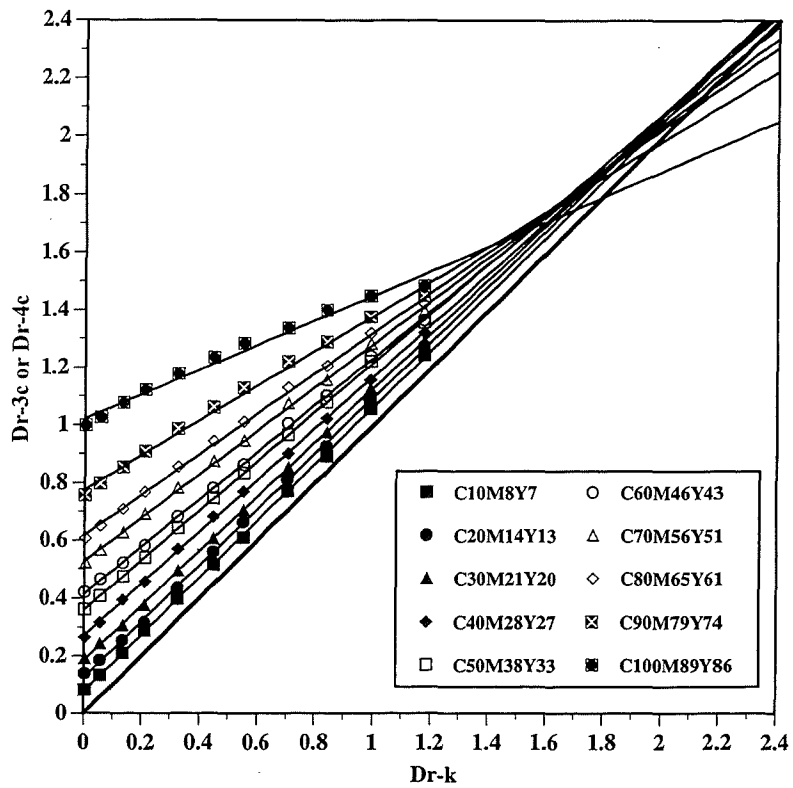


Fig. 3.6 (b) Sub-additivity diagram for red-colorimetric densities (D_r) of IRIS ink device. (Each line is plotted using a least-squares technique)

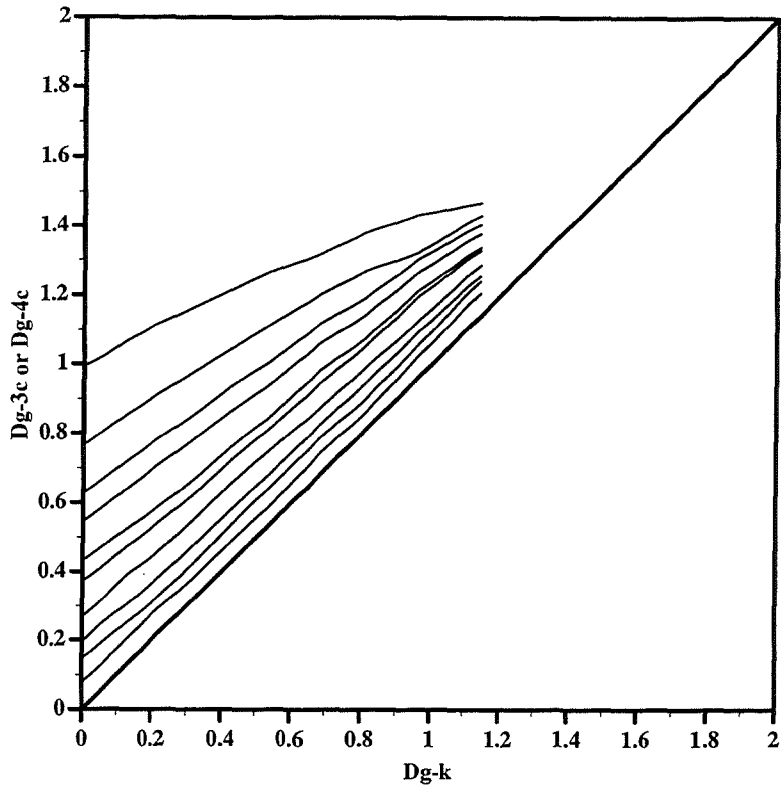


Fig. 3.7 (a) Sub-additivity diagram for green-colorimetric densities (D_g) of IRIS ink device.

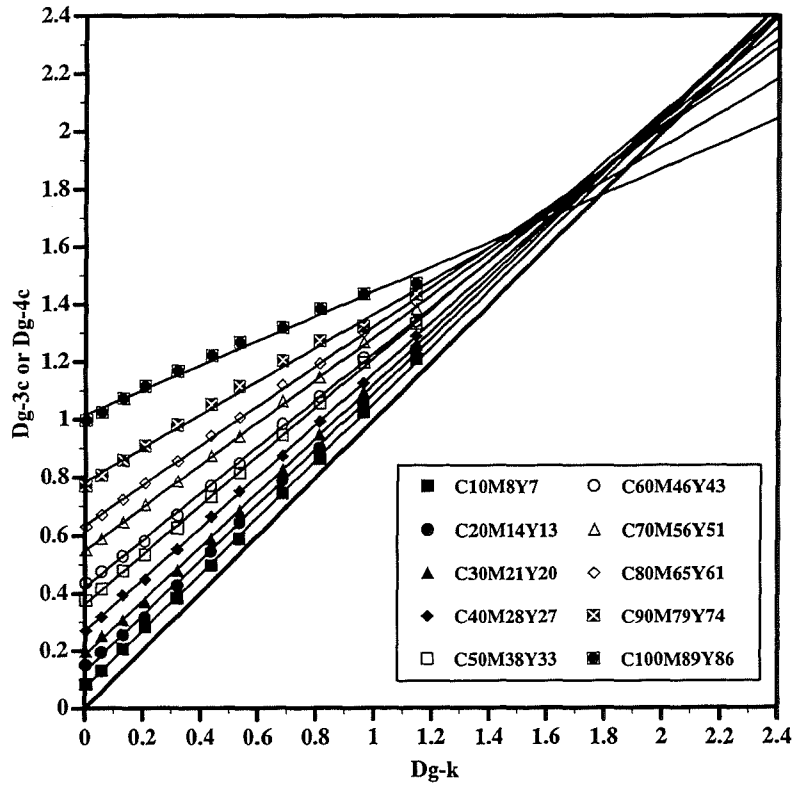


Fig. 3.7 (b) Sub-additivity diagram for green-colorimetric densities (D_g) of IRIS device. (Each line is plotted using a least-squares technique)

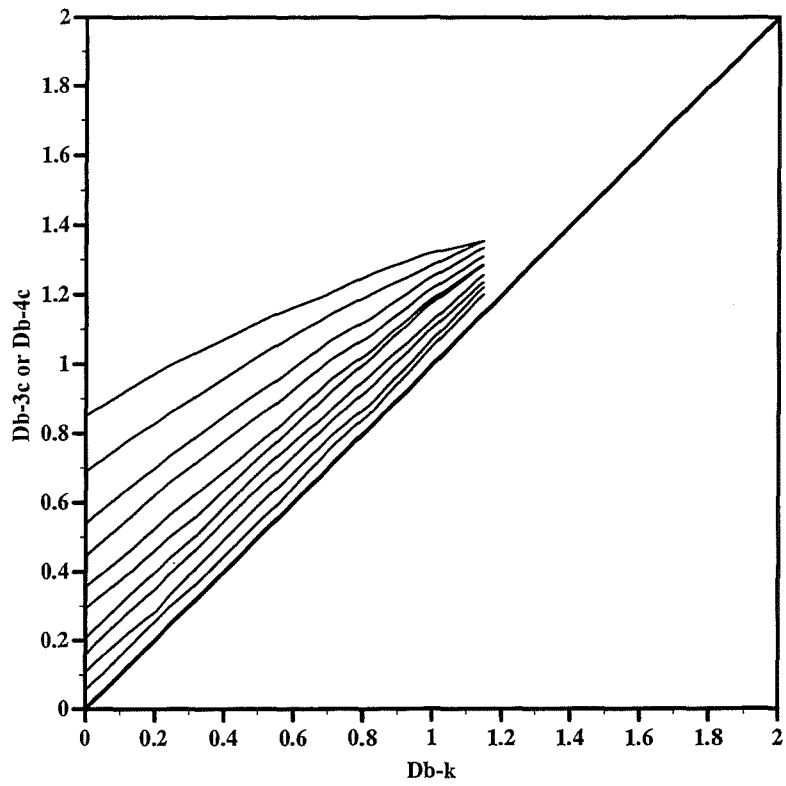


Fig. 3.8 (a) Sub-additivity diagram for blue-colorimetric densities (Db) of IRIS device.

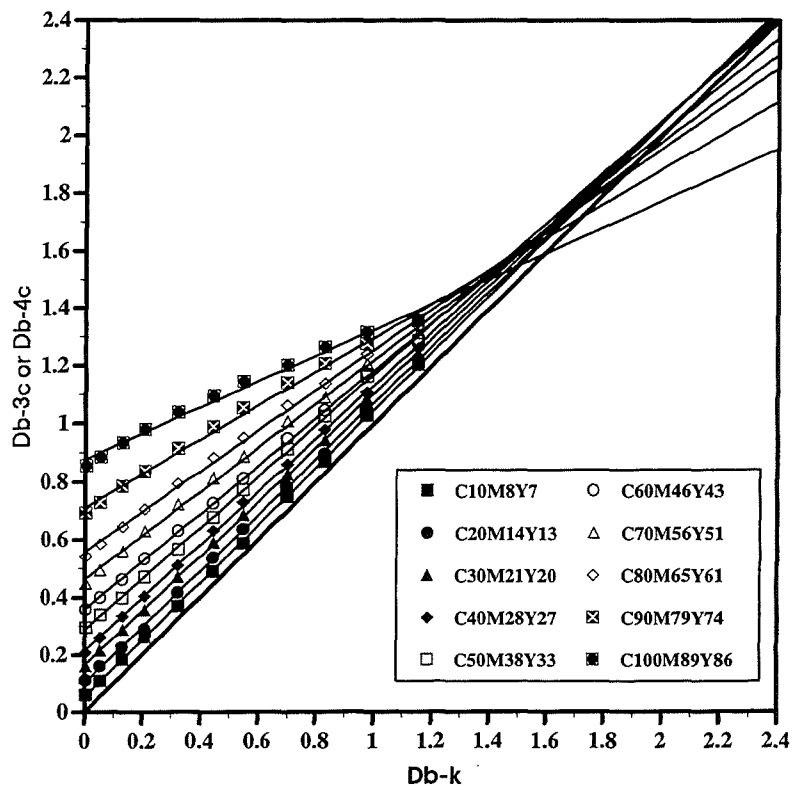


Fig. 3.8 (b) Sub-additivity diagram for blue-colorimetric densities (Db) of IRIS device. (Each line is plotted using a least-squares technique)

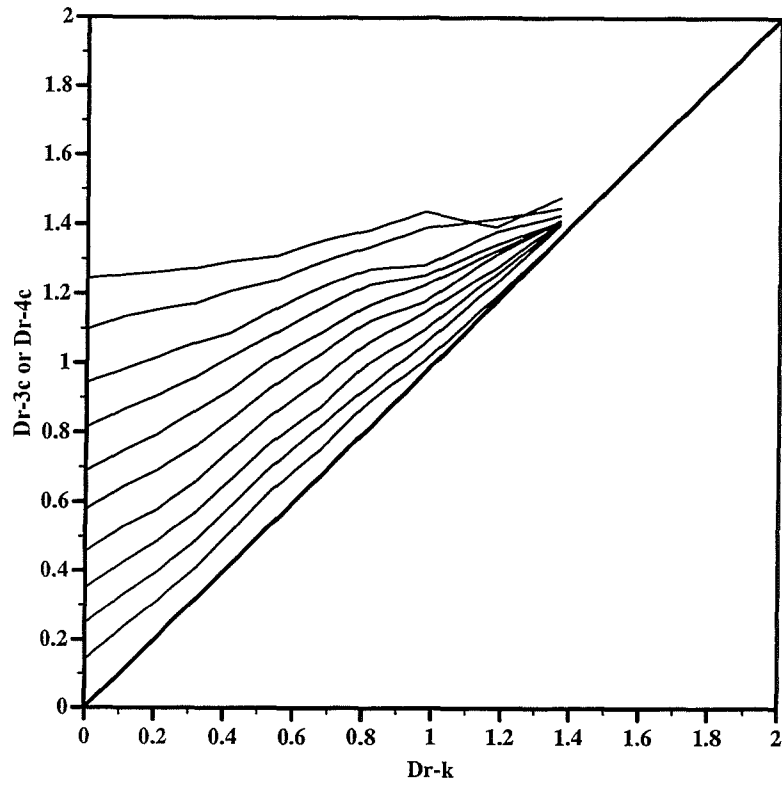


Fig. 3.9 (a) Sub-additivity diagram for red-colorimetric densities (Dr) of Cromalin device.

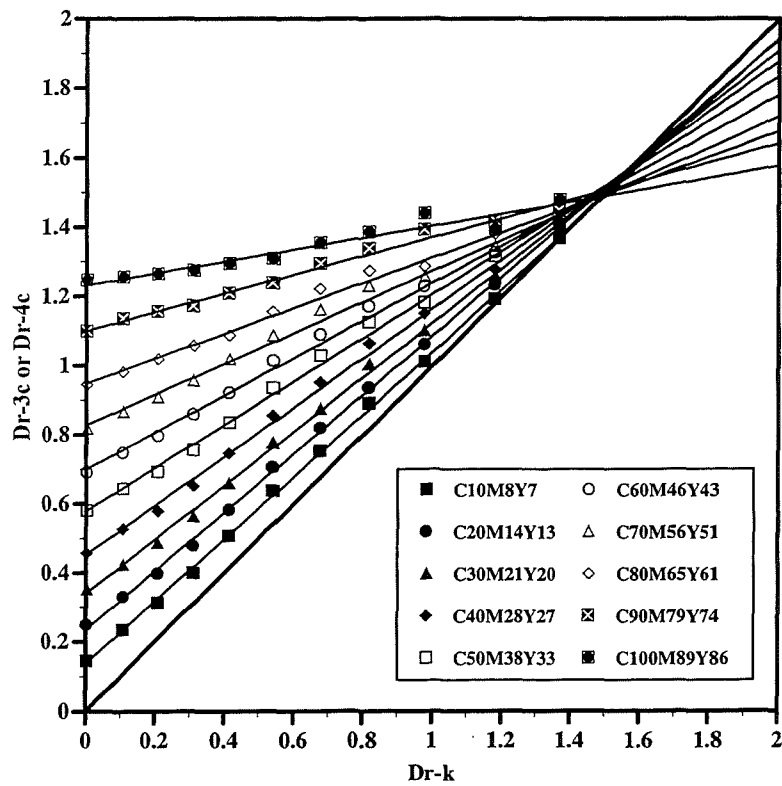


Fig. 3.9 (b) Sub-additivity diagram for red-colorimetric densities (Dr) of Cromalin device. (Each line is plotted using a least-squares technique)

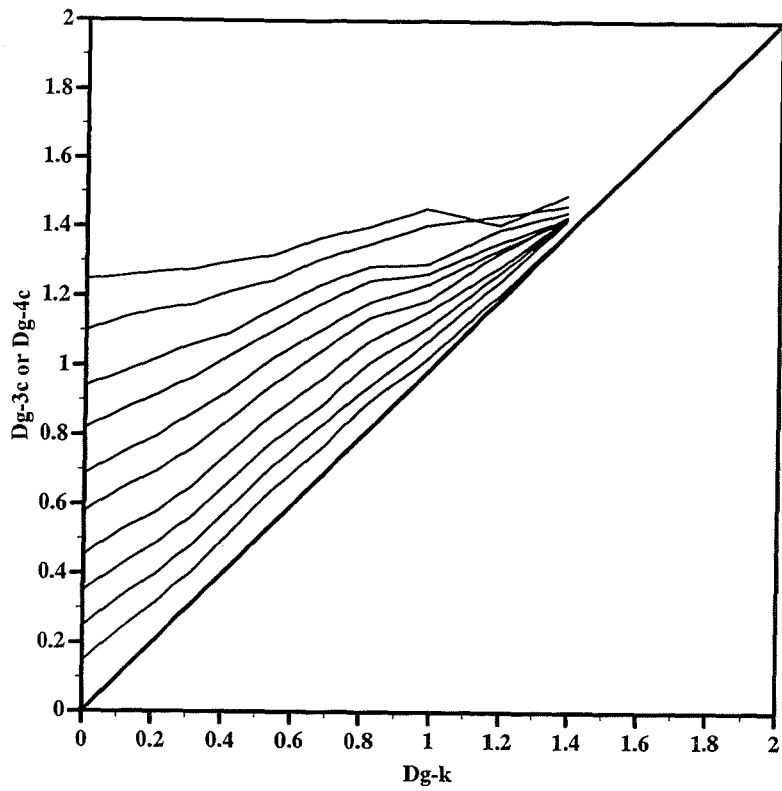


Fig. 3.10 (a) Sub-additivity diagram for green-colorimetric densities (D_g) of Cromalin device.

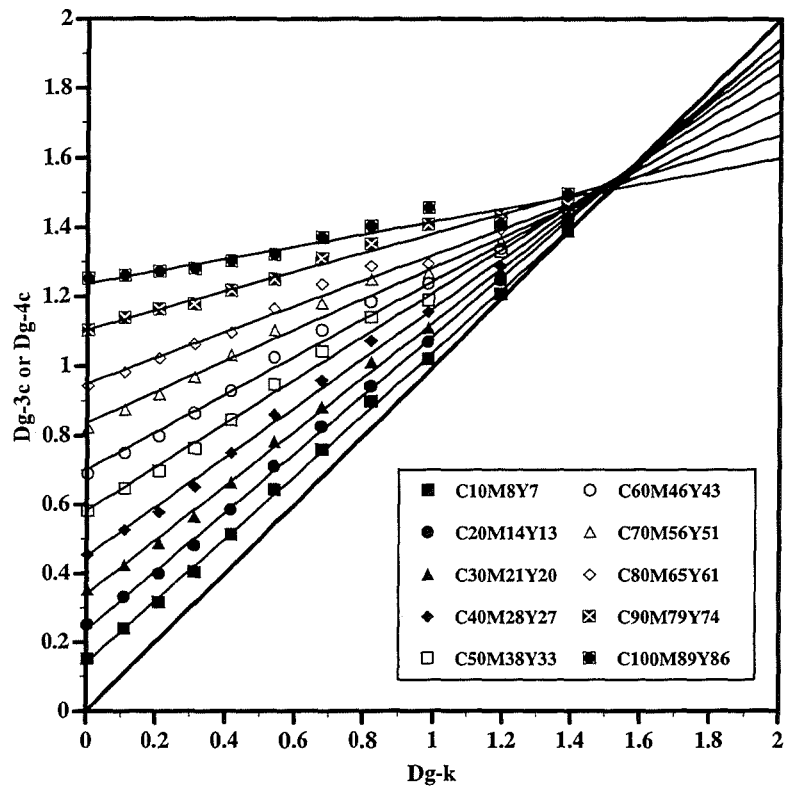


Fig. 3.10 (b) Sub-additivity diagram for green-colorimetric densities (D_g) of Cromalin device. (Each line is plotted using a least-squares technique)

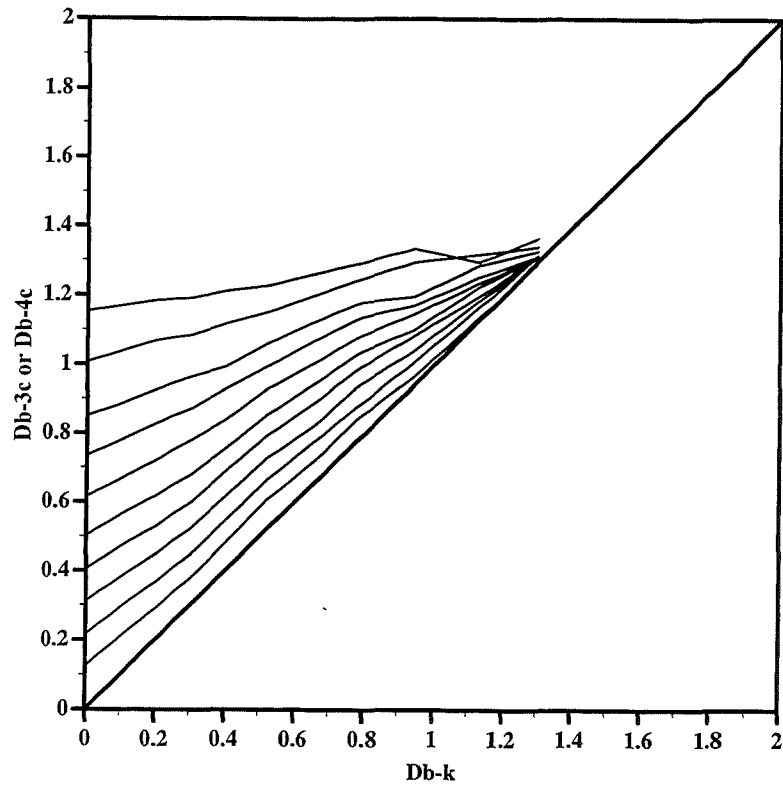


Fig. 3.11 (a) Sub-additivity diagram for blue-colorimetric densities (Db) of Cromalin device.

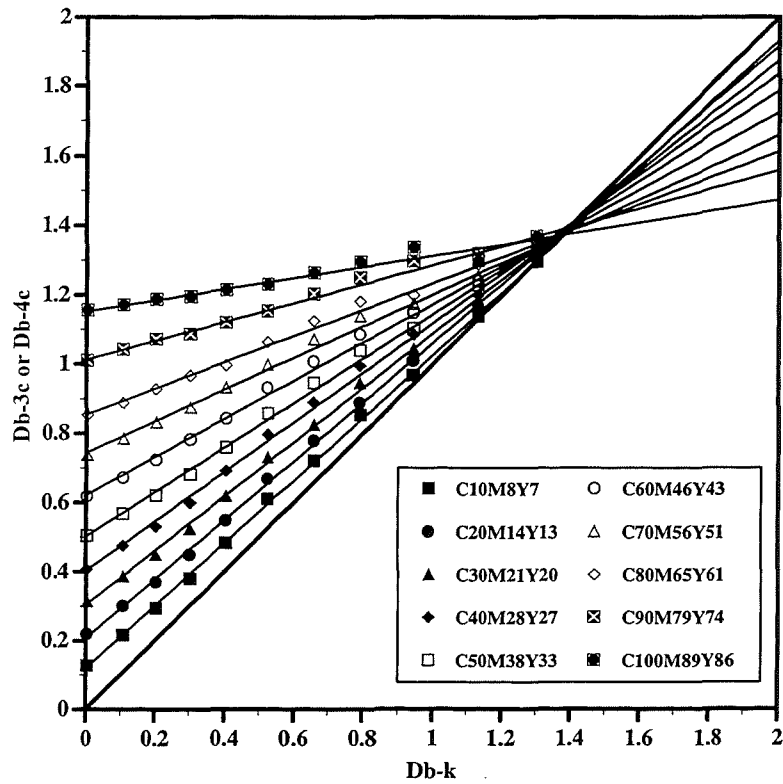


Fig. 3.11 (b) Sub-additivity diagram for blue-colorimetric densities (Db) of Cromalin device. (Each line is plotted using a least-squares technique)

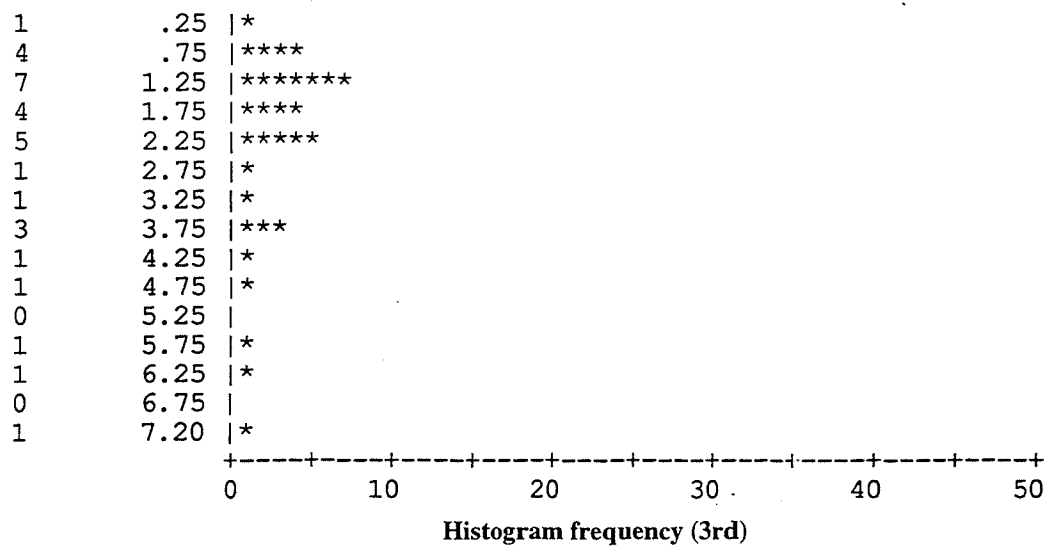
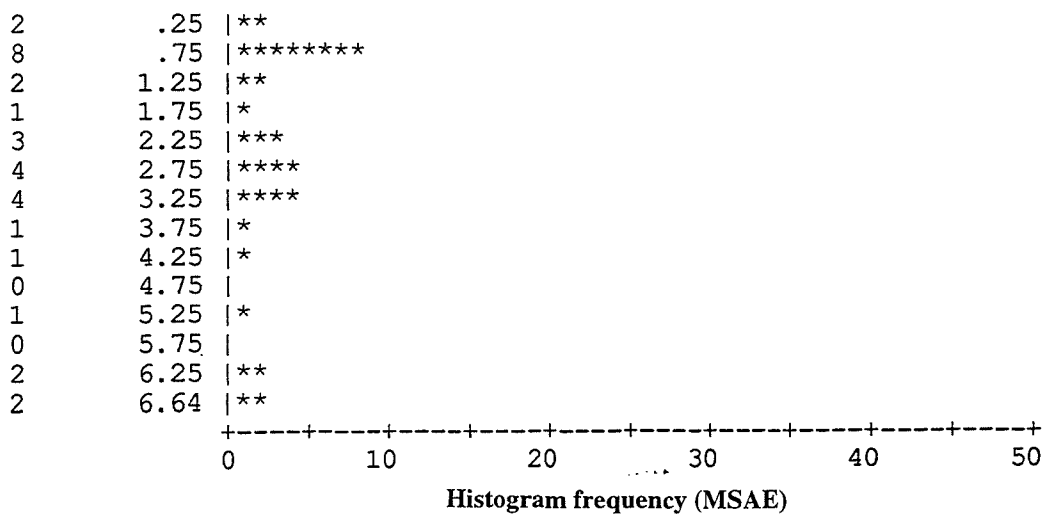
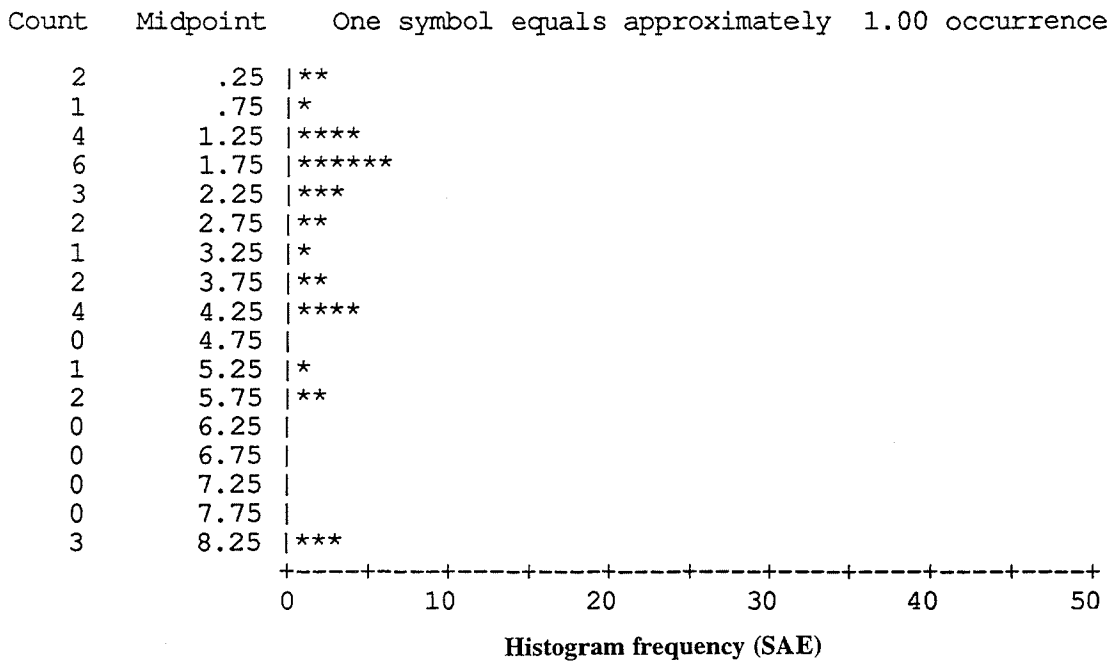


Fig. 3.12 (a) The $\Delta E(\text{CMC})$ distributions for the 5 forward BPA models tested using the 31 data set (IRIS device).

Count Midpoint One symbol equals approximately 1.00 occurrence

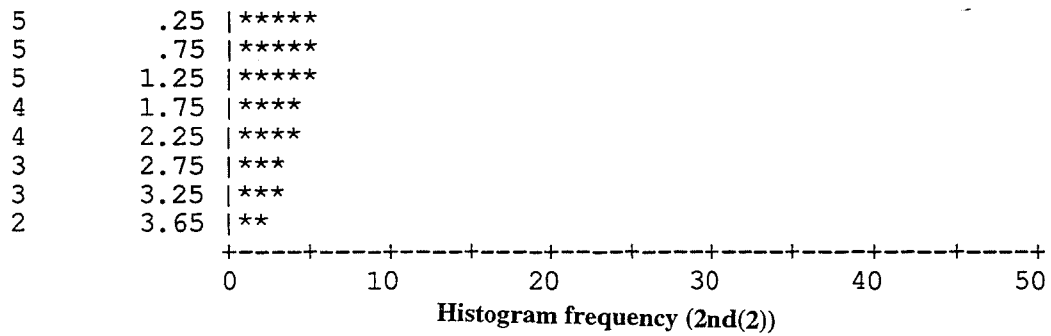
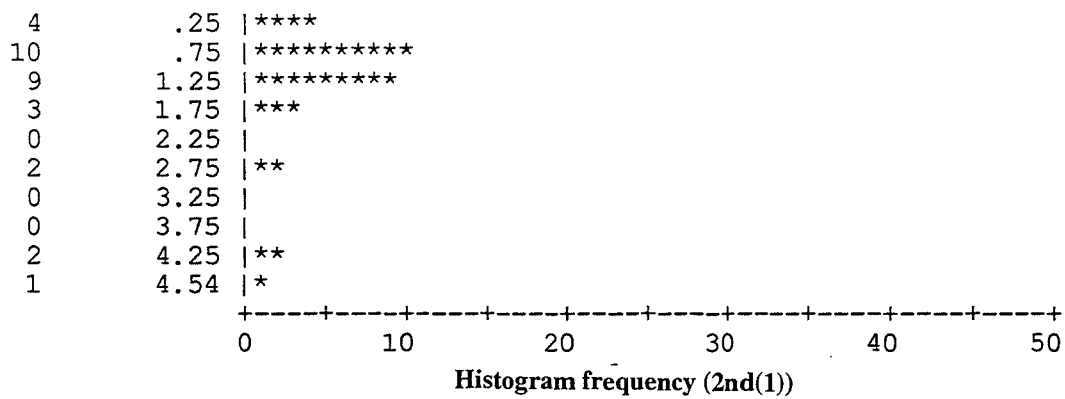


Fig. 3.12 (a) The $\Delta E(\text{CMC})$ distributions for the 5 forward BPA models tested using the 31 data set (IRIS device). (continued)

Count Midpoint One symbol equals approximately 1.00 occurrence

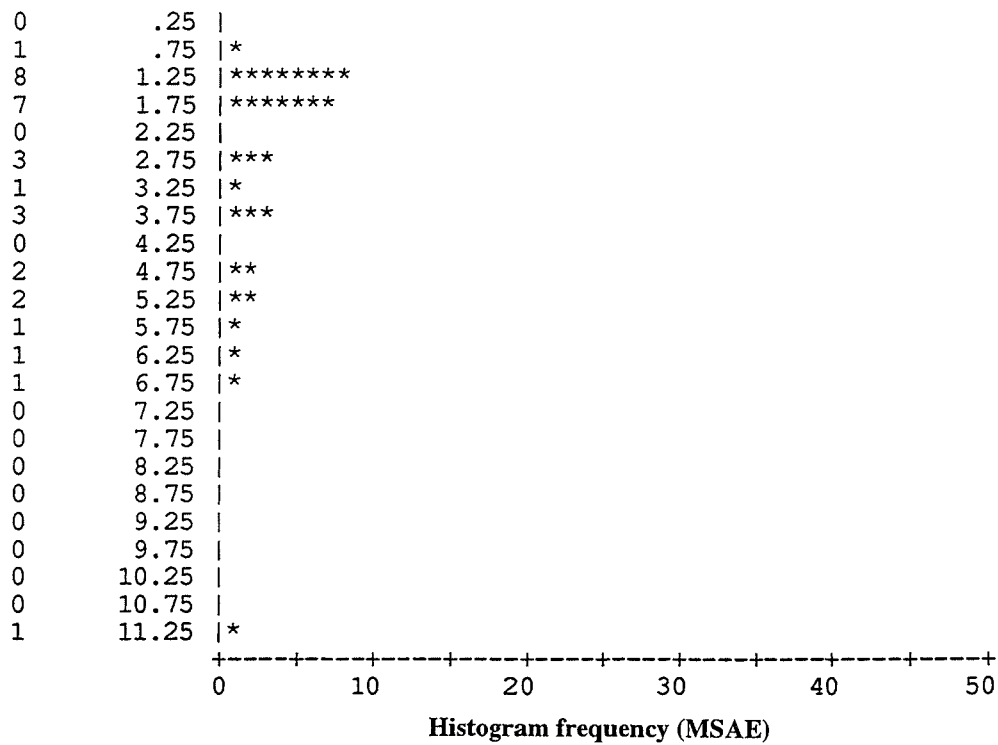
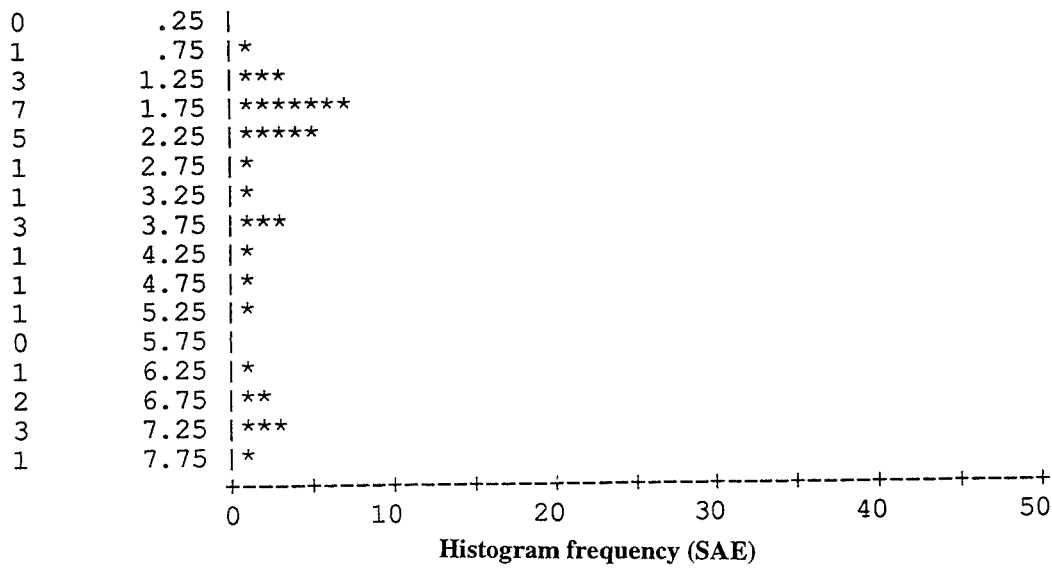
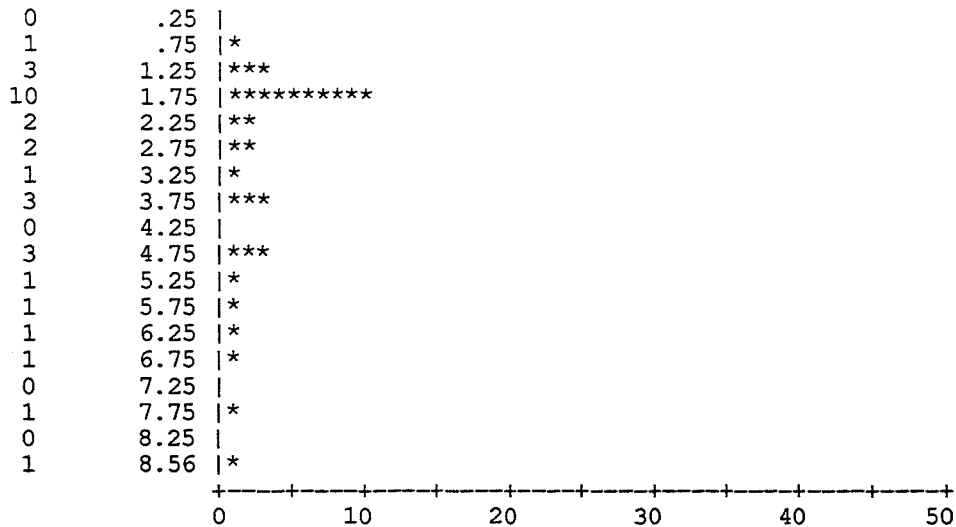
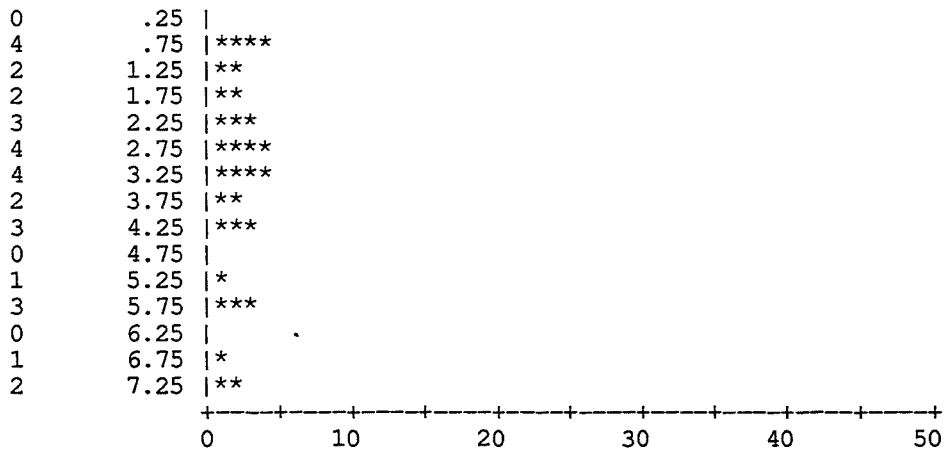


Fig. 3.12 (b) The $\Delta E(\text{CMC})$ distributions for the 5 forward BPA models tested using the 31 data set (Cromalin device).

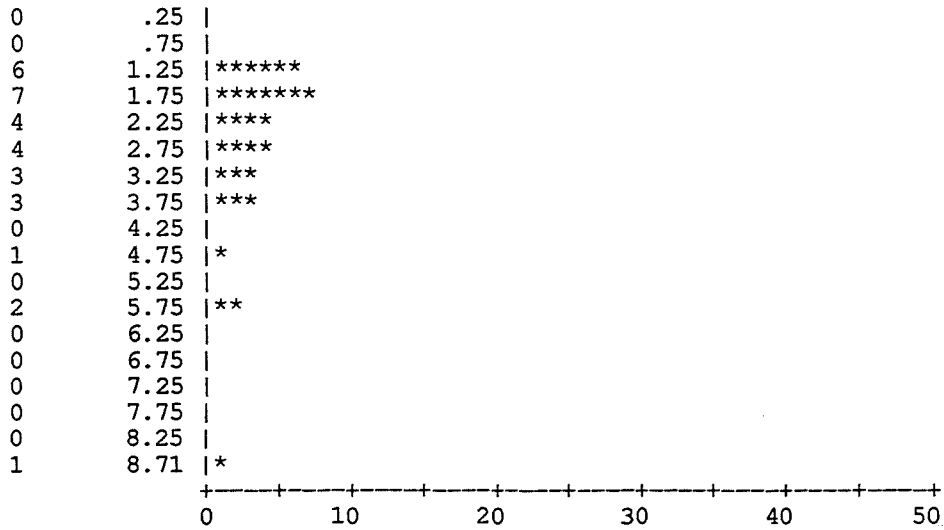
Count Midpoint One symbol equals approximately 1.00 occurrence



Histogram frequency (3rd)



Histogram frequency (2nd(1))



Histogram frequency (2nd(2))

Fig. 3.12 (b) The $\Delta E(\text{CMC})$ distributions for the 5 forward BPA models tested using the 31 data set (Cromalin device). (continued)

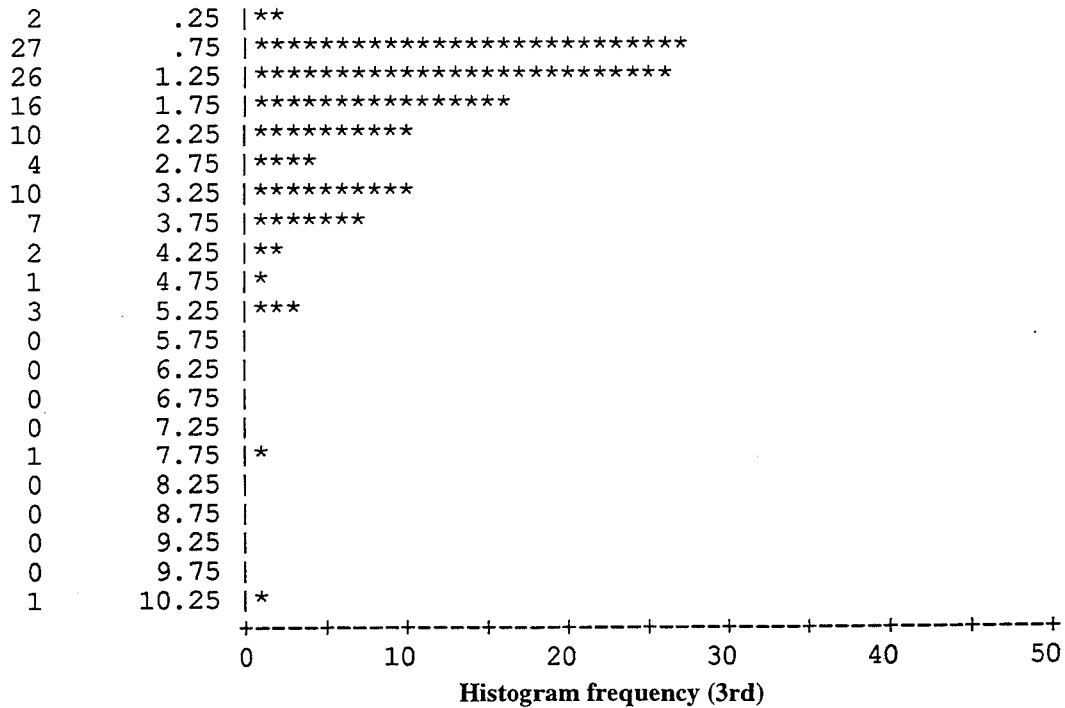
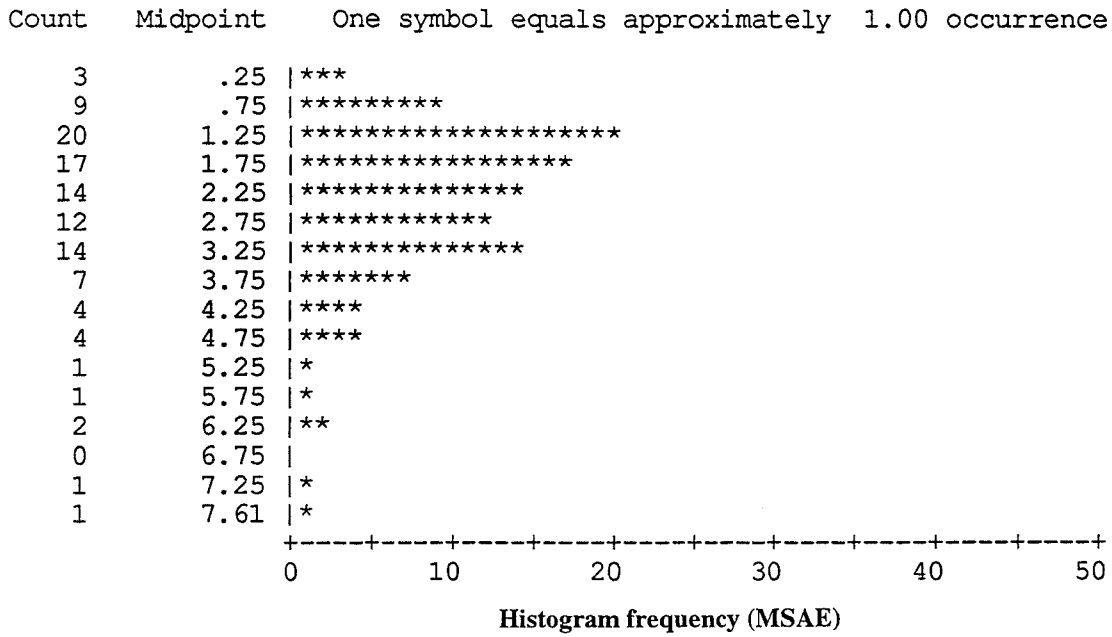


Fig. 3.13 (a) The $\Delta E(\text{CMC})$ distributions for the 5 forward BPA models tested using the 110 data set (IRIS device).

Count Midpoint One symbol equals approximately 1.00 occurrence

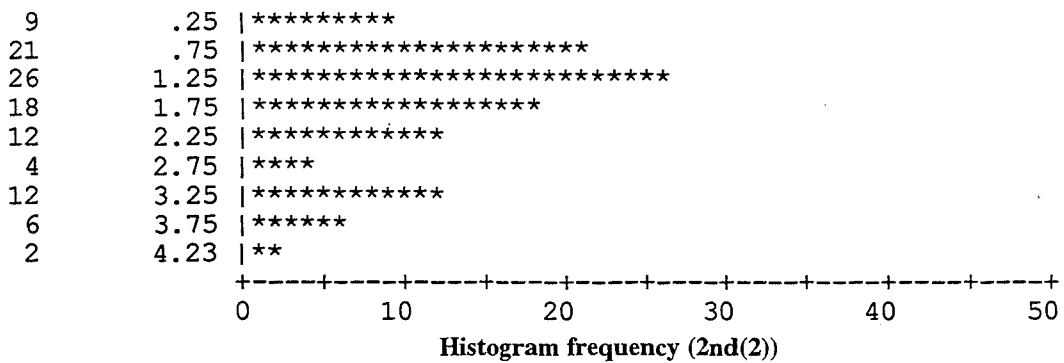
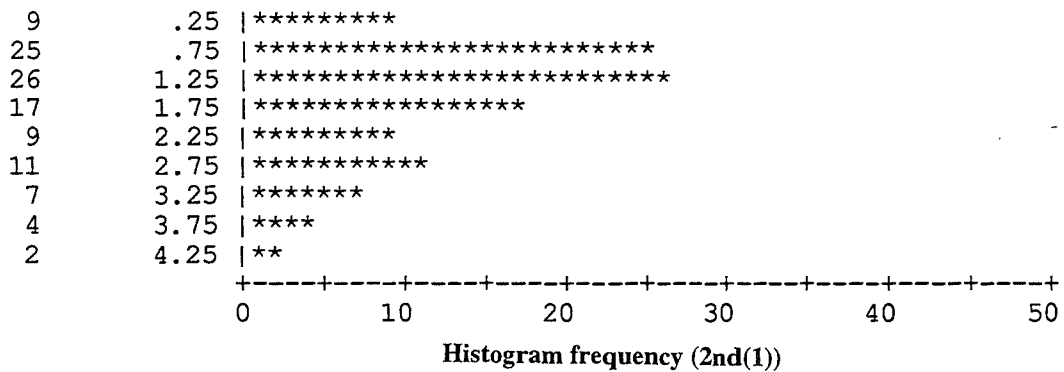
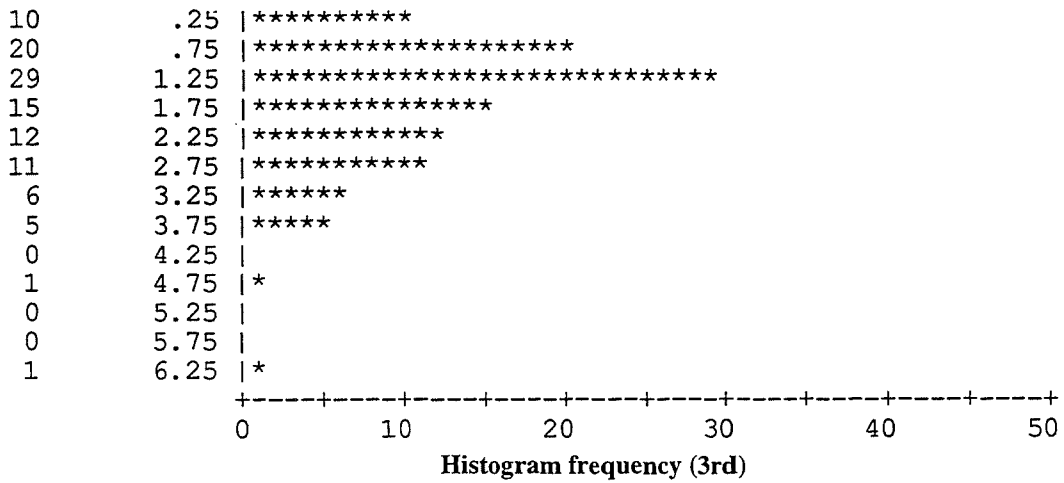


Fig. 3.13 (a) The $\Delta E(\text{CMC})$ distributions for the 5 forward BPA models tested using the 110 data set (IRIS device). (continued)

Count Midpoint One symbol equals approximately 1.00 occurrence

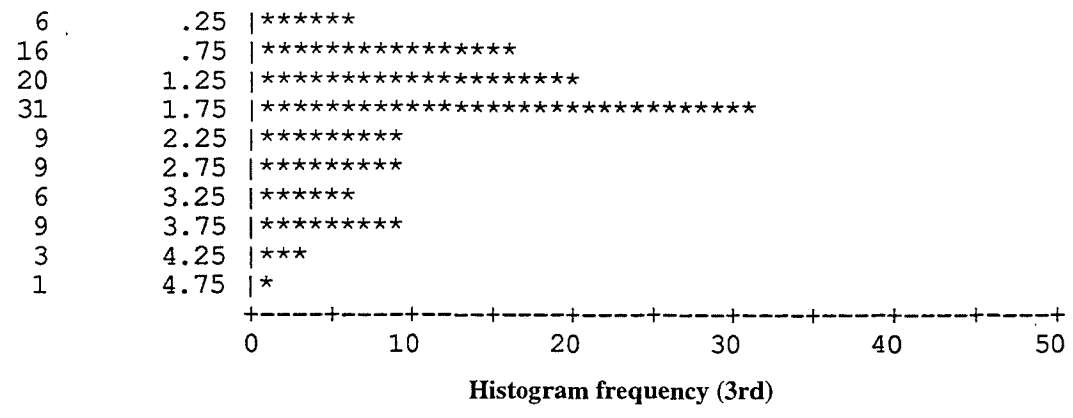
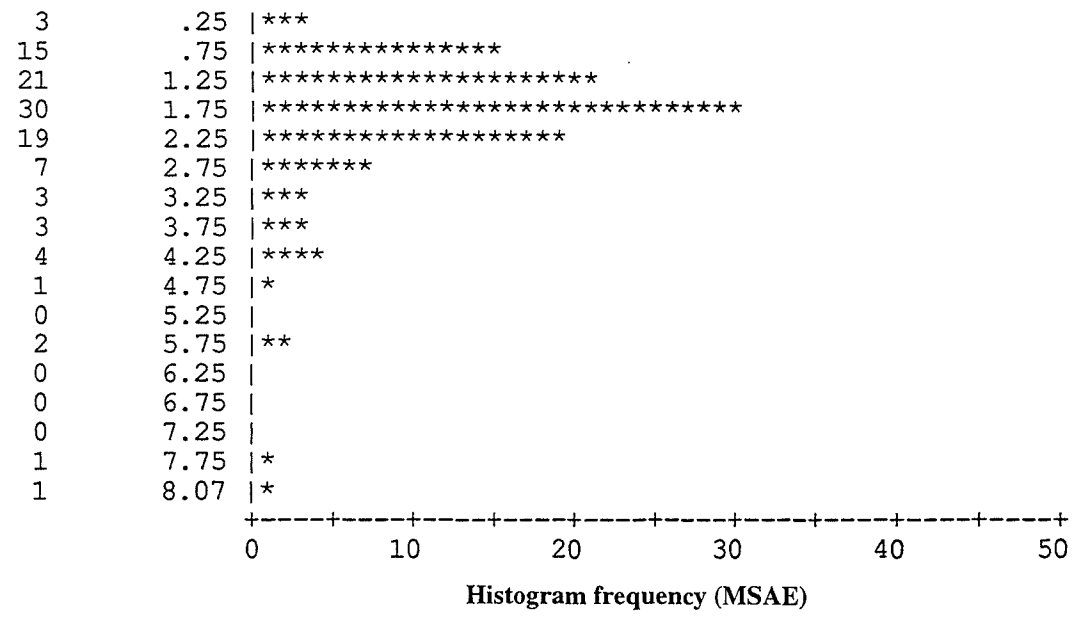
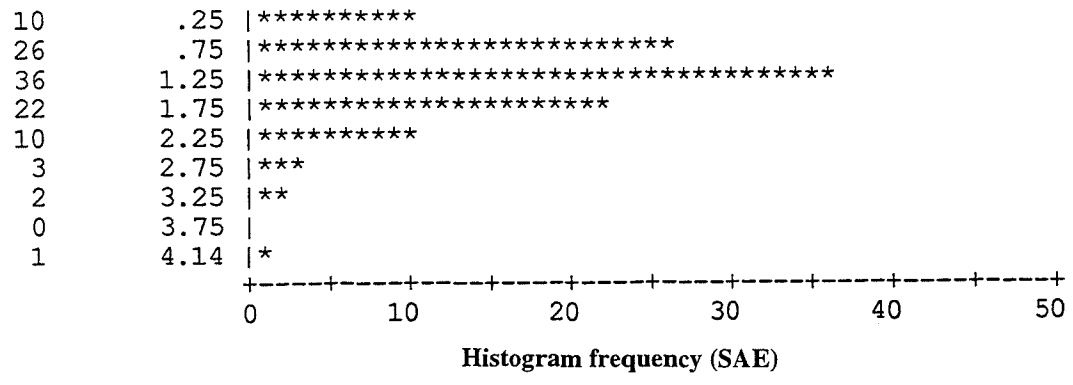


Fig. 3.13 (b) The $\Delta E(\text{CMC})$ distributions for the 5 forward BPA models tested using the 110 data set (Cromalin device).

Count Midpoint One symbol equals approximately 1.00 occurrence

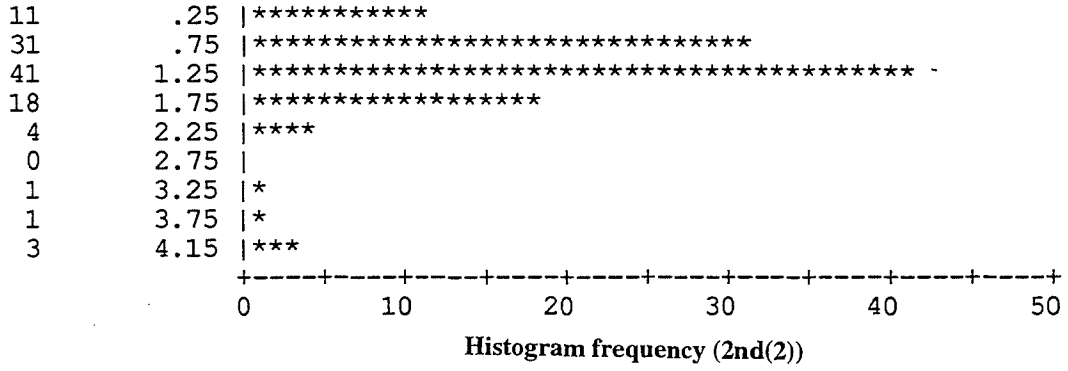
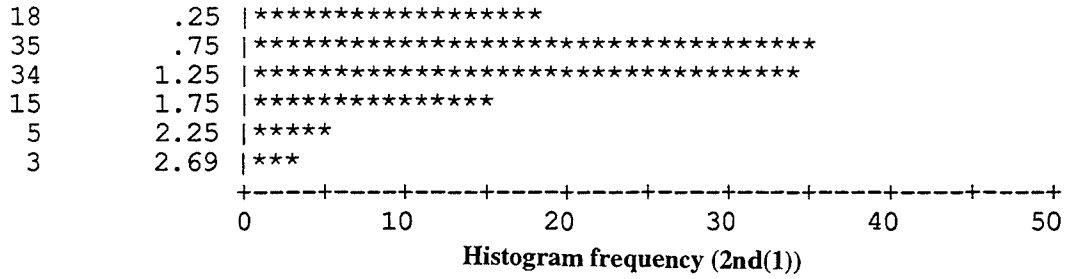


Fig. 3.13 (b) The $\Delta E(\text{CMC})$ distributions for the 5 forward BPA models tested using the 110 data set (Cromalin device). (continued)

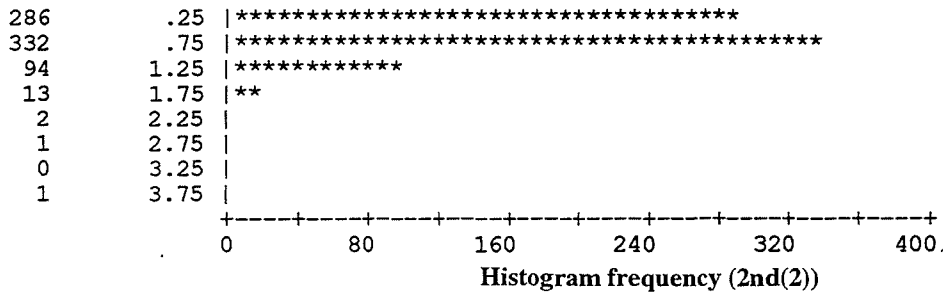
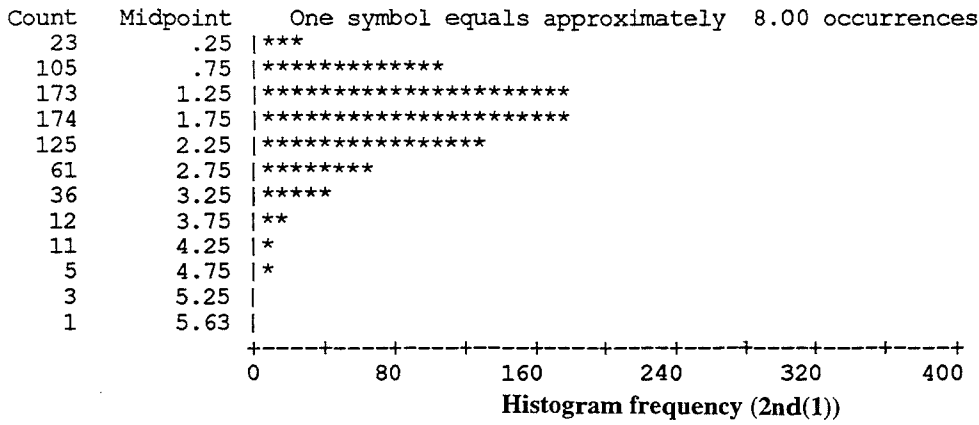


Fig. 3.14 (a) The $\Delta E(\text{CMC})$ distributions for the 2 forward 2nd BPA models tested using the cube data set (IRIS device).

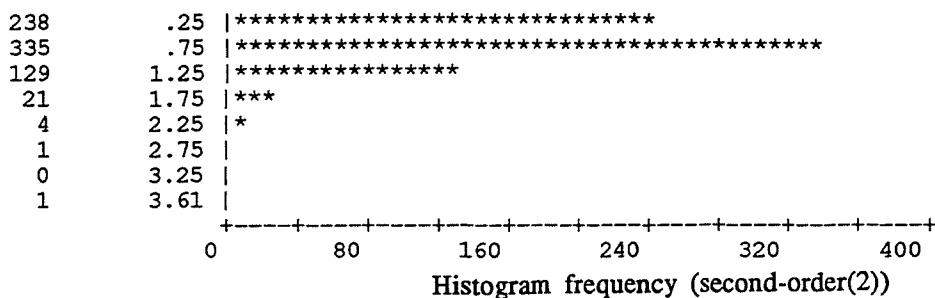
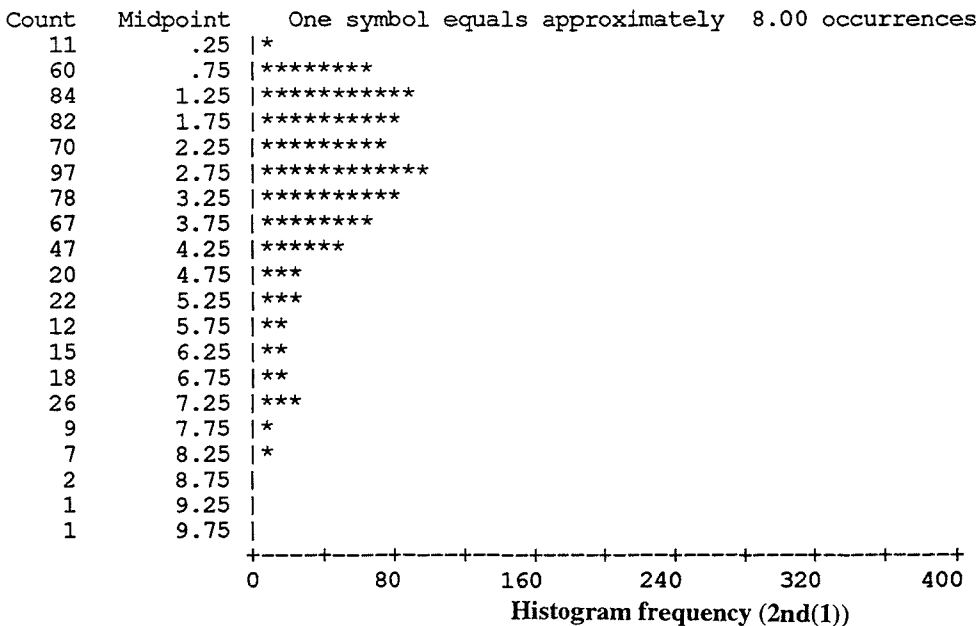


Fig. 3.14 (b) The $\Delta E(\text{CMC})$ distributions for the 2 forward 2nd BPA models tested using the cube data set (Cromalin device).

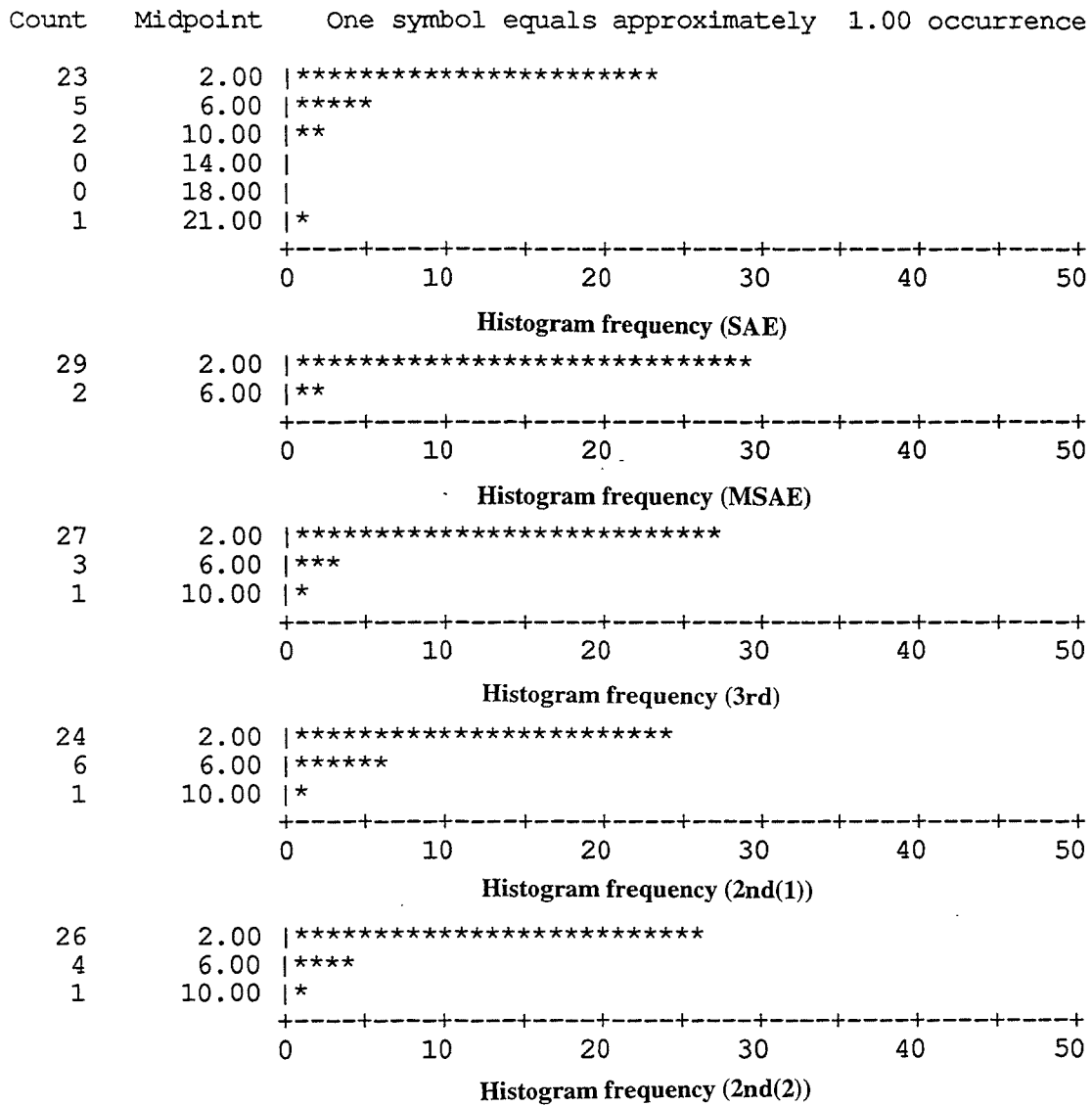


Fig. 3.15 (a) The $|\Delta FDA_{3c}|$ distributions for the 5 reverse BPA models tested using the 31 data set (IRIS device).

Count Midpoint One symbol equals approximately 2.00 occurrences

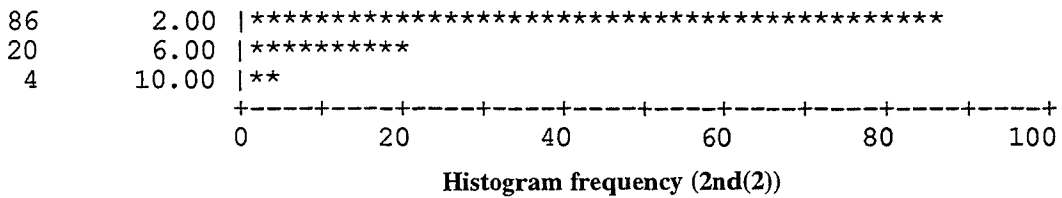
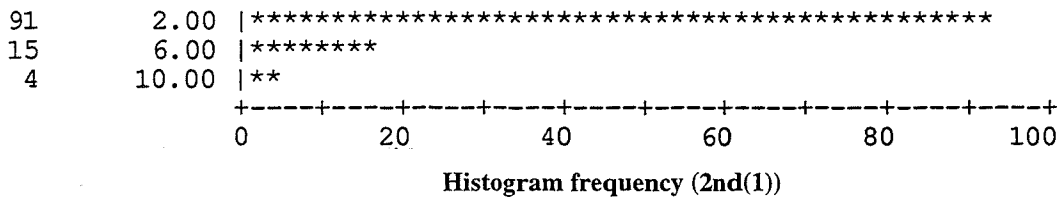
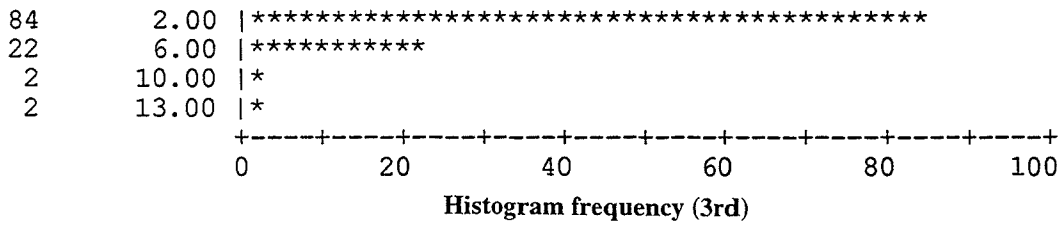
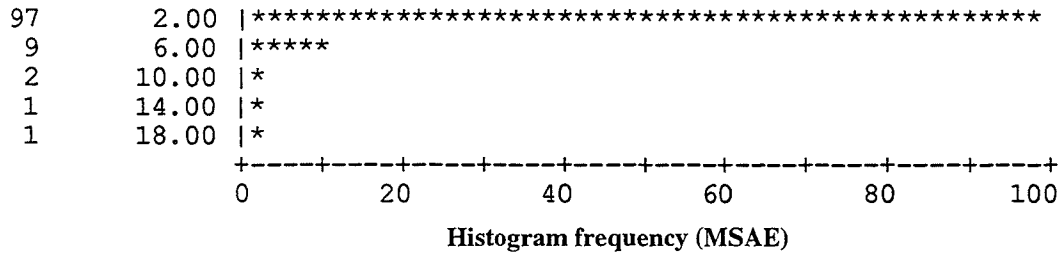
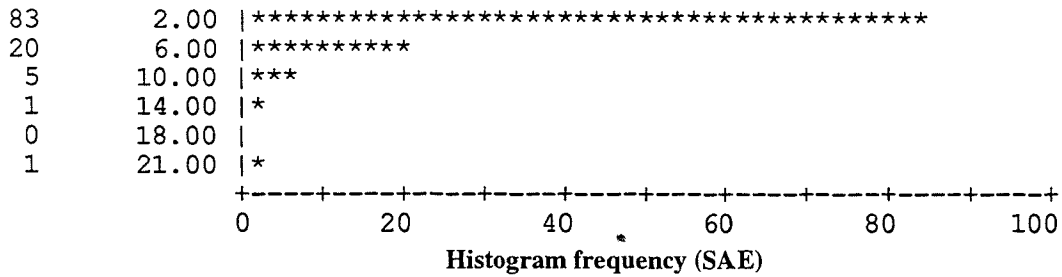


Fig. 3.15 (b) The $|\Delta FDA_{3c}|$ distributions for the 5 reverse BPA models tested using the 110 data set (IRIS device).

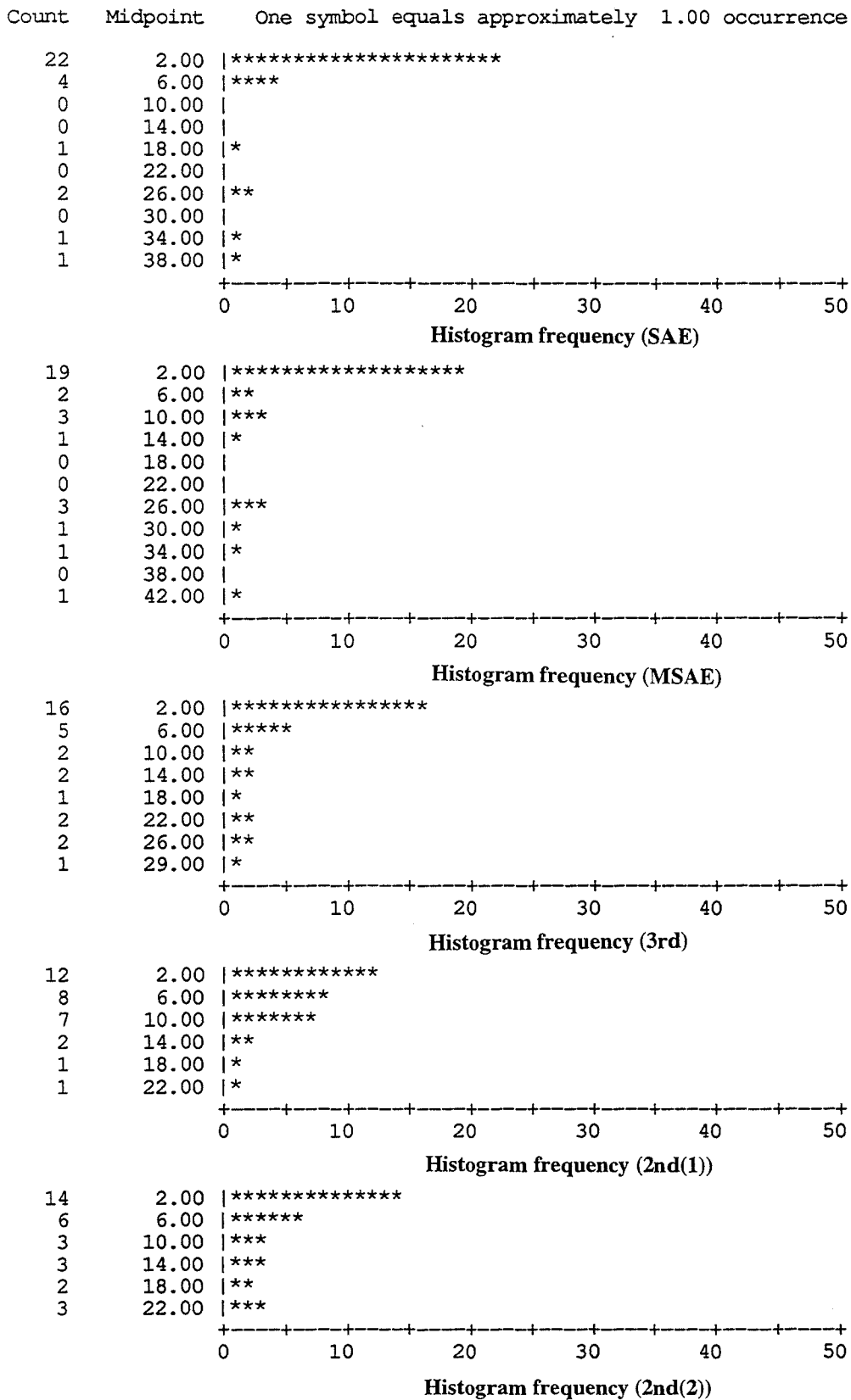
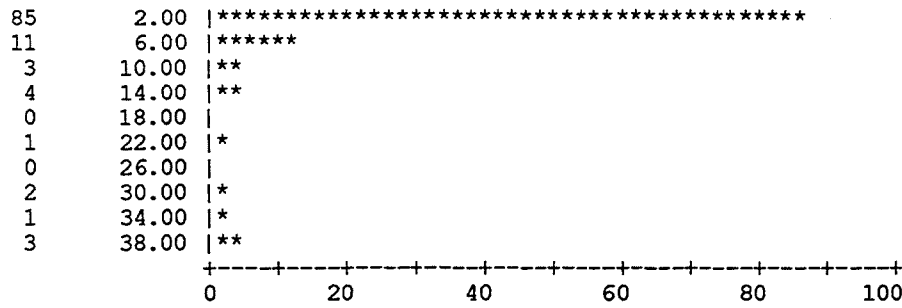
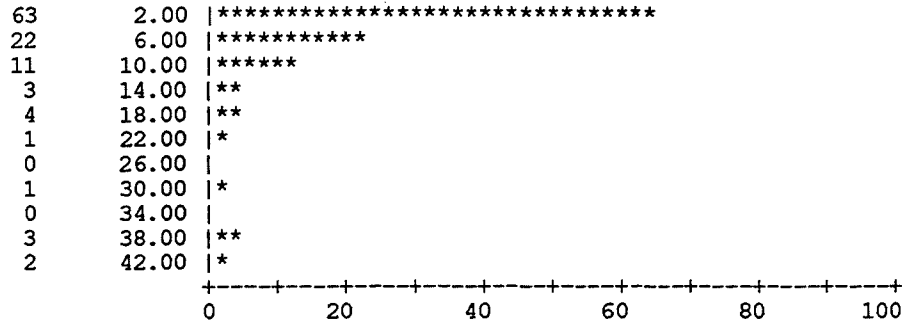


Fig. 3.16 (a) The $|\Delta FDA_{3c}|$ distributions for the 5 reverse BPA models tested using the 31 data set (Cromalin device).

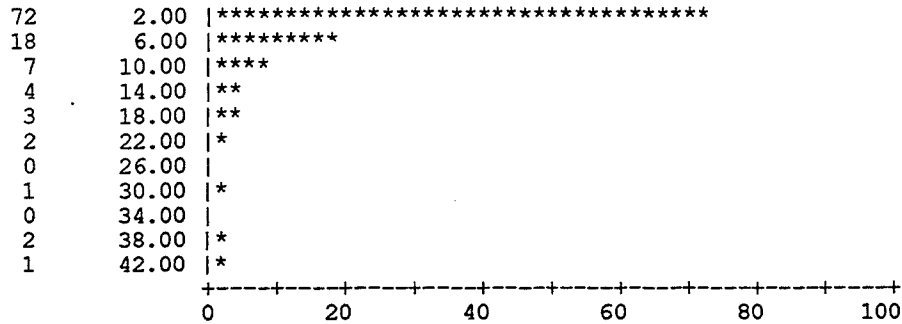
Count Midpoint One symbol equals approximately 2.00 occurrences



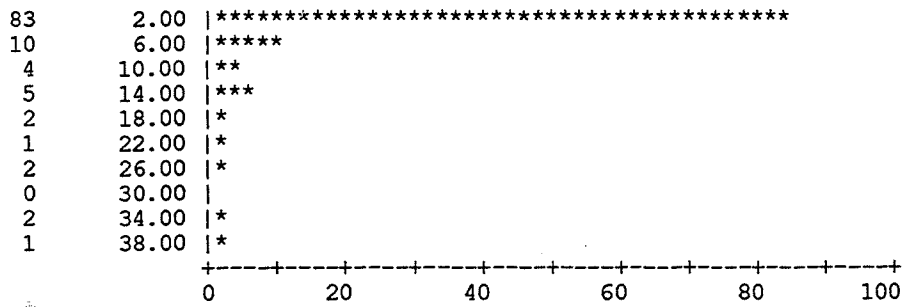
Histogram frequency (SAE)



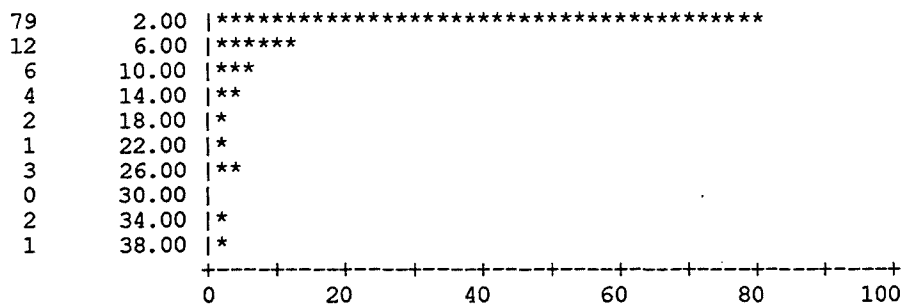
Histogram frequency (MSAE)



Histogram frequency (3rd)



Histogram frequency (2nd(1))



Histogram frequency (2nd(2))

Fig. 3.16 (b) The $|\Delta FDA_{3c}|$ distributions for the 5 reverse BPA models tested using the 110 data set (Cromalin device).

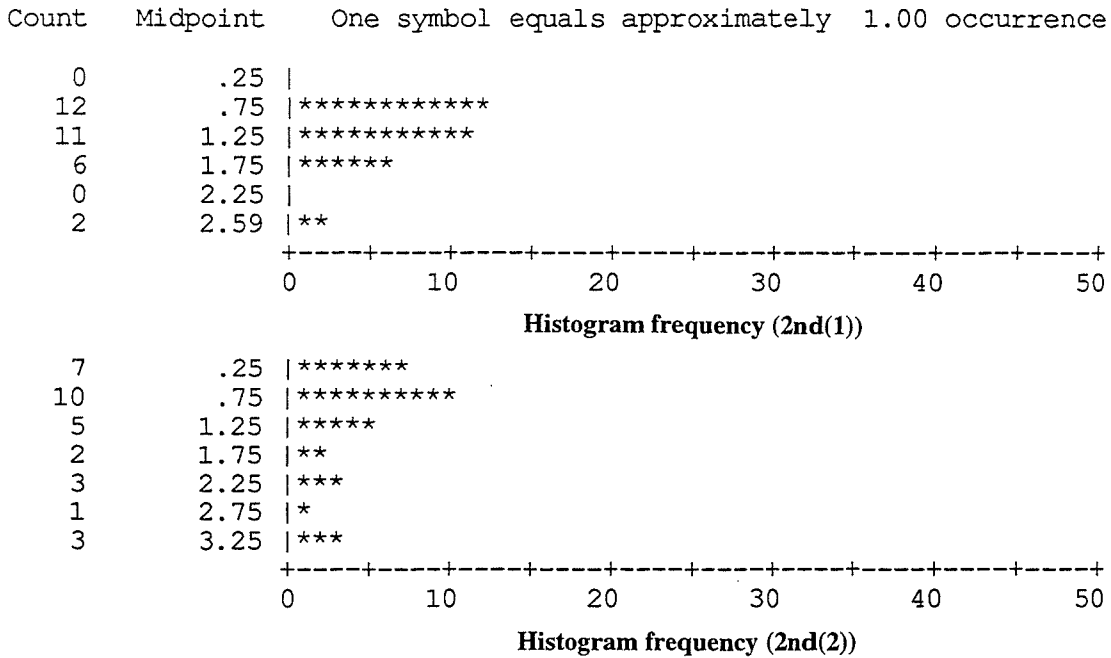


Fig. 3.17 (a) The $\Delta E(\text{CMC})$ distributions for the 2 reverse 2nd BPA models tested using the 31 data set (K ink is known) (IRIS device).

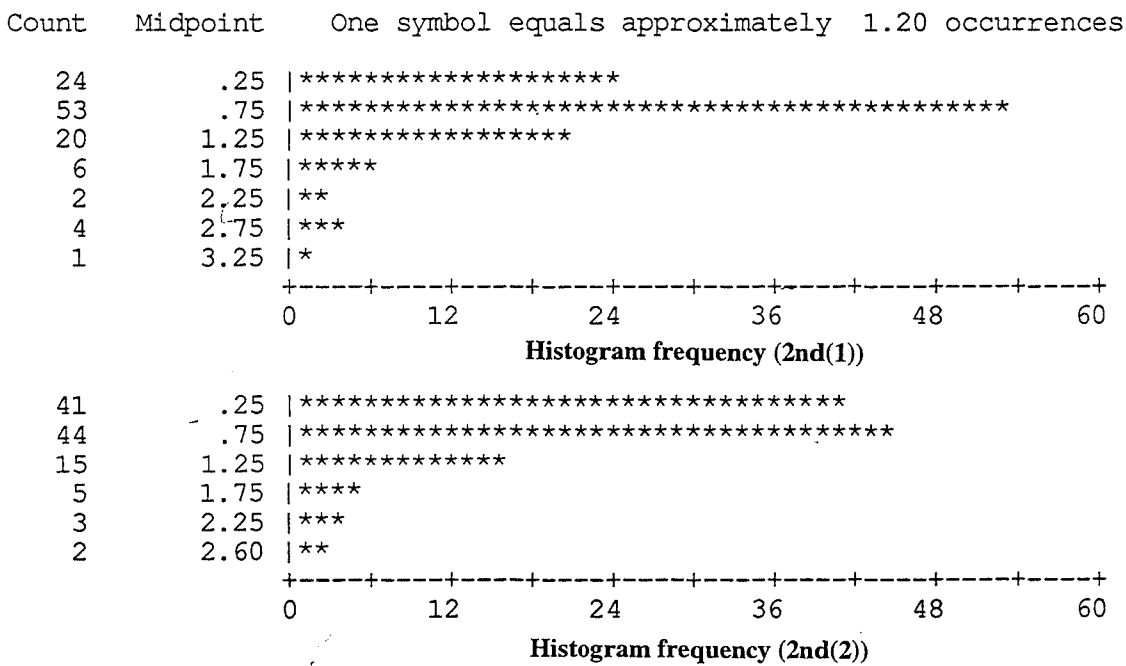


Fig. 3.17 (b) The $\Delta E(\text{CMC})$ distributions for the 2 reverse 2nd BPA models tested using the 110 data set (K ink is known) (IRIS device).

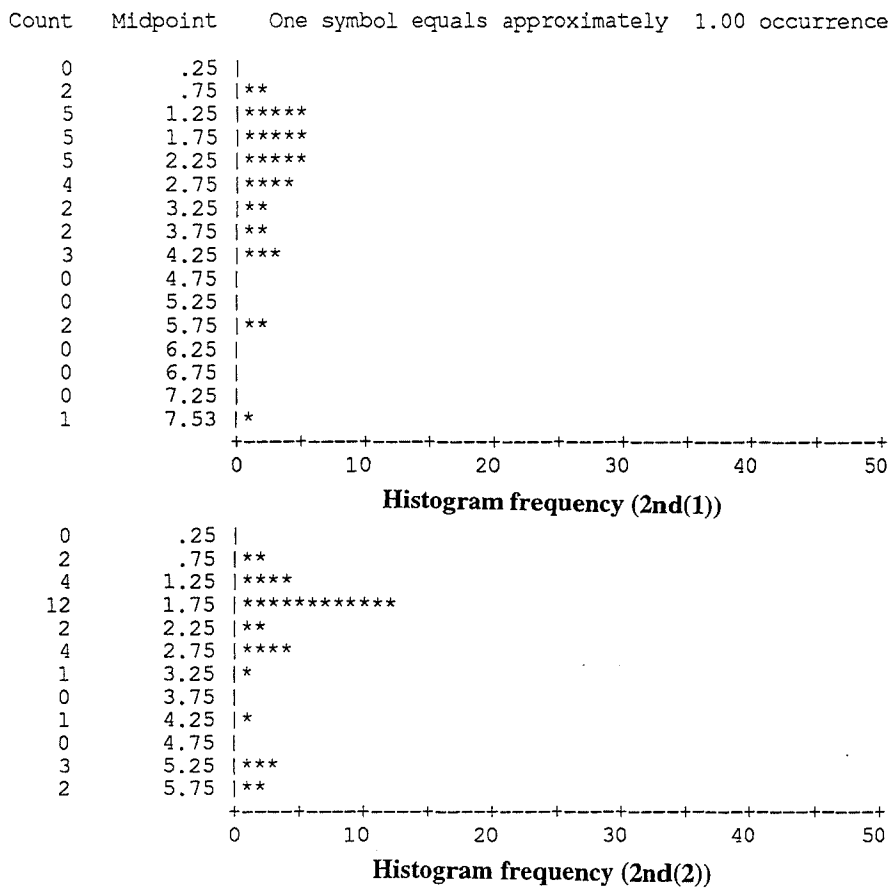


Fig. 3.18 (a) The $\Delta E(\text{CMC})$ distributions for the 2 reverse 2nd BPA models tested using the 31 data set (K ink is known)(Cromalin device).

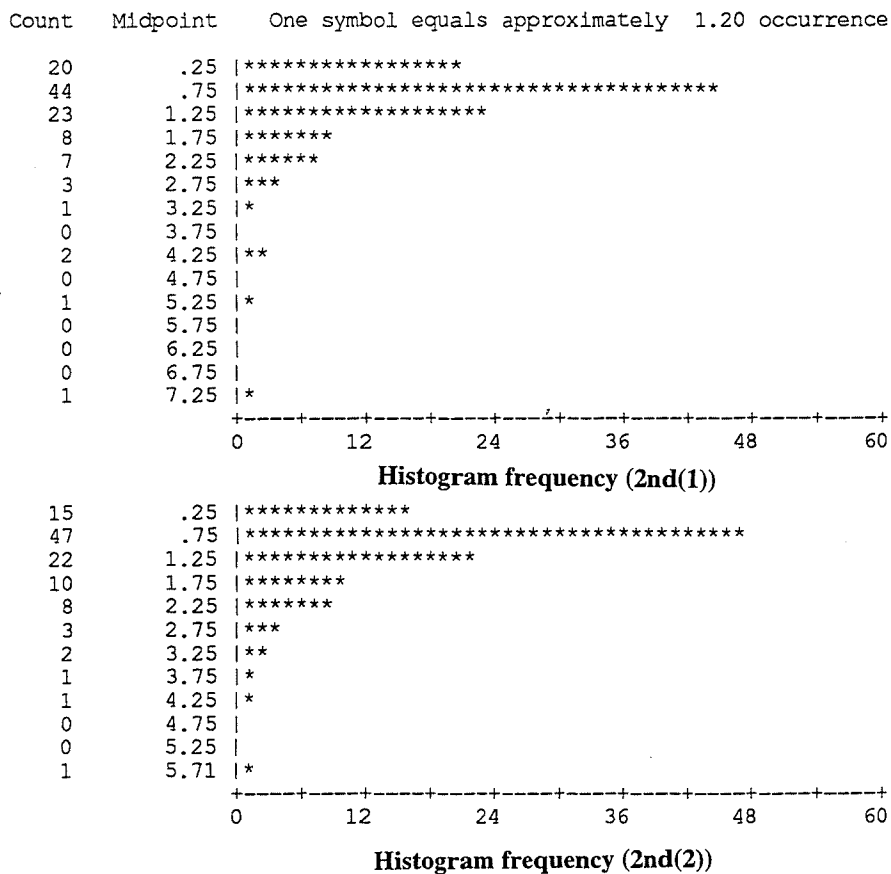


Fig. 3.18 (b) The $\Delta E(\text{CMC})$ distributions for the 2 reverse 2nd BPA models tested using the 110 data set (K ink is known)(Cromalin device).

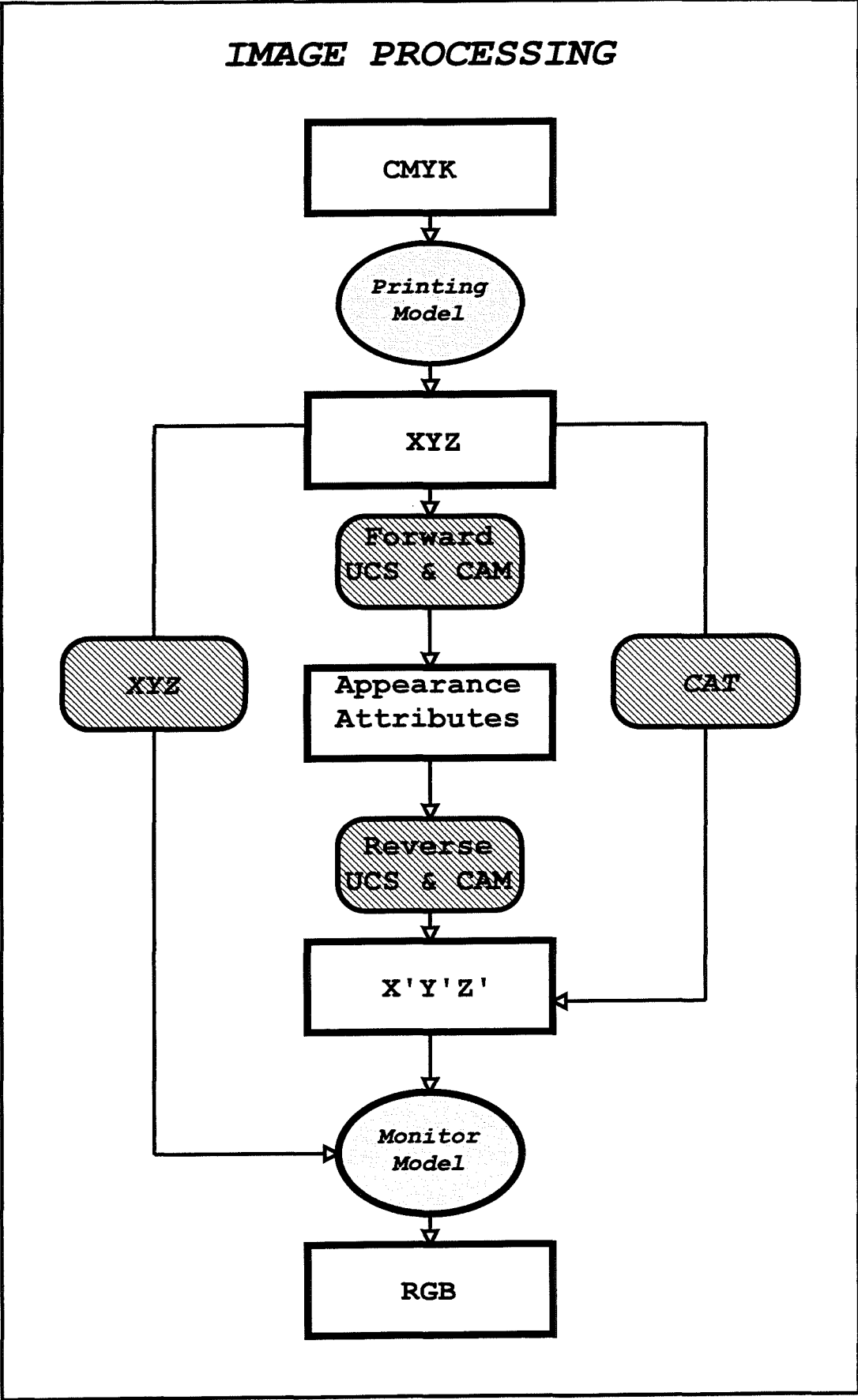


Fig. 4.1 Flow chart showing the image processing procedures. The UCS, CAM and CAT processes represent uniform colour space, colour appearance model and chromatic adaptation transform respectively.

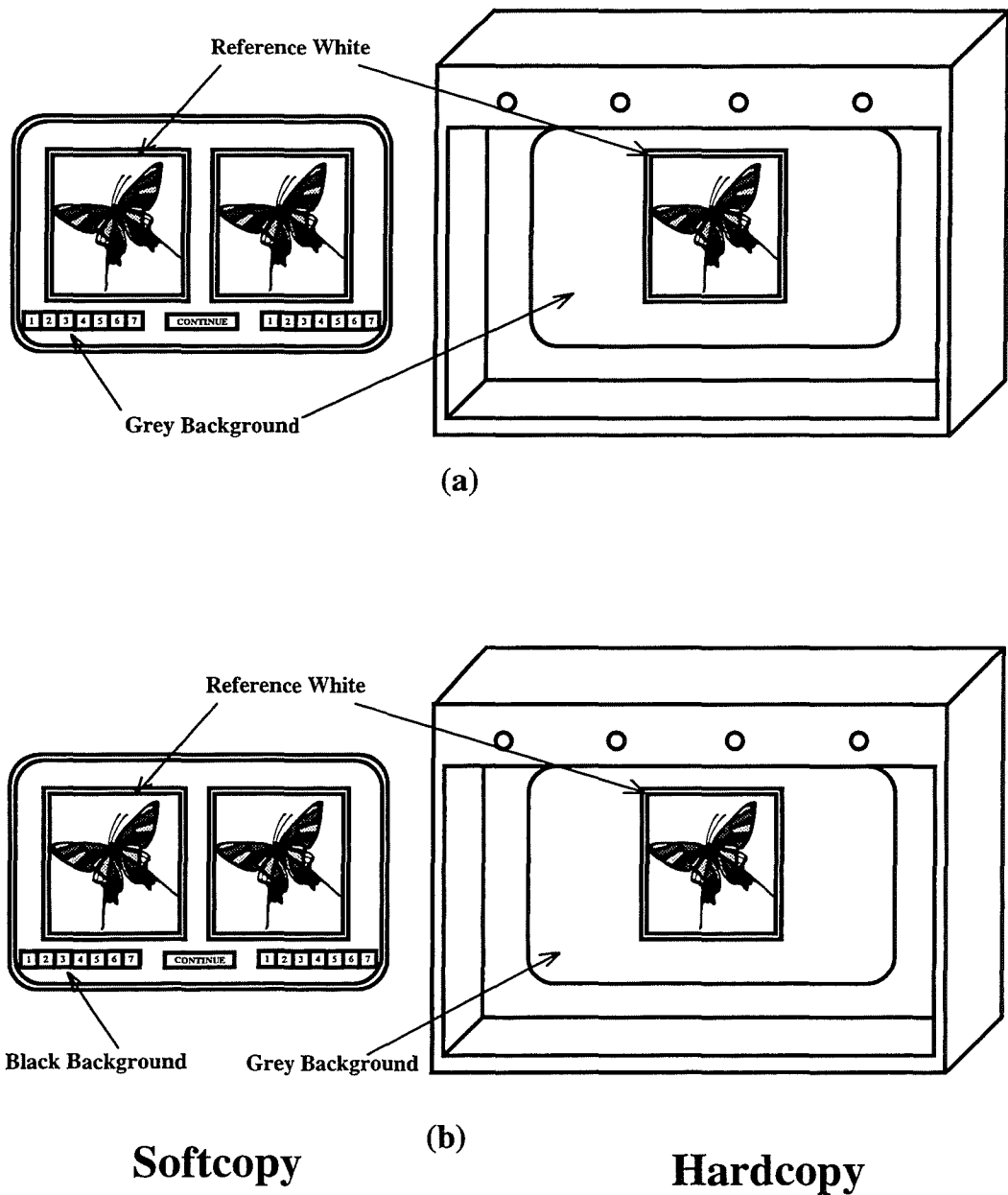


Fig. 4.2 The experimental viewing configuration for a) a simultaneous (SS) display using a symmetric condition, b) a simultaneous (SS) display using a asymmetric condition (Background difference/With white border), c) a simultaneous (SS) display using a asymmetric condition (Background difference/Without white border), and d) a toggling (TG) display.

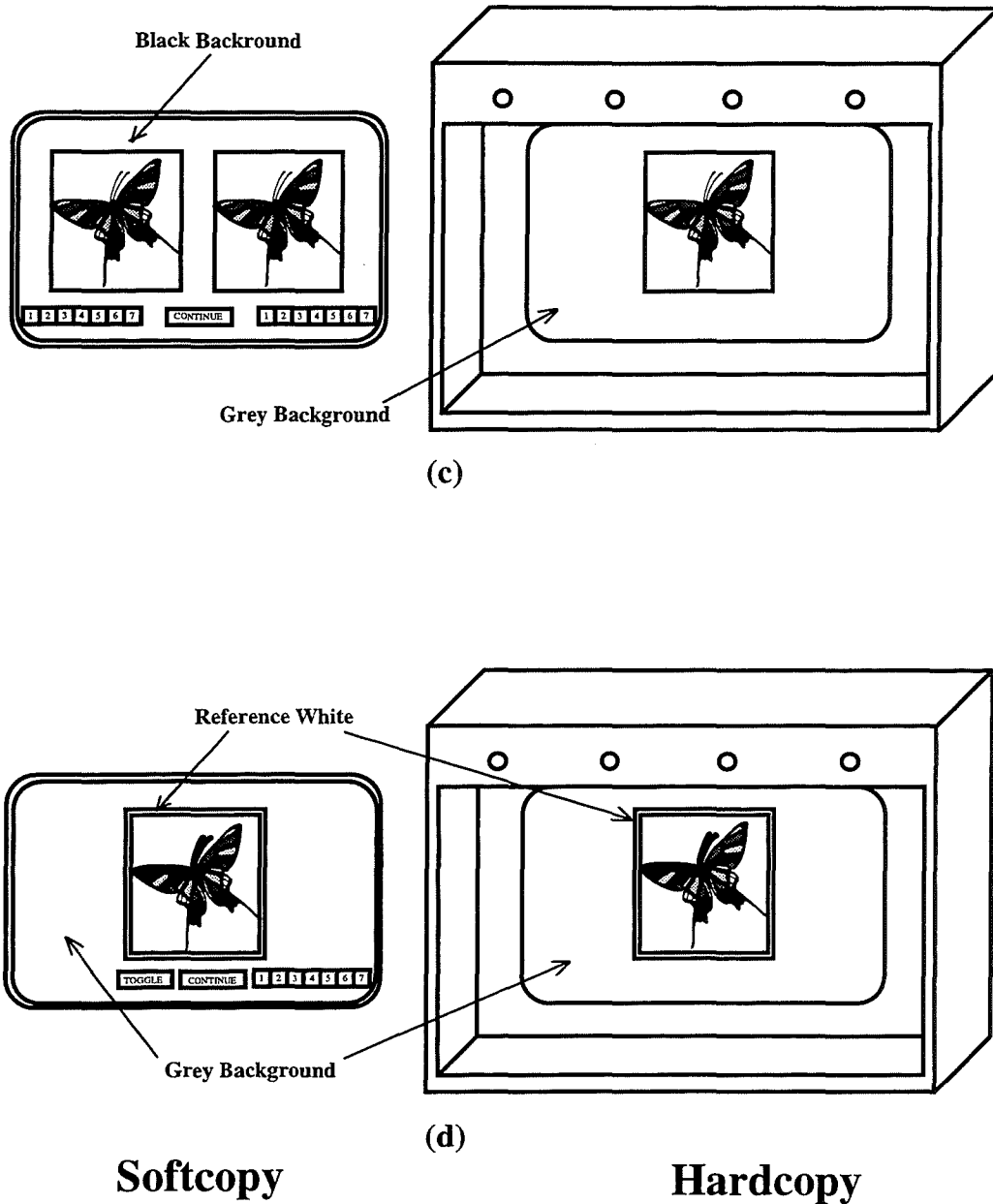


Fig. 4.2 The experimental viewing configuration for a) a simultaneous (SS) display using a symmetric condition, b) a simultaneous (SS) display using a asymmetric condition (Background difference/With white border), c) a simultaneous (SS) display using a asymmetric condition (Background difference/Without white border), and d) a toggling (TG) display. (continued)

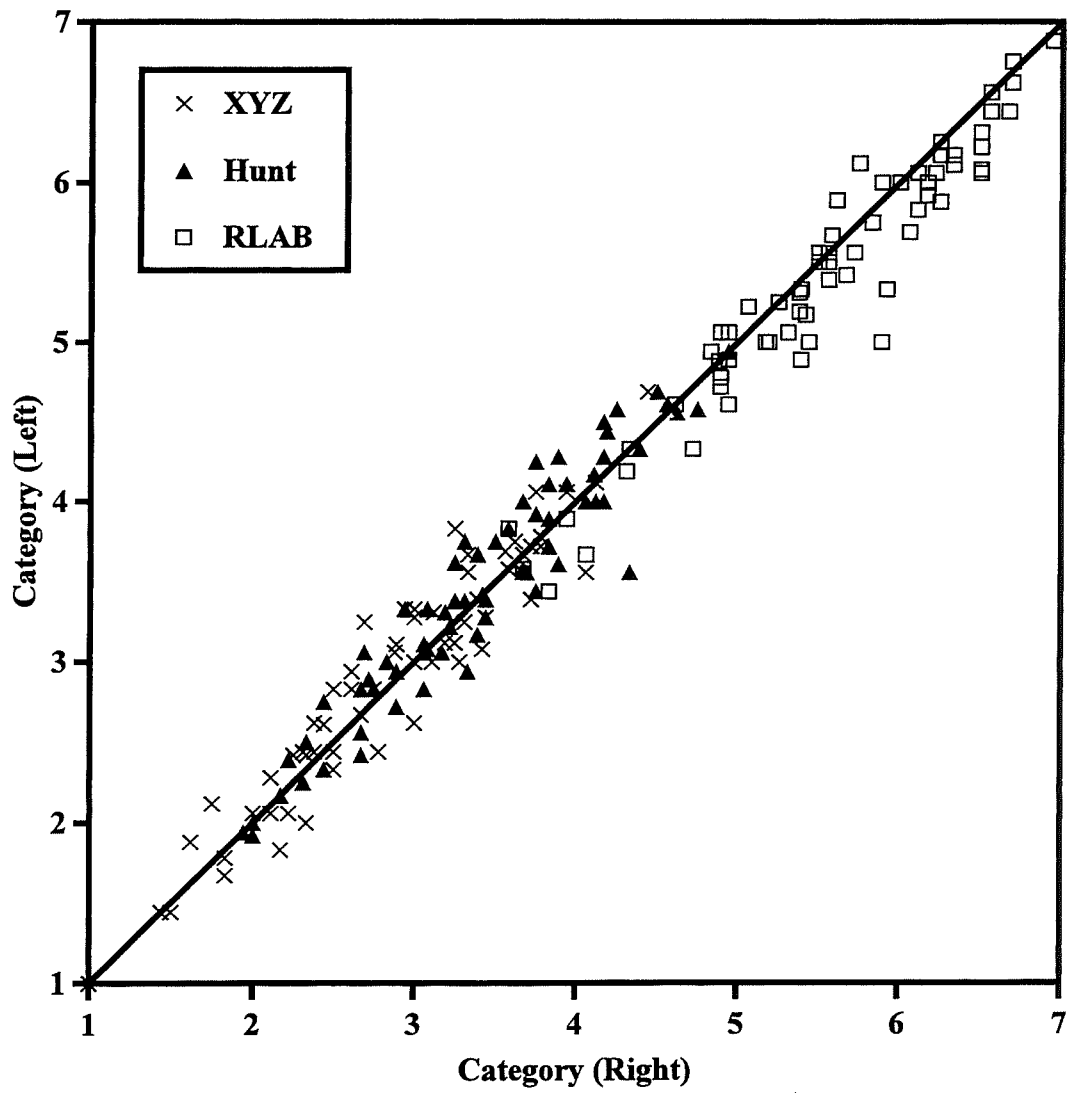
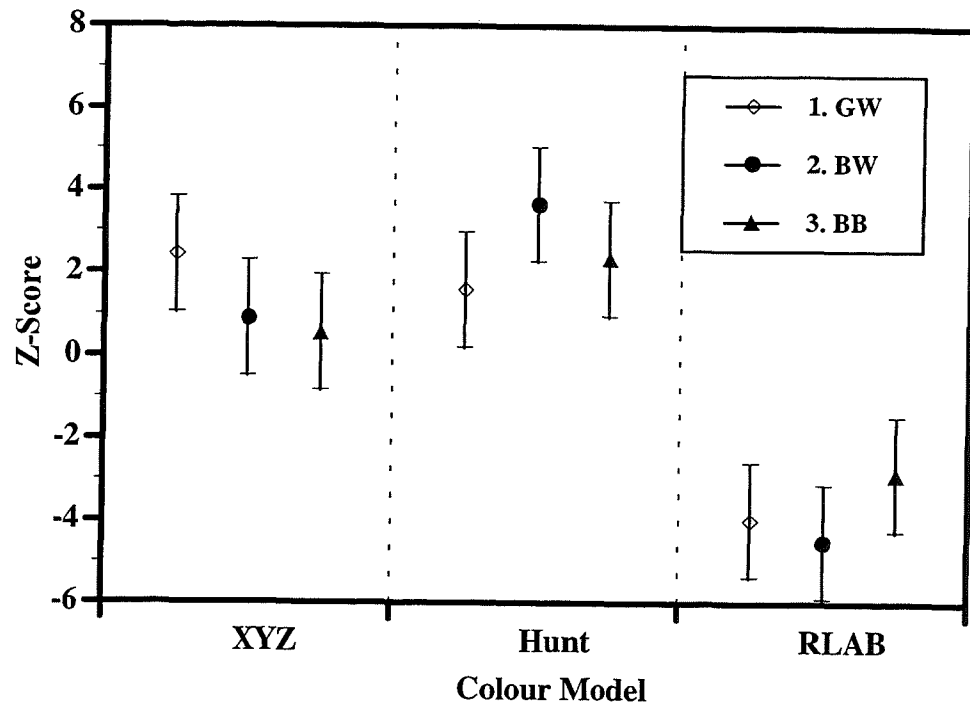
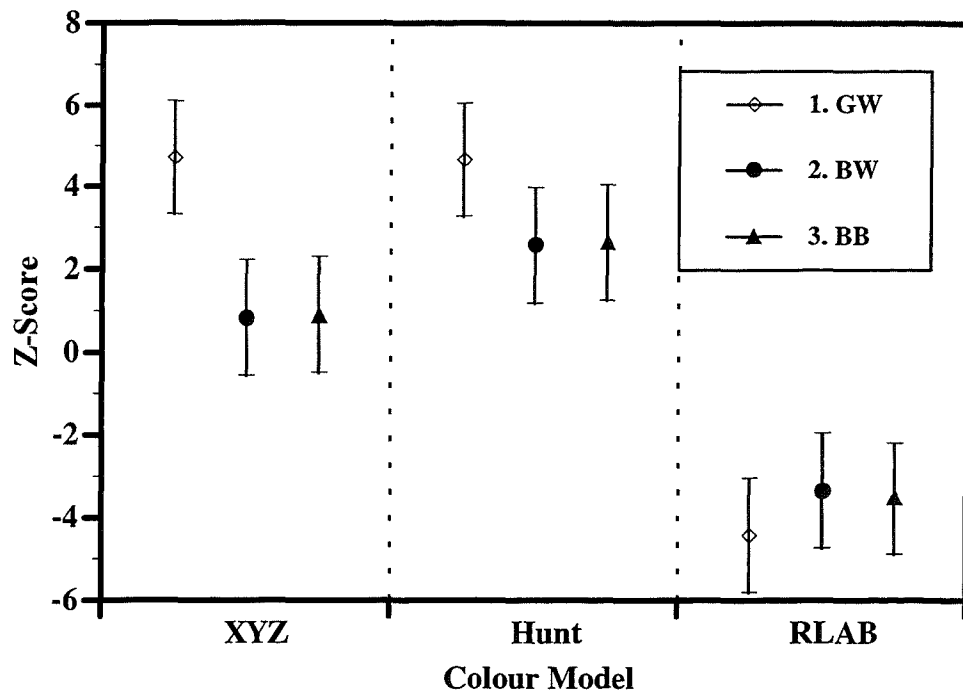


Fig. 4.3 The plot of category results for the same image displayed on the right and left sides of the monitor screen.

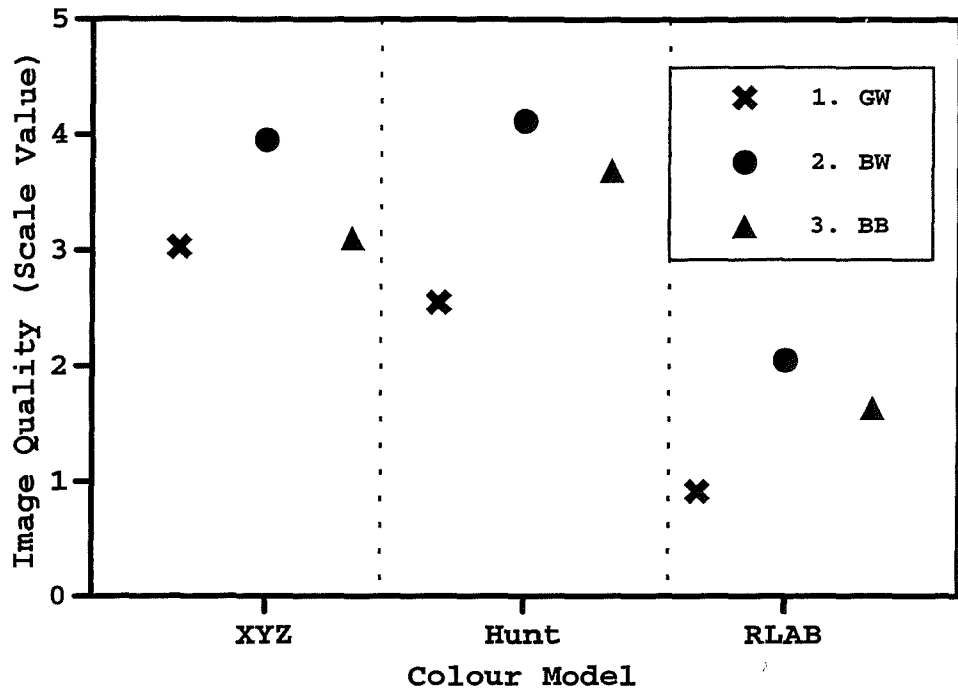


(a) D65

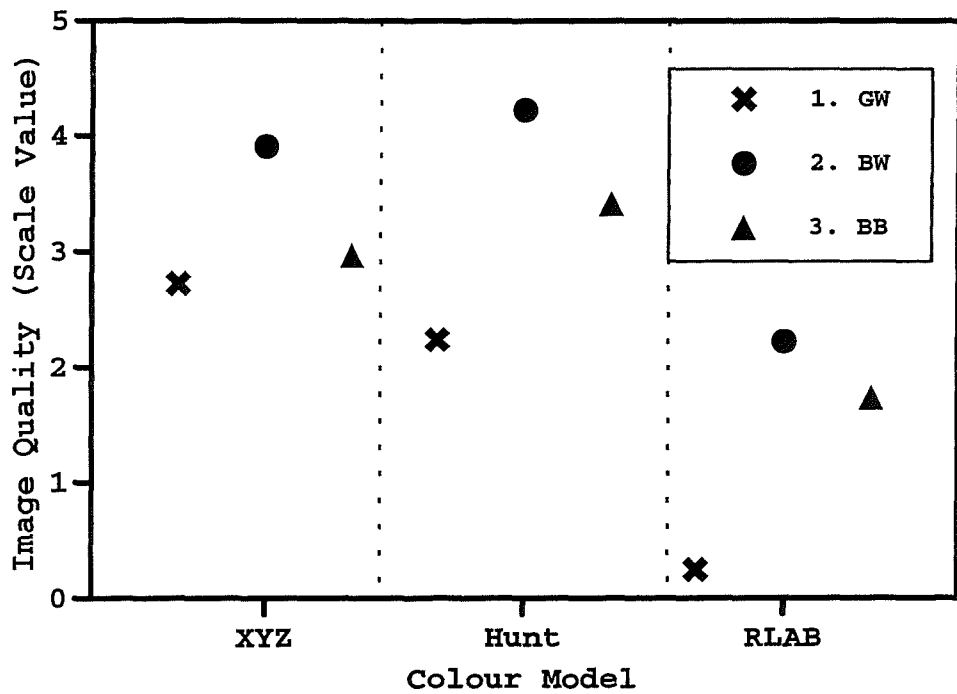


(b) D50

Fig. 4.4 Colour models' performance (combined from six images) evaluated using paired comparison results under a) D65, and b) D50 sources. The GW, BW, and BB represent the situations wherein the grey background with a white border, black background with a white border, and black background without a white border in the softcopy field for Experiments 1, 2, and 3 respectively.

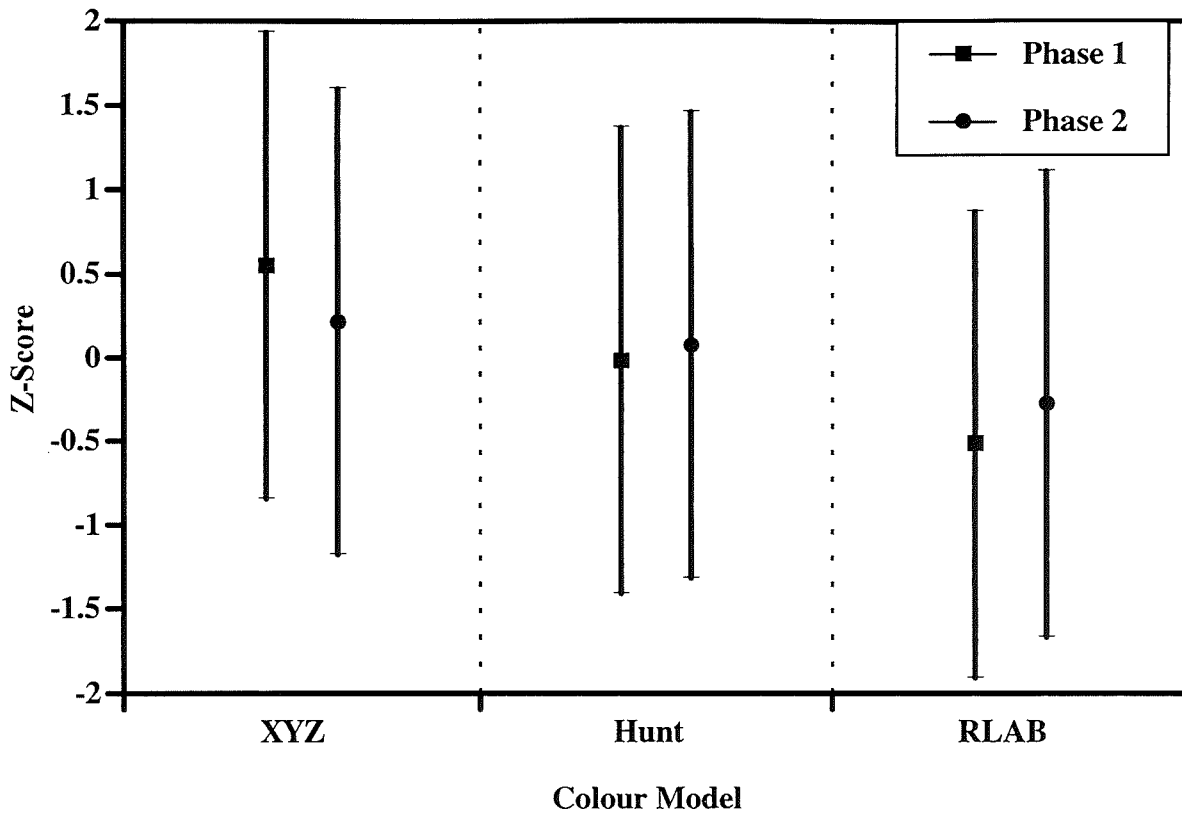


(a) D65

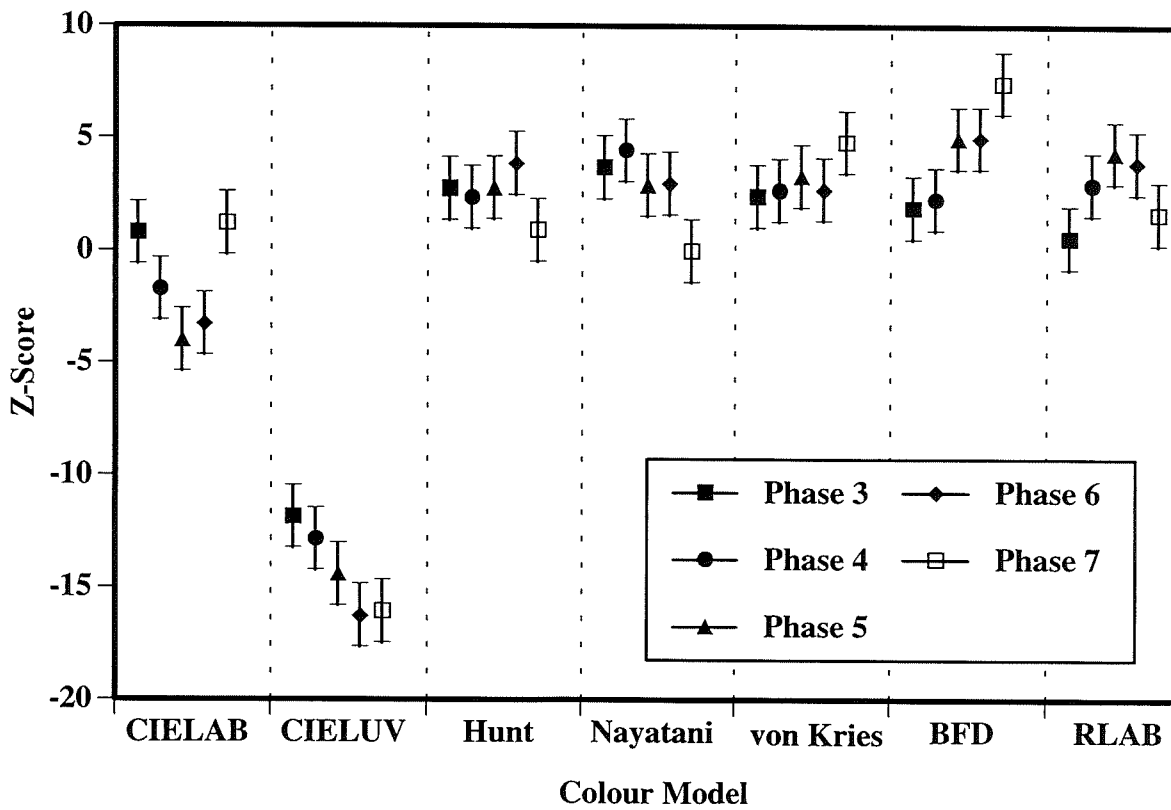


(b) D50

Fig. 4.5 Colour models' performance (combined from six images) evaluated using category judgement results under a) D65, and b) D50 sources. The GW, BW, and BB represent the situations wherein the grey background with a white border, black background with a white border, and black background without a white border in the softcopy field for Experiments 1, 2, and 3 respectively.



(a)



(b)

Fig. 4.6 Colour models' performance (combined from six images) evaluated using paired comparison results from a) Phases 1 and 2, and b) Phases 3 to 7.

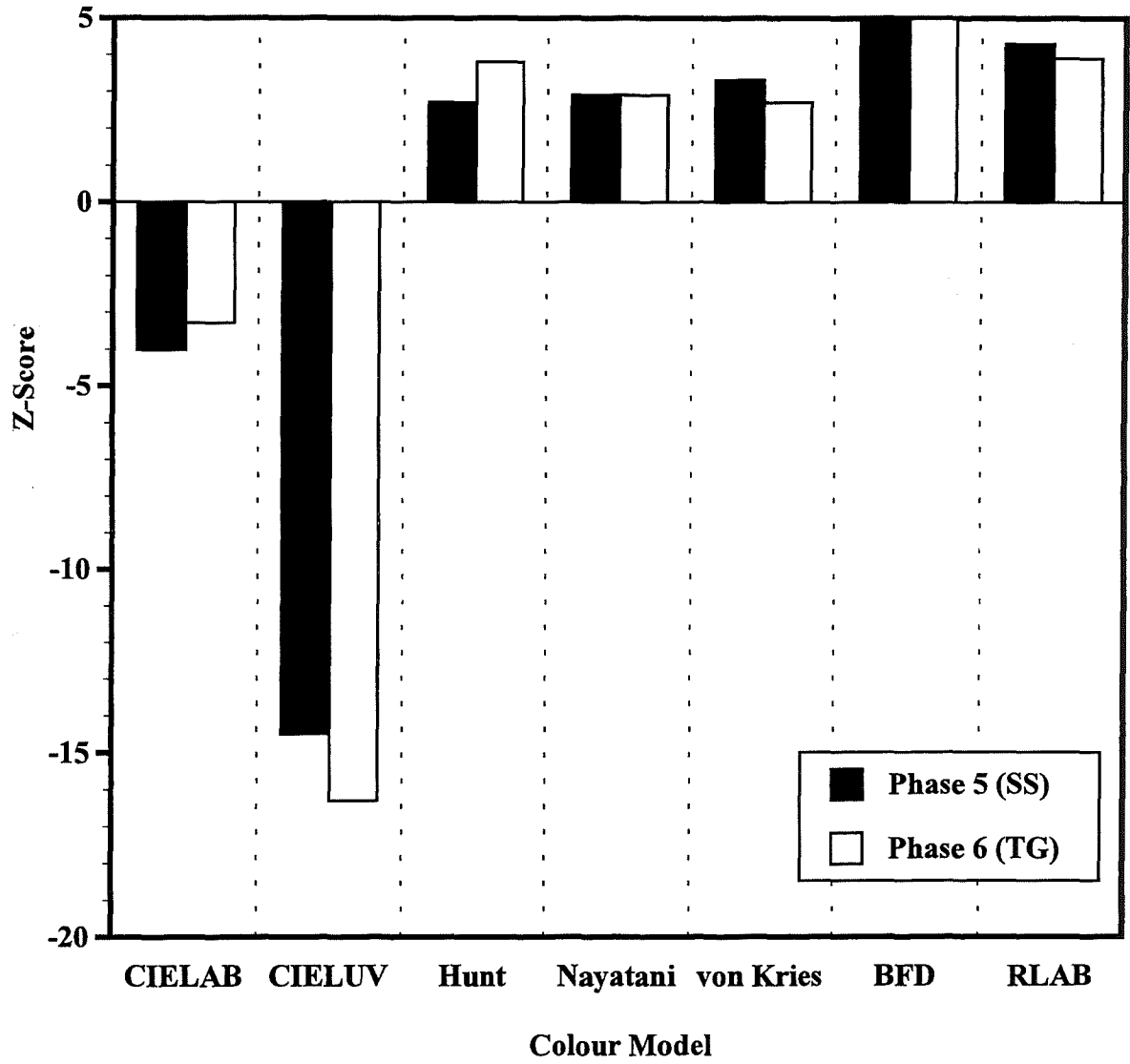
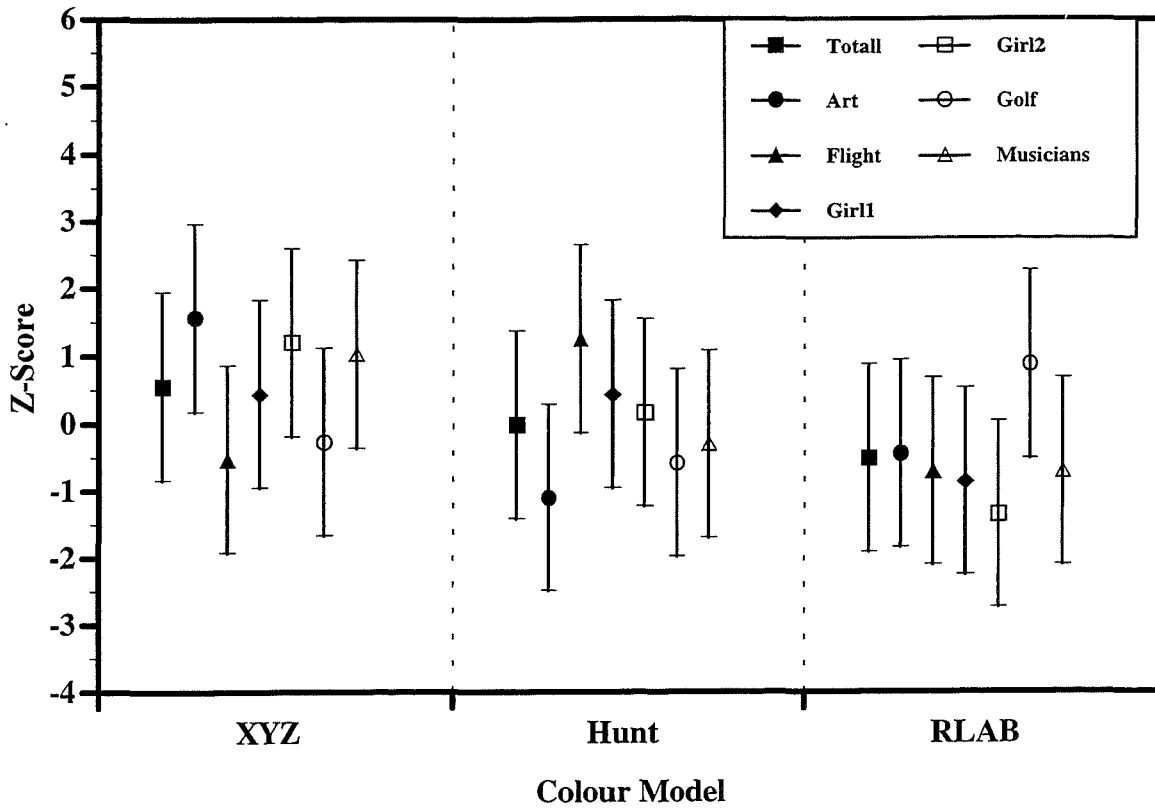
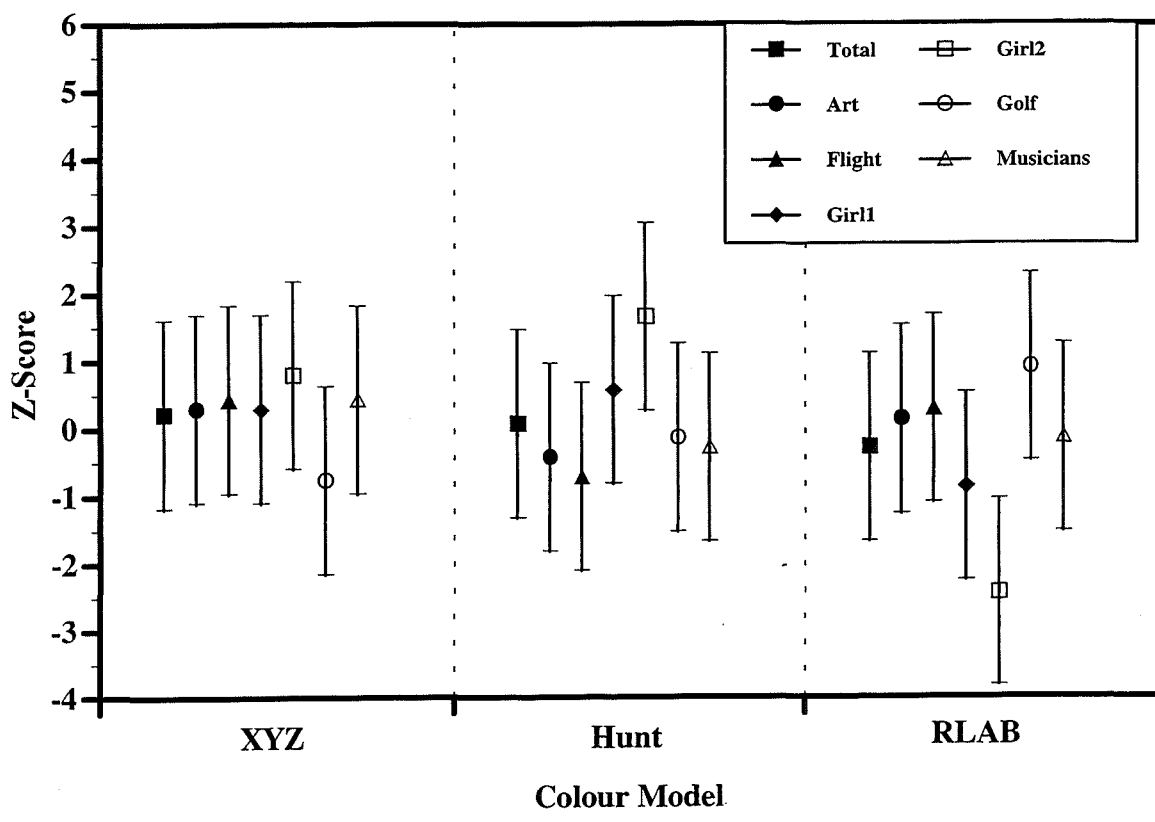


Fig. 4.7 Performance difference between the models using the SS and TG display arrangements for Phases 5 and 6 respectively.

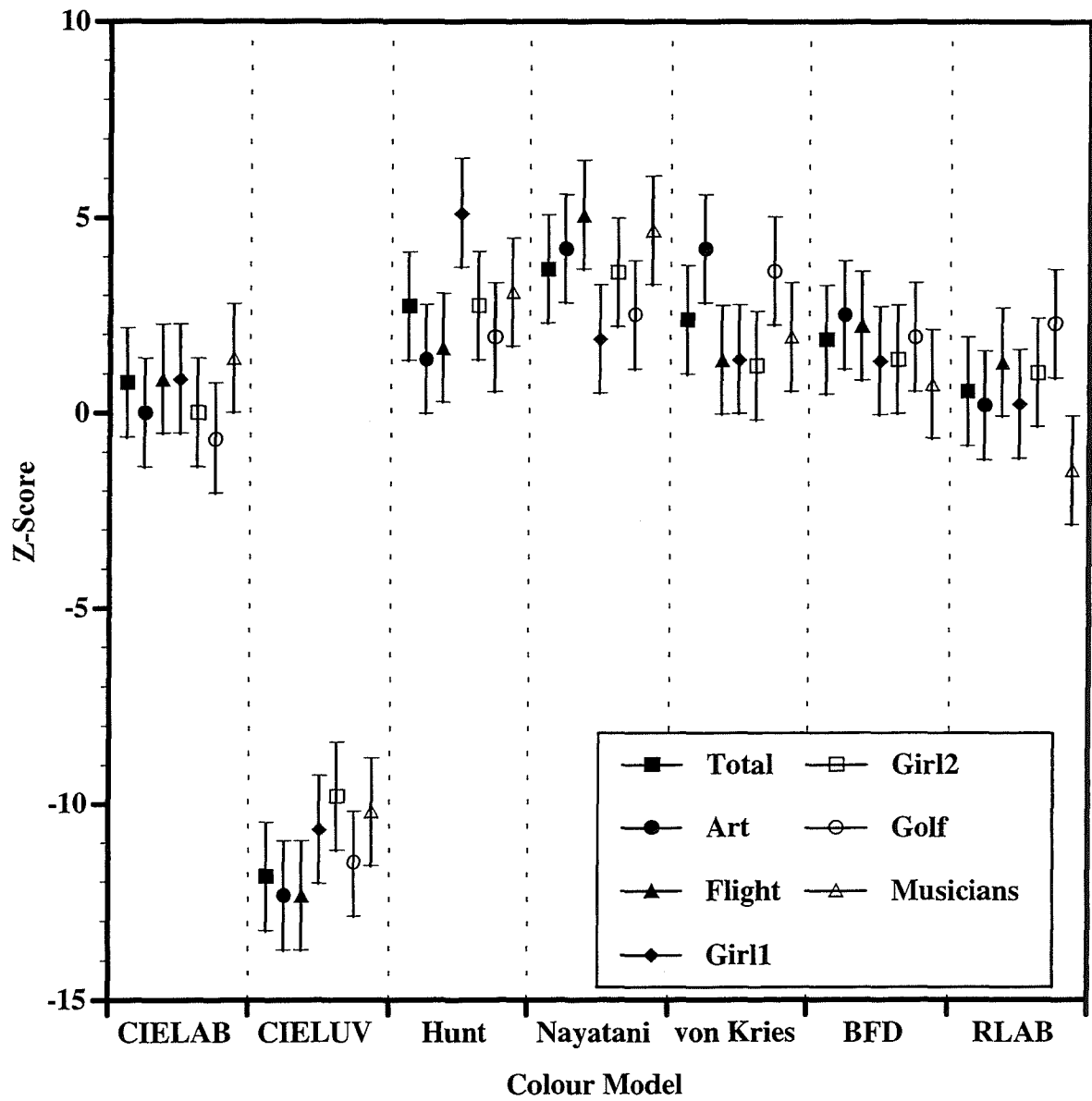


(a)



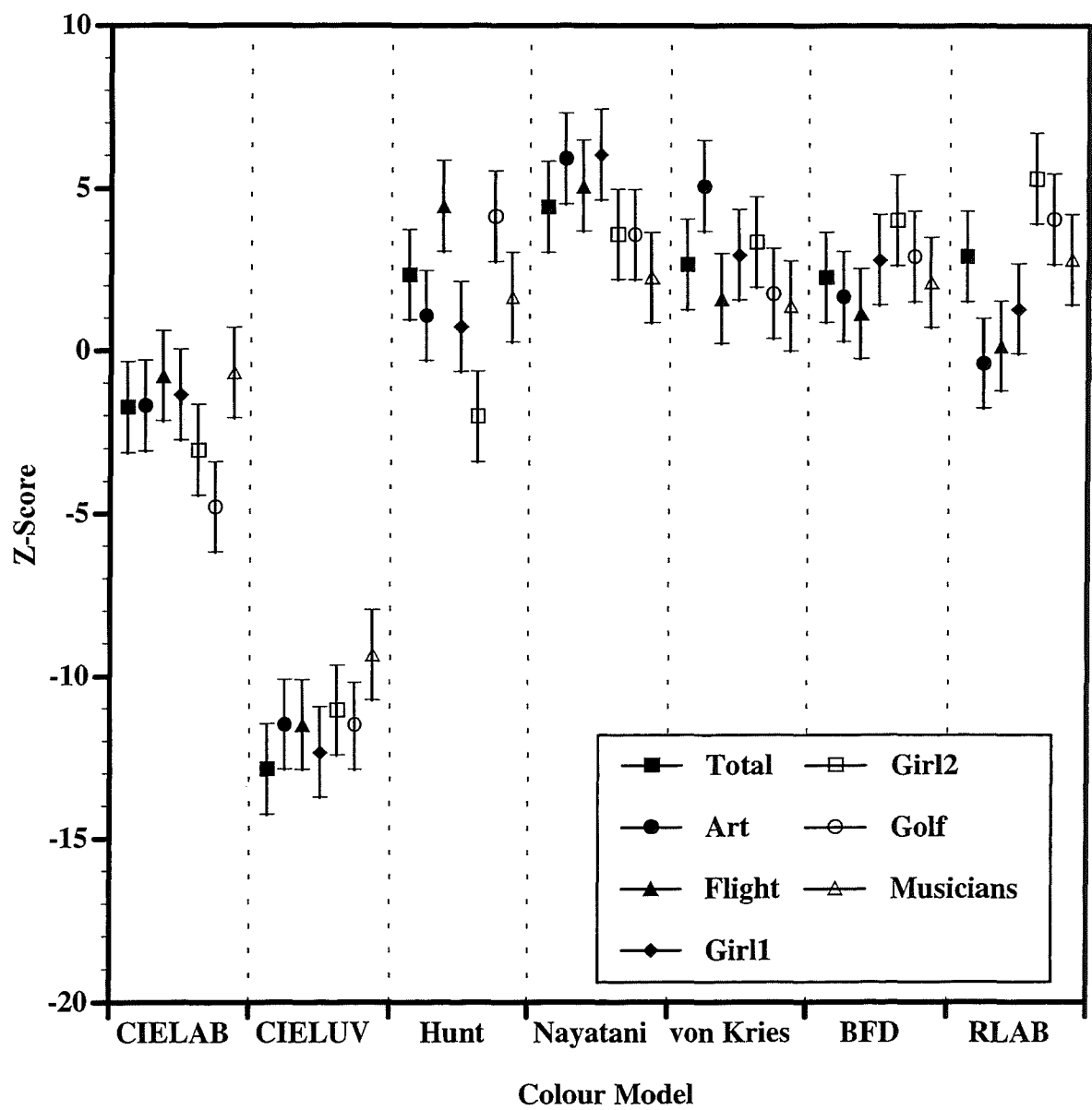
(b)

Fig. 4.8 Colour models' performance (for individual image) evaluated using the paired-comparison method for a) Phase 1, b) Phase 2.



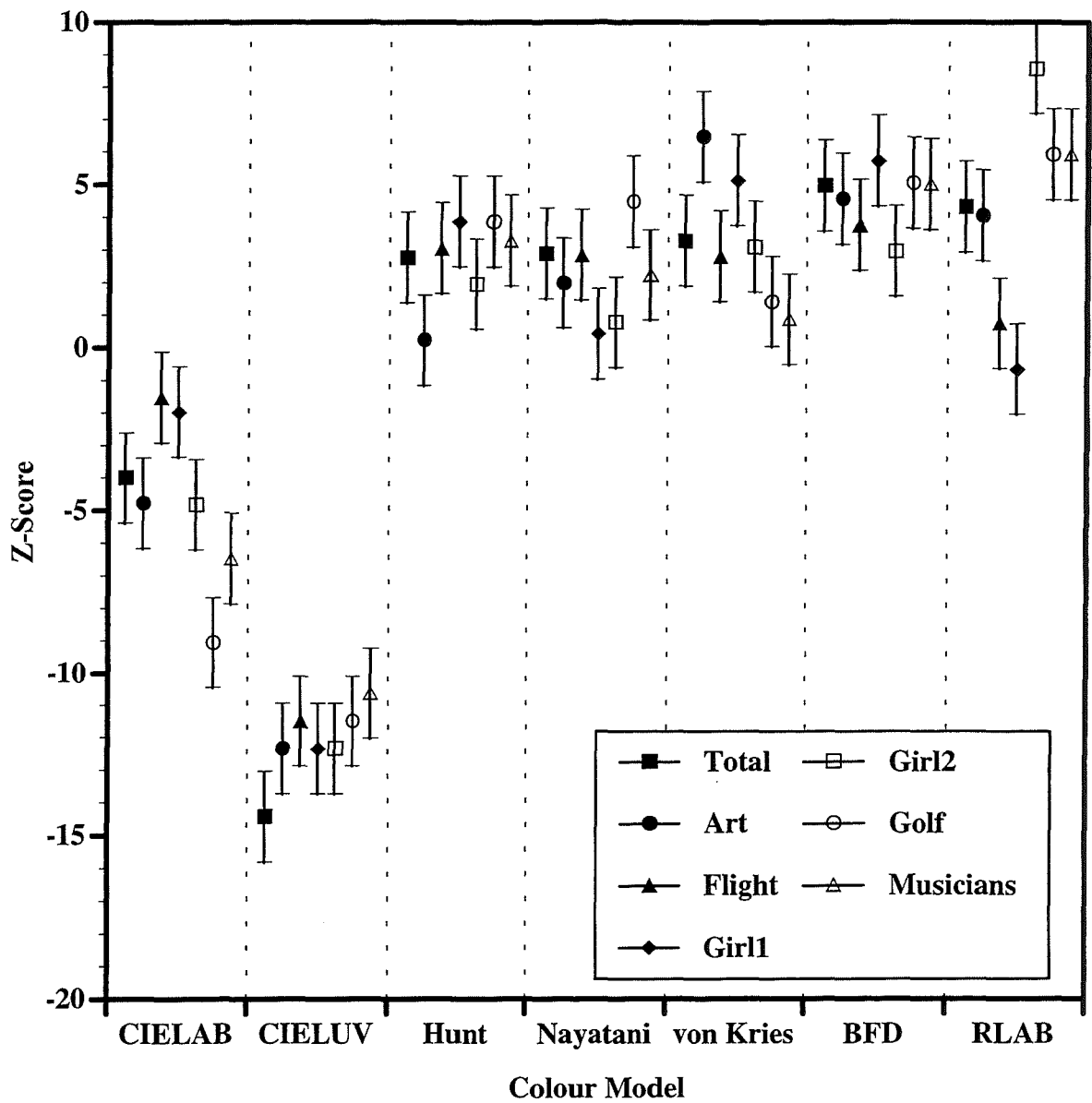
(a)

Fig. 4.9 Colour models' performance (for individual image) evaluated using the paired-comparison method for a) Phase 3, b) Phase 4, c) Phase 5, d) Phase 6, e) Phase 7.



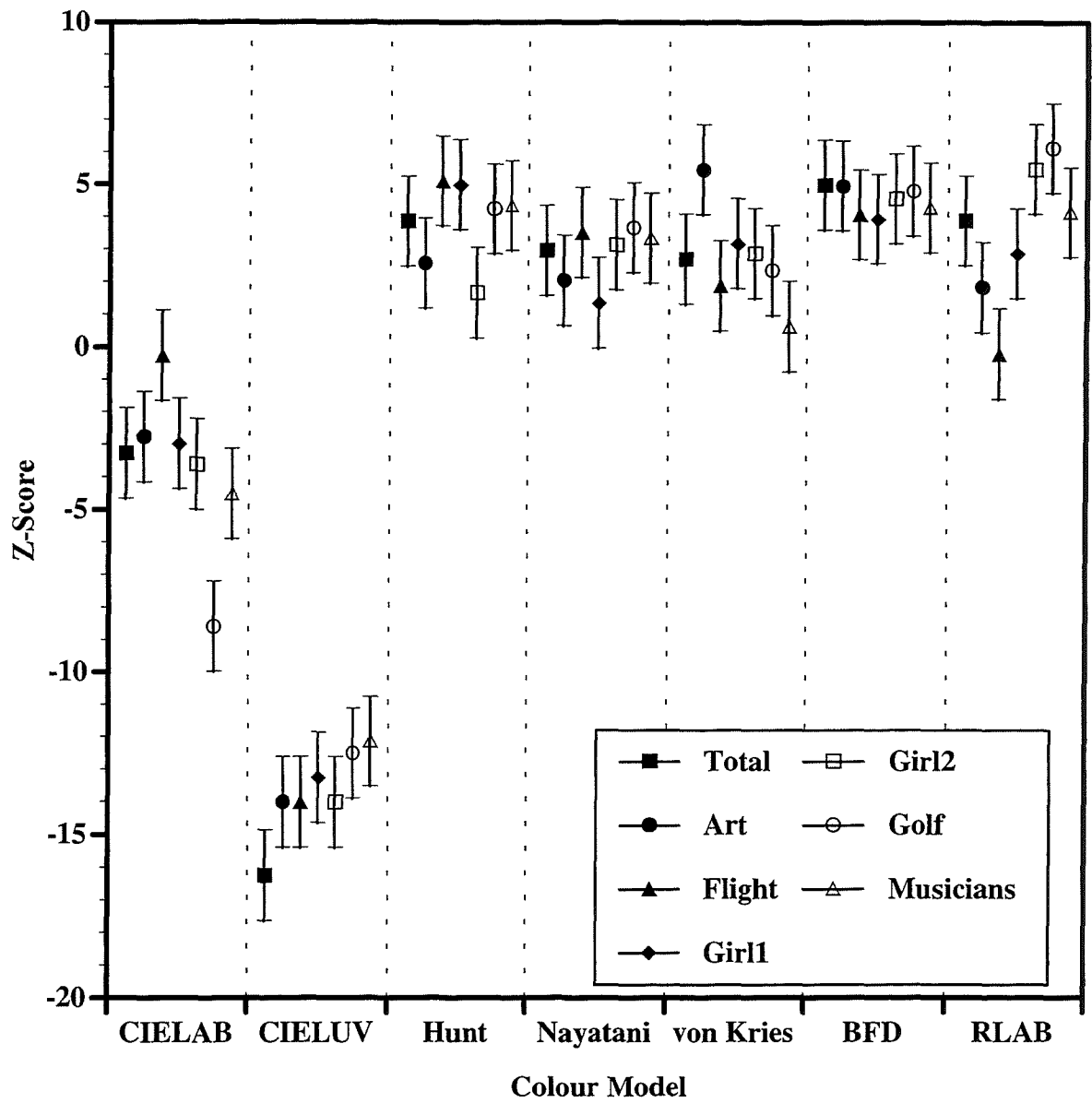
(b)

Fig. 4.9 Colour models' performance (for individual image) evaluated using the paired-comparison method for a) Phase 3, b) Phase 4, c) Phase 5, d) Phase 6, e) Phase 7. (continued)



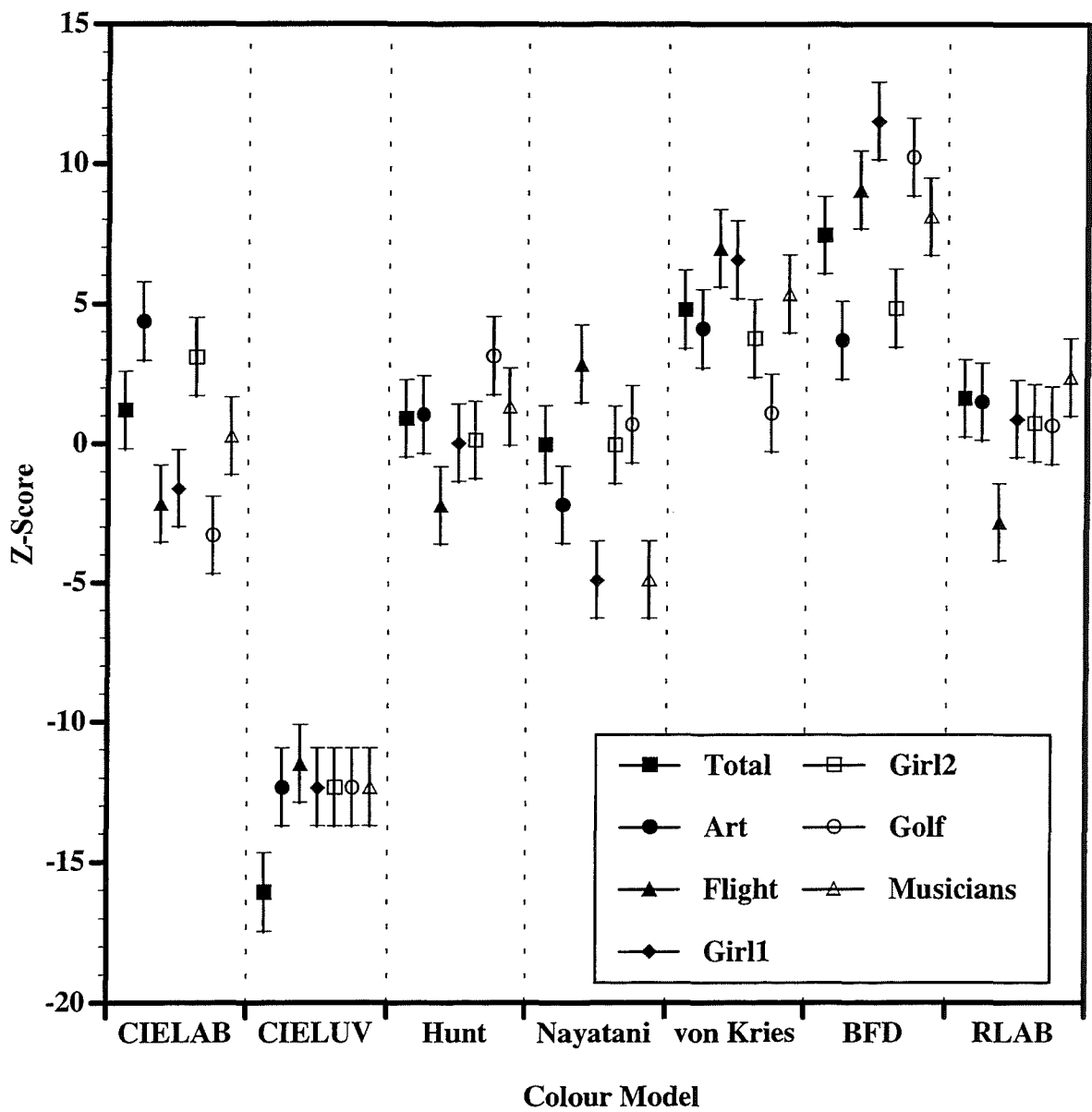
(c)

Fig. 4.9 Colour models' performance (for individual image) evaluated using the paired-comparison method for a) Phase 3, b) Phase 4, c) Phase 5, d) Phase 6, e) Phase 7. (continued)



(d)

Fig. 4.9 Colour models' performance (for individual image) evaluated using the paired-comparison method for a) Phase 3, b) Phase 4, c) Phase 5, d) Phase 6, e) Phase 7. (continued)



(e)

Fig. 4.9 Colour models' performance (for individual image) evaluated using the paired-comparison method for a) Phase 3, b) Phase 4, c) Phase 5, d) Phase 6, e) Phase 7. (continued)

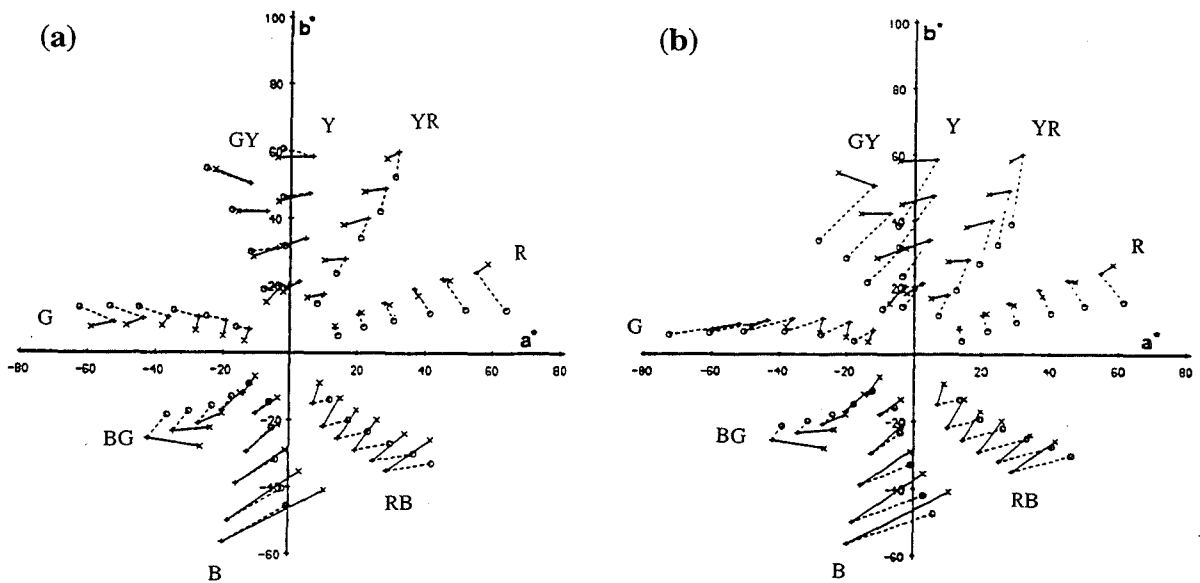


Fig. 5.1 Graphical representation of corresponding a^* , b^* values showing direction and magnitude of the visual results under A (plotted using + symbol) and D65 (plotted using a \times symbol) light sources compared with those predicted by (a) the BFD model, (b) the Hunt model for LUTCHI-Alvey Data Set (plotted using \circ symbol).

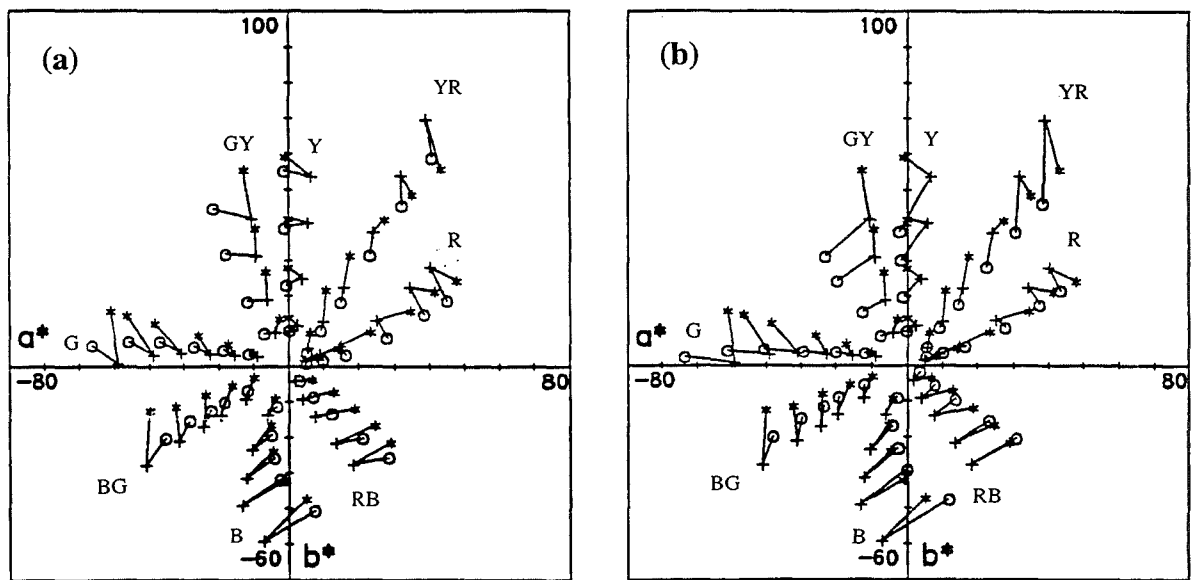


Fig. 5.2 Graphical representation of corresponding a^* , b^* values showing direction and magnitude of the visual results under A (plotted using + symbol) and D65 (plotted using a \times symbol) light sources compared with those predicted by (a) the BFD model, (b) the Hunt model for LUTCHI-Kuo and Luo Data Set (plotted using \circ symbol).

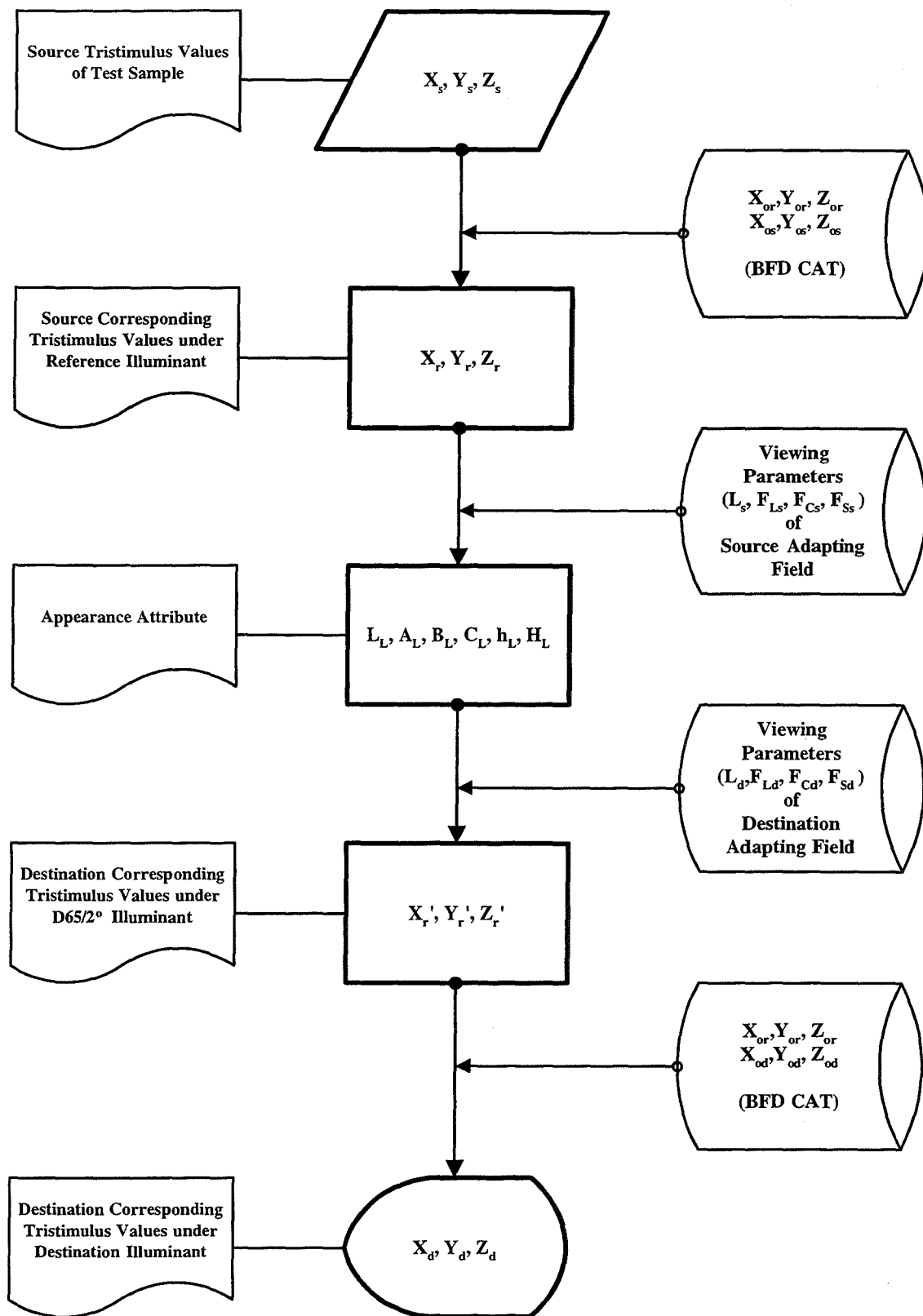


Fig. 5.3 Flow chart for the calculation of LLAB model in predicting corresponding colours.

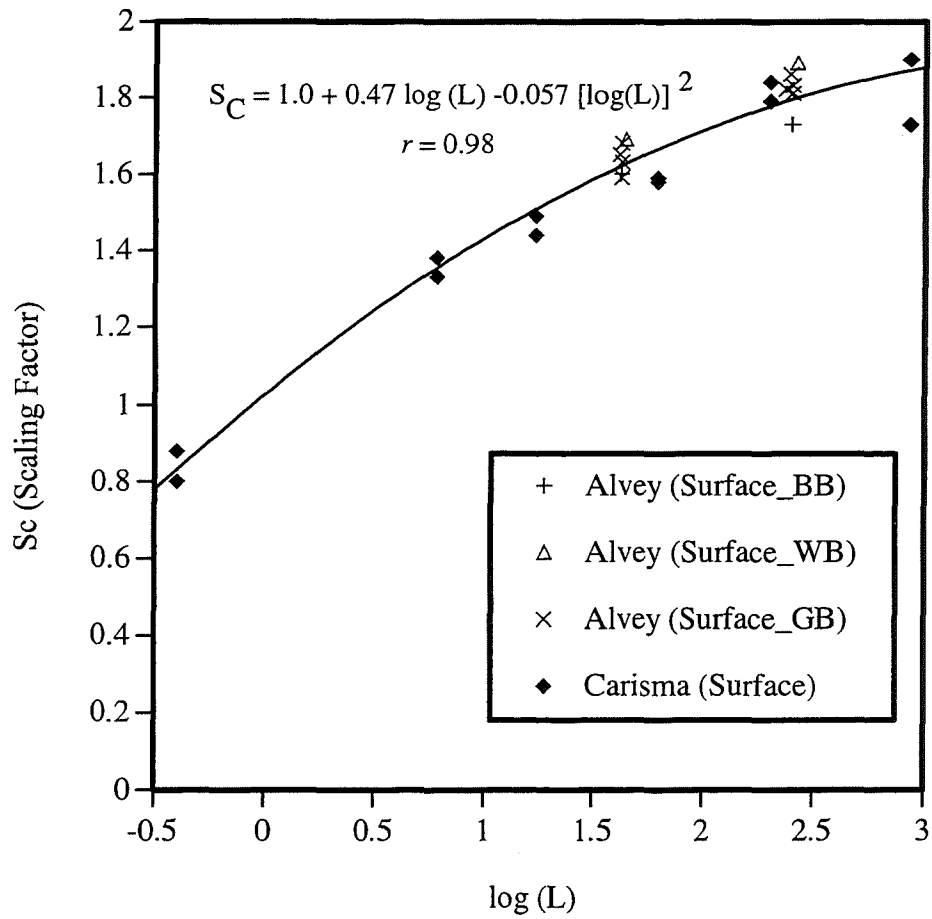


Fig. 5.4 Scaling factor (S_C) vs. $\log(L)$ showing the Hunt effect (the increase in colourfulness due to increase of luminance level).

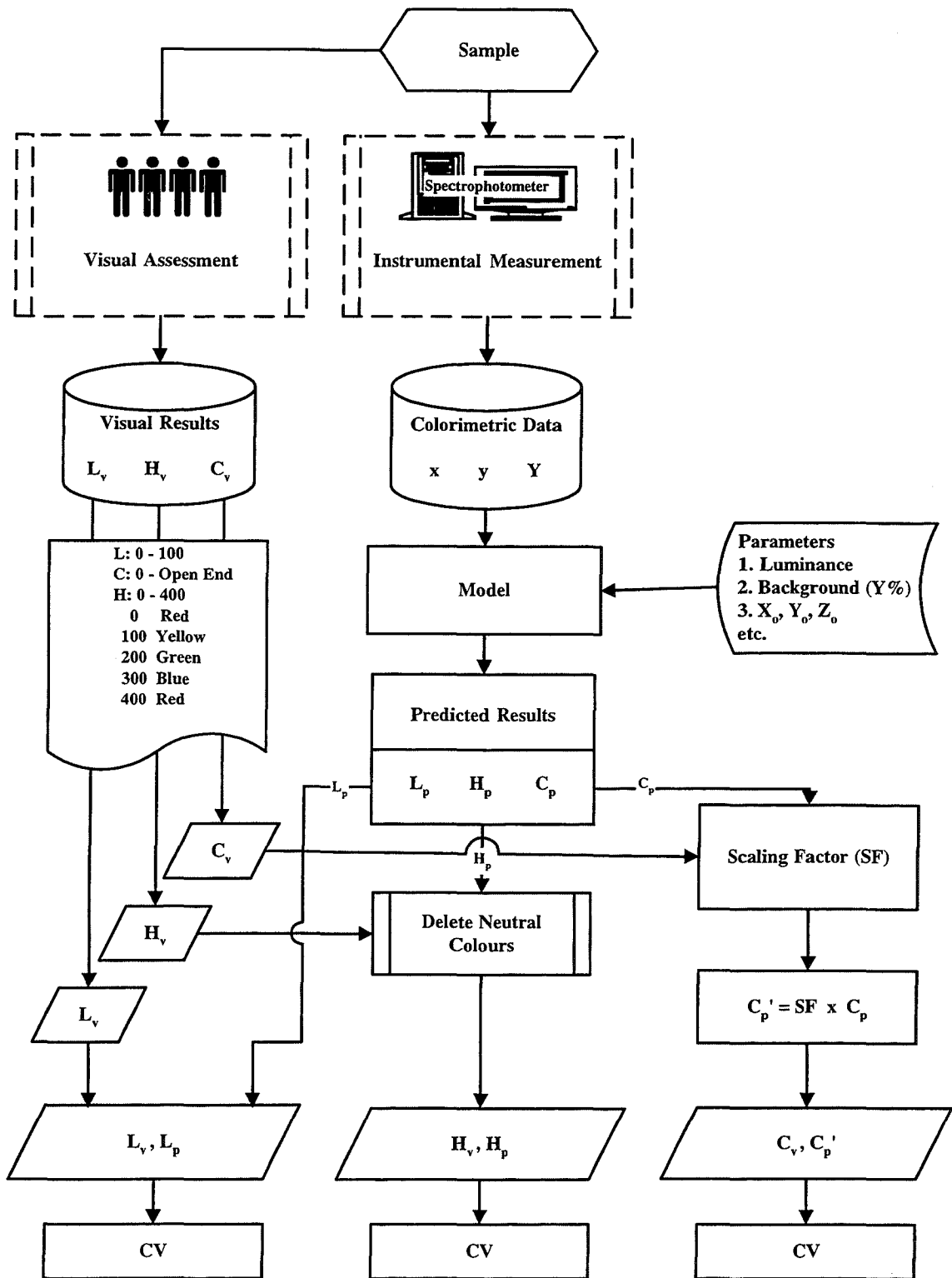


Fig. 5.5 Flow chart for comparing colour models' prediction with visual results.

APPENDICES

APPENDIX A Equations used for black printer algorithms (BPAs).

A.1.1 Forward Model

$$k_r' = a_{1,1} D_{r-3c} + a_{1,2} D_{r-k} + a_{1,3} D_{r-3c}^2 + a_{1,4} D_{r-k}^2 + a_{1,5} D_{r-3c} D_{r-k} + a_{1,6} D_{r-3c}^3 + a_{1,7} D_{r-k}^3 + a_{1,8} D_{r-3c}^2 D_{r-k} + a_{1,9} D_{r-k}^2 D_{r-3c} + a_{1,10}$$

$$k_g' = a_{2,1} D_{g-3c} + a_{2,2} D_{g-k} + a_{2,3} D_{g-3c}^2 + a_{2,4} D_{g-k}^2 + a_{2,5} D_{g-3c} D_{g-k} + a_{2,6} D_{g-3c}^3 + a_{2,7} D_{g-k}^3 + a_{2,8} D_{g-3c}^2 D_{g-k} + a_{2,9} D_{g-k}^2 D_{g-3c} + a_{2,10}$$

$$k_b' = a_{3,1} D_{b-3c} + a_{3,2} D_{b-k} + a_{3,3} D_{b-3c}^2 + a_{3,4} D_{b-k}^2 + a_{3,5} D_{b-3c} D_{b-k} + a_{3,6} D_{b-3c}^3 + a_{3,7} D_{b-k}^3 + a_{3,8} D_{b-3c}^2 D_{b-k} + a_{3,9} D_{b-k}^2 D_{b-3c} + a_{3,10}$$

A.1.2 Reverse Model

$$k_r'' = a_{1,1} D_{r-4c} + a_{1,2} D_{r-k} + a_{1,3} D_{r-4c}^2 + a_{1,4} D_{r-k}^2 + a_{1,5} D_{r-4c} D_{r-k} + a_{1,6} D_{r-4c}^3 + a_{1,7} D_{r-k}^3 + a_{1,8} D_{r-4c}^2 D_{r-k} + a_{1,9} D_{r-k}^2 D_{r-4c} + a_{1,10}$$

$$k_g'' = a_{2,1} D_{g-4c} + a_{2,2} D_{g-k} + a_{2,3} D_{g-4c}^2 + a_{2,4} D_{g-k}^2 + a_{2,5} D_{g-4c} D_{g-k} + a_{2,6} D_{g-4c}^3 + a_{2,7} D_{g-k}^3 + a_{2,8} D_{g-4c}^2 D_{g-k} + a_{2,9} D_{g-k}^2 D_{g-4c} + a_{2,10}$$

$$k_b'' = a_{3,1} D_{b-4c} + a_{3,2} D_{b-k} + a_{3,3} D_{b-4c}^2 + a_{3,4} D_{b-k}^2 + a_{3,5} D_{b-4c} D_{b-k} + a_{3,6} D_{b-4c}^3 + a_{3,7} D_{b-k}^3 + a_{3,8} D_{b-4c}^2 D_{b-k} + a_{3,9} D_{b-k}^2 D_{b-4c} + a_{3,10}$$

where

- $a_{i,j}$ are the optimised coefficients ($i = 1$ to 3 for D_r , D_g and D_b respectively, and j the number of coefficients used). These were obtained by using the Lawson and Hanson's least-squares technique (Lawson and Hanson 1974, Press et al. 1992) to give the closest predictions to those converging densities obtained using Eqn. 3-5-1 (or 3-5-2).
- $(D_{r-4c}, D_{g-4c}, D_{b-4c})$, $(D_{r-3c}, D_{g-3c}, D_{b-3c})$, $(D_{r-k}, D_{g-k}, D_{b-k})$ terms are the red-, green-, and blue- colorimetric densities of four-colour, three-colour component, and black component respectively.

A.2.1 Forward Model

$$D_{r-4c} = a_{1,1} D_{r-3c} + a_{1,2} D_{r-k} + a_{1,3} D_{r-3c}^2 + a_{1,4} D_{r-k}^2 + a_{1,5} D_{r-3c} D_{r-k} + a_{1,6} D_{r-3c}^3 + a_{1,7} D_{r-k}^3 + a_{1,8} D_{r-3c}^2 D_{r-k} + a_{1,9} D_{r-k}^2 D_{r-3c} + a_{1,10}$$

$$D_{g-4c} = a_{2,1} D_{g-3c} + a_{2,2} D_{g-k} + a_{2,3} D_{g-3c}^2 + a_{2,4} D_{g-k}^2 + a_{2,5} D_{g-3c} D_{g-k} + a_{2,6} D_{g-3c}^3 + a_{2,7} D_{g-k}^3 + a_{2,8} D_{g-3c}^2 D_{g-k} + a_{2,9} D_{g-k}^2 D_{g-3c} + a_{2,10}$$

$$D_{b-4c} = a_{3,1} D_{b-3c} + a_{3,2} D_{b-k} + a_{3,3} D_{b-3c}^2 + a_{3,4} D_{b-k}^2 + a_{3,5} D_{b-3c} D_{b-k} + a_{3,6} D_{b-3c}^3 + a_{3,7} D_{b-k}^3 + a_{3,8} D_{b-3c}^2 D_{b-k} + a_{3,9} D_{b-k}^2 D_{b-3c} + a_{3,10}$$

A.2.2 Reverse Model

$$D_{r-3c} = a_{1,1} D_{r-4c} + a_{1,2} D_{r-k} + a_{1,3} D_{r-4c}^2 + a_{1,4} D_{r-k}^2 + a_{1,5} D_{r-4c} D_{r-k} + a_{1,6} D_{r-4c}^3 + a_{1,7} D_{r-k}^3 + a_{1,8} D_{r-4c}^2 D_{r-k} + a_{1,9} D_{r-k}^2 D_{r-4c} + a_{1,10}$$

$$D_{g-3c} = a_{2,1} D_{g-4c} + a_{2,2} D_{g-k} + a_{2,3} D_{g-4c}^2 + a_{2,4} D_{g-k}^2 + a_{2,5} D_{g-4c} D_{g-k} + a_{2,6} D_{g-4c}^3 + a_{2,7} D_{g-k}^3 + a_{2,8} D_{g-4c}^2 D_{g-k} + a_{2,9} D_{g-k}^2 D_{g-4c} + a_{2,10}$$

$$D_{b-3c} = a_{3,1} D_{b-4c} + a_{3,2} D_{b-k} + a_{3,3} D_{b-4c}^2 + a_{3,4} D_{b-k}^2 + a_{3,5} D_{b-4c} D_{b-k} + a_{3,6} D_{b-4c}^3 + a_{3,7} D_{b-k}^3 + a_{3,8} D_{b-4c}^2 D_{b-k} + a_{3,9} D_{b-k}^2 D_{b-4c} + a_{3,10}$$

where

- $a_{i,j}$ are the optimised coefficients ($i = 1$ to 3 for D_r , D_g and D_b respectively) obtained by using the Lawson and Hanson's least-squares technique to give the closest predictions to those measured colorimetric data.
- $(D_{r-4c}, D_{g-4c}, D_{b-4c})$, $(D_{r-3c}, D_{g-3c}, D_{b-3c})$, $(D_{r-k}, D_{g-k}, D_{b-k})$ terms are the red-, green-, and blue- colorimetric densities of the four-colour, three-colour component, and black component respectively.

A.3.1 Forard Model

$$\begin{aligned}
 D_{r-4c} = & a_{1,1} D_{r-3c} + a_{1,2} D_{g-3c} + a_{1,3} D_{b-3c} + a_{1,4} D_{r-k} + a_{1,5} D_{g-k} + a_{1,6} D_{b-k} + \\
 & a_{1,7} D_{r-3c}^2 + a_{1,8} D_{g-3c}^2 + a_{1,9} D_{b-3c}^2 + a_{1,10} D_{r-k}^2 + a_{1,11} D_{g-k}^2 + a_{1,12} D_{b-k}^2 + \\
 & a_{1,13} D_{r-3c} D_{g-3c} + a_{1,14} D_{r-3c} D_{b-3c} + a_{1,15} D_{r-3c} D_{r-k} + a_{1,16} D_{r-3c} D_{g-k} + \\
 & a_{1,17} D_{r-3c} D_{b-k} + a_{1,18} D_{g-3c} D_{b-3c} + a_{1,19} D_{g-3c} D_{r-k} + a_{1,20} D_{g-3c} D_{g-k} + \\
 & a_{1,21} D_{g-3c} D_{b-k} + a_{1,22} D_{b-3c} D_{r-k} + a_{1,23} D_{b-3c} D_{g-k} + a_{1,24} D_{b-3c} D_{b-k} + \\
 & a_{1,25} D_{r-k} D_{g-k} + a_{1,26} D_{r-k} D_{b-k} + a_{1,27} D_{g-k} D_{b-k}
 \end{aligned}$$

$$\begin{aligned}
 D_{g-4c} = & a_{2,1} D_{r-3c} + a_{2,2} D_{g-3c} + a_{2,3} D_{b-3c} + a_{2,4} D_{r-k} + a_{2,5} D_{g-k} + a_{2,6} D_{b-k} + \\
 & a_{2,7} D_{r-3c}^2 + a_{2,8} D_{g-3c}^2 + a_{2,9} D_{b-3c}^2 + a_{2,10} D_{r-k}^2 + a_{2,11} D_{g-k}^2 + a_{2,12} D_{b-k}^2 + \\
 & a_{2,13} D_{r-3c} D_{g-3c} + a_{2,14} D_{r-3c} D_{b-3c} + a_{2,15} D_{r-3c} D_{r-k} + a_{2,16} D_{r-3c} D_{g-k} + \\
 & a_{2,17} D_{r-3c} D_{b-k} + a_{2,18} D_{g-3c} D_{b-3c} + a_{2,19} D_{g-3c} D_{r-k} + a_{2,20} D_{g-3c} D_{g-k} + \\
 & a_{2,21} D_{g-3c} D_{b-k} + a_{2,22} D_{b-3c} D_{r-k} + a_{2,23} D_{b-3c} D_{g-k} + a_{2,24} D_{b-3c} D_{b-k} + \\
 & a_{2,25} D_{r-k} D_{g-k} + a_{2,26} D_{r-k} D_{b-k} + a_{2,27} D_{g-k} D_{b-k}
 \end{aligned}$$

$$\begin{aligned}
 D_{b-4c} = & a_{3,1} D_{r-3c} + a_{3,2} D_{g-3c} + a_{3,3} D_{b-3c} + a_{3,4} D_{r-k} + a_{3,5} D_{g-k} + a_{3,6} D_{b-k} + \\
 & a_{3,7} D_{r-3c}^2 + a_{3,8} D_{g-3c}^2 + a_{3,9} D_{b-3c}^2 + a_{3,10} D_{r-k}^2 + a_{3,11} D_{g-k}^2 + a_{3,12} D_{b-k}^2 + \\
 & a_{3,13} D_{r-3c} D_{g-3c} + a_{3,14} D_{r-3c} D_{b-3c} + a_{3,15} D_{r-3c} D_{r-k} + a_{3,16} D_{r-3c} D_{g-k} + \\
 & a_{3,17} D_{r-3c} D_{b-k} + a_{3,18} D_{g-3c} D_{b-3c} + a_{3,19} D_{g-3c} D_{r-k} + a_{3,20} D_{g-3c} D_{g-k} + \\
 & a_{3,21} D_{g-3c} D_{b-k} + a_{3,22} D_{b-3c} D_{r-k} + a_{3,23} D_{b-3c} D_{g-k} + a_{3,24} D_{b-3c} D_{b-k} + \\
 & a_{3,25} D_{r-k} D_{g-k} + a_{3,26} D_{r-k} D_{b-k} + a_{3,27} D_{g-k} D_{b-k}
 \end{aligned}$$

A.3.2 Reverse Model

$$\begin{aligned}
 D_{r-3c} = & a_{1,1} D_{r-4c} + a_{1,2} D_{g-4c} + a_{1,3} D_{b-4c} + a_{1,4} D_{r-k} + a_{1,5} D_{g-k} + a_{1,6} D_{b-k} + \\
 & a_{1,7} D_{r-4c}^2 + a_{1,8} D_{g-4c}^2 + a_{1,9} D_{b-4c}^2 + a_{1,10} D_{r-k}^2 + a_{1,11} D_{g-k}^2 + a_{1,12} D_{b-k}^2 + \\
 & a_{1,13} D_{r-4c} D_{g-4c} + a_{1,14} D_{r-4c} D_{b-4c} + a_{1,15} D_{r-4c} D_{r-k} + a_{1,16} D_{r-4c} D_{g-k} + \\
 & a_{1,17} D_{r-4c} D_{b-k} + a_{1,18} D_{g-4c} D_{b-4c} + a_{1,19} D_{g-4c} D_{r-k} + a_{1,20} D_{g-4c} D_{g-k} + \\
 & a_{1,21} D_{g-4c} D_{b-k} + a_{1,22} D_{b-4c} D_{r-k} + a_{1,23} D_{b-4c} D_{g-k} + a_{1,24} D_{b-4c} D_{b-k} + \\
 & a_{1,25} D_{r-k} D_{g-k} + a_{1,26} D_{r-k} D_{b-k} + a_{1,27} D_{g-k} D_{b-k}
 \end{aligned}$$

$$\begin{aligned}
 D_{g-3c} = & a_{2,1} D_{r-4c} + a_{2,2} D_{g-4c} + a_{2,3} D_{b-4c} + a_{2,4} D_{r-k} + a_{2,5} D_{g-k} + a_{2,6} D_{b-k} + \\
 & a_{2,7} D_{r-4c}^2 + a_{2,8} D_{g-4c}^2 + a_{2,9} D_{b-4c}^2 + a_{2,10} D_{r-k}^2 + a_{2,11} D_{g-k}^2 + a_{2,12} D_{b-k}^2 + \\
 & a_{2,13} D_{r-4c} D_{g-4c} + a_{2,14} D_{r-4c} D_{b-4c} + a_{2,15} D_{r-4c} D_{r-k} + a_{2,16} D_{r-4c} D_{g-k} + \\
 & a_{2,17} D_{r-4c} D_{b-k} + a_{2,18} D_{g-4c} D_{b-4c} + a_{2,19} D_{g-4c} D_{r-k} + a_{2,20} D_{g-4c} D_{g-k} + \\
 & a_{2,21} D_{g-4c} D_{b-k} + a_{2,22} D_{b-4c} D_{r-k} + a_{2,23} D_{b-4c} D_{g-k} + a_{2,24} D_{b-4c} D_{b-k} + \\
 & a_{2,25} D_{r-k} D_{g-k} + a_{2,26} D_{r-k} D_{b-k} + a_{2,27} D_{g-k} D_{b-k}
 \end{aligned}$$

$$\begin{aligned}
 D_{b-3c} = & a_{3,1} D_{r-4c} + a_{3,2} D_{g-4c} + a_{3,3} D_{b-4c} + a_{3,4} D_{r-k} + a_{3,5} D_{g-k} + a_{3,6} D_{b-k} + \\
 & a_{3,7} D_{r-4c}^2 + a_{3,8} D_{g-4c}^2 + a_{3,9} D_{b-4c}^2 + a_{3,10} D_{r-k}^2 + a_{3,11} D_{g-k}^2 + a_{3,12} D_{b-k}^2 + \\
 & a_{3,13} D_{r-4c} D_{g-4c} + a_{3,14} D_{r-4c} D_{b-4c} + a_{3,15} D_{r-4c} D_{r-k} + a_{3,16} D_{r-4c} D_{g-k} + \\
 & a_{3,17} D_{r-4c} D_{b-k} + a_{3,18} D_{g-4c} D_{b-4c} + a_{3,19} D_{g-4c} D_{r-k} + a_{3,20} D_{g-4c} D_{g-k} + \\
 & a_{3,21} D_{g-4c} D_{b-k} + a_{3,22} D_{b-4c} D_{r-k} + a_{3,23} D_{b-4c} D_{g-k} + a_{3,24} D_{b-4c} D_{b-k} + \\
 & a_{3,25} D_{r-k} D_{g-k} + a_{3,26} D_{r-k} D_{b-k} + a_{3,27} D_{g-k} D_{b-k}
 \end{aligned}$$

where

- $a_{i,j}$ are the optimised coefficients ($i = 1$ to 3 for D_r , D_g and D_b respectively) obtained by using the Lawson and Hanson's least-squares technique to give the closest predictions to those measured colorimetric data.
- $(D_{r-4c}, D_{g-4c}, D_{b-4c})$, $(D_{r-3c}, D_{g-3c}, D_{b-3c})$, $(D_{r-k}, D_{g-k}, D_{b-k})$ terms are the red-, green-, and blue- colorimetric densities of the four-colour, three-colour component, and black component respectively.

Appendix B The paired comparison results in terms of z-scores together with 95% confidence limit for all phases in the main experiment.

Phase	Hard-Copy	Soft-Copy		XYZ	Hunt		RLAB		±95 % CL					
1	D65 (ss)	D65	Total	<u>0.544</u>	-0.023		-0.520		±1.39					
			Art	1.558	-1.108		-0.450		±1.39					
			Flight	-0.537	1.250		-0.713		±1.39					
			Girl1	0.431	0.431		-0.862		±1.39					
			Girl2	1.196	0.159		-1.355		±1.39					
			Golf	-0.282	-0.590		0.872		±1.39					
			Musicians	1.021	-0.307		-0.713		±1.39					
			Total	<u>0.210</u>	0.070		-0.280		±1.39					
			Art	0.291	-0.431		0.140		±1.39					
2	D50 (ss)	D50	Flight	0.422	-0.713		0.291		±1.39					
			Girl1	0.291	0.571		-0.862		±1.39					
			Girl2	0.790	1.652		-2.442		±1.39					
			Golf	-0.765	-0.140		0.905		±1.39					
			Musicians	0.422	-0.282		-0.140		±1.39					
							CIELAB	CIELUV	Hunt	Nayatani	von Kries	BFD	RLAB	±95% CL
			3	D50 (tg)	D65	Total	0.757	-11.879	2.709	<u>3.660</u>	2.365	1.853	0.535	±1.39
						Art	-0.015	-12.361	1.352	4.189	4.189	2.499	0.181	±1.39
						Flight	0.852	-12.361	1.644	5.056	1.340	2.218	1.285	±1.39
Girl1	0.852	-10.667				5.099	1.871	1.352	1.318	0.219	±1.39			
Girl2	-0.014	-09.820				2.722	3.583	1.196	1.352	1.016	±1.39			
Golf	-0.686	-11.514				1.914	2.499	3.616	1.926	2.277	±1.39			
Musicians	1.372	-10.222				3.073	4.654	1.926	0.723	-1.487	±1.39			
Total	-1.753	-12.888				2.317	<u>4.409</u>	2.634	2.242	2.891	±1.39			
Art	-1.705	-11.514				1.059	5.892	5.056	1.652	-0.405	±1.39			
4	D65 (tg)	D93	Flight	-0.796	-11.514	4.439	5.056	1.590	1.124	0.137	±1.39			
			Girl1	-1.370	-12.361	0.723	6.020	2.944	2.792	1.285	±1.39			
			Girl2	-3.067	-11.069	-2.041	3.573	3.335	4.006	5.283	±1.39			
			Golf	-4.808	-11.514	4.127	3.561	1.742	2.890	4.037	±1.39			
			Musicians	-0.697	-09.375	1.632	2.234	1.352	2.089	2.792	±1.39			
			Total	-4.022	-14.450	2.744	2.871	3.260	<u>4.948</u>	4.299	±1.39			
			Art	-4.808	-12.361	0.205	1.968	6.446	4.548	4.037	±1.39			
			Flight	-1.552	-11.514	3.024	2.835	2.780	3.744	0.723	±1.39			
			Girl1	-1.997	-12.361	3.854	0.407	5.111	5.708	-0.686	±1.39			
5	D50 (ss)	D93	Girl2	-4.851	-12.361	1.926	0.766	3.073	2.944	8.538	±1.39			
			Golf	-9.086	-11.514	3.846	4.462	1.387	5.036	5.903	±1.39			
			Musicians	-6.502	-10.667	3.261	2.206	0.844	4.994	5.903	±1.39			
			Total	-3.303	-16.281	3.833	2.937	2.676	<u>4.956</u>	3.854	±1.39			
			Art	-2.792	-14.042	2.540	2.016	5.437	4.931	1.803	±1.39			
			Flight	-0.293	-14.042	5.078	3.500	1.851	4.043	-0.245	±1.39			
			Girl1	-2.998	-13.294	4.963	1.330	3.149	3.913	2.841	±1.39			
			Girl2	-3.638	-14.042	1.631	3.118	2.847	4.533	5.443	±1.39			
			Golf	-8.619	-12.547	4.217	3.646	2.317	4.771	6.108	±1.39			
6	D50 (tg)	D93	Musicians	-4.547	-12.178	4.326	3.317	0.588	4.262	4.115	±1.39			
			Total	1.178	-16.092	0.879	-0.050	4.776	<u>7.423</u>	1.602	±1.39			
			Art	4.342	-12.361	1.016	-2.224	4.092	3.690	1.481	±1.39			
			Flight	-2.196	-11.514	-2.251	2.835	6.957	9.050	-2.844	±1.39			
			Girl1	-1.643	-12.361	0.005	-4.918	6.555	11.524	0.872	±1.39			
			Girl2	3.073	-12.361	0.095	-0.057	3.744	4.818	0.723	±1.39			
			Golf	-3.332	-12.361	3.116	0.669	1.079	10.232	0.634	±1.39			
			Musicians	0.235	-12.361	1.297	-4.918	5.330	8.093	2.359	±1.39			
							A	D65						
7	A (tg)	D65	Total	1.178	-16.092	0.879	-0.050	4.776	<u>7.423</u>	1.602	±1.39			
			Art	4.342	-12.361	1.016	-2.224	4.092	3.690	1.481	±1.39			
			Flight	-2.196	-11.514	-2.251	2.835	6.957	9.050	-2.844	±1.39			
			Girl1	-1.643	-12.361	0.005	-4.918	6.555	11.524	0.872	±1.39			
			Girl2	3.073	-12.361	0.095	-0.057	3.744	4.818	0.723	±1.39			
			Golf	-3.332	-12.361	3.116	0.669	1.079	10.232	0.634	±1.39			
			Musicians	0.235	-12.361	1.297	-4.918	5.330	8.093	2.359	±1.39			

Note:

The figure underlined indicates the best performing model in a particular phase.

Appendix C The category judgement results for all phases in the main experiment.

Phase 1: Hardcopy (in Viewing Cabinet)-D65, Softcopy (on Monitor)-D65 (ss)

Model	Total	Art	Flight	Girl1	Girl2	Golf	Musicians
CIELAB	<u>2.427</u>	<u>2.723</u>	1.675	<u>1.435</u>	<u>2.244</u>	1.008	<u>2.063</u>
Hunt	2.237	2.038	<u>1.973</u>	1.401	1.864	1.070	1.907
RLAB	2.249	2.154	1.470	1.109	1.655	<u>1.450</u>	1.695
Boundary Estimate	Total	Art	Flight	Girl1	Girl2	Golf	Musicians
t1	0.000	0.000	0.000	0.000	0.000	0.000	0.000
t2	0.000	0.000	0.000	0.000	0.000	0.000	0.000
t3	1.241	1.240	0.829	0.000	0.874	0.000	0.829
t4	2.340	2.389	1.908	1.245	1.957	1.106	1.960
t5	3.535	3.599	3.346	2.332	3.147	2.472	2.910
t6	3.535	3.599	3.346	2.332	3.147	2.472	2.910

Phase 2: Hardcopy (in Viewing Cabinet)-D50, Softcopy (on Monitor)-D50 (ss)

Model	Total	Art	Flight	Girl1	Girl2	Golf	Musicians
CIELAB	<u>2.839</u>	2.112	1.941	2.045	2.661	1.359	<u>1.961</u>
Hunt	2.754	2.178	1.601	<u>2.324</u>	<u>3.087</u>	1.487	1.837
RLAB	2.818	<u>2.194</u>	<u>2.001</u>	1.864	1.866	<u>1.851</u>	1.798
Boundary Estimate	Total	Art	Flight	Girl1	Girl2	Golf	Musicians
t1	0.000	0.000	0.000	0.000	0.000	0.000	0.000
t2	0.518	0.000	0.000	0.000	0.000	0.000	0.000
t3	1.549	0.829	0.709	0.531	1.325	0.000	0.761
t4	2.676	2.043	1.875	1.808	2.534	1.207	1.783
t5	3.877	3.155	3.279	2.951	3.866	2.521	3.038
t6	3.877	3.155	3.279	2.951	3.866	2.521	3.038

Phase 3: Hardcopy (in Viewing Cabinet)-D50, Softcopy (on Monitor)-D65 (tg)

Model	Total	Art	Flight	Girl1	Girl2	Golf	Musicians
CIELAB	3.656	3.895	4.382	3.314	3.930	3.062	3.386
CIELUV	<u>1.679</u>	<u>1.660</u>	<u>1.065</u>	<u>1.561</u>	<u>2.072</u>	<u>1.411</u>	<u>1.644</u>
Hunt	4.055	4.134	4.215	<u>3.823</u>	4.167	3.866	3.592
Nayatani	<u>4.188</u>	<u>4.417</u>	<u>4.728</u>	3.512	<u>4.353</u>	3.905	<u>3.979</u>
von Kries	3.981	4.404	4.434	3.565	4.251	<u>4.032</u>	3.343
BFD	3.928	4.297	4.483	3.434	3.940	3.946	3.428
RLAB	3.719	3.903	4.106	3.371	3.650	3.893	3.187
Boundary Estimate	Total	Art	Flight	Girl1	Girl2	Golf	Musicians
t1	0.000	0.000	0.000	0.000	0.000	0.000	0.000
t2	1.543	1.679	1.656	1.407	1.656	1.353	1.311
t3	2.509	2.597	2.631	2.024	2.536	2.335	2.462
t4	3.748	3.919	4.244	3.329	3.854	3.631	3.565
t5	5.143	5.285	5.732	4.694	5.263	5.028	5.116
t6	6.521	6.964	7.392	5.759	6.304	7.100	6.527

Appendix C The category judgement results for all phases in the main experiment.
(continued)

Phase 4: Hardcopy (in Viewing Cabinet)-D65, Softcopy (on Monitor)-D93 (tg)

Model	Total	Art	Flight	Girl1	Girl2	Golf	Musicians
CIELAB	2.276	3.088	2.466	3.470	3.950	1.445	1.907
CIELUV	<i>0.826</i>	<i>1.652</i>	<i>0.254</i>	<i>1.177</i>	1.930	<i>0.381</i>	<i>0.846</i>
Hunt	2.642	3.624	2.876	3.736	3.910	2.690	2.002
Nayatani	<u>3.125</u>	<u>4.092</u>	<u>3.133</u>	<u>4.491</u>	<u>4.864</u>	<u>2.753</u>	<u>2.415</u>
von Kries	2.931	4.086	2.982	4.382	4.599	2.602	2.137
BFD	2.797	3.829	2.810	4.146	4.731	2.487	2.092
RLAB	2.710	3.297	2.518	4.134	4.677	2.516	2.221
Boundary Estimate	Total	Art	Flight	Girl1	Girl2	Golf	Musicians
t1	0.000	0.000	0.000	0.000	0.000	0.000	0.000
t2	0.680	1.221	0.573	1.527	1.833	0.493	0.392
t3	1.604	2.511	1.397	2.719	3.089	1.279	1.271
t4	2.709	3.653	2.738	3.772	4.273	2.423	2.301
t5	3.778	4.672	4.083	5.003	5.489	3.580	3.414
t6	5.266	6.113	4.844	5.891	6.679	4.771	3.795

Phase 5: Hardcopy (in Viewing Cabinet)-D50, Softcopy (on Monitor)-D93 (ss)

Model	Total	Art	Flight	Girl1	Girl2	Golf	Musicians
CIELAB	1.941	2.068	3.098	2.986	2.016	1.135	1.879
CIELUV	<i>0.192</i>	<i>0.504</i>	<i>0.047</i>	<i>0.701</i>	<i>0.482</i>	<i>-0.295</i>	<i>0.799</i>
Hunt	3.081	3.064	3.934	3.662	3.325	3.283	3.188
Nayatani	2.918	3.094	3.623	3.385	3.143	3.302	3.035
von Kries	2.992	<u>3.491</u>	3.763	3.952	3.254	2.938	2.660
BFD	<u>3.286</u>	3.486	<u>3.946</u>	<u>4.000</u>	3.391	<u>3.467</u>	<u>3.384</u>
RLAB	3.038	3.323	3.432	3.229	<u>3.721</u>	3.330	3.326
Boundary Estimate	Total	Art	Flight	Girl1	Girl2	Golf	Musicians
t1	0.000	0.000	0.000	0.000	0.000	0.000	0.000
t2	1.152	1.334	1.833	1.720	1.527	1.237	1.045
t3	2.233	2.356	2.783	2.798	2.561	2.221	2.216
t4	3.227	3.414	3.943	3.834	3.723	3.418	3.421
t5	4.423	4.649	5.158	5.311	5.043	4.489	4.671
t6	4.423	4.841	5.662	5.358	5.744	4.972	4.671

Appendix C The category judgement results for all phases in the main experiment.
(continued)

Phase 6: Hardcopy (in Viewing Cabinet)-D50, Softcopy (on Monitor)-D93 (tg)

Model	Total	Art	Flight	Girl1	Girl2	Golf	Musicians
CIELAB	2.472	2.845	2.663	2.696	2.700	1.289	2.278
CIELUV	0.277	0.212	-0.301	0.389	0.545	0.290	0.423
Hunt	3.487	3.769	3.312	<u>4.107</u>	3.386	3.501	<u>3.725</u>
Nayatani	3.358	3.660	3.172	3.632	3.375	3.493	3.587
von Kries	3.421	4.111	3.011	3.847	3.390	3.286	3.253
BFD	<u>3.656</u>	<u>4.147</u>	<u>3.334</u>	3.787	<u>3.514</u>	3.648	3.630
RLAB	3.290	3.576	2.529	3.719	3.588	3.603	3.593

Boundary Estimate	Total	Art	Flight	Girl1	Girl2	Golf	Musicians
t1	0.000	0.000	0.000	0.000	0.000	0.000	0.000
t2	1.148	1.148	0.806	1.232	1.193	1.076	1.477
t3	2.314	2.342	1.989	2.365	2.371	2.253	2.594
t4	3.299	3.648	3.128	3.464	3.289	3.279	3.666
t5	4.384	4.748	4.281	4.577	4.358	4.366	4.801
t6	5.994	6.028	5.418	6.066	5.575	5.521	4.801

Phase 7: Hardcopy (in Viewing Cabinet)-A, Softcopy (on Monitor)-D65 (tg)

Model	Total	Art	Flight	Girl1	Girl2	Golf	Musicians
CIELAB	1.912	3.095	1.876	1.868	1.962	1.412	1.626
CIELUV	-1.651	-1.325	-1.786	-1.593	-2.087	-1.446	-2.087
Hunt	2.080	2.915	1.812	2.040	1.989	2.674	1.578
Nayatani	1.637	2.230	2.539	1.081	1.301	2.130	0.819
von Kries	2.589	<u>3.400</u>	3.308	2.965	2.041	2.440	2.242
BFD	<u>2.941</u>	3.335	<u>3.512</u>	<u>3.661</u>	<u>2.275</u>	<u>3.226</u>	2.691
RLAB	1.973	3.043	1.737	2.122	1.904	2.181	1.620

Boundary Estimate	Total	Art	Flight	Girl1	Girl2	Golf	Musicians
t1	0.000	0.000	0.000	0.000	0.000	0.000	0.000
t2	1.055	1.552	1.455	0.894	0.617	1.002	0.869
t3	2.083	2.562	2.643	2.206	1.741	2.216	1.859
t4	2.996	3.464	3.837	3.208	2.647	3.185	2.798
t5	4.035	4.593	4.673	4.278	3.612	4.315	3.980
t6	4.035	4.593	4.673	4.278	3.612	4.315	3.980

Note:

The figure underlined indicates the best performing model in a particular phase.

Appendix D Rank order of models' performance using the paired comparison method (using 95% confidence limits). (CL=1.39)

Field Ref.	Image Test	Display	CIELAB	CIELUV	Hunt	Nayatani	von Kries	BFD	RLAB
D50 D65	Art	TG	5	7	3	1	1	3	4
	Flight	TG	2	7	2	1	2	2	2
	Girl1	TG	2	7	1	2	2	2	5
	Girl2	TG	3	7	1	1	3	2	3
	Golf	TG	6	7	3	1	1	3	1
	Musicians	TG	3	7	2	1	2	3	6
	Average			3.50	7.00	2.00	1.00	1.83	2.50
Rank			5	7	3	1	2	4	5
D65 D93	Art	TG	5	7	3	1	1	3	5
	Flight	TG	5	7	1	1	3	3	4
	Girl1	TG	6	7	4	1	2	2	4
	Girl2	TG	5	7	5	2	2	1	1
	Golf	TG	6	7	1	1	4	1	1
	Musicians	TG	6	7	4	1	5	1	1
	Average			5.50	7.00	3.00	1.00	2.83	1.83
Rank			6	7	5	1	4	2	3
D50 D93	Art	SS	6	7	5	4	1	2	2
	Flight	SS	6	7	1	1	1	1	5
	Girl1	SS	4	7	2	4	1	1	4
	Girl2	SS	6	7	2	4	2	2	1
	Golf	SS	6	7	3	2	5	1	1
	Musicians	SS	6	7	3	3	4	1	1
	Average			5.67	7.00	2.67	3.00	2.33	1.33
Rank			6	7	4	5	2	1	2
D50 D93	Art	TG	6	7	3	3	1	1	3
	Flight	TG	5	7	1	2	4	1	5
	Girl1	TG	6	7	1	5	2	1	3
	Girl2	TG	6	7	4	3	3	1	1
	Golf	TG	6	7	2	2	4	2	1
	Musicians	TG	6	7	1	1	5	1	1
	Average			5.83	7.00	2.00	2.67	3.17	1.17
Rank			6	7	2	4	5	1	3
A D65	Art	TG	1	7	4	6	1	1	4
	Flight	TG	4	7	4	3	2	1	4
	Girl1	TG	5	7	3	6	2	1	3
	Girl2	TG	2	7	4	4	1	1	4
	Golf	TG	6	7	2	3	3	1	3
	Musicians	TG	4	7	3	6	2	1	3
	Average			3.67	7.00	3.33	4.67	1.83	1.00
Rank			5	7	3	6	2	1	4
Average			4.83	7.00	2.60	2.47	2.40	1.57	2.87
Rank			6	7	4	3	2	1	5

Appendix E Rank order of models' performance using the category judgement method.

Field	Image	Display	CIELAB	CIELUV	Hunt	Nayatani	von Kries	BFD	RLAB	
Ref.	Test									
D50	D65	Art	tg	6	7	4	1	2	3	5
		Flight	tg	4	7	5	1	3	2	6
		Girl1	tg	6	7	1	3	2	4	5
		Girl2	tg	5	7	3	1	2	4	6
		Golf	tg	6	7	5	3	1	2	4
		Musicians	tg	4	7	2	1	5	3	6
	Average			5.17	7.00	3.33	1.67	2.50	3.00	5.33
Rank			6	7	4	1	2	3	5	
D65	D93	Art	tg	6	7	4	1	2	3	5
		Flight	tg	6	7	3	1	2	4	5
		Girl1	tg	6	7	5	1	2	3	4
		Girl2	tg	5	7	6	1	4	2	3
		Golf	tg	6	7	2	1	3	5	4
		Musicians	tg	6	7	5	1	3	4	2
	Average			5.83	7.00	4.17	1.00	2.67	3.50	3.83
Rank			6	7	5	1	2	3	4	
D50	D93	Art	ss	6	7	5	4	1	2	3
		Flight	ss	6	7	2	4	3	1	5
		Girl1	ss	6	7	3	4	2	1	5
		Girl2	ss	6	7	3	5	4	2	1
		Golf	ss	6	7	4	3	5	1	2
		Musicians	ss	6	7	3	4	5	1	2
	Average			6.00	7.00	3.33	4.00	3.33	1.33	3.00
Rank			6	7	3	5	3	1	2	
D50	D93	Art	tg	6	7	3	4	2	1	5
		Flight	tg	5	7	2	3	4	1	6
		Girl1	tg	6	7	1	5	2	3	4
		Girl2	tg	6	7	4	5	3	2	1
		Golf	tg	6	7	3	4	5	1	2
		Musicians	tg	6	7	1	4	5	2	3
	Average			5.83	7.00	2.33	4.17	3.50	1.67	3.50
Rank			6	7	2	5	3	1	3	
A	D65	Art	tg	3	7	5	6	1	2	4
		Flight	tg	4	7	5	3	2	1	6
		Girl1	tg	5	7	4	6	2	1	3
		Girl2	tg	4	7	3	6	2	1	5
		Golf	tg	6	7	2	5	3	1	4
		Musicians	tg	4	7	5	6	2	1	3
	Average			4.33	7.00	4.00	5.33	2.00	1.17	4.17
Rank			5	7	3	6	2	1	4	
Average				5.43	7.00	3.43	3.23	2.80	2.13	3.97
Rank				6	7	4	3	2	1	5

Appendix F Colour-fidelity category of models' performance using the category judgement method.

Field Hard- copy	Image Soft- copy	Image	Display	CIELAB	CIELUV	Hunt	Nayatani von Kries	BFD	RLAB
D50	D65	Total	tg	4	7	3	3	3	4
		Art	tg	4	6	3	3	3	4
		Flight	tg	3	6	4	3	3	4
		Girl1	tg	4	5	3	3	3	3
		Girl2	tg	3	5	3	3	3	3
		Golf	tg	4	5	3	3	3	3
		Musicians	tg	4	5	3	3	4	4
D65	D93	Total	tg	4	5	4	3	3	3
		Art	tg	4	5	4	3	3	4
		Flight	tg	4	6	3	3	3	4
		Girl1	tg	4	6	4	3	3	3
		Girl2	tg	4	5	4	3	3	3
		Golf	tg	4	6	3	3	3	3
		Musicians	tg	4	5	4	3	4	4
D50	D93	Total	ss	5	6	4	4	4	4
		Art	ss	5	6	4	4	3	4
		Flight	ss	4	6	3	4	4	4
		Girl1	ss	4	6	4	4	3	4
		Girl2	ss	5	6	4	4	4	4
		Golf	ss	6	7	4	4	4	4
		Musicians	ss	5	6	4	4	4	4
D50	D93	Total	tg	4	6	3	3	3	4
		Art	tg	4	6	3	4	3	4
		Flight	tg	4	7	3	3	4	4
		Girl1	tg	4	6	3	3	3	3
		Girl2	tg	4	6	3	3	3	3
		Golf	tg	5	6	3	3	3	3
		Musicians	tg	5	6	3	4	4	3
A	D65	Total	tg	5	7	5	5	4	5
		Art	tg	4	7	4	5	4	4
		Flight	tg	5	7	5	5	4	5
		Girl1	tg	5	7	5	5	4	5
		Girl2	tg	4	7	4	5	4	4
		Golf	tg	5	7	4	5	4	5
		Musicians	tg	5	7	5	6	4	5

Appendix E Rank order of models' performance using the category judgement method.

Field Ref.	Image Test	Display	CIELAB	CIELUV	Hunt	Nayatani	von Kries	BFD	RLAB	
D50	D65	Art	tg	6	7	4	1	2	3	5
		Flight	tg	4	7	5	1	3	2	6
		Girl1	tg	6	7	1	3	2	4	5
		Girl2	tg	5	7	3	1	2	4	6
		Golf	tg	6	7	5	3	1	2	4
		Musicians	tg	4	7	2	1	5	3	6
		Average			5.17	7.00	3.33	1.67	2.50	3.00
	Rank			6	7	4	1	2	3	5
D65	D93	Art	tg	6	7	4	1	2	3	5
		Flight	tg	6	7	3	1	2	4	5
		Girl1	tg	6	7	5	1	2	3	4
		Girl2	tg	5	7	6	1	4	2	3
		Golf	tg	6	7	2	1	3	5	4
		Musicians	tg	6	7	5	1	3	4	2
		Average			5.83	7.00	4.17	1.00	2.67	3.50
	Rank			6	7	5	1	2	3	4
D50	D93	Art	ss	6	7	5	4	1	2	3
		Flight	ss	6	7	2	4	3	1	5
		Girl1	ss	6	7	3	4	2	1	5
		Girl2	ss	6	7	3	5	4	2	1
		Golf	ss	6	7	4	3	5	1	2
		Musicians	ss	6	7	3	4	5	1	2
		Average			6.00	7.00	3.33	4.00	3.33	1.33
	Rank			6	7	3	5	3	1	2
D50	D93	Art	tg	6	7	3	4	2	1	5
		Flight	tg	5	7	2	3	4	1	6
		Girl1	tg	6	7	1	5	2	3	4
		Girl2	tg	6	7	4	5	3	2	1
		Golf	tg	6	7	3	4	5	1	2
		Musicians	tg	6	7	1	4	5	2	3
		Average			5.83	7.00	2.33	4.17	3.50	1.67
	Rank			6	7	2	5	3	1	3
A	D65	Art	tg	3	7	5	6	1	2	4
		Flight	tg	4	7	5	3	2	1	6
		Girl1	tg	5	7	4	6	2	1	3
		Girl2	tg	4	7	3	6	2	1	5
		Golf	tg	6	7	2	5	3	1	4
		Musicians	tg	4	7	5	6	2	1	3
		Average			4.33	7.00	4.00	5.33	2.00	1.17
	Rank			5	7	3	6	2	1	4
Average				5.43	7.00	3.43	3.23	2.80	2.13	3.97
Rank				6	7	4	3	2	1	5

Appendix F Colour-fidelity category of models' performance using the category judgement method.

Field Hard- copy	Image Soft- copy	Image	Display	CIELAB	CIELUV	Hunt	Nayatani von Kries	BFD	RLAB
D50	D65	Total	tg	4	7	3	3	3	4
		Art	tg	4	6	3	3	3	4
		Flight	tg	3	6	4	3	3	4
		Girl1	tg	4	5	3	3	3	3
		Girl2	tg	3	5	3	3	3	3
		Golf	tg	4	5	3	3	3	3
		Musicians	tg	4	5	3	3	4	4
D65	D93	Total	tg	4	5	4	3	3	3
		Art	tg	4	5	4	3	3	4
		Flight	tg	4	6	3	3	3	4
		Girl1	tg	4	6	4	3	3	3
		Girl2	tg	4	5	4	3	3	3
		Golf	tg	4	6	3	3	3	3
		Musicians	tg	4	5	4	3	4	4
D50	D93	Total	ss	5	6	4	4	4	4
		Art	ss	5	6	4	4	3	4
		Flight	ss	4	6	3	4	4	4
		Girl1	ss	4	6	4	4	3	4
		Girl2	ss	5	6	4	4	4	4
		Golf	ss	6	7	4	4	4	4
		Musicians	ss	5	6	4	4	4	4
D50	D93	Total	tg	4	6	3	3	3	4
		Art	tg	4	6	3	4	3	4
		Flight	tg	4	7	3	3	4	4
		Girl1	tg	4	6	3	3	3	3
		Girl2	tg	4	6	3	3	3	3
		Golf	tg	5	6	3	3	3	3
		Musicians	tg	5	6	3	4	4	4
A	D65	Total	tg	5	7	5	5	4	5
		Art	tg	4	7	4	5	4	4
		Flight	tg	5	7	5	5	4	5
		Girl1	tg	5	7	5	5	4	5
		Girl2	tg	4	7	4	5	4	4
		Golf	tg	5	7	4	5	4	5
		Musicians	tg	5	7	5	6	4	5